Inducible Depletion of Cardiac Thymosin β4: Development and Shortcomings of a Popular Technique in Cardiac Research

A thesis submitted for the degree of Doctor of Philosophy and the Diploma of Imperial College

by

Jonas Maximilian Lexow

National Heart & Lung Institute

Hammersmith Campus

Imperial College London

September 2012

Abstract

In reference to recent studies highlighting the importance of Thymosin beta 4 (Tβ4) during embryonic development and its therapeutic potential, an inducible cardiac-specific knockdown of Tβ4 was established to investigate the outcomes of loss of function in adult mammalian hearts. *Tβ4shRNAflox/MerCreMer* mice were generated with the aim of depleting cardiac Tβ4 expression by RNA interference in a tamoxifen-dependent fashion. *In vivo, in vitro* and *ex vivo* approaches showed that tamoxifen treatment of *Tβ4shRNAflox/MerCreMer* mice does not result in significant down-regulation of *Tβ4* mRNA or protein in the heart. Interestingly, higher levels of Tβ4 were identified in cardiac fibroblasts compared to cardiomyocytes. The above analyses suggest that an inducible knockout of *Tβ*4 would be a more direct, more reliable and more effective means to study loss of function in the adult mammalian heart.

In the course of the study, an adverse cardiac phenotype was observed in tamoxifen-treated *MerCreMer*-positive animals, consisting of perivascular and interstitial fibrosis, decreased cardiac function, a marked inflammatory response and increased expression of factors involved in cardiac remodelling and hypertrophy. This was not related to *MerCreMer* gene copy number (homo/heterozygosity) but found to be associated with tamoxifen dose, mode of delivery and genetic background. A thorough analysis of related literature revealed that a number of recent publications have failed to include tamoxifen-treated *αMHC/MerCreMer* controls and some of the presented data may be affected by Cre toxicity. In conclusion, *αMHC/MerCreMer* mice should be included as controls in the analysis of future studies or alternative inducible systems considered.

Recent analyses revealed that *IGF-1Ea* overexpression in the heart improves the outcome of myocardial infarction in mice. This process has been described on the molecular level but a comprehensive analysis of the subcellular structure of *αMHC/IGF-1Ea* hearts had not previously been performed. A detailed transmission electron microscope analysis of *αMHC/IGF-1Ea* hearts revealed previously not described large electron-dense structures inside *αMHC/IGF-1Ea* cardiomyocytes. The structures resembled large autophagolysosomes although markers of autophagy were neither found to be associated with the structures nor upregulated in the hearts of *αMHC/IGF-1Ea* mice. Intriguingly lysosomes were identified in the proximity of the structures potentially implying a role in turnover of intracellular material. These results provide further insights into the diverse roles of IGF-1Ea in the heart.

Acknowledgements

I thank my supervisor Nadia Rosenthal for her support, inspiration, for making science fun and for always putting seemingly small things into a bigger context. She has removed barriers from my imagination and creativity, always encouraging me to follow my ideas and express my views and I am very grateful for having had the opportunity to work for her. I am deeply indebted to my secondary supervisor Maria Paola Santini who always supported me with great dedication, perseverance and unquestionable optimism, especially in times of great frustration. She has taught me countless invaluable lessons. I am grateful to Padmini Sarathchandra for helping me throughout the project. She is the best collaborator I could have wished for, an excellent histologist and a fantastic cook. I thank Tommaso Poggioli for sharing some great times with me both inside and outside the lab, in the UK and abroad and for the camaraderie and friendly competition. Furthermore, I thank Elham Zarrinpashneh who always shared her vast technical knowledge with me - she was fantastic to work and celebrate with and I share a unique friendship with her.

I especially thank my PhD buddy Borggia Seemampilai, my lunch buddies Janine Beale, Kalyani Panse and Alba Singla for the fun, my climbing partner Sebastian Krumscheid for keeping my head level, Jerome Sohier and Athinoula Meli for the fun as well as Napachanok Mongkoldhumrongkul, Murali Padala, Najma Latif, Marzieh Zamani, Jenny Zobel and Phillip Gabriel for always staying positive and encouraging me.

I furthermore would like to thank Cheryl Costello for her support and guidance, especially in all matters regarding the College. I thank Leanne Felkin for her optimism and support with everything related to RNA and Reneé Germack for her practical cell culture advice. I am grateful to Paul Barton, Enrique Lara-Pezzi and Nigel Brand for open ears, advice and excellent sense of humour. Big thanks also to the BSU staff and especially Sandra Peak and Emma Rowley who have done a fantastic job and always helped me with the quite substantial *in vivo* component of this work. Furthermore, I am most grateful to Imperial College London for providing a vibrant and inspirational environment to conduct research and enjoy studying.

I especially thank my parents Jürgen and Monika Lexow, my brothers and sisters Maria Lexow, Jakob Lexow, Matthias Lexow, Johanna Lexow and Magdalena Lexow who have been an oasis of calm in stormy times and without whom I would not have been able to start a PhD.

No words are enough to thank Andrea Bauer for sharing this experience with me, for picking me up when I was down and carrying me through countless difficult times, for making sacrifices and for taking diversions to support me. For the support and joy she has given me over the years I will be indebted to her forever. She has made this work possible and the whole experience worthwhile. Thank you.

Declaration

All the work described in this thesis was performed by the author except were specifically indicated below or in the text. Figure 1.3 and Figure 1.6 were obtained from the respective publications (Bock-Marquette *et al.* 2004; Santini *et al.* 2007). The BioAnalyzer run shown in Figure 2.9 was performed by Leanne Felkin. Sectioning and stainings of Figure 2.3, Figure 3.10, Figure 4.1, Figure 4.2, Figure 4.4 and Figure 4.7 were performed by Padmini Sarathchandra. Immunofluorescence stainings shown in Figure 3.2, Figure 3.8, Figure 3.14 and Figure 3.17 were performed by Padmini Sarathchandra. For Figure 6.1, Figure 6.2, Figure 6.3 and Figure 6.4 transmission electron microscope samples were processed with assistance of Padmini Sarathchandra and ultra-thin sectioning performed by Padmini Sarathchandra. Sectioning, microscopy and recording of images displayed in Figure 6.5 were performed by Bart Wagner. Immunogold sample preparation, ultra-thin sectioning, staining and image recording was performed by Padmini Sarathchandra for Figure 6.6, Figure 6.7, Figure 6.8 and Figure 6.14.

Abbreviations

1D – One-dimensional

2D – Two-dimensional

αMHC – α myosin heavy chain

Ang II – Angiotensin type II

APS – Ammonium persulfate

ARB – Angiotension type II receptor blocker

Atg - Autophagy-related protein

β-ME – β-Mercaptoethanol

BSA – Bovine serum albumin

BW – Body weight

CABG – Coronary artery bypass graft

cDNA – Complementary cDNA

CLN 3 – Ceroid-lipofuscinosis 3

CMV - Cytomegalovirus

CO_2 – Carbon dioxide

Col1 - Collagen type-1

Col2 – Collagen type-2

Col3 - Collagen type-3

CTGF - Connective tissue growth factor

CTX – Cardiotoxin

CVD – Cardiovascular disease

DEPC - Diethylpyrocarbonate

ddH_2O – Double de-ionized H_2O

dH_2O – Distilled H_2O

DNA – Deoxyribonucleic acid

DTT - Dithiothreitol

E. coli - Escherichia coli

ECHO – Echocardiography

ECL – Enhance chemiluminescence

ECM – Extracellular matrix

EF – Ejection fraction

EMBL – European Molecular Biology Laboratory

EPC – Endothelial progenitor cell

ER – Oestrogen receptor

EtOH – Ethanol

F-actin – Filamentous actin

FBS – Fetal bovine serum

FCS – Fetal calf serum

FLP – Flippase

frt – FLP recombination target

FS – Fractional shortening

G-actin – Globular actin

Gal-3 – Galectin 3

HBSS – Hank's buffered salt solution

HGF - Hepatocyte growth factor

hMLH1 – Human *MutL* homologue 1

HUVEC - Human vein endothelial cells

HW – Heart weight

HW/BW ratio - Heart-weight-to-body-weight ratio

IFNγ – Interferon γ

IL – Interleukin

ILK – Integrin-linked kinase

IMS – Industrial methylated spirit

IP – Intraperitoneal

IRS - Insulin receptor substrate

IVC – Inferior vena cava

kDa – Kilodalton

LC3 - Microtubule-associated protein 1 light chain 3

LC_{50} – Median lethal dose

LCA – Left coronary artery

LDH assay – Lactate dehydrogenase assay

LiW – Liver weight

LiW/BW – Liver-weight-to-body-weight ratio

LuW – Lung weight

LuW/BW ratio - Lung-weight-to-body-weight ratio

LV –Left ventricle

LVIDd – Left ventricular inner diameter diastole

LVIDs – Left ventricular inner diameter systole

MCP-1 - Monocyte chemoattractant protein

MeOH - Methanol

MGB – Minor grove binder

min – Minute(s)

MIP1α - Macrophage inflammatory protein 1α

mIR – microRNA

MMP - Matrix metalloproteinase

MRI - Magnetic resonance imaging

MSC - Mesenchymal stem cells

mTOR – Mammalian target of rapamycin

MWCO – Molecular weight cut-off

NCL – Neuronal ceroid lipofuscinosis

NCM – Neonatal cardiomyocytes

NFκB - Nuclear factor κ-light-chain-enhancer of activated B cells

Ni^{2+} - Nickel

O_2 – Oxygen

PBS – Phosphate buffered saline

PCI – Percutaneous coronary intervention

PCR - Polymerase chain reaction

PCTA – Percutaneous transluminal angiogplasty

PFA – Paraformaldehyde

PFN – Profilin

PMN - Polomorphonuclear leukocytes

POP - Prolyl oligopeptidase

RIPA – Radioimmunoprecipitation

RISC - RNA-induced silencing complex

RNA – Ribonucleic acid

RNAi – RNA interference

RT – Room temperature (~25 °C)

rtPCR – Real-time PCR

rtTa – Reverse tetracycline-responsive transcriptional activator

RV – Right ventricle

SDF-1α - Stromal derived factor-1α

SD – Standard deviation

SDS – Sodium dodecyl sulfate

SERCA2a - Sarco/endoplasmic reticulum Ca2+-ATPase

shRNA - Short hairpin RNA

SirT1 – Sirtuin 1

SV40 - Simian virus 40

TBS – Tris-buffered saline

TE – Tris-EDTA

TEM – Transmission electron microscopy

TetO - Tet operator

TNFα - Tumor necrosis factor α

TOR – Target of Rapamycin

tTa - Tetracycline-responsive transcriptional activator

UTR – Untranslated region

VASP - Vasodilator-stimulated phosphoprotein

VEGF- Vein endothelial growth factor

WH2 - Wiskott-Aldrich Syndrome protein homology domain 2

WHO – World Health Organisation

Wt1 – Wilm's tumour gene 1

Index

Abstract **2**

Acknowledgements **3**

Declaration **5**

Abbreviations **6**

Index **10**

List of Figures **15**

List of Tables **19**

Chapter 1 - Introduction **20**

1.1 The mammalian heart **20**

1.2 Cardiovascular disease **20**

1.2.1 Coronary heart disease 21

1.2.1 Hypertrophy, cardiac remodelling and heart failure 21

1.3 Current treatments of coronary heart disease and heart failure **22**

1.3.1 Invasive interventional cardiology 23

1.3.2 Pharmacological intervention 24

1.3.3 Device therapy for cardiovascular disease 24

1.3.4 Novel approaches to prevent or cure heart failure 25

1.4 Thymosin β4 ..... **27**

1.4.1 The thymosin protein family 27

1.4.2 Thymosin β4 structure and actin binding function 28

1.4.3 N-acetyl-seryl-aspartyl-lysyl-proline 31

1.4.4 Thymosin β4 function 32

1.4.5 Thymosin β4 and the heart 37

1.5 Insulin-like growth factor 1 ..... **40**

1.5.1 Insulin-like growth factor 1 structure and post-translational modifications 40

1.5.2 Insulin-like growth factor 1 signalling 42

1.5.3 IGF-1 and its propeptides in cardiac regeneration 43

1.5.4 Autophagy 49

1.6 Researching factors for cardiac protection: Transgenics, global and inducible knockout and knockdown mice 50

1.6.1 Global versus tissue specific gene overexpression 50

1.6.2 Global gene knockout 51

1.6.3 The Cre/*loxP* system 51

1.6.4 Cre driver strains: *αMHC/MerCreMer* mice 52

1.6.5 RNA interference-mediated knockdown 53

1.7 Hypothesis 55

Chapter 2 - Methodology 56

2.1 Mouse models 56

2.1.1 *αMHC/MerCreMer* mice 56

2.1.2 *Tβ4shRNAflox* mice 56

2.1.3 *αMHC/IGF-1Ea* mice 57

2.1.4 Genotyping 58

2.1.5 Experimental MI: Left anterior descending coronary artery ligation 60

2.1.6 Mouse model of myocardial infarction: Left anterior descending coronary artery ligation 61

2.2 Conditional knockdown of Thymosin β4 63

2.2.1 Tamoxifen delivery 63

2.3 Echocardiography 63

2.3.1 Transthoracic echocardiography 64

2.4 Tissue harvesting from mice 66

2.5 Protein biochemistry 68

2.5.1 Protein extraction 68

2.5.2 Protein quantification 68

2.6 Protein immunoblotting 70

2.6.1 Western blotting procedure for normal sized proteins 70

2.6.2 Western blotting procedure for small proteins and peptides 73

2.7 RNA extraction 73

2.7.1 RNA isolation from cells 74

2.7.2 RNA isolation from tissue 74

2.7.3 RNA quantification and quality control 75

2.8 mRNA copy number analysis 76

2.8.1 cDNA synthesis 76

2.8.2 Real-time polymerase chain reaction 77

2.8.3 Autophagy PCR Array 80

2.9 gDNA extraction for gene copy number analysis 82

2.9.1 DNA quantification and quality control 83

2.10 *Cre* gene copy number analysis 84

2.11 Histology 85

2.11.1 Staining of OCT embedded sections 85

2.11.2 Paraffin-embedding of tissue 86

2.11.3 Masson's Trichrome Staining 86

2.12 Transmission electron microscopy 87

2.12.1 Immunogold labelling 88

2.13 Production of recombinant V5-His$_6$-tagged thymosin β4-V5/His protein 88

2.13.1 Cloning of Tβ4 89

2.13.2 Confirmation of positive clones 91

2.13.3 Tβ4-V5-His protein expression in *E. coli* 91

2.13.4 Tβ4-V5-His protein expression in mammalian cells 92

2.13.5 Purification of His-tagged recombinant proteins 92

2.14 Immunoprecipitation 93

2.15 Thymosin β4 knockdown in neonatal cardiomyocyte preparations from mice. 94

2.15.1 Neonatal cardiomyocyte preparation 94

2.15.2 Induction of Cre recombinase *in vitro* 96

2.16 Isolation of adult cardiomyocytes 97

2.17 Statistics 98

2.18 Real-time PCR probes 99

2.19 Antibodies 100

Chapter 3 - Tamoxifen-dependent Cardiomyocyte-specific Knockdown of Thymosin β4 101

3.1 Introduction 101

3.2 Thymosin *β4* knockdown by tamoxifen administration in the diet 101

3.3 Cardiac function following tamoxifen diet 103

3.4 *Thymosin β4* knockdown via intraperitoneal tamoxifen injections 108

3.4.1 MerCreMer localisation following tamoxifen injections 111

3.4.2 Cardiac function and morphology 3-4 weeks following tamoxifen injections 112

3.4.3 Cardiac physiology and function of *Tβ4shRNAflox/MerCreMer* animals 6 weeks following tamoxifen treatment 114

3.4.4 Assessment of *Thymosin* β4 knockdown following tamoxifen injections 116

3.5 Thymosin β4 knockdown in vitro 118

3.5.1 Neonatal cardiomyocyte culture 118

3.6 *Ex-vivo* investigation of *thymosin β4* knockdown in adult cardiomyocyte preparations isolated by Langendorff perfusion 119

3.7 Discussion 123

3.7.1 Tβ4 knockdown *in vivo* 123

3.7.2 Tβ4 knockdown *in vitro* 124

3.7.3 Assessment *ex-vivo* 124

3.7.4 Limitations *in vivo* 125

3.7.5 Limitations *in vitro* 126

3.7.6 General considerations 126

3.7.7 Summary 128

Chapter 4 - Cardiac Fibrosis in Tamoxifen-treated *αMHC/MerCreMer* Mice 129

4.1 Introduction 129

4.2 Cardiac morphology of *Tβ4shRNAflox/MerCreMer* animals following tamoxifen treatment 129

4.3 Abnormal cardiac function and morphology in *αMHC/MerCreMer* mice following tamoxifen treatment 133

4.4 Mechanism of MerCreMer-induced fibrotic phenotype 137

4.5 Discussion 144

4.5.1 *αMHC/*MerCreMer in the literature 146

4.5.2 Potential solutions to the problem of inducible Cre-mediated toxicity 147

4.5.3 Summary 151

Chapter 5 - Work in Progress: Alternative Approaches to Investigate the Role of Thymosin β4 in Cardiomyocytes 152

5.1 Introduction 152

5.2 Proteomics – Identification of Tβ4-interacting proteins 152

5.3 Pitfalls of recombinant protein production for proteomics 155

5.4 Discussion 158

5.4.1 Summary 159

Chapter 6 - Work in Progress: Transmission Electron Microscope Analysis *αMHC/IGF-1Ea* Transgenic Hearts and the Role of IGF-1Ea in Cardiac Autophagy 160

6.1 Introduction 160

6.2 Large electron-dense structures in *αMHC/IGF-1Ea* cardiomyocytes 160

6.3 The role of IGF-1Ea in cardiac autophagy 167

6.3.1 Autophagy PCR array results 169

6.4 Discussion 176

6.4.1 Autophagy in *αMHC/IGF-1Ea* hearts 176

6.4.2 α-synuclein and battenin – Markers of neurological disease 178

6.4.3 Summary 180

Final Conclusion 181

Publications and Presentations 183

Publications 183

Presentations 183

Awards 183

References 184

List of Figures

Figure 1.1: Tβ4 gene and peptide structure..... 28

Figure 1.2: Role of Tβ4 in cell migration and intracellular signalling. 34

Figure 1.3: Scar formation is reduced in mice treated with Tβ4 38

Figure 1.4: Schematic representation of the IGF-1 gene and its four isoforms in the rat..... 41

Figure 1.5: Simplified IGF-1 signalling pathway..... 43

Figure 1.6: Fibrosis in *αMHC/IGF-1Ea* transgenic and *wt* mouse hearts following MI..... 47

Figure 1.7: Simplified alternative IGF-1Ea signalling pathway in injured hearts.. 48

Figure 1.8: Simplified graphic representation of autophagy process..... 49

Figure 1.9: Schematic representation of the *αMHC/MerCreMer* transgene. 52

Figure 2.1: Schematic representation of the *Tβ4shRNAflox* transgene. 56

Figure 2.2: Cre-mediated excision of genomic inhibitory target sequences in *Tβ4shRNAflox/MerCreMer* mice. 57

Figure 2.3: Schematic representation of the *αMHC/IGF-1Ea* transgene..... 57

Figure 2.4: Agarose gel (2%) gels of genotyping PCR products..... 60

Figure 2.5: ECHO traces of mouse heart after coronary artery ligation..... 62

Figure 2.6: Left-descending coronary artery ligation in mice..... 62

Figure 2.7: Schematic representation of echocardiography axes. 64

Figure 2.8: Schematic depiction of the mouse heart dissection pattern used..... 67

Figure 2.9: Example of a standard curve used for protein quantification..... 70

Figure 2.10: Assembly of the transfer cassette..... 72

Figure 2.11: Exemplary result of a rtPCR reaction. 79

Figure 2.12: Exemplary result of RNA quality control using a BioAnalyzer 2100. 80

Figure 2.13: Vector used for the generation of recombinant Tβ4..... 90

Figure 2.14: Langendorff setup required for adult cardiomyocyte isolation. 97

Figure 3.1: Baseline cardiac function of *Tβ4shRNAflox/MerCreMer* mice measured by transthoracic ECHO. 102

Figure 3.2: Immunofluorescence staining for Cre on cardiac cryosections. 103

Figure 3.3: Cardiac function measured by transthoracic ECHO following tamoxifen delivery via diet. 104

Figure 3.4: Recordings of physiological parameters after tamoxifen delivery in the diet. .. 107

Figure 3.5: Body weight change of mice after one month of tamoxifen diet. 107

Figure 3.6: *Tβ4* mRNA and protein levels measured by real-time PCR and Western blotting. 108

Figure 3.7: Recordings of physiological parameters after IP tamoxifen injections. 110

Figure 3.8: MerCreMer localisation in the left ventricle of *Tβ4shRNAflox/MerCreMer* animals. 112

Figure 3.9: Cardiac function assessed by ECHO. 113

Figure 3.10: Masson's trichrome staining of cardiac sections. 114

Figure 3.11: Physiological parameters following tamoxifen injections and 6 weeks of rest. 115

Figure 3.12: ECHO results after IP tamoxifen injections and 6 weeks rest. 116

Figure 3.13: rtPCR and Western Blot for Tβ4 following 5 days of tamoxifen injections (20 mg/kg daily). 117

Figure 3.14: Immunofluorescence staining for Tβ4 on cardiac frozen sections. 117

Figure 3.16: *Tβ4* mRNA levels after tamoxifen treatment of neonatal cardiomyocytes *in vitro* measured by rtPCR. 119

Figure 3.17: Immunofluorescence staining for Cre recombinase on left-ventricular cardiac tissue. 121

Figure 3.18: Morphology of adult cardiomyocytes isolated by Langendorff perfusion. 122

Figure 3.19: Determination of *Tβ4* mRNA levels in adult cardiomyocytes by real-time PCR. 122

Figure 4.1: Masson's trichrome staining on cardiac sections following 5 days of tamoxifen injections and 3-4 weeks of rest. 130

Figure 4.2: Masson's trichrome stain of cardiac sections of *Tβ4shRNAflox/MerCreMer* animals and controls following tamoxifen or control injections and 6-7 weeks of rest. 131

Figure 4.3: Cardiac function of *αMHC/MerCreMer* measured by ECHO. 133

Figure 4.4: Masson's trichrome staining of cardiac sections of *αMHC/MerCreMer* animals after tamoxifen injections and 4-5 weeks of rest. 134

Figure 4.5: Left-ventricular inner diameters analysed by ECHO. 135

Figure 4.6: Physiological parameters of *αMHC/MerCreMer* mice measured after tamoxifen or control injections and 4-5 weeks of rest. 136

Figure 4.7: Cardiac sections of tamoxifen treated *αMHC/MerCreMer* mice 3 days after tamoxifen treatment. 137

Figure 4.8: Cytokine expression analysis in tamoxifen treated *αMHC/MerCreMer* animals. 138

Figure 4.9: rtPCR cytokine expression analysis in tamoxifen treated *αMHC/MerCreMer* animals. 139

Figure 4.10: rtPCR for markers of cardiac remodelling 3 days after completion of 5 days tamoxifen (20 mg/kg daily). 139

Figure 4.11: rt-PCR for pro-inflammatory makers in the heart of *αMHC/MerCreMer.* 140

Figure 4.12: rtPCR analysis of anti-inflammatory markers following a single injection of tamoxifen (40 mg/kg). 141

Figure 4.13: rtPCR analysis of markers of cardiac remodelling following a single injection of tamoxifen (40 mg/kg). 141

Figure 4.14: Western blots for markers of apoptosis. 142

Figure 4.15: Western blot analysis for caspase 3. 143

Figure 4.16: Western blotting analysis of Bax expression in *αMHC/MerCreMer* mice..... 144

Figure 5.1: 2% Agarose gel showing the PCR product of *Tβ4* amplification. 153

Figure 5.2: Transformation and protein expression control using β-galactosidase activity assay. 153

Figure 5.3: 2% Agarose gel of *MfeI*-digested vectors. 154

Figure 5.4: Western blot detection of V5 epitopes. 155

Figure 5.5: Fractions eluted after ProBond Ni^{2+}-affinity column purification. 156

Figure 5.6: Coomassie stained gel of HeLa protein lysates after stable transfection and Ni^{2+}column purification. 156

Figure 5.7: Medium from Tβ4-V5-His_6 transfected HeLa cells cultured under serum-free conditions..... 157

Figure 6.1: Electron micrographs of cardiac section from *αMHC/IGF-1Ea* transgenic mice. 161

Figure 6.2: Electron micrographs of cardiac sections from 6 week old *αMHC/IGF-1Ea* mice. 161

Figure 6.3: Electron micrographs of cardiac sections from 2 year old *αMHC/IGF-1Ea* mice. 163

Figure 6.4: Electron micrographs of cardiac sections from 2 year old *αMHC/IGF-1Ea* and *wt* mice. 164

Figure 6.5: Transmission electron micrographs of cardiac sections from 3 month old *αMHC/IGF-1Ea* mice..... 165

Figure 6.6: Immunogold staining of cardiac sections of *αMHC/IGF-1Ea* mice for LAMP1. 166

Figure 6.7: Immunogold staining for cathepsin D on cardiac sections of 3-4 month old αMHC/*IGF-1Ea* mice..... 167

Figure 6.8: LC3 immunogold labelling of *αMHC/IGF-1Ea* cardiac sections..... 168

Figure 6.9: Western blot for markers of autophagy in adult mice. 169

Figure 6.10: Real-time PCR for *IGF-1* in cardiac samples using Taqman® reagents. 172

Figure 6.11: Western blot for α-synuclein using cardiac extracts from 3 month old *wt* and *αMHC/IGF-1Ea* mice. 173

Figure 6.12: Western blot for battenin using cardiac protein samples of 3 month old *wt* and *αMHC/IGF-1Ea* mice. 173

Figure 6.13: Western blot for ubiquitin using cardiac protein extracts of 3 month old *wt* and *αMHC/IGF-1Ea* mice. 174

Figure 6.14: Immunogold staining for IGF-1 on cardiac section of 3 month *αMHC/IGF-1Ea* mice. 175

List of Tables

Table 2.1: Recipes and thermocycler conditions for genotyping PCR 59

Table 2.2: Generation of a standard curve for quantification of unknown protein samples by *DC* protein assay 69

Table 2.3: Recipe list for most common concentrations of bis-acrylamide resolving gels used for 1D protein electrophoresis 71

Table 2.4: Recipe list for bis-acrylamide stacking gel used for 1D protein electrophoresis.. 71

Table 2.5: Recipe for cDNA synthesis 77

Table 2.6: Thermo cycler program for cDNA synthesis 77

Table 2.7: Recipe list for fast real-time PCR reactions 78

Table 2.8: Thermo cycler program for Fast rtPCR reactions 78

Table 2.9: cDNA synthesis for PCR arrays 81

Table 2.10: rtPCR master mix recipe for Mouse Autophagy RT^2 Profiler PCR Array 82

Table 2.11: ABI 7500 FAST rtPCR machine settings for 96-well RT^2 Profiler PCR arrays .. 82

Table 2.12: PCR reaction setup for *Cre* gene copy number analysis using a 96-well reaction plate 84

Table 2.13: Instrument settings for gene copy number analysis using TaqMan® reagents.. 85

Table 2.14: PCR conditions for Tβ4 amplification from cDNA 89

Table 2.15: Real-time PCR probes used during this study 99

Table 2.16: Antibodies used during this study 100

Table 4.1: *Cre* gene copy number analysis 132

Table 4.2: Publications using *αMHC/MerCreMer* mice in experiments without inclusion of tamoxifen-treated *αMHC/MerCreMer* controls 146

Table 6.1: Autophagy PCR array results 169

Chapter 1 - Introduction

1.1 The mammalian heart

The four chambered mammalian heart is a sophisticated midline organ which circulates blood through the lungs and the organs in two serial vascular circuits. The pulmonary circuit facilitates the removal of waste products, such as carbon dioxide (CO_2), re-oxygenation of the blood and exchange of heat at the blood air barrier in the alveoli. The systemic circulation is required for oxygen (O_2), nutrient/waste and water transport and also to regulate the body temperature. The vasculature also functions as a transport route for cells and signalling molecules.

Despite playing a central role in distributing nutrients and oxygen throughout the body, the adult mammalian heart itself cannot regenerate when blood supply via the coronary arteries fails and the myocardium is damaged. However, two recent reports have challenged this central dogma of cardiac research. Zebrafish hearts retain a substantial regenerative capacity throughout adult life involving factors that are also known to exist in mammals (Lien *et al.* 2006). While this regenerative capacity is not observed in adult mammalian hearts, Porrello *et. al* recently demonstrated that in the early post-natal days, mice can indeed regenerate significant proportions of lost myocardium (Porrello *et al.* 2011). These studies bear promise that by identifying the correct factors involved in the regenerative process, a dormant regenerative program could be re-activated in damaged adult mammalian myocardium. The loss of cardiac tissue is the consequence of disrupted blood supply by arterial occlusion or injury which leads to hypoxia or anoxia and the build-up of toxic waste products which over time inevitably results in death of the cells in the affected area. Circulation can be restored by removal of the obstruction or more long term by angiogenesis, the formation of blood vessels from an existing vascular network. After blood flow is restored, lost cells can be replaced via diverse mechanisms and are able to regenerate large parts of various organs. While in the heart, endothelial cells and fibroblasts can undergo mitosis to replace lost cells, cardiomyocytes cannot be replaced in sufficient numbers in mammals. Thus the injured myocardium is exposed to a number of molecular and biophysical changes which over time in most cases results in heart failure and death.

1.2 Cardiovascular disease

Cardiovascular diseases (CVD) encompass a diverse spectrum of acquired and congenital conditions in human, ranging from valvular disease to hypertrophy, myocardial infarction (MI) and heart failure. CVD is the leading cause of death worldwide (World Health Organisation 2003). 16.7 million (29.2%) of deaths recorded by the World Health Organisation (WHO) in

the World Health Report 2003 were caused by CVD. Opposing the old dogma, that CVD is a disease of industrialised nations, approximately 80% of deaths occur in middle-income countries. This thesis focuses on coronary heart disease and the development of novel treatment strategies to more effectively reduce its individual and societal burden.

1.2.1 Coronary heart disease

Almost half of the deaths due to CVD (7.2 million) are caused by coronary or ischemic heart disease (World Health Organisation 2003). Coronary artery disease predominantly refers to the occlusion of a coronary artery supplying the myocardium. MI is most frequently caused by primary coronary events, such as plaque erosion, rupture or dissection affecting the coronary artery but can be secondary to previous ischaemic, hypertensive or anaemic cardiac events or following cardiac intervention such as percutaneous coronary intervention (PCI) or coronary artery bypass graft (CABG, Davies *et al.* 1976; Thygesen *et al.* 2007). Patients experiencing classical angina pectoris as a consequence of MI can be swiftly diagnosed by a combination of medical history, ECG, as well as imaging by echocardiography (ECHO), coronary angiography, magnetic resonance imaging (MRI) and by biomarker analysis. Circulating levels of troponin T and troponin I are markers of cardiomyocyte necrosis, have high clinical sensitivity and are measured at the onset of symptoms but can remain elevated until 7-14 days after infarct (Panteghini *et al.* 2001; Anderson *et al.* 2007; Thygesen *et al.* 2007). A wider panel of novel biomarkers are currently under investigation to improve differential diagnoses in patients visiting chest pain clinics (Lin *et al.* 2012). Following the diagnosis of MI, a number of pharmacological treatments and interventions are available, which will be discussed in the following sections.

In addition to the high death toll, the disability and individual suffering associated with MI and heart failure, long term treatment of patients suffering coronary heart disease is costly and poses an increasing burden on societies. In the UK alone 2.6 million people are living with coronary heart disease (British Heart Foundation 2005). Finding modern, cost-effective treatments is imperative to relieve the socio-economic burden and improve patient quality of life. Although, substantial advancements have been made in cardiac research to improve cardiac function, after acute injury or chronic disease, a long term cure and regeneration of the heart remains a yet unachieved ultimate goal.

1.2.1 Hypertrophy, cardiac remodelling and heart failure

Given recent advances in management of acute MI increasing numbers of patients are surviving the initial cardiac insult and are thus suffering from the long term consequences of the loss of functional myocardial tissue and subsequent scarring (British Heart Foundation 2005). While cardiac hypertrophy also describes the physiological growth of cardiac cells

and muscle for example during pregnancy or regular exercise, it is mainly associated with the pathological gain of mass due to overcompensation of the organ after chronic or acute insult (reviewed in McMullen and Jennings 2007). This is attributed to increased cardiomyocyte size rather than increase in cell abundance. In the setting of MI, scar tissue formation stabilises the heart from immediate dilatation but it cannot make up for the local loss of contractile tissue (reviewed in Cleutjens and Creemers 2002). This loss of cardiac contractility results in overload of the remaining cardiomyocytes which thus become hypertrophic and thereby increase wall thickness and overall size of the organ. This process is further modulated by the release of a number of cytokines and growth factors (Sugden 1999; Asakura *et al.* 2002; Liao 2002). Over time, the initially improved contraction of the heart due to the compensated cardiac hypertrophy frequently deteriorates into a decompensated hypertrophy associated with higher risk of life-threatening arrhythmias and reduced coronary flow reserve (reviewed in Sugden 1999). The structural and haemodynamic changes of the heart following scarring and maladaptive hypertrophy are also associated with electrophysiological changes, such as prolongation of action potential duration and Ca^{2+} transients (Richard *et al.* 1998; Wickenden *et al.* 1998), reviewed in Shih Shih *et al.* 2010). This is the result of chronic overload insult and in most cases ultimately leads to end-stage heart failure. This is generally accompanied by a range of neurohumoral changes, such as alterations in aldosterone and angiotensin type II (Ang II) levels which modify collagen type 2 (Col2) synthesis and thereby increase fibrosis (Delcayre and Swynghedauw 2002). The remodelling process ultimately cumulates in end stage heart failure (Pfeffer and Braunwald 1990). This describes a state at which cardiac function has degraded below the minimal functionality required to maintain basal body functions. Blood supply and drainage from the lungs and system is insufficient resulting in cyanosis and oedema. End stage heart failure is associated with increased apoptosis in cardiomyocytes, decreased sarco/endoplasmic reticulum Ca2+-ATPase (SERCA2a) and increased SERCA inhibitor phospholamban (Bartling *et al.* 1999; Minamisawa *et al.* 1999). It is furthermore accompanied with an increase in inflammatory markers. As such, pro-inflammatory cytokines tumour necrosis factor α (TNFα), interleukin (IL) 1β, IL-6, IL-8, monocyte chemoattractant peptide 1 (MCP1) and macrophage inflammatory protein 1α (MIP1α) were shown to be upregulated in heart failure patients (Levine *et al.* 1990; Testa *et al.* 1996; Aukrust *et al.* 1998; Aukrust *et al.* 1999; Damas *et al.* 2000; Adamopoulos *et al.* 2001).

1.3 Current treatments of coronary heart disease and heart failure

In the acute setting of an MI, intervention is desired at three disease stages. First, oxygen and nutrient supply needs to be re-established, as well as removal of toxic waste products

from the affected region of the myocardium. Second, acute inflammation needs to be reduced to avoid ongoing damage to healthy tissue surrounding the site of injury and to allow salvaging of damaged structures. Third, the lost or damaged myocardium needs to be regenerated to restore cardiac function. This would entail replacement of dead myocardium with new cardiomyocytes, their correct insertion and functional connection to the surrounding tissue and prevention of fibrosis, hypertrophy and adverse remodelling of the heart. Endogenously, this could hypothetically be achieved by infiltration and differentiation of a variety of putative progenitors, by mitosis of existing cardiomyocytes or by the differentiation of cardiac stem cells that already reside in the heart (Beltrami *et al.* 2001; Beltrami *et al.* 2003; Pitchford *et al.* 2009). However, endogenous repair and substitution of cardiomyocytes has been shown to be insufficient in adult mammals, and the damaged myocardium is quickly replaced by proliferating fibroblasts secreting extracellular matrix (ECM) to provide mechanical support thus producing the infamous scar.

1.3.1 Invasive interventional cardiology

PCI or percutaneous transluminal angioplasty (PCTA) involves catheterisation of the coronary artery and mechanical widening of the blood vessel by means of an intracoronary balloon (Gruntzig and Schneider 1977). This technique has been a phenomenal success and has been further improved significantly by the development of the intracoronary stent which is implanted at the time of angioplasty to prevent re-occlusion of the coronary artery (Sigwart *et al.* 1987). More recently stents coated with sirolimus or paclitaxel to prevent stent thrombosis by ingrowth of vascular cells have been successfully introduced into clinical practice (Morice *et al.* 2002; Grube *et al.* 2003). There is compelling clinical evidence from registry studies that drug eluting stents are superior to bare metal stents and substantially reduce the need for target-vessel revascularisation (Tu *et al.* 2007). In a Swedish study registry, however, an increased mortality in the patient group receiving drug-eluting stents compared to bare metal stent recipient was found, highlighting the need for a large, prospective, randomised clinical trial for clarification (Lagerqvist *et al.* 2007). While PCI is the first choice of invasive treatment for acute MI, it is associated with a number of risks predominantly the aforementioned stent-stenosis, but also myocardial or vessel damage from the stent, arrhythmia and bleeds. A more classical but significantly more invasive means of restoring myocardial perfusion is CABG which was first performed in 1961 (Goetz *et al.* 1961). This involves autologous transplantation of one or multiple blood vessels sourced from patient's thigh (saphenous vein) or thorax (left internal mammary artery) to circumvent or 'bypass' the stenotic coronary vessel (Favaloro *et al.* 1971; Ohki *et al.* 2002).

1.3.2 Pharmacological intervention

There are a number of pharmacological treatment options which are aimed at resolving the thrombus or preventing re-stenosis. The NICE thrombolytic therapy guidelines are based on 14 clinical trials and give recommendation to the use of plasminogen-activating drugs for this purpose (NICE guidelines October 2002). Thrombolytic medication needs to be administered early, usually no later than 6-12h following onset of symptoms. In the UK, 4 thrombolytic agents are available: alteplase, reteplase, streptokinase and tenecteplase. All of the above are given in combination with the anti-platelet drug Aspirin and, except streptokinase, with the anticoagulant heparin. Thrombolytic therapy has a risk of haemorrhagic stroke which is associated with a high mortality and affects 0.5% - 1% of patients (NICE 2002, Thrombolytic therapies). Thrombolytic therapy is often combined with anti-thrombotic therapy. Historically, heparin and aspirin have been used as anti-thrombotic agents while platelet glycoprotein IIb/IIIa inhibitors came into use in the 1990s (reviewed in Brodie 2008). Developed in the late 1990s, clopidogrel is now the main anti-thrombotic pharmacological intervention. Similar to thrombolytic therapy, there is a risk of severe complications associated with anti-thrombotic treatment with the main risk being bleedings which range from insignificant gastrointestinal bleeds to major haemorrhages, blood loss and stroke. More recently, a new drug called bivalirudin was developed which acts directly on thrombin and shows a reduced incidence of bleedings (Stone *et al.* 2006).

1.3.3 Device therapy for cardiovascular disease

Mechanical assist devices or left ventricular assist devices (LVADs) are mechanical pumps that are used to assist cardiac function, traditionally as a bridge-to-transplant (Goldstein and Oz 2000; Zeltsman and Acker 2002). Mechanical unloading of the heart was shown to reduce the expression of apoptotic markers in cardiomyocytes during end stage heart failure. Furthermore, it was found that preceding LVAD therapy improved patient outcomes after transplantation compared to patients immediately receiving a donor heart (Frazier *et al.* 1995; Bartling *et al.* 1999). Cardiogenic shock is the most common acute cause of death following MI (5% - 10%) and patients not responding to pharmacological intervention or PCI were shown to benefit from LVAD implantation as well (Thiele *et al.* 2007). Early reports about patients that could be weaned from their mechanical assist device, after their hearts had recovered to a surprising degree, prompted an ongoing research into a so called bridge-to-recovery approach (Muller *et al.* 1997). Combining LVAD therapy with a pharmacological regime consisting of lisinopril, carvedilol, spironolactone and the angiotensin type II receptor blocker (ARB) losartan and subsequent concomitant treatment with the β2-adrenergic receptor agonist clenbuterol supports the recovery of a dilated, failing heart, allowing for explantation of the LVAD (Birks *et al.* 2006; Birks *et al.* 2012). In this recovering patient

population, the functional improvement is accompanied by overall normalisation of cell size, reduced phospholamban expression and increased levels of SERCA2a (Yacoub 2001).
A caveat of the existing clinical data on bridge-to-recovery is the small sample size and a large prospective, randomised, double-blind multicentre clinical trial would be required to ascertain the observed effect. While device therapy is a step in the right direction, the COMET trial has revealed that despite optimal pharmacological (ACE inhibitors and β-blockers) and device therapy, 50% of congestive heart failure patients die within 4 years after onset of the first symptoms (Bristow *et al.* 2005; Yndestad *et al.* 2006). Consequently, in the absence of alternative treatments, heart transplantation remains in most cases the last resort. However, even after transplant, the survival rate in the first 5 years post-operation is only 80% (Lloyd 2010). Furthermore, in the USA only 2500 heart transplants can be performed annually due to severely limited availability of donor hearts and this highlights the need for novel approaches to treat acute and chronic heart disease.

1.3.4 Novel approaches to prevent or cure heart failure

Cardiac myocytes are naturally turned over in the adult human heart, although to a very limited degree with about 50% of cells being replaced by *de novo* generated cardiomyocytes over a lifetime (Bergmann *et al.* 2009). Depending on age, the annual turnover rate is between 0.45% and 1%. Thymidine radiolabelling experiments in mice showed that 0.0006% of adult cardiomyocytes proliferate under physiological conditions while 0.0038% of cardiomyocyte proliferate in the borderzone following MI (Soonpaa and Field 1998). This endogenous regeneration is insufficient considering the disproportionately large loss of heart muscle tissue that generally occurs during MI. Nevertheless, these studies demonstrated for the first time the intrinsic capability of the heart to regenerate. This encourages research into mechanisms and techniques that could enhance the natural regenerative response of the heart. Novel cell based and molecular approaches try to coax cardiac cells into a more proliferative state to be able to respond to loss of myocardium due to injury in a more timely and comprehensive manner. To achieve this, a number of cell or factor based approaches are currently being evaluated.
Cell injection: In the BOOST trial catheter mediated infusion of coronaries with autologous bone marrow cells following PCI was assessed (Wollert *et al.* 2004). This resulted in a slight increase (6.7%) of left-ventricular ejection fraction compared to controls 6 months post intervention (Meyer *et al.* 2006). However, no difference was found after 18 months follow-up casting doubt over the long term benefit of this treatment. Another cell population that was investigated in pre-clinical studies, are $lin^-/c\text{-}kit^+$ progenitor cells (Beltrami *et al.* 2003). These stem cells reside in the heart and were found to be able to differentiate into myocytes, smooth muscle and endothelial cells in infarcted rat heart. Injecting $lin^-/c\text{-}kit^+$ cells into the

borderzone of an experimental MI in rats was shown to salvage parts of the myocardium. These findings prompted early phase clinical trials in which c-kit$^+$ cardiac stem cell treatment after MI and CABG improved cardiac function (Bolli *et al.* 2011). However, their limited availability and accessibility renders them currently unsuitable for application in the clinics (Schuldt *et al.* 2008). Cardiosphere-derived cell infusion into the coronaries was also shown to decrease scar mass and increase viable myocardium, but as for c-kit$^+$ cells, or indeed all autologous cell transplantation approaches in general, cardiosphere treatment suffers from high cost associated with this highly specialised and individualised technique (Makkar *et al.* 2012). Many of the observed beneficial effects of cell injections are attributed to factors secreted by stem cells rather than their actual engraftment (Gnecchi *et al.* 2008). Identifying these factors and the mechanisms by which they improve cardiac function or prevent cardiac deterioration could provide novel therapies that could have significant advantages over cell therapy due to the reduced risk of tumorigenicity, stenosis and immune reactions.

Factors inducing progenitor cells or mitosis: In order to replace coronary vasculature, to improve perfusion of poorly supplied areas of myocardium, the generation of new vessels by angiogenesis is pivotal. VEGF treatment induces angiogenesis and increases recruitment of circulating endothelial progenitor cells (EPCs, Kalka *et al.* 2000). While in theory, revascularisation could assist to rescue parts of the myocardium, this cannot be achieved in a timely manner and is no alternative to PCI as an immediate intervention. Considerable damage to the myocardium would have already occurred, highlighting that research has to focus on ways to improve the healing process of injured myocardium. A range of interesting candidates for factor based therapies are currently under investigation and these could be involved in improving the regenerative capacity of the heart or to reduce further damage to the heart after initial ischaemic insult. As such, G-CSF treatment of patients in a recent clinical trial reduced cardiac remodelling and improved cardiac function, potentially by mobilising stem cells from the bone marrow (Orlic *et al.* 2001; Ince *et al.* 2005). TWEAK, a member of the TNF factor family, is another factor potentially enhancing the endogenous regenerative capacities and was shown to induce cardiomyocyte proliferation in vitro (Novoyatleva *et al.* 2009).

Next to improving regeneration, inhibition of factors contributing to cardiac pathology could be a complementary approach to improve outcomes. For example, the inhibition of p38 MAP kinase was shown to reduce scarring and wall thinning and to significantly improve cardiac function in a rat model of MI (Engel *et al.* 2006). Replenishing lost myocardium, however, remains the holy grail of cardiac research and one approach addressing this involves the stimulation of cardiomyocyte cell cycle re-entry. This is a particularly interesting approach, since research has shown that after birth, mouse cardiomyocytes briefly retain the ability to proliferate but this is lost within the first postnatal days coinciding with cessation of cyclin A2

expression (Yoshizumi *et al.* 1995; Porrello *et al.* 2011). Cyclin A2 is a potent regulator of the cell cycle and drives cell cycle progression through G1/S and G2/M phases (Sherr and Roberts 1995). Inducing cardiomyocyte cycle re-entry by adenoviral vector mediated overexpression of *cyclin A2* in rat myocardium at the time of experimental MI was shown to improve wall thickness in the infarct border zone and improve cardiac function (Woo *et al.* 2006). While it is not clear whether these improvements are attributable to true cell cycle re-entry of adult cardiomyocytes or due to induction of a hyperproliferative potential of side population cells, these promising results call for further testing of cyclin A2 in clinical trials. Further candidates potentially promoting cardiac regeneration include periostin and neuregulin 1, which were separately shown to stimulate cell cycle re-entry of cardiomyocytes after MI, thereby reducing fibrosis and improving cardiac function (Kuhn *et al.* 2007; Bersell *et al.* 2009).

As opposed to cell-based treatments, factor-based approaches have the significant advantage that they can be generated industrially, can be easily stored and distributed, are generally not immunogenic and potentially have a lower risk of causing cancers. There is an on-going effort to identify and characterise further molecules that could activate endogenous mechanisms to act at the three stages of re-vascularisation, reduction of inflammation and regeneration of myocardium. Two factors that appear to be promising candidates to achieve this are thymosin β4 (Tβ4) and the locally acting insulin-like growth factor 1Ea (IGF-1Ea) isoform.

1.4 Thymosin β4

Thymosins derive their name from their first isolation from calf thymus in the 1960s (Klein *et al.* 1965). The extract of a whole thymus was isolated in fractions, with fraction 5 containing the α, β and γ thymosins (Goldstein *et al.* 1977).

1.4.1 The thymosin protein family

The thymosins are divided into α, β and γ subgroups according to their isoelectric points: α for highly acidic pH <5, β for pH 5-7 and γ for basic pH >7. Before this classification it was believed that thymosin was a single 14 kDa hormone (Goldstein *et al.* 1972; Huff *et al.* 2001). Today, three α thymosins were isolated: thymosin α1, thymosin des(25-28) α1 and the 7 amino acid longer thymosin α11 (Goldstein *et al.* 1977; Caldarella *et al.* 1983). All α thymosins are derived from prothymosin α by enzymatic cleavage (Haritos *et al.* 1984).

The name thymosin β4 (Tβ4) was given in reference to it being the fourth β-thymosin to be sequenced in 1981 after isolation from fraction 5 using a combination of ion exchange chromatography and gel filtration (Low *et al.* 1981). Together with Tβ4, mammals express a

second β-thymosin, which is thymosin β10 (Tβ10) in some species (human, rat, mouse, rabbit, cat) or thymosin β15 (Tβ15) in others (calf, pig, sheep). Mouse Tβ4 and Tβ10 are 43 and 44 amino acids long, have a MW of ~5 kDa and share 100% identity with their human orthologs (Safer *et al.* 1990; Gerhard *et al.* 2004). Tβ15 was also discovered in humans, however only in tumours, prostate cancer cells and embryonic brain tissue and is devoid from other tissues under physiological conditions (reviewed in Bao *et al.* 1996; Smart *et al.* 2007; Dhaese *et al.* 2009). Tβ15 represents its own subclass distinct from the other β-thymosins (Tβ4, Tβ10) with regard to its N-terminal amino acid sequence (Dhaese *et al.* 2009). However, it shares a functional similarity with Tβ4 in terms of its actin binding properties. Thymosin NB is the human homologue of rat Tβ15 but its two isoforms are also referred to as Tβ15a and Tβ15b (Banyard *et al.* 2007). Given its role in the development and progression of prostate cancer, Tβ15 is a putative biomarker for this disease. Tβ15 was furthermore shown to have pro-angiogenic and anti-migratory properties in rats (Koutrafouri, Leondiadis *et al.* 2003; Dhaese *et al.* 2007). With regards to its amino acid sequence, Tβ4 is very similar to the β-thymosins 10 and 15 and to the thymosins 8, 9, discovered in other organisms (Low and Goldstein 1984; Bao *et al.* 1996; Li *et al.* 1996; Dhaese *et al.* 2009). All β-thymosins are acetylated at their N-terminal alanine (Tβ4, 10) or serine (Tβ15) respectively (Hannappel 2010).

1.4.2 Thymosin β4 structure and actin binding function

The Tβ4 gene consists of 2.13 kB genomic DNA and contains three exons, of which exon 2 and exon 3 code for the Tβ4 peptide (**Figure 1.1 A**, Li *et al.* 1996; Waterston *et al.* 2002).

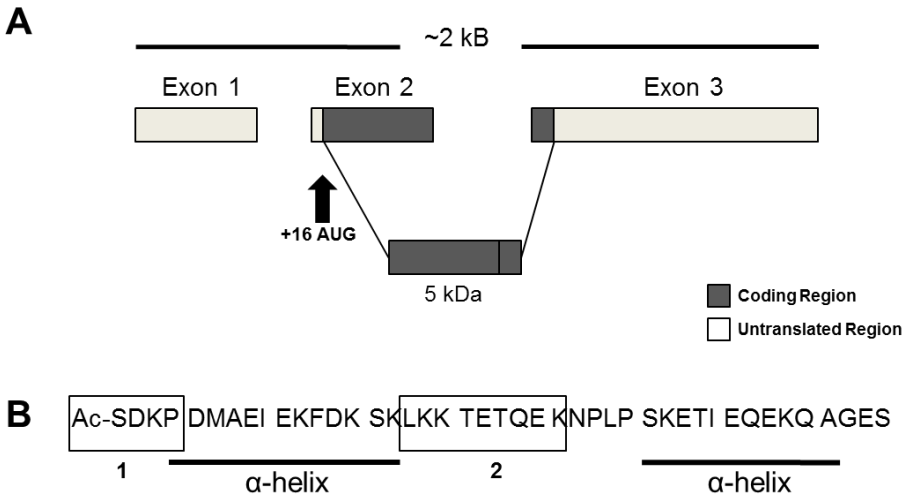


Figure 1.1: Tβ4 gene and peptide structure. (A) Simplified depiction of the Tβ4 gene (not to scale). (B) Amino-acid sequence and domains of Tβ4. 1 - N-terminal Ac-SDKP peptide, 2 - Actin binding domain (Li *et al.* 1996; Huff *et al.* 2001).

Tβ4 was already synthesised in 1981 by automated solid phase synthesis due to an early interest in the immunomodulary role of thymosins suggested by their apparent involvement in T lymphocyte maturation (reviewed in Hannappel 2010). It is now established that Tβ4 is a highly conserved peptide in the animal kingdom, being almost identical in human, rat, mouse, cat, calf, horse, pig, sheep, chicken and gecko. Between different species its length varies from 40 to 44 amino acids and it is the most abundant β-thymosin in mammals (Huff *et al.* 2001). Historically, it was characterised to have a molecular weight of 4982 Da and an isoelectric point of 5.1 However, more recent data support a PI around 4.58 which is similar to the value calculated *in silico* (4.82, Low and Goldstein 1982, EMBL WWW Gateway to Isoelectric Point Service, http://www3.embl.de/cgi/pi-wrapper.pl 22-06-2010, Hannappel 2010). Unlike the α-thymosin subclass, β-thymosins are not derived from a larger precursor peptide. As mentioned previously, cDNA analysis of human, mouse and rat Tβ4 indicate a length of 44 amino acids, however the mature peptide is only 43 amino acids long since the initiator methionine is removed after translation and the freed N-terminal alanine is acetylated (Hannappel 2010). A further post-translational modification of Tβ4 involves phosphorylation at two sites (threonine-21 and threonine-23), which was demonstrated in HeLa cells but not in human platelets (Zahedi *et al.* 2008). The function of these post-translational modifications is not yet fully understood although a role in actin interaction has been proposed. Furthermore, the transglutamination of Tβ4 residues Gln-23 and Gln-36 and to some degree Gln-39 has been successfully demonstrated, but has not yet been described *in vivo* (Huff *et al.* 1999). In physiological solutions, Tβ4 appears to be unstructured but contains two alpha helices, one consisting of residues 5-15 and the second of residues 30-40, interconnected by a flexible linker (Zarbock *et al.* 1990; Stoll *et al.* 1997). Apart from N-terminal acetylation and transglutamination, another post-translational modification involves enzymatic removal of the N-terminal Ac-SDKP tetrapeptide, which will be discussed in more detail in the next section.

All β-thymosins sequester globular actin (G-actin) and this interaction has probably been the most studied aspect of this peptide (Huff *et al.* 2001). Tβ4 prefers binding of ATP-G-actin over ADP-G-actin and it was shown that the nine amino acid long motif (17LKKTETQEK25) involved contains the three hydrophobic residues 6Met, 9Ile and 12Phe which are essential for this interaction (Safer *et al.* 1991; Van Troys *et al.* 1996; Hertzog *et al.* 2002). The wider actin binding domain of Tβ4 and its orthologues comprises the so called β-thymosin domain, which like the Wiskott-Aldrich Syndrome protein homology domain 2 (WH2) is characterised by a LKKT/V sequence with variable terminal extension (Xue *et al.* 2007). While the interaction of this domain with actin was not directly shown, there is strong indirect evidence that β-thymosin and WH2 domain-containing proteins use their N-terminal extension to make contact to the hydrophobic cleft at the barbed end of G-actin and this interaction regulates

the strength of the interaction (Didry *et al.* 2012). Actin-binding requires the α-helical conformation of the N-terminal part of Tβ4 to allow physical contact of Lys3, Met6, Lys18 and Lys38 of Tβ4 with the actin residues Asp1-Glu4, Gln41 and Glu167 (Huff *et al.* 2001). While C-terminal interactions with G-actin are minimal, point mutations in the C-terminal domain can reverse the function of Tβ4 and WH2 domain-containing proteins from stabilisation of a pool of monomeric actin to a role in promoting of filamentous (F-)actin assembly (Hertzog *et al.* 2004). WH2 domain were found in over 500 eukaryotic proteins, all of which bind actin and are involved in regulating motility but may have positive or negative roles in this process (reviewed in Husson *et al.* 2010). Intriguingly, it was shown that the actin binding domain of Tβ4 is essential for its angiogenic properties and the domain was shown to have comparable pro-angiogenic effects on human vein endothelial cells (HUVEC) to the full peptide (Philp *et al.* 2003).

Tβ4 is present in high cytosolic concentrations throughout the body and in body fluids (Gomez-Marquez *et al.* 1989; Huff *et al.* 2004). It is expressed in most tissues such as brain, spleen, thymus, lung, ovary, kidney, intestine, liver, testis and the heart (Hannappel *et al.* 1982; Gomez-Marquez *et al.* 1989). Its expression was also confirmed in circulatory cells such as lymphocytes, macrophages, granulocytes and is found in very high concentrations in platelets (Hu *et al.* 1981; Xu *et al.* 1982; Gondo *et al.* 1987). Tβ4 concentrations are particularly high in wound fluid highlighting its implication in dermal healing (Frohm *et al.* 1996). Intracellular, it is found diffusely distributed in the cytoplasm, but concentrations can increase focally near stress fibres and it is relatively abundant in the nucleus (Cha *et al.* 2003; Mannherz and Hannappel 2009). This may surprise, given the absence of nuclear localisation signal in the peptide. Nevertheless, exogenous Tβ4 localises to the nucleus and this occurs likely by active transport, potentially involving α/β importins, rather than by passive perfusion due to its small size (Grant *et al.* 1999; Koerner *et al.* 2003; Huff *et al.* 2004; Mannherz and Hannappel 2009). As for the pro-angiogenic properties, facilitation of nuclear localisation of Tβ4 appears to be dependent of the actin binding domain, since after enzymatic cleavage only the N-terminal half of the peptide localises to the nucleus (Huff *et al.* 2004). It was more recently shown *in vitro* that nuclear localisation of Tβ4 can be mediated by hMLH, a protein involved in DNA mismatch repair which contains a nuclear localisation signal (Brieger *et al.* 2007). hMLH appears furthermore to be involved in regulating the expression of Tβ4. In the nucleus, another binding partner called Ku80 has been identified in endothelial cells *in vitro* (Bednarek *et al.* 2008). Ku80 is a subunit of ATP-dependent DNA helicase II and is an essential mediator of the Tβ4-induced expression of PAI-1, providing first clues about a role of Tβ4 in the nucleus which has not yet been well documented. A potential role of nuclear Tβ4 is binding of nuclear actin which is involved in

transcriptional regulation of certain genes but this hypothesis remains to be tested in the future (Vartiainen *et al.* 2007).

Endogenous and exogenous Tβ4 improves various physiological processes, such as wound healing in general and during ageing and diabetes, corneal repair after abrasion, hair growth, neurological recovery in experimental autoimmune encephalitis and cardiomyocyte survival and improved cardiac function in models of MI (Malinda *et al.* 1999; Sosne *et al.* 2001; Philp *et al.* 2003; Bock-Marquette *et al.* 2004; Philp *et al.* 2004; Zhang *et al.* 2009). Some of these functions have been attributed to its N-terminal Ac-SDKP tetrapetide.

1.4.3 N-acetyl-seryl-aspartyl-lysyl-proline

The amino-terminal acetyl-seryl-aspartyl-lysyl-proline (AcSDKP) tetrapeptide (**Figure 1.1**) is cleaved off Tβ4 by prolyl oligopeptidase (POP), a serine peptidase (clan SC, family S9) abundantly present in many tissues and body fluids in mammals (Polgar 2002; Cavasin *et al.* 2004). Tβ4 knockdown in the heart results in up to 62% decreased cardiac AcSDKP underlining the peptide-precursor relationship of Tβ4 and AcSDKP (Smart *et al.* 2007). AcSDKP is a pleiotropic peptide, which shares many angiogenic functions with its precursor Tβ4, such as stimulation of endothelial cell migration and differentiation *in vivo* (Cha *et al.* 2003; Liu *et al.* 2003). At the same time, AcSDKP inhibits proliferation of haematopoietic pluripotent stem cells by inhibiting an S-phase stimulator in these progenitor cells (Lenfant *et al.* 1989; Stephan *et al.* 2000). In rats, this response to AcSDKP elevation was shown to be accompanied by increased secretion of active MMP-1 and a substantial angiogenic response. Increased circulating levels of AcSDKP prevents monocyte/macrophage infiltration, collagen deposition and fibrosis in hearts and kidneys of hypertensive rats (Rhaleb *et al.* 2001; Cavasin *et al.* 2007). In line with these findings it was shown that blocking cleavage of AcSDKP using POP inhibitors leads to perivascular fibrosis in the kidneys and the heart (Cavasin *et al.* 2007). In the setting of cardiac hypertrophy after MI in rats, infusion with AcSDKP resulted in reduced fibrosis by reduction of collagen deposition (Peng *et al.* 2003; Yang *et al.* 2004). POP substrates are limited to a size of 30 amino acids indicating that Tβ4 needs to be enzymatically cleaved before POP can generate the active AcSDKP peptide fragment, but this step has not yet been documented (Myohanen *et al.* 2010).

AcSDKP is upregulated in response to injury and plasma levels of AcSDKP were elevated in patients with renal failure (Suzuki *et al.* 2012). Cardiac levels of AcSDKP were increased 1 week after experimental myocardial infarct in mice (Smart *et al.* 2007). The tetrapeptide can be degraded by angiotensin converting enzyme (ACE), being a class III substrate for the C-active site of ACE (Rousseau *et al.* 1995). Treatment of patients with renal failure with ACE inhibitors was shown to augment AcSDKP plasma concentrations and it was hypothesised

that the cardioprotective effect of ACE inhibitors may indeed be partially mediated by elevating the concentration of this peptide (Rhaleb *et al.* 2001; Inoue *et al.* 2011). In the setting of hypertension, the abundance of macrophage-released galectin-3 (Gal-3) is an indicator of progression into heart failure, since it promotes cardiac inflammation and remodelling (Liu *et al.* 2009). Gal-3–mediated progression was attenuated by AcSDKP administration in rats with overall improved outcomes compared to controls. Furthermore, TGFβ1-mediated differentiation of cardiac fibroblasts into pathological myofibroblasts was attenuated by AcSDKP in human foetal cardiac fibroblast cultures, further highlighting the importance of AcSDKP as an antifibrotic agent (Peng *et al.* 2010). Although these findings highlight the potential of AcSDKP for treatment of cardiovascular disease and while there is some overlap between the observed functions of Tβ4 and the tetrapeptide, AcSDKP supplementation was unable to rescue the cardiac phenotype of a conditional Tβ4 knockdown mouse indicating a more complex function of whole Tβ4 than the one mediated by its AcSDKP domain (Smart *et al.* 2007).

1.4.4 Thymosin β4 function

Tβ4 has a beneficial role in wound healing as well as neuroprotection in the brain (Malinda *et al.* 1997; Popoli *et al.* 2007). It was shown to improve neurological outcomes in a rat model of stroke (Morris *et al.* 2010). After IP injection of Tβ4, increased vessel density and numbers of oligodendrocyte progenitors and myelinating oligodendrocytes were observed at the boundary of the ischaemic lesion. It was furthermore shown to stimulate progenitor cells in the hair follicle (Philp *et al.* 2004). Bulge residing hair follicle stem cell-like cells displayed increased migratory potential and differentiation in response to Tβ4 treatment in culture, as well as elevated MMP-2 expression which promotes hair outgrowth from the follicle.

Another role attributed to Tβ4 is the amelioration of type II diabetes. Initial experiments were based on the observation that Tβ4 was upregulated in regenerating skeletal muscle and acts as a chemoattractant for myoblasts and satellite cell-derived myocytes (Tokura *et al.* 2011). Since myoblast injection into the hindlimbs of diabetic mice was shown to reduce hyperglycemia and hyperinsulinemia, Tβ4 was injected intraperitoneally (IP) into the same type II diabetes mouse model to attract endogenous myoblasts (Ye *et al.* 2009; Zhu *et al.* 2012). This resulted in increased insulin sensitivity accompanied by elevated Akt expression. It is not surprising that given its involvement in cell motility, growth and survival, that Tβ4 is also considered an indicator of malignant progression and metastasis in tumours (Kim *et al.* 2009). For example in malignant lung tumour cells Tβ4 is found to be highly expressed (Clark *et al.* 2000).

Tβ4 is abundant in platelets and is released in pre-thrombotic states upon thrombin stimulation (Huff *et al.* 2002). It is co-released with the transglutaminase factor XIIIa which

crosslinks Tβ4 to various molecules such as fibrin and collagen. Crosslinking to fibrin occurs in a Ca^{2+} and time-dependent manner and in competition with the related Tβ10. Without physical retention, the highly hydrophilic Tβ4 peptide would easily diffuse away from its site of release from platelets. Therefore, Tβ4 tethering is believed to either have a role in the fibrin clot or is retained to create a milieu that supports healing and regeneration. In support of the first hypothesis, Tβ4 was shown to increase the interaction of platelet receptors with their ligands thus promoting local platelet accumulation (Kaur *et al.* 2010). Binding of Tβ4 to fibrinogen in the presence of high concentrations of Tβ4, however, seems to block attachment of activated platelets to fibrinogen. Extracellular Tβ4 induced expression and release of plasminogen activator inhibitor type 1 (PAI-1) in endothelial cells (Al-Nedawi *et al.* 2004; Boncela *et al.* 2006). This is attributed to an intracellular signalling involving the MAPK cascade, which enhances binding of c-Fos/c-Jun to the AP-1 element of the PAI-1 promoter and provides a further role of Tβ4 in clot stability. The second hypothesis is supported by the fact that factor XIIIa-mediated crosslinking to fibrin occurs at the fibrin αC-domain which is associated with tethering of biologically active peptides to increase their local concentration (Huff *et al.* 2002; Makogonenko *et al.* 2004). Furthermore, Tβ4 exerts antimicrobial effects on common pathogens such as *E. coli* and *S. aureus* implying an additional protective function at lesions of the body surface (Tang *et al.* 2002). It is noteworthy that the highest levels of Tβ4 in the body are observed in platelets, since these are the cells that arrive first at the site of injury and by secreting Tβ4 could pre-condition the affected area (Goldstein *et al.* 2012).

In addition to the described roles in actin binding, cell recruitment and acute response to injury, an additional function of Tβ4 is the regulation of inflammation. The immunomodulary role of Tβ4 was elucidated in a mouse model of septic shock. Tβ4 treatment not only decreased levels of inflammatory cytokines IL-1 and TNFα and reduced the infiltration of polomorphonuclear leukocytes (PMN) but also reduced overall the mortality in this model (Badamchian *et al.* 2003). A reduction in PMN-infiltration in response to topical Tβ4 treatment was also observed in a mouse model of corneal alkaline injury (Sosne *et al.* 2002). This was accompanied by reduction of IL-1β and monocyte chemoattractant protein 1 (MCP-1) and MIP-1α, MIP-1β and MIP-2. In corneal cells, as well as other cells types, TNFα is a main driver of inflammation by activating NFκB. This TNFα-mediated activation of NFκB is suppressed by Tβ4 which leads to the observed downregulation of pro-inflammatory cytokines and chemokines in Tβ4-treated corneal cells compared to controls *in vitro* (Sosne *et al.* 2002; Sosne *et al.* 2007). While Tβ4 directly targeted the RelA/p65 subunit of NFκB, it was independently demonstrated to also inhibit TNFα, which leads to a reduction of downstream IL-8 expression (Qiu *et al.* 2011). Furthermore it was shown that Tβ4 interacting protein ILK and PINCH have sensitising effects on TNFα-mediated NFκB activity but these

effects are diminished in the presence of Tβ4. *In vitro* data indicates that in natural killer cells IL-18 regulates Tβ4 expression by a signalling cascade involving p38MAPK and Jun kinase (Lee *et al.* 2011). In addition, Tβ4 increases IL-18-mediated IFNγ expression in a positive feedback loop and this increase can be abolished by knocking down Tβ4 by RNA interference (RNAi). Tβ4 has further less well described roles in the immune system. As such, it was shown to promote antigen presentation on macrophages and to control thymus-dependent lymphocyte maturation but no recent studies have further investigated these mechanisms (Low *et al.* 1981; Tzehoval *et al.* 1989).

The overall anti-inflammatory role of Tβ4 results in less tissue damage from inflammation and consequently decreases fibrosis and improves healing. There are further mechanisms by which Tβ4 is thought to directly reduce scar tissue formation, some of which may be attributable to the AcSDKP fragment, as discussed previously. One of the best researched aspects of Tβ4 is its pro-migratory role. That being said, our current knowledge of the intracellular function and signalling of Tβ4 does not yet explain its extracellular role in stimulating migration and only a few direct interactors have been identified to date (Freeman *et al.* 2011). As previously described, Tβ4 interacts with G-actin in a 1:1 ratio to maintain a dynamic pool of monomeric actin indicating its importance in actin cycling (Safer *et al.* 1991). Actin binding occurs in competition with profilin (PFN), which facilitates the release of Tβ4 from G-actin and thus facilitates F-actin assembly (**Figure 1.2**, Pantaloni and Carlier 1993).

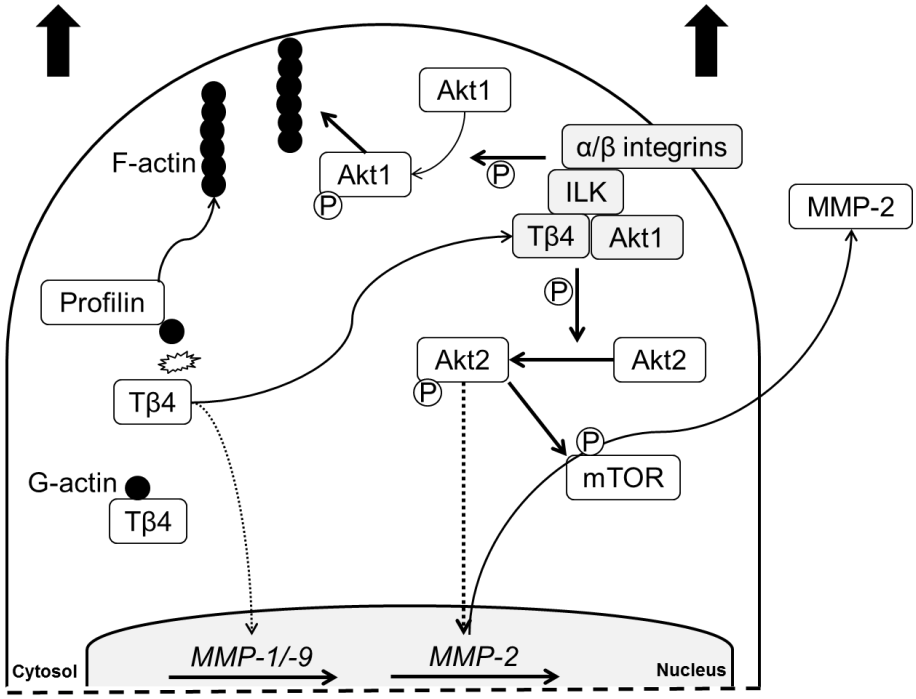


Figure 1.2: Role of Tβ4 in cell migration and intracellular signalling. In migrating cells, Tβ4 is released from monomeric G-actin by profilin (PFN). This allows F-actin formation in the leading edge and utilisation of free Tβ4 in a complex consisting of Akt1/2 and integrin-linked kinase (ILK). This complex

facilitates Akt1 phosphorylation and Akt2-mediated phosphorylation of mTOR. While phosphorylated Akt2 stimulates the transcription of matrix degrading proteins, phospho-mTOR facilitates the release of molecules, such as MMP-2. Tβ4 furthermore induces transcription of MMP-1 and MMP-9 (Philp *et al.* 2006; Qiu *et al.* 2007; Fan *et al.* 2009).

These studies highlight the importance of Tβ4 for reorganisation of the cytoskeleton and cell locomotion. Cytoskeletal modifications are necessary for lammellipodia formation and extension as well as repeated protrusion, adhesion and contraction (Lauffenburger and Horwitz 1996; Pollard and Borisy 2003). This process is further facilitated by Tβ4-induced expression of matrix metalloproteinases (MMP-1, MMP-2 and MMP-9), which are implicated in ECM degradation (Philp *et al.* 2006; Qiu *et al.* 2007). The induction of MMPs was shown to be dependent on the actin binding domain of Tβ4. Fan and co-workers have proposed a Tβ4 signalling pathway in migrating endothelial cells (Fan *et al.* 2009). They indicated that G-actin sequestration by Tβ4 is antagonising cell migration but that this effect, however, is overruled by induction of MMPs resulting in the observed increased migratory potential (Bock-Marquette *et al.* 2004; Fan *et al.* 2009). MMP expression is supposedly induced by the interaction of Tβ4 with integrin-linked kinase (ILK), which leads to the activation of Akt1 and Akt2. Akt2 activation not only induces survival signalling via mTOR, but also regulates production and activity of MMP-2 (Fan *et al.* 2009). Tβ4-ILK-mediated phosphorylation of Akt1 is believed to result in its localisation to the leading edge of the cell and enhance local actin polymerisation.

Consistent with this proposed pathway, Tβ4 was found to be abundant in the leading edge of migrating endothelial cells. F-actin assembly and Tβ4 signalling require the release of Tβ4 from G-actin which is facilitated by PFN (Pantaloni and Carlier 1993). PFN was further shown to interact with pro-migratory factors Rac/Rho, ROCK and proline-rich vasodilator-stimulated phosphoprotein (VASP) and is preferentially localised in the protrusive edge of fibroblasts (Buss *et al.* 1992; Witke 2004). Tβ4-mediated endothelial cell migration and induction of MMPs to degrade ECM have obvious implications in angiogenesis. In line with the observation made by Fan and co-workers, stable overexpression of Tβ4 is pro-migratory most likely due to compensatory mechanisms stabilising F-actin, but cDNA microinjection or transient transfections that instantaneously increase Tβ4 inhibit migration by depolymerisation of actin (reviewed in Mannherz and Hannappel 2009). This is supported by the inverse approach of depleting intracellular Tβ4 by RNA interference (RNAi) which was shown to increase cell motility (Fan *et al.* 2009). Nevertheless, Tβ4 was demonstrated to induce migration of HUVEC *in vitro* and this was shown to be dependent of P2X4 receptor (Freeman *et al.* 2011). Extracellular Tβ4 also increases surface ATP availability by binding F1-F0 ATP synthase which is an extracellular receptor for Tβ4. Tβ4 binds the β-subunit of

F1-F0 ATP synthase providing evidence for a role of Tβ4 in purinergic signalling (Goldstein *et al.* 2012). Tβ4-mediated elevated surface ATP could provide a further explanation for the pro-migratory role of Tβ4 in HUVEC.

The pro-regenerative effects of Tβ4 can be partially attributable to its role in promoting endothelial cell differentiation and angiogenesis (Grant *et al.* 1999). Angiogenesis is the formation of new blood vessel from a pre-existing vascular network and is essential during development, repair and tumour growth (Risau and Flamme 1995). In line with this, high concentrations of Tβ4 were observed in blood vessels and endocardial cushions during development of mouse embryos (Gomez-Marquez *et al.* 1989; Carpintero, Anadon *et al.* 1995; Carpintero *et al.* 1996). In human patients with coronary artery disease, less well developed collateral vessels were shown to be associated with lower circulating levels of Tβ4 (Bicer *et al.* 2011).

A number of experiments *in vitro* further underline the role of Tβ4 in blood vessel formation. In an aortic ring angiogenesis assay, increased vascular sprouting and a doubling of vessel area by increased branching was observed after adding as little as 100 ng of synthetic Tβ4 (Grant *et al.* 1999). In HUVEC, Tβ4 was shown to increase tube formation and HUVEC differentiating into capillary-like tubes displayed a 5-fold increase of intracellular Tβ4 (Grant *et al.* 1995). Further evidence for the relationship between VEGF and Tβ4 was derived from immunofluorescence data indicating that VEGF expression is decreased in the hearts of mouse embryos following cardiac specific knock down of Tβ4 (Smart *et al.* 2007). Earlier reports have suggested that hypoxia inducible factor-1α (HIF-1α) co-localises with Tβ4 in colorectal cancer cells and that Tβ4 induces VEGF by stabilising HIF-1α (Jo *et al.* 2010). However, despite the fact that HIF-1α is found to be upregulated at the same time with Tβ4 and VEGF, there is more recent evidence indicating that Tβ4 induces VEGF expression independently of HIF-1α (Kang *et al.* 2011; Kim *et al.* 2011). Increasing intracellular levels of Tβ4 by adenoviral vector increases VEGF and MMP-7 expression *in vitro* (Cha *et al.* 2003; Wang *et al.* 2004). In a porcine model of MI not only Tβ4 and VEGF but also MMP-9 was found to be upregulated in response to the insult (Shah *et al.* 2011).

In the synovial fluid sampled from the joints of rheumatoid arthritis patients, levels of Tβ4 were strongly associated with levels of the collagenases MMP-9, MMP-13 as well as VEGF measured by ELISA (Choi *et al.* 2011). While an increase of matrix degrading proteins is advantageous in the regenerative setting to resolve scar tissue or allow cell migration, it is associated with increased disease severity in rheumatoid arthritis since it results in further damage to the cartilage. To an extent this holds true for the cardiac setting since increased MMP-9 expression has been linked to more severe left-ventricular dilatation after experimental MI (Ducharme *et al.* 2000). In line with this, diminished numbers of macrophage and reduced collagen deposition were observed in the left ventricle of MMP-9

KO mice. This was accompanied by upregulation of MMP-2, MMP-13 and TIMP-1 indicating the diverse roles of the various ECM degrading enzymes. Enzymatic digestion of ECM is not only important to clear the path for newly forming blood vessels but could be useful in scar resolution during cardiac regeneration to create space for progenitor cells or even new myocytes.

Another mechanism shown to contribute to the diverse effects of Tβ4 is epithelial to mesenchymal transition (EMT). EMT is a process naturally occurring for example during embryogenesis and describes the loss of tissue adhesion by downregulation of adhesive molecules and overall adoption of a promigratory phenotype and ultimately the conversion from an epithelial to mesenchymal phenotype (reviewed in Savagner 2001). This involves downregulation of adhesion molecules, such as E-cadherin, a process which is reiterated during tumour metastasis (reviewed in Vernon and LaBonne 2004). Tβ4 promotes EMT via upregulation of ILK (Huang *et al.* 2007). It was further demonstrated that Tβ4 overexpression results in downregulation of E-cadherin at cellular junctions *in vitro* in colorectal cancer cells (Wang *et al.* 2003). This is further supported by the reverse approach of depleting Tβ4 by RNAi which resulted in increased E-cadherin expression in urinary bladder cancer cells leading to reduced mobility and invasiveness (Wang *et al.* 2012).

1.4.5 Thymosin β4 and the heart

Tβ4 is expressed in the developing and adult animal heart (Hannappel *et al.* 1982; Gomez-Marquez *et al.* 1989). Levels of Tβ4 can increase in the adult animal heart under certain conditions, for example following cardiac injury as demonstrated in pig, zebrafish and mouse. Tβ4 secretion accelerates from 0.06 pg/mL per minute to 0.16 pg/mL per minute (measured in plasma from the right atrium) after left-anterior descending coronary artery occlusion, cardiac arrest and resuscitation in porcine MI/reperfusion model (Shah *et al.* 2011). Tβ4 is highly expressed in embryonic endothelial progenitor cells (eEPC) and in recent studies eEPC-mediated cardiomyocyte survival was shown to be dependent of Tβ4 in a pig ischemia-reperfusion model (Kupatt *et al.* 2005; Hinkel *et al.* 2008). This underlines the beneficial paracrine effects of this molecule which have been well documented previously (Bollini *et al.* 2011; Kraehenbuehl *et al.* 2011). Tβ4 treatment of pigs with experimental MI reduced infiltration of inflammatory cells, pro-inflammatory cytokines and chemokines resulting in overall reduction of inflammation and swelling (Hinkel *et al.* 2008). This study also showed that the functional improvement following endothelial progenitor cell injections is at least partially attributable to Tβ4, since pre-treatment of eEPC with *Tβ4shRNA* prior to injection abolished some of the beneficial effects. Zebrafish have the surprising capability to regenerate functional myocardium after extensive damage. After complete resection of the apex, zebrafish heart can completely regenerate, a process in which upregulation of a Tβ4

orthologue was observed after 3 days and to lesser extent after 7 days (Lien *et al.* 2006). This could indicate that Tβ4 is part of a program that assists in cardiac regeneration. Also in mice, Tβ4 levels measured at one day and one week after ligation were found to be significantly increased (Smart *et al.* 2007). That the mammalian heart is in principle capable of regeneration was demonstrated in a recent study. During early postnatal life the mouse heart remains a highly plastic organ. Neonatal mice can also regenerate myocardium after surgical apex resection with only insignificant hypertrophy or fibrosis during later life but this regenerative potential is limited to the first postnatal days (Porrello *et al.* 2011). Although this intrinsic regenerative capability is lost after 7 days of postnatal life it indicates that cardiac regeneration in mammals is possible, but only in perinatal life. The Srivastava laboratory showed that Tβ4 can rescue the ischemic heart by Akt activation (Bock-Marquette *et al.* 2004). Tβ4-mediated reduction infarct size and improved cardiac function was, however, not able to rescue Akt deficiency since concomitant treatment with the Akt inhibitor Wortmannin abolished this effect (Sopko *et al.* 2011). Overall, either IP or intracardiac injections of Tβ4 after coronary artery ligation resulted in increased early cardiomyocyte survival, markedly reduced scar formation and overall improved function compared to untreated mice (**Figure 1.3**, Bock-Marquette *et al.* 2004).

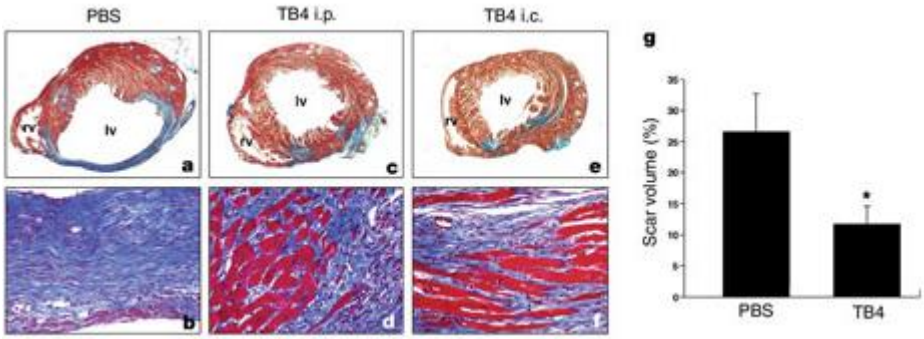


Figure 1.3: Scar formation is reduced in mice treated with Tβ4. Trichrome stain of mouse hearts 14 days after coronary artery ligation. (a, b) Control animals injected with PBS, (c, d) intraperitoneal (i.p.) or (e, f) intracardiac (i.c.) injections of Tβ4. (g) Quantification of scar volume of infarcted hearts following Tβ4 or control treatment (image obtained from Bock-Marquette *et al.* 2004).

In human patients, serum Tβ4 is significantly downregulated in ST-elevated MI (STEMI) patients at time of PCI, but levels return to those of controls 48h following successful intervention (Yesilay *et al.* 2011). PINCH, ILK and α-parvin are components of focal adhesions and are upregulated during dilated cardiomyopathy in humans (Sopko *et al.* 2011). This was also observed in overloaded and infarcted hearts in mice. PINCH, ILK and α-parvin expression was further increased by Tβ4-treatment indicating that Tβ4 potentially

augments a natural endogenous response to cardiac injury. *In vitro*, pre-conditioning of cardiac fibroblasts with Tβ4 resulted in decreased intracellular ROS, increased superoxide dismutase expression and catalase expression and reduced the Bax/Bcl2 expression ratio (Kumar and Gupta 2011). Furthermore, collagen type-1 (Col1), collagen type-3 (Col3) and connective tissue growth factor (CTGF) expression were reduced. This was confirmed in mice, where Tβ4 treatment was also shown to significantly reduce Col1 and Col3 expression in the heart following MI (Sopko *et al.* 2011).

The aforementioned role of Tβ4 in recruiting stem/progenitor cells further contributes to the improved outcomes after experimental MI in mice, with the epicardium being one of the most recently suggested sources for cardiomyocyte, endothelial and smooth muscle precursors (Smart *et al.* 2007; Smart *et al.* 2011). Exogenous Tβ4 was indeed shown to induce the recruitment of epicardium-derived progenitor cells following infarct. In the cardiovascular system of early mouse embryos Tβ4 is present mainly in blood vessels and endocardial cushions (Gomez-Marquez *et al.* 1996). Additionally, Tβ4 expression was observed in the ventricular myocardium, in the outflow tract, the pericardium and endocardium of mice at embryonic day 10 (E10, Smart *et al.* 2002). Smart and co-workers further established that Tβ4 promotes endothelial cell differentiation and epicardial cell migration and vasculogenesis during embryonic development (Smart *et al.* 2007). According to this study, epicardium-derived cells (EPDCs) undergo EMT and are subsequently recruited to the myocardium by Tβ4, to form either endothelial cells or a smooth muscle collateral support. The endothelial fate is determined by the vasculogenic growth determinants VEGF and basic fibroblast growth factor (bFGF), while the arteriogenic factors platelet-derived growth factor (PDGF) and transforming growth factor β (TGFβ) direct the cells towards smooth muscle fate. Tβ4 expression is vital for this process and accordingly for overall development of the heart. This was proven by RNAi-mediated Tβ4 knockdown during development, which resulted in impaired vasculogenesis and defects of the myocardium and embryonic lethality in mice. Pre-treatment of mice with Tβ4 was shown to prime epicardial cells to migrate into the myocardium during MI and this leads to improved cardiac outcomes (Smart *et al.* 2011). EPDC migration was traced by GFP and YFP expression under the control of *Wilm's tumour gene 1* (*Wt1*) promoter. While *Wt1* is not expressed in the adult epicardium, this embryonic expression pattern can be re-iterated by Tβ4 treatment. Cells were transiently labelled by EGFP expression under the control of the *Wt1* promoter which was activated by Tβ4 treatment as well as cardiac injury. Permanent labelling was achieved in the adult by use of a tamoxifen-inducible Cre recombinase under the control of the *Wt1* promoter which permanently activated EYFP transgene expression. In the myocardium these cells expressed cardiomyocyte-specific markers such as cardiac troponin-T, sarcomeric α-actinin and connexin-43.

In summary, these studies demonstrate that molecules which are involved in embryonic development could provide a means to stimulate a similar program in the adult heart. Tβ4-mediated induction of cell migration, angiogenesis and survival signalling in the setting of myocardial injury, make it a strong candidate to treat human heart disease. The fact that some, if not most, of these effects are exerted in a paracrine fashion, indicates an additional strength of this peptide. This potential has received recognition by the industry and Tβ4 is tested in several early-phase clinical trials (RegeneRx Biopharmaceuticals Inc., Bethesda, MD, USA). Unlike growth factors, Tβ4 has the additional advantage that it does not bind to heparin, thus allowing it to penetrate deep into tissues to exert its actions locally (Goldstein *et al.* 2012). A recent dose escalating phase I clinical trial in healthy subjects investigated systemic Tβ4 injections at pharmacologically relevant concentrations and concluded that it can be considered relatively safe since no severe adverse events were reported (Ruff *et al.* 2010).

1.5 Insulin-like growth factor 1

The name insulin-like growth factor-1 (IGF-1) derives from early observations in the 1960s when the then called somatomedin C was shown to have overlapping functions with insulin, while not being detectable by anti-insulin antibodies (Froesch *et al.* 1963). In 1976 the name was changed into IGF-1 to better describe its similarity to insulin and its growth promoting function (Rinderknecht and Humbel 1976). IGF-1 has been characterised as an anabolic protein mediating muscle growth and repair and fulfilling a host of critical functions during development and throughout life (Stewart and Rotwein 1996). Its importance during embryonic development was highlighted by the phenotype of *IGF-1*-deficient mice which display substantially reduced body weight at birth, growth retardation and during adult life weigh a third less than age-matched *wt* mice (Baker *et al.* 1993; Liu *et al.* 1998). IGF-1 stimulates glucose transport and utilisation in animals including humans and reduces circulating amino acids by decreasing protein degradation (Jacob *et al.* 1989). High levels of IGF-1 can result in hypoglycaemia due to increased glucose uptake.

1.5.1 Insulin-like growth factor 1 structure and post-translational modifications

The amino acid sequence of the precursor of IGF-1 was first determined in 1983 from human liver cDNA (Jansen *et al.* 1983). Less than ten years later, the complete structure of the IGF-1 gene had been identified in the rat (Shimatsu and Rotwein 1987; Hoyt *et al.* 1992; Simmons *et al.* 1993). It consists of more than 90 kb genomic DNA distributed over six exons and five intronic regions (**Figure 1.4**, Winn *et al.* 2002).

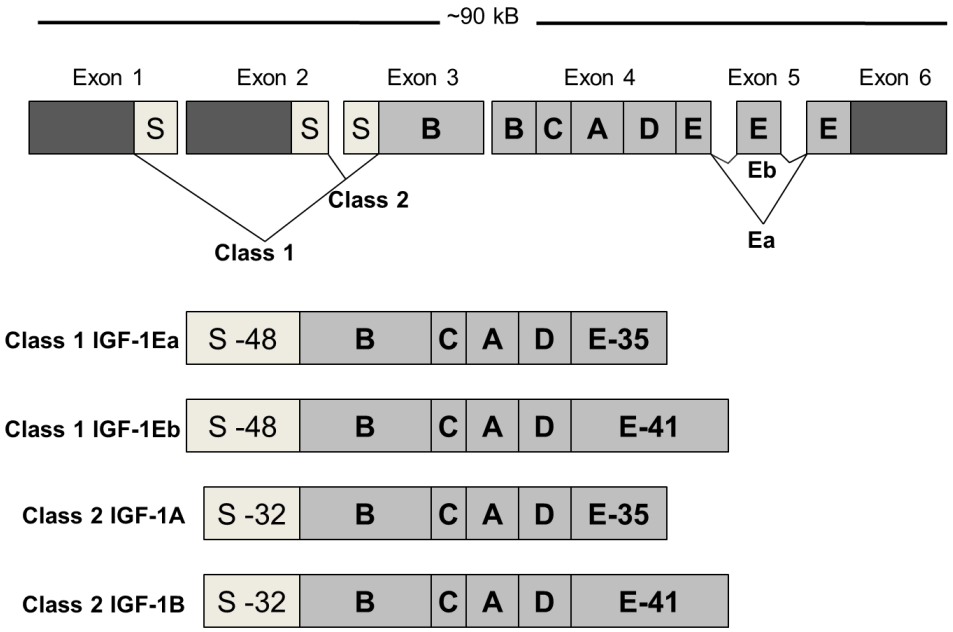


Figure 1.4: Schematic representation of the IGF-1 gene and its four isoforms in the rat. Expression of class 1 and 2 signal peptides and Ea and Eb carboxy-terminal peptides are regulated by alternative splicing (not to scale). S - signal peptide, E – extension peptide (Winn *et al.* 2002; Dobrowolny *et al.* 2005; Barton 2006).

Alternative splicing of Exon 1 and 2 produces two different amino-terminal signal peptides according to which the isoforms are classified into class 1 or class 2 molecules. Exon 3 and 4 are present in all transcripts of IGF-1 and are followed by differentially spliced exons 5 and 6, which give rise to two different carboxy-terminal extension peptides Ea and Eb. Various translation initiation site (AUG) are found along IGF-1 transcripts, indicating differential regulation on a translational level after splicing (Simmons *et al.* 1993). Both the signal peptide as well as the extension peptide undergo proteolytic cleavage to yield the 70 amino acid (7649 Da) long mature form of IGF-1 (Yang *et al.* 1995). The carboxy-terminal Ea peptide is highly conserved across mammalian species, while there is some divergence in the Eb peptide sequence (Hepler *et al.* 1990). The Ea peptide contains an N-glycosylation motif which is absent from the highly basic Eb peptide (Shimatsu and Rotwein 1987). To date, there is no consensus on the functions of both the Ea and Eb peptide (Santini *et al.* 2007). The sequence of the signalling peptide affects the efficiency of translation initiation and is a target for glycosylation on the IGF-1 precursor peptide (Simmons *et al.* 1993; Yang *et al.* 1995). As such, it defines the different localisation and function of the two IGF-1 classes (Musaro and Rosenthal 2002). The class 1 IGF-1 is described as the local isoform, opposed to the circulating class 2 molecule. Class 1 molecules are expressed by most, if not all tissues and act in an auto- or paracrine fashion while IGF-1 class 2 are mainly expressed

in the liver as endocrine signalling molecules in response to growth hormone (GH) stimulation.

Recent studies using decellularised tissue preparations have indicated that the function of the extension peptides (Ea and Eb) is their retention *in situ* and provides a rationale why unlike the processed mature IGF-1 they are not found in circulation (Hede *et al.* in press).

1.5.2 Insulin-like growth factor 1 signalling

Extracellular IGF-1 binds IGF-1 receptor (IGF-1R), which in turn autophosphorylates eight intracellular tyrosine residues (**Figure 1.5**, Kato *et al.* 1994). Phosphorylated IGF-1R activates insulin receptor substrates (IRS), preferentially IRS-1 (Rother *et al.* 1998). Activated IRS are highly potent regulators upstream of Ras-MAPK and phosphoinositide 3-kinase (PI3K) signalling cascades (Myers *et al.* 1994; Tanaka *et al.* 1996). PI3K phosphorylates Akt, also known as protein kinase B (PKB), and its signalling was shown to regulate heart growth during development (Alessi *et al.* 1996; Shioi *et al.* 2000). Akt, a serine/threonine kinase, in turn phosphorylates target of rapamycin (TOR), which is not essential but sufficient to mediate phosphorylation of the S6 ribosomal subunit (Sekulic *et al.* 2000). Mammalian TOR (mTOR), is achieving this as part of the mTORC1 protein complex, which phosphorylates various serine and threonine residues on the p70S6 kinase (p70S6K, Isotani *et al.* 1999). Phosphorylated p70S6K is recognised and further phosphorylated by phosphoinositide-dependent kinase 1 (PDK1) in a final activating step (Pullen *et al.* 1998). Hyperphosphorylated p70S6K activates 40S ribosomal subunit 6, which is stimulating protein synthesis and cell cycle progression (Chung *et al.* 1992; Chung *et al.* 1994; Ferrari and Thomas 1994).

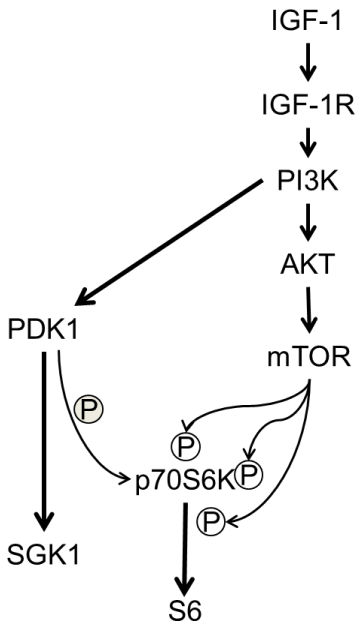


Figure 1.5: Simplified IGF-1 signalling pathway. Upon binding of extracellular IGF-1, IGF-1R autophosphorylates itself. Hyperphosphorylated IGF-1R activates PI3 kinase which subsequently phosphorylates Akt and PDK1. Akt then phosphorylates mTOR. Phosphorylated PDK1 and mTOR hyperphosphorylate p70S6K, which in turn activates the ribosomal subunit S6, which induces protein synthesis. PDK1 may alternatively activate SGK1, independently of mTOR, which mediates cell cycle progression and survival signalling.

Alternatively, IGF-1 signalling through PI3K can activate the growth factor serum- and glucocorticoid-regulated kinase 1 (SGK1) via PDK1, independently of mTOR (Kobayashi and Cohen 1999; Park *et al.* 1999). Activated SGK1 translocates to the nucleus and is considered the nexus between several intracellular signalling and phosphorylation cascades (Buse *et al.* 1999; Park *et al.* 1999). SGK1 mediates cell cycle progression and cell survival signalling by phosphorylating forkhead transcription factor FKHRL1 (FOXO3a), p300 and NFκB (Brunet *et al.* 2001; Tai *et al.* 2009). Additionally, SGK1 upregulates K+ channels, which contributes to its proliferative function (Gamper *et al.* 2002). Like Tβ4, IGF-1 is present in platelets where it is involved in autocrine signalling (Karey and Sirbasku 1989; Hers 2007). It was shown to bind platelet IGF-1R to induce insulin receptor substrate (IRS)/PI3K/Akt signalling and induce platelet aggregation.

1.5.3 IGF-1 and its propeptides in cardiac regeneration

IGF-1: IGF-1 treatment of embryonic cardiomyocytes in culture was shown to have anti-apoptotic effects by suppressing DNA fragmentation, bax and caspase-3 cleavage (Wang *et al.* 1998). It was also shown to increase proliferation of G_0/G_1 arrested HUVECs (Ma *et al.* 2009). In human heart transplant patients low serum levels of IGF-1 were found to be

associated with the development cardiac allograft vasculopathy and IGF-1 supplementation has been proposed as a treatment for recipients with low serum IGF-1 (Aharinejad *et al.* 2012). Conversely, ACE inhibitor treatment is associated with elevated circulating levels of IGF-1 in patients with ischaemic heart disease however there is some indication that high IGF-1 levels increase mortality in the elderly (Chisalita *et al.* 2011). However in a prospective cohort study (PRIME), high IGF-1 serum levels were shown to be protective against coronary artery disease (Ruidavets *et al.* 2011).

Both IGF-1 and IGF-1R are expressed in the heart during embryonic development in rats (Haskell and Tucker 1994). In order to study the importance of IGF-1R in cardiac progenitor cells, myocardial human cardiac stem cell (hCSC) were isolated from patients undergoing elective cardiac surgery for ischaemic heart disease (D'Amario *et al.* 2011). A patient subgroup characterised by higher expression of IGF-1R on hCSC compared to the other patients was identified. In this group, hCSC retained a “young” phenotype with long telomeres, enhanced cell proliferation and attenuated apoptosis and marked expression of IGF-1 and IGF-2. The cardioprotective role of IGF-1R was demonstrated in IGF-1R overexpressing mice, which were shown to be resistant to experimental type I diabetes-induced cardiomyopathy (Huynh *et al.* 2010). Intriguingly in zebrafish, that can regenerate lost myocardium, a gene duplication event resulted in two similar copies of the *IGF-1R* gene termed *igf-1ra* and *igf-1rb* (Maures *et al.* 2002).

There are a number of cardioprotective effects associated with IGF-1 overexpression or supplementation. For example myocardial hypoxia/reperfusion normally results in inhibited respiratory chain citrate synthase and mitochondrial complex IV and V activity but this was shown to be ameliorated by IGF-1 pre-treatment (Pi *et al.* 2007). It also increased mitochondrial membrane potential and decreased ROS, indicating that IGF-1-mediated cardioprotection is partially achieved by stabilising mitochondria. It was furthermore demonstrated that IGF-1 treatment increases the current through the L-type Ca^{2+}-channel in cardiomyocytes via PI3Kα-mediated Akt activation and this was hypothesised to assist in contractility and cardiac growth (Sun *et al.* 2006). Furthermore, IGF-1 enhanced grafting of fluorescently labelled mesenchymal cells in the heart in a rat model of MI (Enoki *et al.* 2010). However, this effect was lost after 1 month, indicating that either the selected cell type is inappropriate or that the effect of IGF-1 is only transiently improving cell engraftment. Nevertheless, increased neovascularisation and reduced cardiomyocyte apoptosis were observed at 3 days as well as 1 month following injury. Virally transducing mesenchymal stem cells (MSC) to induce overexpression of IGF-1 activated survival molecules Akt and PI3K as well as antiapoptotic Bcl-xL and increased the secretion of stromal derived factor-1α (SDF-1α, Haider *et al.* 2008). Transplanting transduced MSCs into rat myocardium after experimental MI resulted in an increased recruitment of $ckit^+$, $MDR1^+$, $CD31^+$ and $CD34^+$ cell

populations which likely contribute to the observed functional improvement compared to hearts treated with non-transduced MSCs.

More recent designs involved novel biomaterials as carriers for IGF-1. As such, alginate-based injectable beads were shown to be an excellent mode of delivering IGF-1 to the heart (Ruvinov *et al.* 2011). The biomaterial confers protection from proteolysis, which normally poses a significant deterrent to injected factors due to the adverse conditions *in situ*. In a rat model of MI, sequential release of IGF-1 and hepatocyte growth factor (HGF) using this technique demonstrated attenuated apoptosis, infarct expansion and scar fibrosis alongside increased angiogenesis and density of mature blood vessels and induced cell cycle re-entry of cardiomyocytes. Combinatorial therapy of IGF-1 and HGF was further investigated in a porcine model of MI (Ellison *et al.* 2011). IGF-1 and HGF were perfused into the culprit artery following reperfusion. This increased the abundance of c-kit^{+}/CD45^{-} endogenous porcine CSC, improved cardiac myocyte survival and reduction of fibrosis and hypertrophy. For this study and a clinically relevant experimental design of 60 min ischaemia and injection of factors after 30 min reperfusion had been used, highlighting the potential of this approach in clinical use. Another recent study tethered IGF-1 to self-assembling peptide nanofibres and co-injected these together with CSC into the MI borderzone in rat (Padin-Iruegas *et al.* 2009). This was designed to allow for gradual release of IGF-1 to promote activation and differentiation of injected and resident CSC. The approach was successful, showing increased formation of *de novo* myocytes compared to injecting either cells or IGF-1 alone. While overall cardiac function was improved by this combination therapy, long term functionality of these new myocytes was not assessed.

Despite these promising results, circulating IGF-1 was also shown to contribute to cardiac hypertrophy by downregulating anti-hypertrophic micro RNAs (mIRs, Hua *et al.* 2012). Mice were subjected to aortic banding to induce cardiac hypertrophy. mIR1 and mIR133a were significantly reduced in *wt* mice resulting in heart enlargement (Hua *et al.* 2012). This effect was abolished in mice with IGF-1 deficiency in the liver. mIR-1 negatively regulates cardiac hypertrophy by downregulating GATA4, Mef2a and calmodulin and mIR-133a regulates proteins RhoA, GDP-GTP exchange protein and Cdc42 which are all implicated in this process (Care *et al.* 2007; Ikeda *et al.* 2009). In neonatal rat cardiomyocyte cultures, IGF-1-mediated hypertrophy is abolished by overexpression of mIR-1 and mIR133a (Hua *et al.* 2012).

IGF-1Eb: While a substantial amount of research has been directed towards fully processed IGF-1 a significant effort has been made to understand the diverse roles of the IGF-1Ea and IGF-1Eb propeptides which somewhat differ from circulatory IGF-1. Recent research has shown that expression of IGF-1Eb in the brain is increased following traumatic cerebral

injury in rats indicating that this isoform potentially plays a role in a natural defence mechanism (Schober *et al.* 2012). In the heart, early experiments have already shown the beneficial effect of cardiac-specific IGF-1Eb isoform overexpression (Li *et al.* 1997). Mice overexpressing IGF-1Eb in the heart showed decreased expansion of the lesion by apoptosis and necrosis as well as reduced remodelling following experimental MI. Another beneficial effect of IGF-1Eb was observed in the setting of diet-induced cardiomyopathy. A number of pathological changes in mice are associated with high fat diet reflecting the situation in human (Zhang *et al.* 2012). These include reduced fractional shortening, glucose intolerance, increased circulatory IL-6 and insulin, cardiac hypertrophy (indicated by increased wall thickness and increased end systolic/end-diastolic dimensions) and reduced circulatory IGF-1. This was accompanied by increased ROS, apoptosis, mitochondrial dysfunction and reduced ATP on the molecular level. While also presenting an obese phenotype in response to high fat diet, mice overexpressing the IGF-1Eb isoform in the heart did not show increased ROS production, apoptosis or mitochondrial dysfunction. In addition, insulin signalling and cardiac contractility where preserved while glucose intolerance and cardiac hypertrophy were not reduced.

IGF-1Ea: ROS reducing properties have also been attributed to the locally acting IGF-1Ea isoform *in vitro*. Overexpression of IGF-1Ea, but not IGF-1, conferred protection from Ang II-mediated oxidative stress and hypertrophy in HL-1 and neonatal cardiomyocytes (Vinciguerra *et al.* 2010). In recent years IGF-1Ea has received considerable attention as a putative candidate for therapy of cardiac conditions. Although IGF-1Ea is widely expressed in neonatal tissues, high expression in the adult seems to be restricted to the liver, but increases in extrahepatic tissues after injury (D'Ercole *et al.* 1984; Hill and Goldspink 2003). In skeletal muscle, this increase triggers the activation of satellite cells and increases protein synthesis (Hill and Goldspink 2003). In mice, muscle specific overexpression of IGF-1Ea increases numbers of myogenic progenitors, promotes healing after muscle injury and reduces muscle loss in cachexia and ageing (Musaro *et al.* 2001; Musaro *et al.* 2004).
Cardiomyocyte-specific overexpression of IGF-1Ea in mice was shown to support recovery and reduce scar formation after MI, also reducing pro-inflammatory cytokines IL-1β and IL-6, while anti-inflammatory IL-4 and IL-10 expression were increased compared to *wt* mice (**Figure 1.6**, Santini *et al.* 2007).

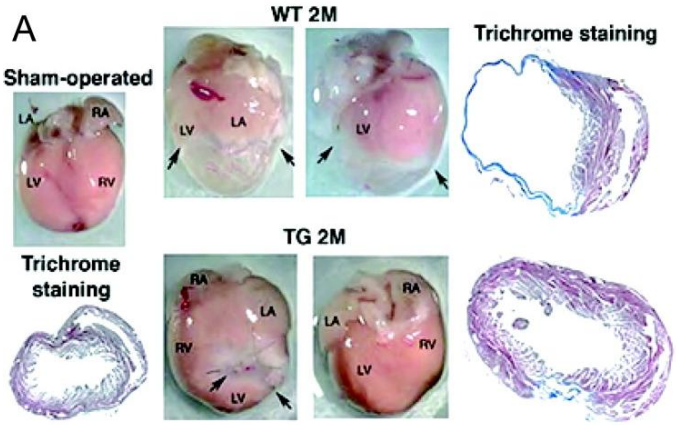


Figure 1.6: Fibrosis in *αMHC/IGF-1Ea* transgenic and *wt* mouse hearts following MI. (A) Whole mount and Masson's trichrome analysis of sham-operated control *wt* heart (left). *wt* (top panels) and *αMHC/IGF-1Ea* hearts (bottom panels) 2 months following coronary artery ligation. Arrows indicate fibrotic tissue. LA - left atrium, LV - left ventricle, RA - right atrium, RV - right ventricle (image obtained from Santini *et al.* 2007).

Furthermore, decreased apoptosis was observed at the site of the lesion, which is at least in part attributable to the IGF-1Ea-mediated increase in the expression of UCP-1, metallothionein 2 and the cardioprotective molecule adiponectin. While contributing to preserved organ function in the setting of MI, IGF-1Ea overexpression in cardiomyocytes does not produce sustained hypertrophy under physiological conditions.

Despite being downstream of IGF-1/PI3K signalling and its role as a cardioprotective mediator and key regulator of physiological heart growth, Akt does not seem to mediate IGF-1Ea cardioprotection since this seems to involve an alternative signalling pathway (**Figure 1.7**, Matsui *et al.* 1999; Fujio *et al.* 2000; DeBosch *et al.* 2006; Santini *et al.* 2007).

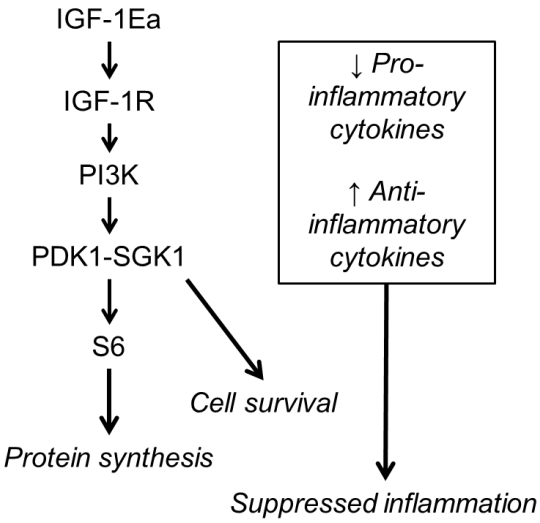


Figure 1.7: Simplified alternative IGF-1Ea signalling pathway in injured hearts. In animals that overexpress IGF-1Ea in the heart, an alternative signalling cascade was identified. IGF-1R binds IGF-1Ea and transduces the signal through PI3K, PDK1 and SGK1. While PDK1 phosphorylation leads to S6 ribosomal subunit activation and protein synthesis, SGK1 induces cell survival signalling. The observed effects in vivo include increased expression of anti-inflammatory cytokines pro-inflammatory molecules are suppressed (Santini *et al.* 2007).

PDK1 can directly phosphorylate p70S6K and activate the PI3K dependent kinase SGK1, which was shown to regulate cardiomyocyte survival (Pullen *et al.* 1998; Aoyama *et al.* 2005). It has been proposed that many functions attributed to Akt are potentially mediated by SGK, which has an inactivating function on Akt, but is a strong contributor to cell survival signalling in its own right (Kobayashi and Cohen 1999; Lang and Cohen 2001). In line with this, no Akt-PDK1 complex formation in the heart and a downregulation of mTOR was observed in uninjured and challenged hearts of *IGF-1Ea* transgenic mice (Santini *et al.* 2007). In contrast, an increase in the levels of phosphorylated PDK1, PDK1-SGK1 complex formation and S6 phosphorylation were observed. Taken together, these results indicate that in the hearts of mice overexpressing IGF-1Ea, survival signalling is directed by an alternative pathway via PDK1 and SGK1 and not via mTOR of the classical pathway. Increased cell proliferation was detected in the vessels close to the lesion in IGF-1Ea overexpressing mice after MI suggesting that IGF-1Ea may additionally be responsible for the recruitment of endogenous EPCs (Santini *et al.* 2007). In summary, the presented evidence indicates that IGF-1, IGF-1Ea and IGF-1Eb are interesting candidates for future approaches to enhance cardiac repair after chronic or acute injury.

1.5.4 Autophagy

In addition to the described cardioprotective mechanisms, IGF-1 also modulates autophagy. Autophagy is an essential mechanism of normal cell homeostasis, as it regulates the lifetime of organelles (predominantly mitochondria) and long-lived proteins and is mediated by autophagy-related proteins (Atg). Macromolecules and organelles destined for autophagic recycling are enucleated by a double membrane vesicle called phagophore (**Figure 1.8**, reviewed in Mizushima *et al.* 2003 and Levine and Kroemer 2008).

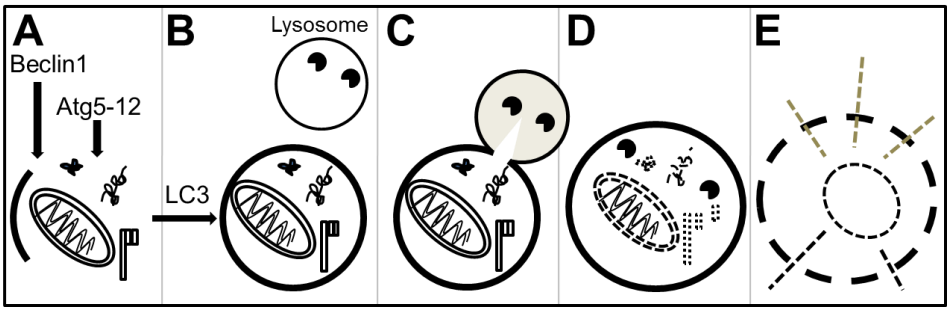


Figure 1.8: Simplified graphic representation of autophagy process. (A) Nucleation of cytosolic macromolecules and organelles into the pre-phagophore complex is mediated by Beclin1 and the Atg5-Atg12 complex. (B) LC3 conversion and insertion into autophagosomal membrane completes autophagosome formation. (C) Fusion of lysosome with the mature autophagosome. (D) Degradation of autophagolysosomal contents by lysosomal enzymes. (E) Release of nutrients and breakdown products release into the cytoplasm.

Once phagophore assembly is completed, the now mature autophagosome fuses with lysosome to give rise to the late autophagolysosome. After degradation of the internalised content, the autophagolysosome dissociates and amino acids and other products are released into the cytoplasm. Hence it is upregulated during starvation to provide nutrients for essential basal protein synthesis (Maiuri *et al.* 2007). Impaired autophagy results in various diseases such as Lafora disease, Fabry disease and heart failure (Tannous *et al.* 2008; Chevrier *et al.* 2010; Knecht *et al.* 2010). This highlights the importance of autophagy not only as provider of nutrients but also as a cell maintenance mechanism to remove defective protein and organelles. Autophagosome assembly starts with the binding of beclin-1 (Atg6) to PI3K and p150 to initiate nucleation of the pre-phagophore (reviewed in Petiot *et al.* 2000; Yang *et al.* 2005). LC3I (Atg8) and Atg 12 are activated in a first step by Atg7 (Noda *et al.* 2011). LC3I activation further involves lipidation by covalent cross-linking to phosphatidylethanolamine yielding the active LC3II form, which is inserted into the autophagosomal membrane (Kabeya *et al.* 2000). Atg12 is covalently linked to Atg5 by Atg10 and this Atg5-Atg12 complex, like LC3II, is essential for autophagosomal membrane formation (Shintani *et al.* 1999). Most Atgs are only required for formation of the

autophagosome and LC3II appears to be the only more permanent marker of autophagosomal membranes (Kabeya *et al.* 2000). After fusion with the lysosome, the autophagolysosomal contents are degraded by lysosomal hydrolases (reviewed in Mitsushima *et al.* 2007). The resulting breakdown products, such as amino acids, are released back into the cytoplasm by molecules called vacuolar effluxers and can be recycled (Yang *et al.* 2006).

While autophagy is critical for physiological function of post-mitotic tissues, it was shown that it needs to be carefully regulated in the heart to support normal cardiac function (Kostin *et al.* 2003; Tsujimoto and Shimizu 2005; Tannous *et al.* 2008).

1.6 Researching factors for cardiac protection: Transgenics, global and inducible knockout and knockdown mice

Some of the most ground breaking discoveries of basic molecular mechanisms have been made in yeast, bacteria, plants or cell culture. However, for the study of human physiology and disease on the organ level, the use of *in vivo* animal models is indispensable and is a main driver of translational research.

Both IGF-1Ea and Tβ4 have been shown to reduce inflammation, increase myocyte survival, reduce scar volume and overall to preserve cardiac function in animal models of ischaemic injury. The substantially improved outcome after experimental MI following IGF-1Ea and Tβ4 supplementation in animals indicates the importance of further examining their mode of action to fully understand their function and evaluate potential risks. The animal models used in the present study to better our understanding of the function of Tβ4 and IGF-1Ea will be described in the next sections.

1.6.1 Global versus tissue specific gene overexpression

Global gene overexpression in all tissues is achieved in transgenic animals by introducing transgenes under promiscuous, often viral promoters such as simian virus 40 (SV40) and cytomegalovirus (CMV, Qin *et al.* 2010). The disadvantage of this approach is that the overexpression of genes has different effects in different tissues. The effect of gene overexpression in one tissue can affect the tissue of interest for example by paracrine signalling, hormone secretion, cell interaction or metabolic changes. To circumvent this limitation, the use of tissue-specific promoters to overexpress genes of interest was developed. Every tissue has its own specific gene expression profile and the knowledge of when promoters are active (for example during which developmental stage) allows for precise timing of transgene expression within the tissue of interest. The choice of promoter

will also affect how strongly the transgene will be expressed. The myosin heavy chain family of proteins, which form the subunit of cardiac myosin, are by weight the most dominant contractile protein in vertebrate skeletal and cardiac muscle (Ng *et al.* 1991). *βMHC* is predominantly expressed in the heart during embryonic development but cardiac *aMHC* is strongly expressed during late gestational stages and throughout postnatal life (Gulick *et al.* 1991). The timing of its expression and its cardiomyocyte specificity have made *αMHC* a popular promoter to express transgenes exclusively in ventricular myocardium. For this study, two mouse strains expressing transgenes under the control of the *αMHC* promoter were used: *αMHC/IGF-1Ea* and *αMHC/MerCreMer* mice.

1.6.2 Global gene knockout

A global or conventional knockout describes the loss of a gene in every tissue and can be achieved by introducing into embryonic stem cells DNA that has a certain degree of sequence homology with the region of the target gene, but is lacking vital parts or the full gene to be studied (Capecchi 1989). The standard technique involves gene targeting by homologous recombination in mouse embryonic stem cells *in vitro* and subsequent introduction of positively selected knockout clones into a mouse embryo at the blastocyst stage (Grant and Silva 1994). The introduced cells become part of the host blastocyst and this gives rise to chimeric mice which are backcrossed into the strain of interest to purify the genetic background. As is true for global overexpression of transgenes, conventional or global knockouts suffer the caveat of off-target effects, which can affect observations in the tissue of interest. In order to achieve temporally and spatially controllable downregulation of genes without these confounding factors, the Cre/*loxP* system is now frequently used to study gene function in physiological and pathological conditions.

1.6.3 The Cre/*loxP* system

Complementing global knockouts, cutting edge inducible gene manipulation has found its way into the mainstream of basic research. Among the most popular techniques to induce genetic modifications *in vivo* is the Cre/*loxP* system. Bacterial DNA *loxP* sequences are recognised by Cre recombinase (Enterobacteria phage P1 cyclization recombinase), an enzyme derived from P1 bacteriophage (Sternberg and Hamilton 1981; Sauer and Henderson 1988). Cre facilitates homologous recombination of DNA at these *loxP* sites, which results in the excision of the flanked sequence and the leading *loxP* site. The choice of promoter driving Cre confines this recombination to a specific tissue or developmental stage. Furthermore, expression of Cre can be regulated by external means for example by the use of heat inducible promoters. The use of tissue specific Cre driver strains has been a success story in mouse research and the European Conditional Mouse Mutagenesis Program Tools

for Functional Annotation of the Mouse Genome (EUCOMMTOOLS) is currently developing further 500 Cre ES cell lines to stream-line translational research based on the Cre/*loxP* technology. This is part of an international effort to generate thousands of crosses to floxed alleles as part of the International Knockout Mouse Consortium (IKMC) program (www.knockoutmouse.org, Skarnes *et al.* 2011).

1.6.4 Cre driver strains: *αMHC/MerCreMer* mice

A host of Cre driver strains have been generated in the recent years, allowing for tissue specific Cre transgene expression in virtually every organ. As discussed previously the *αMHC* promoter remains one of the most frequently used promoters to achieve transgene expression restricted to the cardiac ventricles,. The *αMHC/MerCreMer* strain (also referred to as *αMHC/CreERT*^{2}) was generated by cloning *MerCreMer* cDNA into a vector downstream of the *αMHC* promoter (**Figure 1.9**, Gulick *et al.* 1991; Zhang *et al.* 1996).

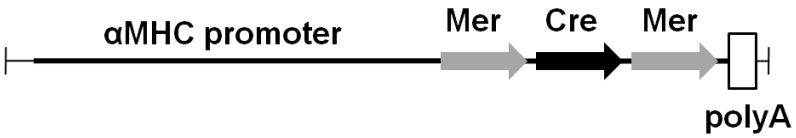


Figure 1.9: Schematic representation of the *αMHC/MerCreMer* transgene. Not to scale (Sohal *et al.* 2001).

MerCreMer refers to a fusion protein consisting of the Cre enzyme core and two flanking Mer domains. The mutated oestrogen receptor (Mer) domains were generated by mutating the glycine at position 525 of the oestrogen receptor to arginine (G525R), hence abolishing the binding of oestrogen/17β-oestradiol (Danielian *et al.* 1993). Mer binds the synthetic oestrogen analogue tamoxifen or its metabolite 4-hydroxytamoxifen with high affinity. Fusion-proteins containing Mer domains are restricted to the cytoplasm but upon binding of tamoxifen are shuttled to the nucleus in a steroid receptor-like mechanism, comparable to ligand-bound oestrogen receptor (Feil *et al.* 1996; Kocanova *et al.* 2010). Nuclear exclusion of MerCreMer is safeguarded heat shock protein 90 (Hsp90) which binds MerCreMer in the cytoplasm (Koitabashi *et al.* 2009). Upon tamoxifen binding to Mer domains Hsp90 dissociates from the fusion-protein which can subsequently enter the nucleus. The fusion of two Mer domains to the Cre enzyme core instead of one leads to more tightly regulated Cre activity (Zhang *et al.* 1996). To generate the *αMHC/MerCreMer* strain, transgene DNA was injected into pronuclei of fertilised oocytes of *FVB* mice (Sohal *et al.* 2001). The *FVB* founders were backcrossed into a *C57Bl/6SV129* background and maintained as a *C57Bl/6* strain.

The success of the conditional genomic deletion or knockout can be determined by PCR or by investigating the corresponding reduction of mRNA or protein. The time required for sufficient reduction of the target gene can vary from 6 days to 4 weeks depending on the route of administration and dose of tamoxifen (Kiermayer *et al.* 2007; Andersson *et al.* 2010; Stokke *et al.* 2010). Serum tamoxifen peaks 3-6 h following oral administration and tamoxifen is rapidly metabolised into its active form 4-hydroxytamoxifen, while the predominant metabolite *N*-desmethyltamoxifen reaches peak levels only after 24-48 h following administration (Robinson *et al.* 1991). Oral administration of 200 mg/kg tamoxifen every 24h resulted in tamoxifen accumulation over for 4 days before a plateau was reached. For this work, tamoxifen pellets and tamoxifen injections were used at concentrations established in previous studies (Welle *et al.* 2009).

1.6.5 RNA interference-mediated knockdown

RNA interference (RNAi) is a post-transcriptional regulatory mechanism that was discovered in the late 1990s by Andrew Fire and Craig Mello, who were jointly awarded the Nobel prize for this work in 2006 (retrieved 22/07/2012, source: http://www.nobelprize.org/nobel_prizes/medicine/laureates/2006/press.html/, Fire *et al.* 1998). RNAi is a technique that exploits the endogenous double stranded RNA (dsRNA) degradation machinery involving an RNase III (Tuschl *et al.* 1999). Small interfering RNA (siRNA) can be directly introduced into the cell or the respective code be inserted into the genome depending of the model system. Endogenous small RNA transcripts form larger hairpin or stem-loop structure. This is truncated at both the 5' and 3' ends by the endonuclease drosha in the nucleus yielding a so called pre-miRNA (Han *et al.* 2006). This stem-loop pre-miRNA of around 50-60 nucleotides length is cleaved to produce double-stranded siRNA of ~22 nucleotides length by removal of the loop and is transported to the cytoplasm (Elbashir *et al.* 2001, reviewed in Kim 2005). This process is catalysed by dicer, a member RNase III family (Bernstein *et al.* 2001). This short double- stranded siRNA associates with members of the diverse argonaute protein family to form the RNA-induced silencing complex (RISC) and simultaneously processed into a single-stranded guide strand (reviewed in Parker and Barford 2006). The complementary 'passenger strand' is degraded in the process (Matranga *et al.* 2005). The role of the guide strand is targeting the correct mRNA by Watson-Crick base-pairing of its 5' end to the 3' UTR of the target (reviewed in Martin and Caplen 2007). Once bound to the target mRNA, there are a variety of pathways inhibiting the formation of a protein product. For example, a RISC complex containing argonaute 2, also referred to as 'slicer', which has an RNase H-like catalytic domain, is able to degrade the target mRNA (Song *et al.* 2004). This form of post-transcriptional regulation is

referred to as knockdown and is clearly distinct from a knockout as it does not affect the genome sequence.

1.7 Hypothesis

1. Tβ4 is a molecule of diverse physiological functions that has been shown to improve various disease conditions. Given the importance of Tβ4 during embryonic development, the increase of endogenous Tβ4 during cardiac injury and the absolute requirement for Tβ4 during cardiac development, a loss of function in the adult mouse heart was expected to potentially have small effects under physiological conditions. I hypothesised that following MI Tβ4 depletion would show more significant effects, the nature of which could provide further clues about the role of Tβ4 in the heart.

2. Complementary to the analysis of an adult Tβ4 knockdown phenotype *in vivo,* the production of a recombinant Tβ4 molecule *in vitro* for the use in proteomics was aimed at advancing the mechanistic understanding Tβ4 and to identify novel interactors of the peptide in the heart.

3. The beneficial effect of IGF-1Ea overexpression or supplementation to the heart following experimental MI has been well documented. The subcellular morphology of *αMHC/IGF-1Ea* cardiomyocytes however had not been previously assessed. To gain novel insights into the working mechanisms of IGF-1Ea in the heart a transmission electron microscope analysis cardiac tissue from *αMHC/IGF-1Ea* mice was to be performed.

Chapter 2 - Methodology

2.1 Mouse models

Animal models provide unparalleled insights into disease mechanisms and novel therapeutic approaches. In cardiovascular research, animals such as zebrafish, mouse, rat, guinea pig, cat, dog and pig are used to study myocardial infarction, heart failure and regeneration (Corr *et al.* 1978; Gao *et al.* 2010; Guo *et al.* 2012; Johnson *et al.* 2012; Jopling *et al.* 2012; Rosenblatt-Velin *et al.* 2012; So *et al.* 2012). The plethora of transgenic mice available, their ease of breeding, handling and relatively cheap maintenance makes them the favourite *in vivo* tool for developmental and pre-clinical studies.

2.1.1 *αMHC/MerCreMer* mice

αMHC/MerCreMer (B6.FVB(129)-Tg(Myh6-cre/Esr1*)1Jmk/J) mice were purchased from JAX lab.

2.1.2 *Tβ4shRNAflox* mice

Tβ4shRNAflox mice were generated in Paul Riley's laboratory at University College London. This mouse was created with the aim to downregulate *Tβ4* mRNA by RNAi. *Tβ4shRNAflox* mice contain a *Tβ4 short hairpin RNA* (*Tβ4shRNA*) transgene with a leading 5T stop sequence inhibiting its expression (Smart *et al.* 2007). The stop sequence is flanked by *loxP* sites and can therefore be removed by Cre recombinase resulting in the expression of *Tβ4shRNA* (**Figure 2.1**).

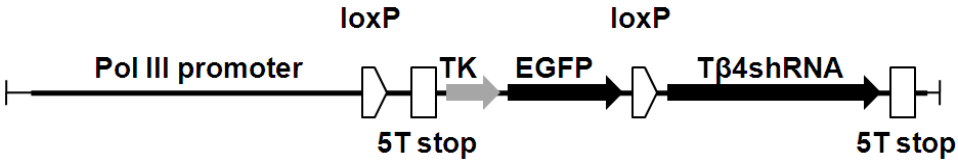


Figure 2.1: Schematic representation of the *Tβ4shRNAflox* transgene. Not to scale (Smart *et al.* 2007).

By crossbreeding *Tβ4shRNAflox* mice with a Cre driver strain, expression of the shRNA can be induced. In this project, *αMHC/MerCreMer* mice were crossbred with *Tβ4shRNAflox* animals to allow for controlled knockdown of *Tβ4* by inducible expression of the *Tβ4shRNA* (**Figure 2.2**).

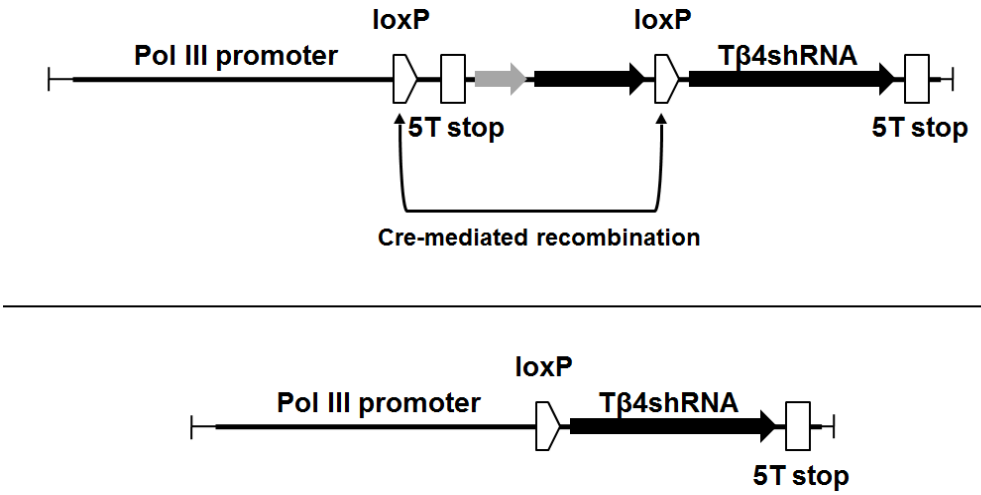


Figure 2.2: Cre-mediated excision of genomic inhibitory target sequences in *Tβ4shRNAflox/MerCreMer* mice. MerCreMer fusion protein translocates to the nucleus upon tamoxifen administration (top panel). Nuclear MerCreMer recombines DNA at *loxP* sites, excising the inhibitory 5T sequence. This results in the expression of Tβ4shRNA (lower panel). Not to scale (Smart *et al.* 2007).

The *pol III* promoter driving the expression of the *Tβ4shRNA* is not tissue specific but the *αMHC* promoter driving MerCreMer fusion protein expression limits recombination to cardiomyocytes. Consequently, MerCreMer activation will results in expression of *Tβ4shRNA* and subsequent knockdown of *Tβ4* in the cardiac ventricles.

2.1.3 *αMHC/IGF-1Ea* mice

Transgenic *αMHC/IGF-1Ea* mice were generated on the *FVB* background in Nadia Rosenthal's laboratory at the EMBL Monterotondo using standard techniques (**Figure 2.3**, (Santini *et al.* 2007).

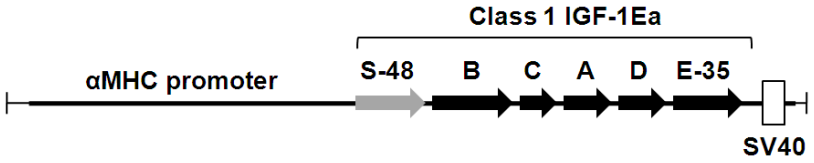


Figure 2.3: Schematic representation of the *αMHC/IGF-1Ea* transgene. Not to scale (Santini *et al.* 2007).

Briefly, rat *IGF-1Ea* cDNA was cloned into an expression vector under the control of the *αMHC* promoter. This was achieved by random insertion of the rat *IGF-1Ea* transgene DNA into the genome, as opposed to targeted insertion.

2.1.4 Genotyping

Mice were anaesthetised briefly using 3% (v/v) isofluorane (Merial Animal Health Ltd., Harlow, UK). A 5 mm piece of tail was removed and animals marked with numbered metal ear tags. Tails were digested at 56 °C overnight in 0.05 mg/mL proteinase K (Roche Applied Science, Burgess Hill, UK, # 03115801001). Digested samples were vortexed and centrifuged at 16,000 g for 10 min at 4 °C. The supernatant containing the DNA was directly used to amplify the relevant transgene DNA by PCR (GeneAmp PCR System 9700, Applied Biosystems, Carlsbad, CA, USA).
The following primers were used:

αMHC/IGF-1Ea
Sense: 5'-TTCCTGTCTACAGTGTCTGTG-3'
Antisense: 5'-GAGCTGACTTTGTAGGCTTCA-3'

αMHC/MerCreMer
Sense: 5'-AACATTCTCCCACCGTCAGT-3'
Antisense: 5'-CATTTGGGCCAGCTAAACAT-3'

Tβ4shRNAflox
Sense: 5'-TGCATGTCGCTATGTGTTCTG-3'
Antisense: 5'-AAGTCGTGCTGCTTCATGTG-3'

Table 2.1: Recipes and thermocycler conditions for genotyping PCR.

Transgene	**Recipe**	**Thermocycler conditions**	**Size of amplicon**
αMHC/IGF-1Ea	30 µL reactions: 6 µL Buffer (5x) 1.2 µL $MgCl_2$ (25 mM) 0.6 µL dNTP (10mM) 3 µL *IGF-1Ea* rev/fw primer mix (10µM) 0.3 µL Taq Polymerase 17.9 µL ddH_2O + 1 µL sample DNA	5 min at 94 °C 35x 1 min at 94 °C 1 min at 52 °C 20 s at 72 °C 7 min at 72 °C ∞ 4 C	440 bp
Tβ4shRNAflox	30 µL reactions: 6 µL Buffer (5x) 1.2 µL $MgCl_2$ (25 mM) 0.6 µL dNTP (10mM) 3 µL *Tβ4shRNAflox* rev/fw primer mix (10µM) 0.3 µL Taq Polymerase 17.9 µL ddH_2O + 1 µL sample DNA	5 min at 94 °C. 35x 1 min at 94 °C 1 min at 60 °C 20 s at 72 °C 7 min at 72 °C ∞ 4 C	703 bp
αMHC/MerCreMer	25 µL reactions: 5 µL Buffer (5x) 2 µL $MgCl_2$ (25 mM) 0.5 µL dNTP (10mM) 1 µL *Cre* rev/fw primer mix (10µM) 0.2 µL Taq Polymerase 14.3 µL ddH_2O + 1 µL sample DNA	5 min at 95 °C 30x 30 s at 95 °C 45 s at 56 °C 45 s at 72 °C 7 min at 72 °C ∞ 4 C	350 bp

Buffer, MgCl2, taq polymerase and dNTP were purchased from Promega, Southampton, UK (# M8306 and U1240).

PCR products were electrophoresed at 100 V (PowerPac300, Bio-Rad Laboratories, Hemel-Hempstead, UK) on 2% (w/v) agarose gels prepared using 1X TAE buffer (0.4 M, 10 mM EDTA) containing 10 µL/mL ethidium bromide. Gels were analysed using GeneSnap v7.07 software and a SynGene ChemiGenius2 gel documentation system (SynGene, Cambridge, UK).

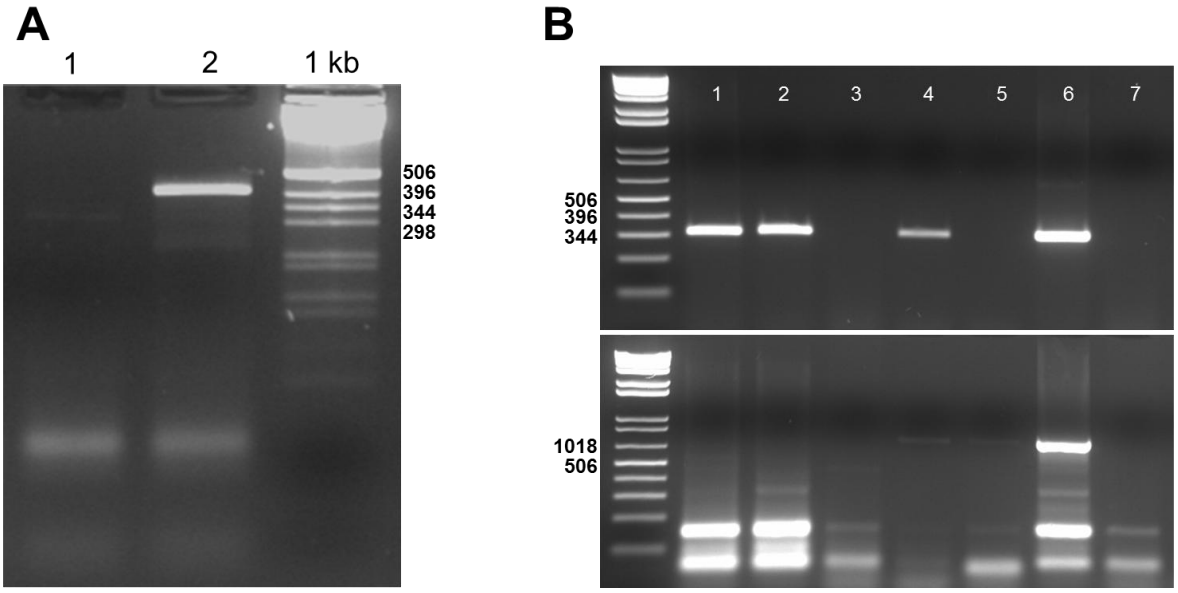


Figure 2.4: Agarose gel (2%) gels of genotyping PCR products. (A) Lane 1 shows results for a *wt* mouse with a faint aspecific band at ~350 bp. Lane 2 shows the characteristic band at 440 bp for a *IGF-1Ea* transgenic animal. (B) PCR results for *MerCreMer* (top panel) and *Tβ4shRNAflox* (lower panel) transgenes of various genotypes. Lanes 1 and 2: *MerCreMer*, Lane 3: *wt*, Lane 4: *Tβ4shRNAflox/MerCreMer*-double transgenic (faint), Lane 5: *Tβ4shRNAflox* (faint), Lane 6: double transgenic positive control and Lane 7: *wt* negative control. A 1 kb molecular weight marker (Invitrogen, Carlsbad, CA, USA, # 10787-018) was used as reference.

2.1.5 Experimental MI: Left anterior descending coronary artery ligation

Ligation of the left anterior descending coronary artery (LCA) is the most accurate model of MI in animals and is used from large mammals, such as pig and dog to small animals, such as rat and mouse (Podzuweit *et al.* 1981; Richeson *et al.* 1982; Salto-Tellez *et al.* 2004). LCA ligation in mice was first developed in 1995 and has since been constantly developed further to increase reproducibility and experimental outcome as well as to improve animal welfare by decreasing the duration of surgery and unnecessary trauma (Michael *et al.* 1995). More recently, models of ischaemia-reperfusion have increased in popularity since they reflect today's clinical practice of re-establishing blood supply through the affected coronary vessel by PCI and stent (Ellison *et al.* 2011). For the present work, the simpler and more time effective standard experimental MI was chosen over ischaemia-reperfusion.

2.1.6 Mouse model of myocardial infarction: Left anterior descending coronary artery ligation

The left anterior descending coronary artery (LCA) ligation protocol described by Salto-Tellez and colleagues was used with some significant improvements especially regarding the intubation technique (Salto-Tellez *et al.* 2004). Mice between 3 and 4 month of age were weighed and then anaesthetised in a small animal induction chamber using 4% (v/v) isofluorane (Merial Animal Health Ltd., Harlow, UK). After approximately 4 min, depth of anaesthesia was sufficient to proceed with intubation. The non-invasive intubation technique developed by Hamacher and co-workers was the preferred option over the commonly used tracheotomy (Hamacher *et al.* 2008). Mice were removed from the induction chamber and hung on a self-built stand by passing a suture under their incisor teeth. A fibre optic light was placed in front of the throat to illuminate the larynx. The tongue was retracted using atraumatic forceps to reveal clear view on the trachea with the characteristic epiglottal opening and closing motion visible during each breath. A 25 G wire guide was inserted into the trachea and the intubation cannula carefully slid over the wire into the trachea. After removing the guidewire, the animal was placed in a supine position and connected to a small animal respirator (MiniVent Type 845 microrespirator, Harvard Apparatus, Hollston, MA, USA). The respirator was set to 200 µL stroke volume at 110 strokes per minute. Both front paws were taped to the working surface and the chest was shaved. Prior to the first incision, the animals were injected subcutaneously with 0.002 mg of analgesic buprenorphine (Vetergesic®, Reckit Benckiser Healthcare UK Ltd., Hull, UK). A single 15 mm incision in parallel to the sternum was made into the skin covering the left lower quadrant in the area covering the 3rd intercostal space. The left pectoralis major muscle and lower muscle layers were retracted to allow access to the 3rd intercostal space. Blunt forceps were used to tear the tissue between the 3rd and the 4th ribs. Particular attention was paid to avoiding damage to the lower side of the ribs, which are lined with blood vessels and nerves. Four retractors were used to retract the 3rd and 4th rib and permit access the thoracic cavity. The pericardium was carefully opened to provide adequate exposure of the heart. The LCA was identified with the aid of a Leica S6E microscope at 8x magnification (Leica Microsystems, Milton Keynes, UK). A 8/0 polyamide suture (Ethicon, Johnson & Johnson, Brussels, Belgium) was passed underneath the LCA, through the myocardium and carefully tightened in a double-double square knot to restrict blood supply to the lower left ventricle. The success of the ischemia was controlled by observing blanching of the lower left ventricle. The pericardium was allowed to slide back into its original position and the retractors were removed. The intercostal space was closed by two non-continuous sutures using non-absorbable 6/0 polypropylene suture material (Ethicon, Johnson & Johnson, Brussels, Belgium). Previously retracted muscles were pushed back in their native position and the skin was sutured using

the 6/0 polypropylene material. Isofluorane delivery was terminated and animals kept on pure oxygen until independent breathing was setting in. Following LCA ligation animals had access to wet diet and were allowed to recover in a 30 °C incubator overnight. Additional injections of pain relief were administered as described above, 6 hours following the procedure and optionally the next morning if signs of pain and distress were observed. Extent of infarct was assessed by Echocardiography (ECHO) (**Figure 2.5**).

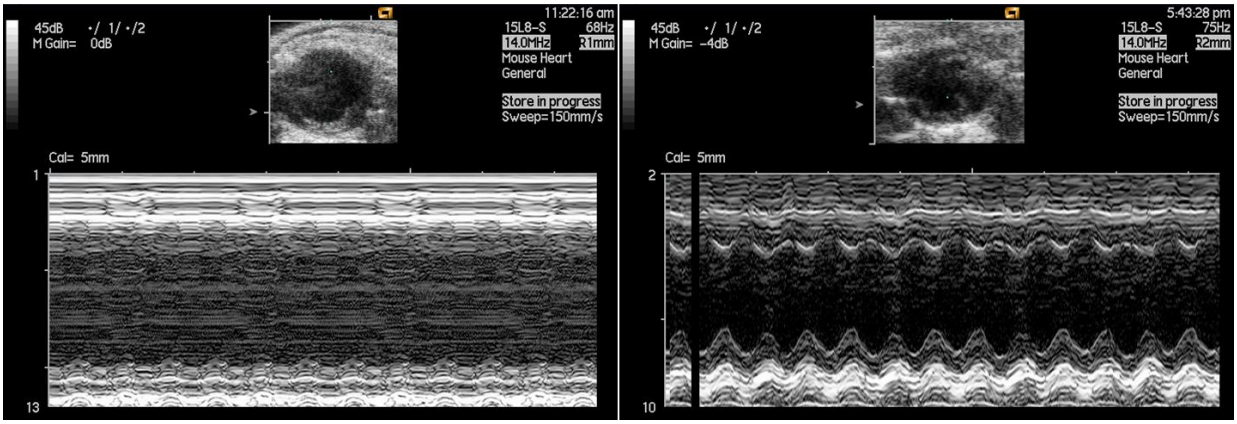


Figure 2.5: ECHO traces of mouse heart after coronary artery ligation. M-mode ECHO recordings of mouse heart 1 month following LCA ligation (left panel) and under physiological conditions (right panel).

Histology was used to investigate tissue remodelling and fibrosis after 1 month (**Figure 2.6**).

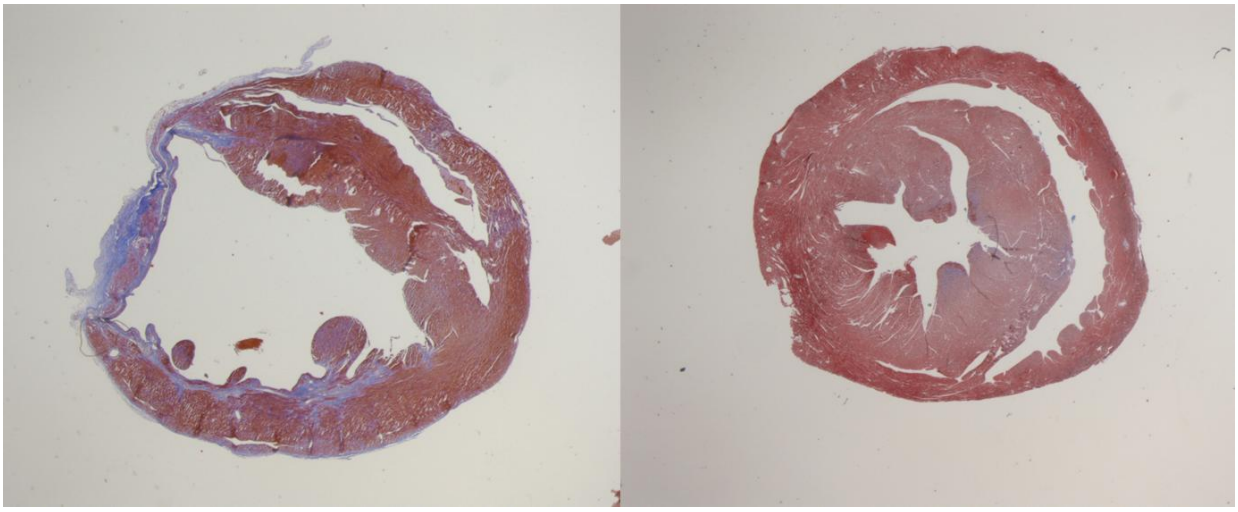


Figure 2.6: Left-descending coronary artery ligation in mice. Masson's Trichrome staining of mouse heart 1 month following coronary artery ligation (left panel) and normal heart (right panel).

2.2 Conditional knockdown of Thymosin β4

Double transgenic *Tβ4shRNAflox/MerCreMer* mice were treated with tamoxifen to induce nuclear localisation of MerCreMer and subsequent excision of an inhibitory sequence flanked by *loxP* sites. This was aimed to induce *Tβ4shRNA* expression and subsequent downregulation of *Tβ4* mRNA (see Chapter 3).

2.2.1 Tamoxifen delivery

Choosing the appropriate method of tamoxifen delivery to mice carrying the MerCreMer transgene is essential to ensure sufficient abundance of MerCreMer in the nucleus for long enough to allow successful recombination of targeted *loxp* sites with minimal impact on general health and homeostasis. Tamoxifen can be delivered via diet, drinking water or by IP injections (Gail *et al.* 1999; Andersson *et al.* 2010). With the aim to avoid unnecessary distress for the animals, I initially opted for tamoxifen delivery via diet. This avoided handling and restraining the animals as for gavage (delivery in drinking water) or IP injections. IP injections were later used after unexpected problems arose from feeding tamoxifen chow as described in Chapter 3.

Tamoxifen delivery via diet: Normal chow was replaced by tamoxifen containing (0.025% w/w) chow (Harlan Laboratories, Horst, The Netherlands, # TD.110069) for two weeks. Nuclear translocation was assessed immediately after two weeks by immunofluorescence analysis for Cre on cardiac sections. To avoid any potential transient side effects of tamoxifen, experimental outcome of knockdown was assessed after additional two weeks recovery.

Tamoxifen delivery via IP injections: Tamoxifen (Sigma-Aldrich, Gillingham, UK, # T5648) was dissolved in 100% Ethanol to a concentration of 100 mg/mL. It was then further diluted 1/10 in soybean oil (Sigma-Aldrich, Gillingham, UK, # S7381) to a final concentration of 10 mg/mL. Animals were manually restrained and injected IP in the lower left quadrant of the abdomen to reduce the risk of unintentional damage to the liver. Tamoxifen was delivered at 20 mg/kg daily over five consecutive days or as a single injection of 40 mg/kg. Control injections consisted of pure EtOH diluted in soybean oil at identical concentration. Animals were rested for 4-11 weeks before assessment of experimental outcomes.

2.3 Echocardiography

Cardiac function of mice was determined by echocardiography (ECHO). Several different ultrasound-based techniques such as transthoracic, transoesophageal and epicardial surface ECHO and intravascular, transjugular or transperitoneal ultrasound are available for small animal research. The latter 4 techniques have the disadvantage of being invasive.

Transthoracic ECHO was shown to be the best approach in terms of procedure and temporal/spatial resolution to permit the most accurate estimation of cardiac function in the mouse (Gardin *et al.* 1996).

2.3.1 Transthoracic echocardiography

Cardiac function was assed using a Siemens Acuson Sequoia 256 workstation and a 14.0 MHz 15L8-S transducer (Siemens Healthcare, Camberley, UK). Aqueous ultrasound gel (Ana Wiz, Hersham, UK, # UGEL250) was pre-warmed to 37 °C to increase signal transduction and prevent hypothermia of the mice. Low level of anaesthesia was induced in the mice using 3% (v/v) isofluorane in oxygen and further maintained at 1.5% (v/v) isofluorane via facemask. The animals were placed in a supine position on a heated pad to maintain a stable body temperature and the thorax was shaved from the sternum to the left side, from the lowest rib to the left axilla and commercially available hair removal cream was used to remove residual hair. A thin layer of ultrasound gel was applied on the shaved area and a generous amount was placed on the probe before commencing the measurement. Short axis view measurements were obtained with treatment and genotype blind to the investigator. Traces were recorded at least in duplicate over consecutive days and results averaged. This was aimed at eliminating user bias and reducing variation. The term “short axis” refers to measuring the lumen of the left ventricle at an angle parallel to the base of the heart. Long axis refers to measurements taken along the axis from the tip of the apex to the base of the heart (**Figure 2.7**).

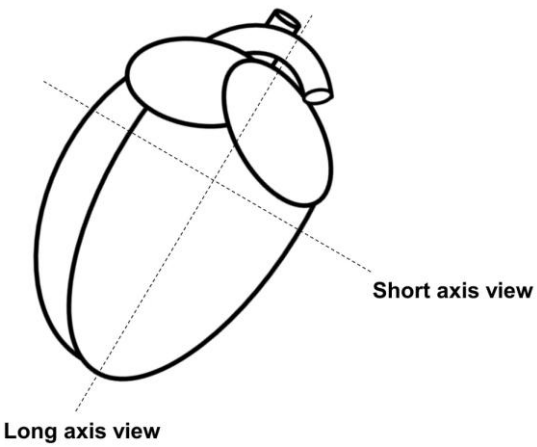


Figure 2.7: Schematic representation of echocardiography axes. Short axis and long axis ECHO planes are indicated by the dashed lines.

Left-ventricular ejection fraction (EF) and fractional shortening (FS) were determined. EF refers to the fraction of blood volume that is ejected during systole (stroke volume) in relation to the maximum cardiac volume during diastole. M-mode and two-dimensional (2D) mode

measurements were performed at a sweep speed of 150 mm/s. Before continuing with data analysis, residual ultrasound gel was removed, animals were allowed to recover from anaesthesia and placed back in their cages. The analysis of M-mode traces was performed by manually measuring the anterior wall thickness, lumen of the LV and the thickness of the posterior wall using the ECHO workstation. LV EF and FS were calculated using the formulas shown in below.

Short axis M-mode:

$EF = [(\text{end-diastolic}^3 - \text{end-systolic}^3)/\text{end-diastolic}^3] \times 100\ (\%)$

$FS = [(\text{end-diastolic} - \text{end-systolic})/\text{end-diastolic}] \times 100\ (\%)$

Left-ventricular inner diameters during systole and diastole (LVIDs/d) were also determined from M-mode ECHO traces. EF measured in 2D-mode provides more accurate results and is the method of choice to measure cardiac function in human patients. This is attributable to the fact that in a two-dimensional measurement only one dimension has to be interpolated, whereas in M-mode, a linear measurement is used for volume calculations (two dimensions interpolated). This mathematical caveat and the increased susceptibility to measuring inaccuracies (e.g. accidental offset from the correct measuring line or angle) indicate that where possible 2D EF measurements should be preferred over M-mode analysis. Measurements obtained in 2D-mode were analysed by manually delineating the inner and outer boundaries of the left-ventricular myocardium. Ejection fraction and fractional shortening were calculated using the formula indicated below.

Short axis 2D-mode:

$EF = [(\text{end-diastolic area} - \text{end-systolic area})/\text{end-diastolic area}] \times 100\ (\%)$

Calculation of 2D EF using the area method, as described above, is reasonably accurate but less accurate than using end-diastolic/systolic volumes (Wisneski *et al.* 1981). Determination of 2D EF using the volume method was not available during this study due to technical limitations of the ultrasound equipment.

2.4 Tissue harvesting from mice

Mice were weighed, anaesthetised using 4% (v/v) isofluorane and placed in a supine position on the procedure surface. Ventilation with isofluorane was maintained via facemask. Sufficient depth of anaesthesia was controlled by monitoring responsiveness to pain. A semi-lunar shaped incision was made into the peritoneal cavity of the mouse using a scissor. Intestines and fat tissue were carefully pushed out of the peritoneal cavity to the left using a cotton bud. Great care was taken not to damage the digestive organs to prevent bacterial contamination of the area. Following this step, the inferior vena cava (IVC) was identified proximal to the right kidney. A 25 G needle was used to slowly draw up to 1 mL of blood from the IVC just above the point where it gives rise to the right renal vein. The blood was transferred to a Vacutainer tube (Fisher Scientific, Loughborough, UK, # VCT-090-050W). The syringe was briefly rinsed and then filled with PBS. Two incisions were made through the rib cage left and right of the sternum. The sternum was folded back over the head of the mouse. The IVC and abdominal aorta were severed to allow drainage of blood and buffer following the injection of 0.5 to 1 mL of PBS into the left ventricle. Transcardiac flushing was performed slowly and carefully to avoid overstretching of the left ventricle to avoid tissue damage. This had to be prevented to maintain structural integrity and to avoid molecular changes in response to overstretching potentially causing interference during subsequent RNA expression analysis. The heart was carefully removed from the thorax without damaging it with the scissors and without applying excessive pressure on the myocardium with the forceps. It was then placed in a dish with PBS and allowed to further purify itself from any residual blood by on-going contractions. The heart was then carefully blotted dry on a tissue, atria removed and cardiac mass recorded. It was then placed back into the dish containing PBS (4 °C) and dissected with a scalpel. The dissection pattern used to ensure tissue availability for all required analyses is shown in **Figure 2.8**.

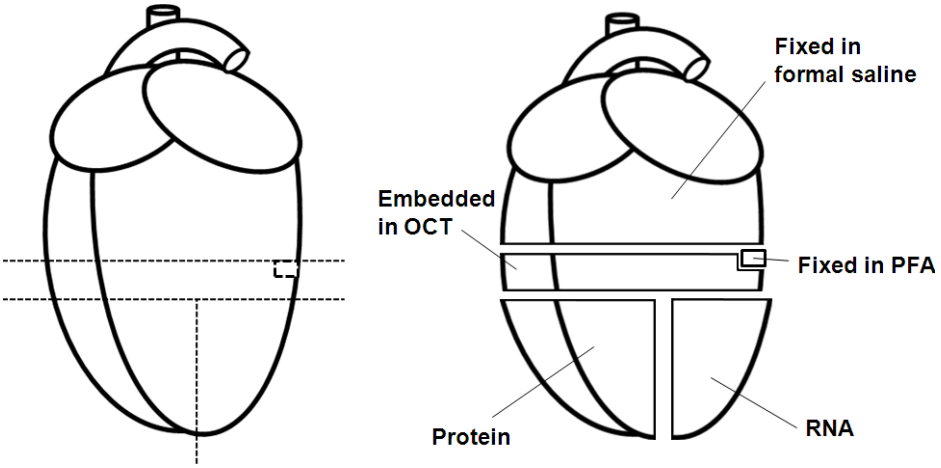


Figure 2.8: Schematic depiction of the mouse heart dissection pattern used. To obtain samples for most standard applications from a single specimen, hearts were dissected into 5 pieces as indicated in the cartoon above. Formal saline-fixed tissue was used for immunohistochemistry and histological staining, the OCT embedded ring for cryosections, the PFA fixed specimen of the left ventricle for electron microscopy analysis and each half of the lower ventricles for protein and RNA isolation respectively.

Tissue samples for the study of RNA and protein composition were minced carefully to remove any residual blood, placed in 2 mL microcentrifuge tubes and frozen immediately in liquid nitrogen. Samples destined for paraffin embedding and transmission electron microscopy (TEM) analysis were placed in a 2 mL tube containing formal saline and 4% (w/v) paraformaldehyde (PFA) in 0.2 M phosphate buffer respectively and stored at 4 °C overnight to allow for sufficient crosslinking. 0.2 M phosphate buffer consisted of aqueous mono (NaH_2PO_4 * H_2O) and di-basic (Na_2HPO_4 * 2 H_2O) phosphate buffers adjusted to pH 7.2. Formal saline and PFA was replaced by 0.2 M phosphate buffer after overnight incubation at 4 °C. To preserve tissue for immunofluorescence staining of cryosections, a small ring of cardiac tissue from the middle of the heart was placed in a square mold containing sufficient OCT compound to cover the sample. This was followed by immediate freezing in liquid nitrogen. Quick freezing of OCT embedded samples prevents formation of tissue-damaging ice crystals which appear during slow freezing on dry ice. In addition to cardiac samples, four 1 cm pieces of tail were removed in addition. Three pieces were stored in -80 °C freezers for future DNA isolation and the remaining piece was used for re-genotyping the animals after sacrifice, as described in Section 2.1.4. Lungs and livers were dissected, blotted dry and weights recorded.

2.5 Protein biochemistry

Investigation of cardiac protein composition is important to understand how altered mRNA expression profiles translate into changes on the protein level.

2.5.1 Protein extraction

Tissue samples destined for protein isolation stored at -80 °C were kept on dry ice prior to isolation. 1x RIPA buffer (20 mM Tris-HCl (pH 7.5), 150 mM NaCl, 1 mM Na_2EDTA, 1 mM EGTA, 1% NP-40, 1% sodium deoxycholate, 2.5 mM sodium pyrophosphate, 1 mM β-glycerophosphate, 1 mM Na_3VO_4, 1 µg/ml leupeptin) containing 1x DTT (1.25 M, Cell Signaling, Danvers, MA, USA, # 9806) and a cocktail of protease and phosphatase inhibitors (Roche Applied Science, Burgess Hill, UK, # 11206893001, 04906845001) was prepared following manufacturer's instructions. The whole isolation procedure was carried out on ice to prevent degradation or dephosphorylation of proteins. The tissue sample was transferred into a glass homogeniser, 300 µL RIPA buffer were added and the sample homogenised by rotating the pestle while carefully sliding it in and out of the glass shaft. Homogenised tissue suspension was transferred to a fresh 1.5 mL tube on ice and further disrupted by three brief continuous pulses (~1 s each) at 90 W using a Vibra Cell sonicator (Sonics & Materials, Newtown, CT, USA). The samples were centrifuged at 16,000 g for 20 min in a pre-cooled (4 °C) microcentrifuge (Heraeus, Osterode, Germany) to pellet insoluble tissue fragments and cellular debris. The supernatant was transferred into a fresh 1.5 mL tube. After protein quantification, aliquots of known concentrations were prepared and the stock samples stored long term at -80 °C.

2.5.2 Protein quantification

Proteins were quantified using the *DC* protein assay following manufacturer's instructions (Bio-Rad Laboratories, Hemel-Hempstead, UK, # 500-0116). The colorimetric quantification kit is an improvement of the classical Lowry assay, which is based on Folin reduction (Lowry *et al.* 1951). This is achieved in a two-step reaction: protein samples are exposed to copper in an alkaline solution before Folin is added and subsequently reduced (loss of 1-3 oxygen atoms) by the protein-copper complexes. This results in a colour shift to blue with a peak absorbance at 750 nm (Peterson 1979). The amount of Folin reduced in the reaction is proportional to the quantity of protein available and hence allows absorbance values to be related to protein concentration. A standard curve was prepared from a bovine serum albumin (BSA) sample of known concentration. Concentrations used are displayed in **Table 2.2**.

Table 2.2: Generation of a standard curve for quantification of unknown protein samples by *DC* protein assay. BSA protein concentrations for each of the 9 data points are indicated.

mg/mL BSA final	0	0.2	0.4	0.6	0.8	1.0	1.2	1.6	2.0
BSA (2mg/mL)	0	5	10	15	20	25	30	40	50
ddH_2O	50	45	40	35	30	25	20	10	0

Protein samples from larger pieces of cardiac tissue were highly concentrated and could therefore not be measured directly, since absorbance values would exceed the linear range of the standard curve. Consequently samples were diluted 1/10 in ddH_2O before measurement. To allow for automated evaluation of the absorbance using a µQuant microplate reader (Bio-Tek Instruments, Potton, UK), 5 µL of the BSA dilutions for the standard curve as well as the 5 µL of each sample were pipetted in separate wells of a 96-well cell culture plate. Following the manufacturer's instructions, 25 µL solution A/S (alkaline copper tartrate solution; consisting of 1mL reagent A and 20 µL reagent S) and 200 µL solution B (Folin reagent) were added to each well. After 15 min incubation in the dark the absorbance at 750 nm was stable for at least 1h. Samples were measured in duplicate to correct for pipetting errors. Absorbance measurements for the each standard were plotted against their know concentration and the slope *m* and the intersection with the y-axis *b* of the linear regression line calculated by MS Excel (Microsoft, Reading, UK).

Formula of a linear function:

$$f(x) = m * x + b$$

By inserting the measured absorbance *f(x)* for each sample into the formula, it was possible to deduct the concentration *x* for each sample. The coefficients of determination R^2 were calculated in MS Excel and were consistently >0.99 indicating a good fit of the data points with the linear regression meaning that it is highly likely to get correct predictions from the regression line (**Figure 2.9**).

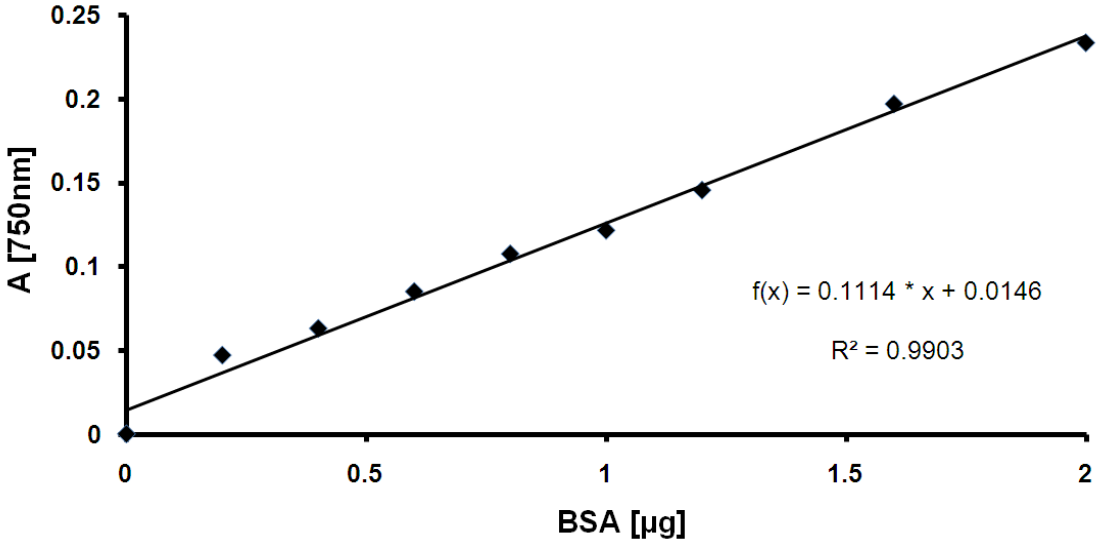


Figure 2.9: Example of a standard curve used for protein quantification. DC protein assay was used to determine absorbance at 750 nm of BSA samples of known concentrations. The absorbance of each protein concentration was assayed in duplicate and averaged. The coefficient of determination R^2 is indicated.

2.6 Protein immunoblotting

The protein immunoblot was developed in 1981 in the Laboratory of W. Neal Burnette and is also known as Western blot in reference to Edwin Southern and his Southern blot (Burnette 1981). Protein samples to be analysed were quantified (see Section 2.5.2), diluted to a standard concentration and combined with reducing SDS sample buffer (1X SDS sample buffer final, 1X DTT final, Cell Signaling, Danvers, MA, USA, # 7722). The protein solution was boiled at 95 °C for 5 minute to denature the proteins and briefly centrifuged to collect vapour droplets. After boiling, the samples were stored at -20 °C or immediately loaded onto a 1D polyacrylamide gel.

2.6.1 Western blotting procedure for normal sized proteins

Electrophoresis acrylamide gels were self-made for proteins >10 kDa. A commercially available 30% solution of acrylamide mix (29:1) with the cross-linker bis-acrylamide (Bio-Rad Laboratories, Hemel-Hempstead, UK, # 161-0157) was used. The volume percentage of acrylamide and cross-linker in the total volume determines the pore size of the gel with higher total percentages resulting in smaller pore sizes in the gel. Consequently, lower percentage gels (≤ 10%) were used to analyse proteins of higher molecular weight, while higher percentage gels (≥ 12%) were used to achieve better separation of smaller proteins. **Table 2.3** shows the recipes used for the preparation of the resolving/separation gels.

Electrophoresis and transfer were carried out using a BioRad Mini-PROTEAN® system (Bio-Rad Laboratories, Hemel-Hempstead, UK, # 165-8000, 165-8004).

Table 2.3: Recipe list for most common concentrations of bis-acrylamide resolving gels used for 1D protein electrophoresis. The volumes indicated (5 mL total) are sufficient for 1 gel in a 0.75 mm cast.

	Percentage of bis-acrylamide gels		
Components	**10%**	**12%**	**15%**
ddH_2O	1.9 mL	1.6 mL	1.1 mL
Acrylamide mix (30%)	1.7 mL	2.0 mL	2.5 mL
1.5 M Tris (pH 8.8)	1.3 mL	1.3 mL	1.3 mL
SDS (10%)	50 mL	50 µL	50 µL
TEMED	2 µL	2 µL	2 µL
Ammonium persulfate	50µL	5 µL	5 µL

The components were added to a 15 mL tube in the order displayed. Ammonium persulfate (APS) and tetramethylethylenediamine (TEMED, Bio-Rad Laboratories, Hemel-Hempstead, UK, # 161-0700, 161-0801) catalyse the polymerisation of acrylamide and were added immediately before the gel was poured into the cast. The solution was transferred into the cast using a 5 mL serological pipette. The cast was filled to approximately 2 cm below the top to keep sufficient space for the stacking gel. The surface of the gel was covered with 100% EtOH to level the surface as well as to prevent it drying from drying. The gel was allowed to polymerise for 15 min before the EtOH cover layer was removed. In the meantime the stacking gel was prepared in a 15 mL plastic tube according to the recipe shown in **Table 2.4**.

Table 2.4: Recipe list for bis-acrylamide stacking gel used for 1D protein electrophoresis. Volumes indicated (1 mL total) are for sufficient for 1 gel in a 0.75 mm cast.

Components	**5% bis-acrylamide gel**
ddH_2O	0.68 mL
Acrylamide mix (30%)	0.17 mL
1.5 M Tris (pH 8.8)	0.13 mL
SDS (10%)	10 µL
TEMED	1 µL
Ammonium persulfate	10 µl

Using a 5 mL serological pipette the stacking gel was transferred into the remaining space of the cast and the comb was carefully inserted in the top. The gel was allowed to polymerise, stored for several days at 4 °C or used immediately for 1D separation of proteins.

1D gel electrophoresis: The gel was assembled into the Bio-Rad system and placed inside the buffer reservoir which was then filled with 1x electrophoresis tank buffer (25 mM tris base, 0.192 M glycine, 0.1% (v/v) SDS). Boiled protein solution was pipetted into the wells leaving one well for running a pre-stained molecular weight marker (Invitrogen, Carlsbad, CA, USA, # LC5800). Samples were electrophoresed at 150 V (PowerPac300, Bio-Rad Laboratories, Hemel-Hempstead, UK) at RT until the running dye reached to lower bottom of the gel.

Protein transfer: The gel was removed from the system and placed onto 0.45 µm pore size nitrocellulose membrane (Bio-Rad Laboratories, Hemel-Hempstead, UK, # 162-0150). Gel and membrane were placed into a transfer cassette between 2 layers of Whatman 3 MM Chr chromatography paper (Thermo Fisher Scientific, Loughborough, UK, # CJF-500-050X) and a fibre pad on each side (**Figure 2.10**). The transfer cassette was then inserted between anode and cathode of the Mini Trans-blot Cell Electrophoretic Transfer Cell (Bio-Rad Laboratories, Hemel-Hempstead, UK, # 170-3930) with the nitrocellulose membrane located between the gel and the anode.

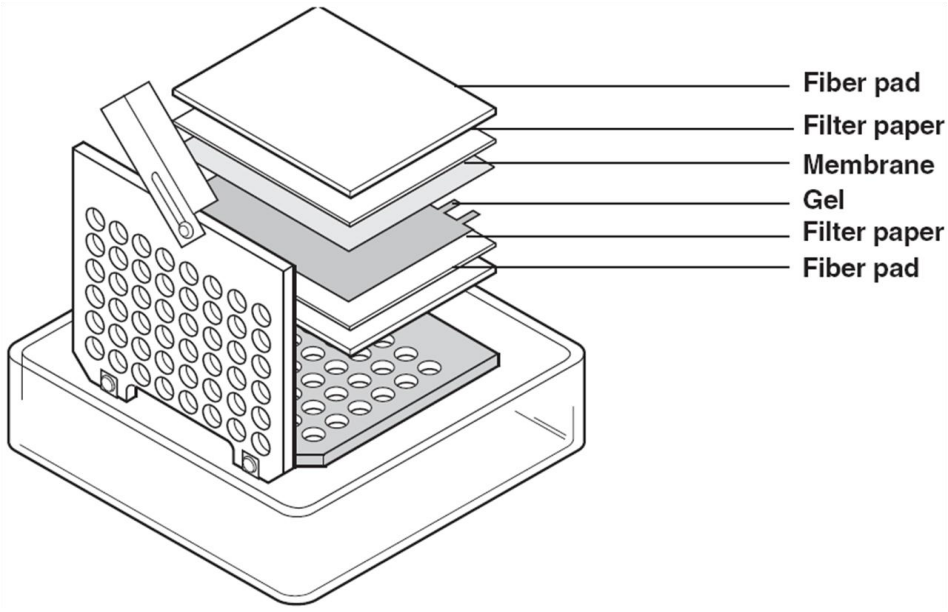


Figure 2.10: Assembly of the transfer cassette. The gel and nitrocellulose membrane were placed between 2 layers of chromatography paper. The resulting stack was placed between filter pads and secured in the transfer cassette (Bio-Rad Laboratories [Internet], Hercules, CA, Mini Trans-Blot® Electrophoretic Transfer Cell Instruction Manual, ©2011, Cited 27/02/2012, Available from: http://www.bio-rad.com/webroot/web/pdf/lsr/literature/M1703930.pdf).

The buffer tank was filled with transfer buffer (Tris base 25 mM, 0.192 M glycine, 15% (v/v) MEOH) and the protein transferred to the nitrocellulose membrane at 100 V for 2 h at 4 °C. *Blocking:* To prevent aspecific binding of the primary antibody, membranes were blocked in 5% (w/v) BSA blocking solution (TBS-T, 50 mM tris, 150 mM NaCl, 0.1% (v/v) Tween, pH 8) for 1 h at RT.

1° antibody: The membrane was incubated overnight at 4 °C in 5 mL of 5% (w/v) BSA blocking solution containing the primary antibody (concentrations dependent on antibody specificity).

1st washing: After overnight incubation the membrane was washed twice in 1X TBS-T (0.1%) for 5 min at RT. *2° antibody:* Secondary antibodies targeting the Fc portion of the respective primary antibody were used at a dilution of 1:2000 in 5% (w/v) milk blocking solution. The membrane was incubated for 1 h at RT. *2nd washing:* The membrane was washed twice in 1X TBS-T (0.1%) for 15 min at RT.

Following the second wash, the membrane was incubated in ECL for 5 min and exposed to Amersham Hyperfilm ECL in a darkroom (GE Healthcare, Little Chalfont, UK, # 28-9068-37). Quantification of band intensity was performed using ImageJ 1.45S.

2.6.2 Western blotting procedure for small proteins and peptides

Proteins smaller <10 kDa were resolved using commercially available Tris-Tricine gradient gels ranging from 10-20% (Bio-Rad Laboratories, Hemel-Hempstead, UK, # 456-3114). The electrophoresis procedure was performed as described in the previous section with some deviations. During electrophoresis, two different buffers were used: anode buffer (0.2 M tris, pH 8.9) and cathode buffer (0.1 M tris base, 0.1 M tricine, 1% (v/v) SDS). The cathode buffer was placed inside the inner reservoir between two gels (or a gel and a buffer dam) and the anode buffer filled in the outer reservoir. The samples were electrophoresed for ~1 h 45 min. The transfer setup was used as described above using a modified transfer buffer (25 mM tris base, 0.192 M glycine, 40% v/v MeOH). Increased MeOH concentrations promote small peptide transfer to the membrane. Blotting and development were carried out as described in Section 2.6.1.

2.7 RNA extraction

Extraction of RNA from cells or tissues requires two steps: disruption and homogenisation (QIAGEN Ltd [Internet], Hilden, RNeasy® Mini Handbook 09/2010, ©2003-2012, Cited 27/02/2012, Available from: www.qiagen.com/literature/render.aspx?id=352). Disruption is necessary to release the RNA by breaking down tissue and cell/organelle membranes and has to occur immediately after the sample is removed from ice to expose the RNA to

protective buffers. Homogenisation is required to reduce viscosity of the sample by shearing DNA and other high-molecular-weight cell components to allow optimal binding of the RNA to the column during purification.

2.7.1 RNA isolation from cells

In a fume cabinet TRIzol reagent (Invitrogen, Carlsbad, CA, USA, # 15596-026) was added to the wells of cultured cells: 500 µL/well for 12 well plates and 1 mL/well for 6 well plates. Cells were mechanically disrupted and detached by scraping the wells with a bent pipette tip and the suspension transferred to a 2 mL centrifuge tube. For isolation from pelleted cells, TRIzol reagent was directly added to the cell pellet and the suspension transferred to a 2mL tube. To assist homogenisation and to shear released genomic DNA, the suspension was passed ten times through a 23 G syringe needle before storage at -80 °C or immediate processing. 200 µL chloroform for each mL TRIzol used were added and the samples incubated for 3 min at RT before 15 min centrifugation at 16,000 g at 4 °C. This separates the protein debris, the organic phase, the DNA containing interphase and the RNA containing aqueous phase. The latter was transferred to a new 2 mL centrifuge tube. 0.56 volumes of EtOH (100%) were added and the solution and any precipitate were transferred to an RNeasy Mini spin column. RNA isolation was performed according to the manufacturer's protocol using the RNeasy Mini Kit (QIAGEN, Crawley, UK, # 74104) including optional DNase I (QIAGEN, Crawley, UK, # 79254) treatment to remove contaminating DNA. This isolation procedure is based on ion exchange chromatography. By varying the pH and/or salt concentration in the buffers, RNA is either bound or released from the silica membrane. Small RNAs (< 200 bp) such as miRs are lost during this procedure.

2.7.2 RNA isolation from tissue

Frozen tissue was placed in RLT lysis buffer (1% (v/v) β-ME) and disrupted by use of a rotor-stator homogeniser (Polytron PT 2500 E), which achieves tissue/cell disruption and homogenisation simultaneously by fluid turbulence and mechanical shearing. Samples were loaded on QIAshredder columns (QIAGEN, Crawley, UK, # 79654), centrifuged for 2 min at 16,000 g to further disrupt any remaining cellular components. The tissue lysates was enzymatically digested by adding 1 mL proteinase K (0.35 mg/mL, Roche Applied Science, Burgess Hill, UK, # 03115879001) and incubation at 55 °C for 10 min. Digested proteins and cellular debris were pelleted by centrifugation at 16,000 g for 3 min and 1.5 µL of supernatant transferred to a 2 mL centrifuge tube. 1 mL EtOH was added and the sample (including precipitates) transferred to an RNeasy Mini spin column. Downstream purification was performed using an RNeasy mini kit (QIAGEN, Crawley, UK, # 74104) including optional DNase I digestion, as described in section 2.7.1.

2.7.3 RNA quantification and quality control

After RNA elution in nuclease-free H_2O, RNA aliquots were diluted in Tris-EDTA buffer (TE, 100 mM tris-HCl, 10 mM EDTA, pH 8.0). Shifting to this slightly alkaline pH increases the ability to detect protein contamination by photospectrometry (Wilfinger *et al.* 1997). When a low yield was expected e.g. after isolation from cells in culture with eluent volumes of 35 µL, 5 µL RNA solution were diluted in 55 µL TE buffer. If larger yields were anticipated e.g. in tissue-derived preparations, RNA was eluted in 50 µL H_2O and 1 µL RNA was added to 59 µL TE for measurement. After blanking against 60 µL TE, the light absorbances of the diluted samples were measured in a UVette plastic cuvettes (Eppendorf, Cambridge, UK, # 0030 106.318) over a spectrum of wavelengths using a photospectrometer (BioPhotometer plus, Eppendorf, Cambridge, UK). At 260 nm wavelength, the linear range for accurate quantification is A_{260} = 0.10-1.0. In TE, the ratio between the absorbance measured at 260 nm and 280 nm (A_{260}/A_{280}) should ideally range between 1.9 and 2 to indicate good sample purity. Depending on the sample type (specific cell lines/tissues etc.) and on the buffer pH the actual A_{260}/A_{280} value can be slightly higher or lower. Contaminating proteins and some chemicals such as phenol absorb light at a wavelength of 230 nm. A_{260}/A_{230} ratios >1.7 indicate sufficient purity of RNA from these contaminants. The concentration of RNA in the sample was determined by applying the Beer-Lambert law.

Beer-Lambert law:

$$A = \varepsilon * c * l$$

A = Absorbance
ε = Extinction coefficient
c = Concentration
l = Path length (of the cuvette)

The extinction coefficient of RNA (ε_{RNA}) is 0.025 $mg/mL^{-1}cm^{-1}$. Consequently the concentration of RNA (c_{RNA}) can be calculated by the following formula considering that l = 1 cm.

$$c_{RNA} = 40\ \mu g/mL * A_{260} * \text{dilution factor}$$

Following quantification, RNA samples were either stored at -80 °C or immediately used for complementary DNA (cDNA) synthesis (Section 2.8.1).

2.8 mRNA copy number analysis

The most robust and widely used technique to study mRNA transcript abundance in whole organs, tissues or specific cells is real-time polymerase chain reaction (rtPCR). As the name indicates, this technique is based on specific sequence amplification by PCR. To achieve this, two separate reactions are required. First, the mRNA sequence needs to be reversely transcribed into complementary DNA (cDNA). This process is non-specific, meaning that a cDNA copy is generated for every polyadenylated strand of RNA present. cDNA is synthesised by the commercial enzyme Multiscribe® Reverse Transcriptase which is a recombinant protein derived from Moloney murine leukaemia virus reverse transcriptase (Stoye and Coffin 1987), Applied Biosystems [Internet], Carlsbad, CA, TaqMan® Reverse Transcription Reagents, © 2012, Cited 16/04/2012, Available from: http://products.invitrogen.com/ivgn/product/4304134?ICID==Search-Product). The relative quantity of a particular cDNA can be determined by rtPCR using a highly expressed internal standard, such as 18S ribosomal subunit or GAPDH as a reference. The amount of the corresponding cDNA is directly proportional to the amount of the mRNA of interest in the original RNA sample.

2.8.1 cDNA synthesis

RNA samples stored at -80 °C were thawed on ice. The reverse transcription reaction was setup on ice using the chemicals shown in **Table 2.5**. Briefly, a master mix was prepared containing all components except the RNA and was aliquoted into nuclease-free PCR tubes. RNase inhibitors (Applied Biosystems, Carlsbad, CA, USA, # N8080234) were included to prevent RNA degradation before or during reverse transcriptase PCR.

Table 2.5: Recipe for cDNA synthesis. All reagents were supplied with the MultiScribe® reverse transcription kit (Applied Biosystems, Carlsbad, CA, USA, # N8080234).

Components	**Volume**
RT Buffer (10X)	1.0 µL
Random Hexamers (50 µM)	0.5 µL
dNTP Mixture (10 mM)	2.0 µL
$MgCl_2$ Solution (25 mM)	2.2 µL
RNase inhibitor	0.2 µL
MultiScribe® MuLV Reverse Transcriptase	0.625 µL
Nuclease-free H_2O (Sigma-Aldrich Company Ltd., Gillingham, UK, # W4502)	0.475 µL
RNA (100 ng/µL)	1 µL
Total Volume	10 µL

RNA was added in the last step and the tubes loaded on a PHC-3 Thermal Cycler (Techne Bibbi Scientific, Stone, UK). Thermocycler conditions for cDNA synthesis are displayed in **Table 2.6**.

Table 2.6: Thermo cycler program for cDNA synthesis.

Stage	**Duration**	**Temperature [°C]**
1 cycle	10 min	25
	30 min	48
	5 min	95

cDNA was either stored at -20 °C or immediately used for rtPCR. Stock cDNA (~10 ng/µL) was diluted 1/5 to achieve a final concentration of ~2 ng/µL which was used for subsequent rtPCR. The concentration of 10 ng/µL of the cDNA stock solution was not precisely determined but estimated based on the amount of RNA used for cDNA synthesis.

2.8.2 Real-time polymerase chain reaction

Real-time polymerase chain reaction (rtPCR) was performed on a ABI 7500 FAST (Applied Biosystems, Carlsbad, CA, USA) platform using Fast optical tubes and 96-well plates (0.1 mL, Applied Biosystems, Carlsbad, CA, USA, # 4358297, 403012) and Taqman® Fast Advanced Master Mix (Applied Biosystems, Carlsbad, CA, USA, # 4444557). A master mix for all samples was prepared according to **Table 2.7** (omitting the cDNA) and aliquoted into the reaction wells.

Table 2.7: Recipe list for fast real-time PCR reactions. The concentration of cDNA is estimated from the amount of RNA used during the reverse transcription reaction. For genes of interest (GOI) with low transcript abundance, higher volumes of cDNA (e.g. 4 µL for measuring cytokines) were used.

Components	**Volume**
Taqman® Fast Advanced Master Mix	10 µL
18S Reference (20X)	1 µL
GOI Probe (20X)	1 µL
Nuclease-free H_2O (Sigma-Aldrich Company Ltd., Gillingham, UK, # W4502)	5 µL
cDNA (~2 ng/µL)	3 µL
Total Volume	20 µL

Finally cDNA samples were added, the plates sealed using optical adhesive film (Applied Biosystems, Carlsbad, CA, USA, # 4311971) and centrifuged for 3 minutes at 1500 g to remove any air bubbles from the bottom of each well potentially introduced during pipetting. **Table 2.8** shows the cycler conditions for the rtPCR reaction.

Table 2.8: Thermo cycler program for Fast rtPCR reactions.

Stage	**Temperature [°C]**	**Time**
Hold	95	10 min
40 Cycles	95	15 s
	60	60 s

The probe for the gene of interest (GOI) is frequently labelled with the reporter dye FAM™ at the 5' end and a non-fluorescent quencher (NFQ) as well as minor grove binder (MGB) situated at the 3' end. FAM™ is fluorescent dye emitting light at 520 nm upon excitation. In the native state of the probe, NFQ suppresses FAM™ fluorescence by Förster-type energy transfer (Förster 1948). MGBs increase melting temperature (T_m) and hence allow for design of shorter probes (Afonina *et al.* 1997; Kutyavin *et al.* 1997). A reference probe, labelled with a 5' VIC® reporter dye and a TAMRA™ quencher at the 3' end, is used for simultaneous analysis with the target gene a process referred to as duplex rtPCR. Upon excitation VIC emits light at 580 nm. Following hybridisation of each probe to their respective target cDNA, DNA polymerase cleaves off the FAM™ or VIC™ labels during the PCR reaction. Without quenching, free FAM™/VIC® emit a detectable fluorescent signal. The intensity of light emitted can be directly correlated to the number of target strands in the reaction. The cycle at which the emitted light reaches a certain threshold (set at the beginning of the linear range) defines the cycle threshold (Cт). The Cт of the GOI is normalised against the Cт of a

housekeeping gene, the expression of which must not be affected by the experiment (i.e. the drug used to treat the cells or animals). The housekeeping gene used throughout this study was the 18s ribosomal subunit.

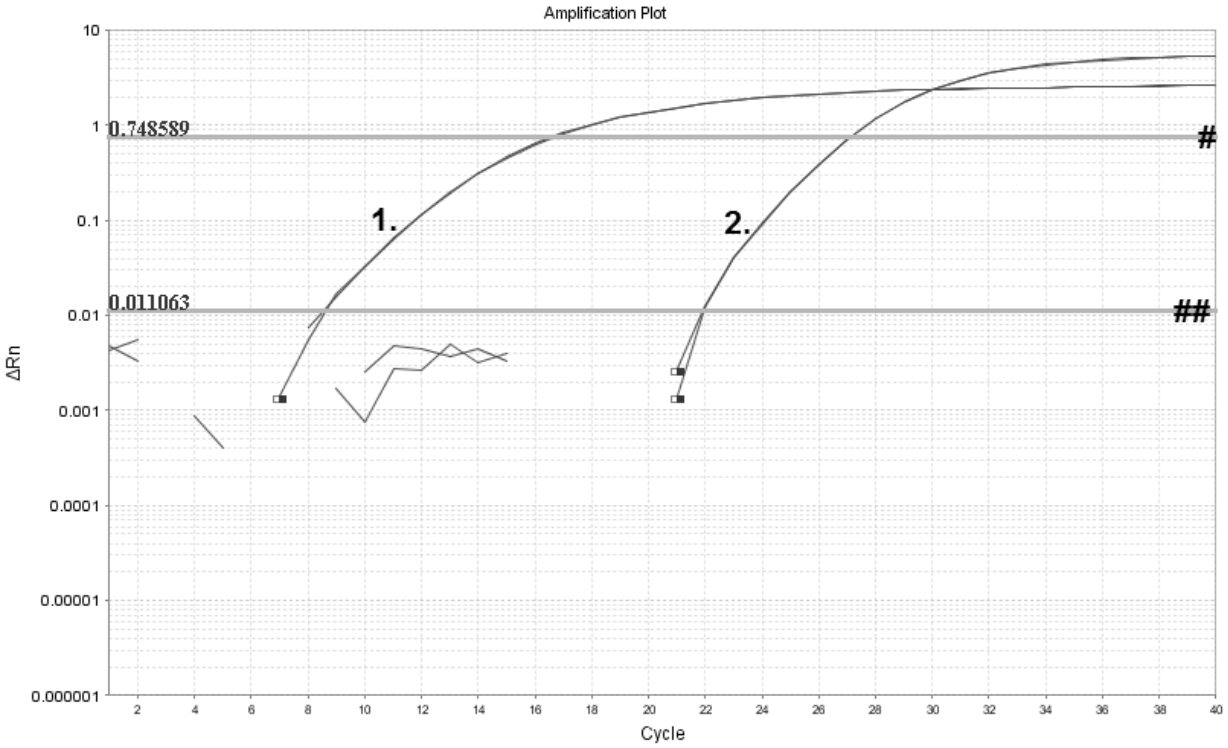


Figure 2.11: Exemplary result of a rtPCR reaction. (1.) Amplification curves of 18s reference. (2) Amplification curves of the GOI. The experiment was performed in duplicate and good matching of curves for individual targets was observed. (#) Cycle threshold (ΔCT) and (##) baseline are indicated.

The ΔCT value is achieved by subtracting C_{T18s} from C_{TGOI}, as indicated in the formula below.

Example calculation for determination of the relative expression:

$$\Delta C_T = C_{TGOI} - C_{T18s}$$

$$\text{Relative expression} = 2^{-\Delta Cm - \Delta Cm\ ref}$$

ΔC_{Tref} refers to the ΔCT value of the sample which is arbitrarily set as the expression reference (most commonly a sample of the control group). The relative expression of this sample is consequently 1.

The real-time PCR was performed in duplicate for each cDNA to decrease the impact of small pipetting inaccuracies. The resulting relative expression values were averaged. Validation of probes that are order made, such as the Tβ4 probe used in this study, is good

practice to ensure comparable PCR efficiencies between the mRNA of interest and the reference gene. This was performed by comparing expression of the GOI and the reference gene over a range of cDNA concentrations (0.03 to 25 ng) to generate a standard curve for each PCR from which the respective efficiencies were deducted.

2.8.3 Autophagy PCR Array

The RT^2 Profiler PCR Array (SABiosciences QIAGEN, Crawley, UK, # PAMM-084C-2) was used which contains a 96-well plate pre-primed with probes to 83 genes involved in the autophagy pathway. RNA was isolated from tissue following the protocol but commercial sterile nuclease-free water (Sigma-Aldrich Company Ltd., Gillingham, UK, # W4502) was used instead of DEPC treated ddH_2O. RNA purity and integrity were assessed using an Agilent BioAnalyzer 2100 (**Figure 2.12**, Agilent, Wokingham, UK). RNA integrity numbers (RIN) were routinely >8.0 indicating adequate RNA quality of the samples for PCR array analysis (minimum RIN >7, (Schroeder *et al.* 2006).

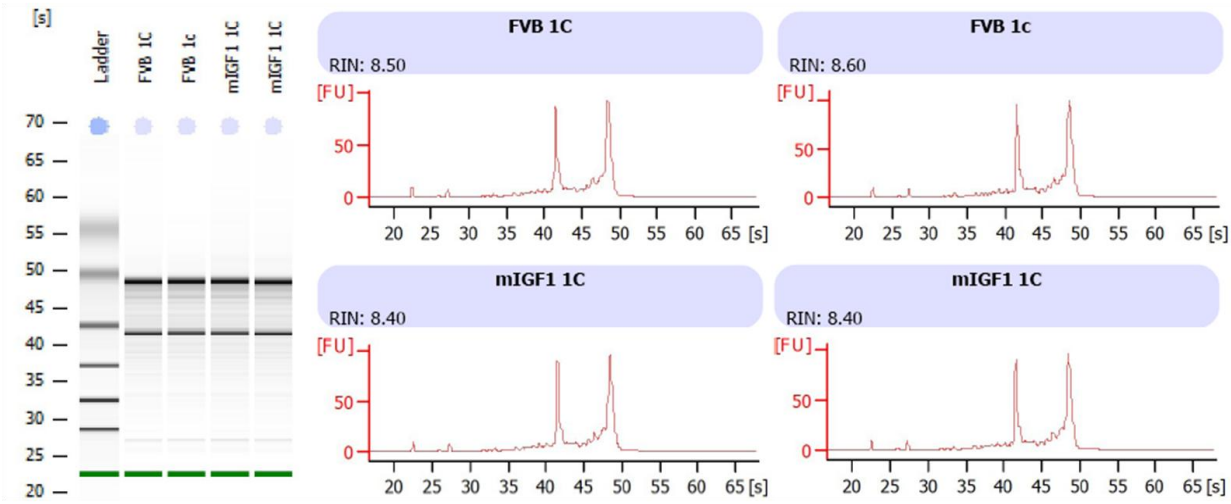


Figure 2.12: Exemplary result of RNA quality control using a BioAnalyzer 2100. Bands on the left panel represent 18s (lower band) and 28 ribosomal (upper band) subunits. RIN values are indicated above the electropherograms on the four panels on the right and are >8. Smearing or shouldering of the peaks of 18s/28s ribosomal subunits is not observed in any of the electropherograms.

As opposed to conventional rtPCR reactions, several GOIs are analysed on a PCR array simultaneously. Hence, the cDNA was added to the master mix during this experiment while the probes have been pre-plated into the wells by manufacturer. *Genomic DNA elimination*: As a precautionary measure, RNA is pre-treated before cDNA synthesis to remove any potentially remaining gDNA contamination. 1 µg of clean RNA and 2 µL of the proprietary gDNA Elimination Buffer (5X) were combined in a PCR tube and the total volume brought up

to 10 µL using nuclease-free H_2O. Components were mixed and incubated for 5 min at 42 °C and cooled on ice for at least 1 min. *cDNA synthesis:* cDNA was synthesised using the RT^2 First Strand Kit (SABiosciences QIAGEN, Crawley, UK, # C-03-330401) using the recipe displayed in **Table 2.9**.

Table 2.9: cDNA synthesis for PCR arrays. Quantities shown are for a single sample to be used on a single PCR array 96-well plate.

Components	**Volume**
RT Buffer 3 (5X)	4 µL
Primer & External Control Mix	1 µL
RT Enzyme Mix 3	2 µL
Nuclease-free H_2O (Sigma-Aldrich Company Ltd., Gillingham, UK, # W4502)	3 µL
cDNA (after gDNA elimination)	10 µL
Total Volume	20 µL

After adding all components to a PCR tube, the cDNA synthesis reaction is initiated by incubating the mixture for exactly 15 min at 42 °C. The reaction was stopped immediately by transferring the tube to a second heat block at 95 °C for 5 min. 91 µL of nuclease-free H_2O were added and the sample kept on ice followed by long term storage at -20 °C or used immediately. To investigate differential regulation of genes associated with autophagy, a Mouse Autophagy RT^2 Profiler PCR Array (SABiosciences QIAGEN, Crawley, UK, # PAMM-084C-2) containing 84 relevant probes was used. The plate included 5 different reference housekeeping genes to determine the relative expression of each of the 84 targets genes, as well as 1 mouse genomic DNA contamination control, 3 reverse transcription controls and 3 positive PCR controls. The rtPCR master mix was prepared in 50 mL falcon tube according to **Table 2.10**.

Table 2.10: rtPCR master mix recipe for Mouse Autophagy RT^2 Profiler PCR Array (96-well plate).

Components	Volume
RT^2 SYBR Green ROX qPCR Mastermix (2X, SABiosciences QIAGEN, Crawley, UK, # 330520)	1350 µL
Diluted First Strand cDNA Synthesis Mix	102 µL
Nuclease-free H2O (Sigma-Aldrich Company Ltd., Gillingham, UK, # W4502)	1248 µL
Total Volume	2700 µL

Precisely 25 µL were added to each well of the 96-well plate. The plate was sealed using the provided adhesive film and centrifuged for 1 min at 1,000 g to remove air bubbles. The plate was inserted into the ABI 7500 FAST rtPCR system which was programmed as indicated in **Table 2.11**.

Table 2.11: ABI 7500 FAST rtPCR machine settings for 96-well RT^2 Profiler PCR arrays (modified from SABiosciences QIAGEN [Internet], Crawley, RT2 Profiler PCR Array Handbook 11/2011, ©2011, Cited 16/04/2012, Available from: http://www.sabiosciences.com/Manual/1070190.pdf).

Stage	Temperature [°C]	Time
Hold	95	10 min
40 Cycles	95	15 s
	60	60 s

The experiment was performed in triplicate, using 3 separate plates for cardiac RNA samples of *αMHC/IGF-1Ea* transgenic mice and 3 separate plates for FVB control mice. This allowed statistical evaluation of the results without reproduction of data by single-gene rtPCR. Evaluation of raw data was performed using the SABiosciences online tool (SABiosciences QIAGEN, Crawley, UK).

2.9 gDNA extraction for gene copy number analysis

Genomic DNA was isolated from mouse tail samples using a QIAGEN DNeasy Blood and Tissue kit (QIAGEN, Crawley, UK, # 69504). The columns used in this kit contain a silica membrane which binds DNA (QIAGEN Ltd [Internet], Hilden, DNeasy® Blood & Tissue Handbook 07/2006, ©2003-2012, Cited 28/02/2012, Available from: http://www.qiagen.com/literature/render.aspx?id=523). Consecutive washes with buffers

containing high concentrations chaotropic salts (guanidine hydrochloride) remove water from hydrated macromolecules, which promotes DNA binding to silica and denatures proteins. 180 µL ATL lysis buffer and 20 µL proteinase K (QIAGEN, Crawley, UK, # 19131) were added to each tail sample in a 1.5 mL microcentrifuge tube. The sample was incubated overnight at 56 °C, thoroughly vortexed the following day and incubated for additional 30 min at 56 °C. To remove any undigested solids and debris the samples were centrifuged at 20,000 g for 5 min and the supernatant transferred to a fresh 1.5 ml tube. Although RNA does not generally amplify during normal PCR, it is good practice to remove unwanted nucleic acids to reduce the risk of interference. Residual RNA was removed by adding 4 µL of RNase A (100 mg/mL, QIAGEN, Crawley, UK, # 19101), mixing the sample, incubating at RT for 2 min and then vortexing again for 15 s. 200 µL of buffer AL (containing guanidine hydrochloride) and 200 µL EtOH (100%) were mixed separately, added to each sample and the suspension mixed immediately by vortexing to yield a homogenous solution. The suspension was loaded onto DNeasy Mini spin column and centrifuged at 6,000 g for 1 min. The flow-through was discarded and the membrane bound DNA washed with 500 µL buffer AW1 (containing guanidine hydrochloride), followed by a wash with 500 µL of buffer AW2. Buffers AW1 and AW2 contain EtOH to ensure that DNA remains precipitated on the membrane while other contaminants are washed out. The column was dried by centrifuging for 1 min at 20,000 g. 200 µL buffer AE (10 mM Tris-HCl, 0.5 mM EDTA; pH 9.0) were added directly on the membrane to rehydrate the DNA. The sample was incubated at RT for 1 min and then centrifuged for 1 min at 6,000 g to elute the purified gDNA.

2.9.1 DNA quantification and quality control

DNA concentrations were determined by spectrophotometry as previously described for RNA with minor deviations. As during RNA quantification, the absorbance is strongly dependent on pH. DNA sample were diluted 1/5 (v/v) in 10 mM Tris-HCl (pH 7.5). The linear range for this assay is between 0.1 and 1.0 absorbance units at 260 nm. Using the absorbance measured at a wavelength of 260 nm (A_{260}) the concentration of DNA (c_{DNA}) in the sample was determined using the following formula:

$$C_{DNA} = 50\ \mu g/mL * A_{260} * \text{dilution factor}$$

A_{260}/A_{280} values for purified DNA routinely ranged between ~1.8-2.0 indicating good purity of the DNA. A_{260}/A_{230} ratios were measured to detect any potential protein contamination in the sample.

2.10 *Cre* gene copy number analysis

The relative abundance of Cre gene copies was determined using a TaqMan® Copy Number Assay (Applied Biosystems, Carlsbad, CA, USA, # Mr00635245_cn). Procedure and principle are identical to mRNA copy number analysis with two exceptions: 1. synthesis of cDNA is not required since the starting material is gDNA and 2. a reference gene with a known copy number has to be selected as internal reference. During this study mouse transferrin receptor gene (*Tfrc*), chromosome 16, cytoband 16qB3 was selected. It is present in two copies in the diploid mouse genome. The Reference Assay (Applied Biosystems, Carlsbad, CA, USA, # 4458366) contains two primers and a VIC® dye labelled TAMRA™ probe. The assay to target *Cre* (Applied Biosystems, Carlsbad, CA, USA, # Mr00635245_cn) contains *Cre* specific primers and a FAM™ dye labelled MGB probe. As recommended by the manufacturer, TaqMan® Genotyping Master Mix (Applied Biosystems, Carlsbad, CA, USA, # 4371355) as opposed to conventional TaqMan® Universal Master Mix was used during this study. After isolation and purification gDNA samples were diluted in nuclease-free water to a concentration of 5 ng/µL. The PCR reaction mix was prepared as indicated in **Table 2.12**.

Table 2.12: PCR reaction setup for *Cre* gene copy number analysis using a 96-well reaction plate (modified from Applied Biosystems [Internet], Carlsbad, CA, TaqMan® Copy Number Assays Manual 09/2010, ©2010, Cited 16/04/2012, Available from: http://tools.invitrogen.com/content/sfs/manuals/cms_062368.pdf).

Reaction Mixture Component	**Volume**
2X TaqMan® Genotyping Master Mix	10 µL
TaqMan® Copy Number Assay (20X)	1 µL
TaqMan® Copy Number Reference Assay (20X)	1 µL
Nuclease-free H_2O (Sigma-Aldrich Company Ltd., Gillingham, UK, # W4502)	4 µL
gDNA (5 ng/µL)	4 µL
Total Volume	**20 µL**

A master mix containing all components except gDNA was prepared and loaded on MicroAmp® *Fast* Optical 96-well reaction plates (Applied Biosystems, Carlsbad, CA, USA, # 4349609) before adding gDNA to each well. The reaction plates were sealed with optical adhesive film (Applied Biosystems, Carlsbad, CA, USA, # 4311971) and inserted into the ABI 7500 Fast System real-time PCR instrument. The run was performed using the conditions displayed in **Table 2.13**.

Table 2.13: Instrument settings for gene copy number analysis using TaqMan® reagents (modified from Applied Biosystems [Internet], Carlsbad, CA, TaqMan® Copy Number Assays Manual 09/2010, ©2010, Cited 16/04/2012, Available from: http://tools.invitrogen.com/content/sfs/manuals/cms_062368.pdf).

Stage	Temperature [°C]	Time
Hold	95	10 min
40 Cycles	95	15 s
	60	60 s

Threshold and baseline values were set manually into the linear portion of the amplification curve (log view). C_T values of *Tfrc* and *Cre* were exported into Excel and the relative expression calculated as reported in Section 2.8.2. gDNA samples from C57Bl/6 wt animals were used as negative controls.

2.11 Histology

Investigating abundance and localisation of proteins inside organs, tissues or individual cells provides valuable information about their function frequently obtained by immunofluorescence staining and immunohistochemistry. Briefly, binding of specific antibodies to the protein or peptide of interest in processed tissue sections or cell preparations is following by interaction of a species specific secondary antibody conjugated to a fluorescent label used for detection. The fluorescent tag is excited by laser and the signal captured by fluorescence or confocal microscopy. Depending on the nature of the staining either frozen sections (cryosections) or paraffin-embedded sections are used. While the structural integrity of the tissue is better preserved in the latter technique, epitopes are masked to a higher degree compared to cryosections. The trade-off between structural preservation and good epitope presentation has to be considered depending on the aim of each experiment.

2.11.1 Staining of OCT embedded sections

Samples were harvested from mice and blood removed as described in section 2.4. The full heart or the relevant part thereof was placed in a rectangular plastic mould containing sufficient OCT compound to fully cover the sample. The mould was immediately placed in liquid nitrogen to instantly freeze the sample. Samples were stored at -80 °C. 6-10 µm sections were cut at -20 °C using a Leica CM 850 cryostat (Leica Microsystems, Milton Keynes, UK) and transferred to polysine slides (VWR, Lutterworth, UK, # 631-1349). The slides were allowed to dry at RT and fixed by immersion in acetone (100%) at RT for 5 min.

Slides were then air-dried at RT, wrapped in foil and stored at -20 °C. In preparation for staining, slides were thawed and washed once briefly with PBS. After blocking with 3% (w/v) BSA in PBS, slides were incubated with primary antibody in PBS for 1 h at RT. After three 5 min washes with PBS, slides were incubated with fluorophore-coupled secondary antibody in PBS for 1 h at RT. To mask elastin fibre autofluorescence pontamine skye blue (Sigma-Aldrich, Gillingham, UK, # C8679) was added and the slides incubated for 6 min at RT (Cowen *et al.* 1985). Slides where then washed twice and nuclei stained with DAPI (Sigma-Aldrich, Gillingham, UK, # 32670) at a concentration of 1/20,000 for 7 min each (Kapuscinski 1995). Slides were mounted with PermaFluor™ (Thermo Fisher Scientific, Loughborough, UK, # LVTA006FM) and analysed using a Nikon DMx1200 camera mounted on a Zeiss Axioscope microscope. Images were captured using NIS elements software V (Nikon Instruments, Melvile, NY, USA). Method specificity was tested by use of secondary antibody alone (negative control) which did not result in a specific staining pattern.

2.11.2 Paraffin-embedding of tissue

Samples destined for paraffin embedding were harvested as described in Section 2.4 and placed in 10% v/v formal saline (1.54 M NaCl, 10% v/v formaldehyde). Formaldehyde is a fixative that crosslinks primary amino groups thus preserving tissue and protein integrity. Following overnight incubation at 4 °C, formal saline was replaced with 0.2 M phosphate buffer. Fixed samples stored at 4 °C are stable for years. After fixing, samples were embedded in paraffin using a Leica TP 1020 tissue processor (Leica Microsystems, Milton Keynes, UK). During this process water is removed by an increasing gradient of EtOH before incubation in xylene and embedding into paraffin blocks.

2.11.3 Masson's Trichrome Staining

All dyes used during this procedure were filtered before use. Paraffin-embedded tissue sections were deparaffinised and brought to water by immersion into the following reagents for 2 min each: xylene, xylene, EtOH (100%), EtOH (100%), EtOH (70%), H_2O followed by a final wash under running tab water for 5 min. Slides were transferred into Celestine blue (Sigma-Aldrich, Gillingham, UK, #206342) for 5 min to stain nuclei, followed by a dH_2O wash for 3 min. The sections were then immersed in haematoxylin (Sigma-Aldrich, Gillingham, UK, # HT15), a second nuclear stain for 5 min, washed under running water for 5 min. To stain muscle tissue red, slides were then immersed in acid fucsin (Sigma-Aldrich, Gillingham, UK, #HT15) for 5 min before washing twice by immersion in dH_2O. The slides were then differentiated in phosphomolybdic acid solution (Sigma-Aldrich, Gillingham, UK, # HT15) for 10 min. The dye was drained carefully from the slide but no wash step performed. Slides were then immersed in methyl blue (Sigma-Aldrich, Gillingham, UK, # M6900) to stain

collagen and washed briefly under running tab water. Finally, the sections were dehydrated by increasing EtOH gradient and xylene (70%, 100%, 100%, xylene, xylene), mounted with DPX (VWR, Lutterworth, UK, # LEIC08600E) and dried for 30 min at RT.

2.12 Transmission electron microscopy

Day 1: PFA-fixed samples were removed from the 0.1 M phosphate storage buffer. The ~2 mm^3 tissue blocks were fixed by incubation in 2.5% glutaraldehyde (9 mL 0.1 M phosphate buffer, 1 mL 25% glutaraldehyde, Agar Scientific, Stansted, UK # R1020) for 2 h. Samples were washed twice for 5 min each before 1% osmium tetroxide (Agar Scientific, Stansted, UK, # R1019) in EM buffer was added. Osmium tetroxide fixes lipoproteins of membranes and is consequently very important for structural preservation. Samples were incubated on a rotor in a fume cabinet for 1 h at RT. Samples were then washed twice as described and dehydrated via acetone gradient (50%, 70%, 95%, 100%, 100% acetone - 30 minutes each) and placed in propylene oxide (Agar Scientific, Stansted, UK, # R1080) for 30 min on a rotor. Propylene oxide further dehydrates the samples and facilitates resin penetration into the specimen in subsequent steps. Araldite resin consists of three-components: 100 mL of araldite CY212 (Agar Scientific, Stansted, UK, # R1040) and dodecenyl succinic anhydride (DDSA, Agar Scientific, Stansted, UK, # R1051) mixed with 2 mL crosslinker/accelerator benzyl dimethylamine (1:1 v/v, BDMA, Agar Scientific, Stansted, UK, # R1060). Samples were incubated at RT overnight in a 1:1 mixture of propylene oxide and the epoxy resin araldite (Agar Scientific, Stansted, UK, # R1040) to allow complete penetration of araldite into the sample block. The samples were placed into embedding molds and covered with resin and dried at 60 °C overnight.

Day 2: Samples were placed in pure araldite resin and incubated without a cover, at RT for >2 h on a rotor. This allowed propylene oxide to evaporate from the sample. The resin was replaced by fresh resin and the samples incubated for another 2 h, as described.

Day 3: Using a self-made glass blade, tissue blocks were trimmed and coarse 1 µm sections cut. Coarse sections were placed on a coverslide and quick-stained with 1% toluidine blue (Agar Scientific, Stansted, UK, # R1727) in 1% sodium tetraborate (Borax, Taab, Aldermaston, UK, # B021). Following a quick rinse with water the orientation and integrity of the section was determined by light microscopy. After identification of a suitable cutting area, ultra-thin sections (100 nm) were cut from the block using a diamond blade on a Reichert-Jung Ultracut E ultramicrotome and placed on 200 µm EM copper grids. Ultra-thin sections were stained with 2% aqueous uranyl acetate for 10 min, washed with ddH_2O (three times 5 minutes by immersion in separate baths) and placed on lead nitrate droplets consisting of lead nitrate (Agar Scientific, Stansted, UK, # R1217) in tri-sodium citrate (Agar Scientific,

Stansted, UK, # R1106) for 30 min at RT according to Reynolds' Lead Nitrate stain method. After 10 min, the specimens were washed as described and counterstained with lead citrate (Agar Scientific, Stansted, UK, # R1210) for 10 minutes and washed with ddH_2O. After final stream-washing with ddH_2O the samples were analysed using a Jeol 1200 XE electron microscope (Jeol, Herts, UK) and micrographs captured using a Gatan digital camera (Gatan, Abingdon Oxon, UK).

2.12.1 Immunogold labelling

For immunogold labelling, PFA-fixed cardiac tissue was quenched in 0.5 M ammonium chloride for 30 min to bind free aldehyde hindering staining. Specimens were washed with 0.1 M phosphate buffer and embedded according to the method of Roth *et al.* (Roth *et al.* 1978). Dehydration by graded acetone series was performed at 4 °C (30%, 50%) and -20 °C (70%, 90%, 100%). Samples were then embedded in the acrylic resin Lowicryl HM20 (Agar Scientific, Stansted, UK, # R1210) which was prepared in 1:1 and 1:2 mixtures with MeOH (100%) and incubated for 1 h each at -20 °C. The specimen were then incubated in pure Lowicryl resin over 2 days at -20 °C with 3-4 resin changes in the course. This is performed to eliminate all alcohol from the sample which would disturb sample integrity during sectioning. The specimen were placed in Taab embedding capsules (Taab, Aldermaston, UK, # C050) and covered in Lowicryl resin and the resin cured in a UV box at -20 °C. Sample integrity and orientation was examined using the quick-staining technique before cutting of ultra thin sections as described in Section 2.12. Sections were placed on formvar-coated nickel grids and blocked with Aurion 1% (w/v) BSA-c™ (Aurion, Wageningen, The Netherlands, # 900.022) solution for 30 min following incubation with the respective antibody at concentrations of 1/10 rabbit anti-LC3 (Abgent) or 1/20 rabbit anti-cathepsin D (Merck Calbiochem) for 1 h at RT. Sections were washed three times for 5 min with filtered PBS and incubated with 15 nm gold conjugated anti-rabbit goat IgG (BBInternational BioCell, Cardiff, UK, R14010) at a concentration of 1/100 for 1 h at RT. Post-staining was performed using Reynolds' Lead Nitrate stain method and electron micrographs recorded as described previously.

2.13 Production of recombinant V5-His_6-tagged thymosin β4-V5/His protein

Total RNA was isolated from the hearts of 3 month old male FVB mouse by phenol-chloroform extraction and purified as described in Section 2.7.2. cDNA was produced by one cycle of rtPCR from 200 ng RNA starting material as described (Section 2.8.1). Using *Tβ4* specific primers (forward 5' – ACC ATG TCT GAC AAA CCC GAT ATG – 3' and reverse 5' – CGA TTC GCC AGC TTG CTT CTC TTG - 3'), cDNA was amplified by PCR using *Pfx*

proofreading polymerase (Invitrogen, Carlsbad, CA, USA, # 11708-013) which has a higher fidelity compared to normal *Taq* polymerase.

cDNA sequence of *Tβ4*: 5' AT GTCTGACAAA CCCGATATGG CTGAGATCGA GAAATTCGAT AAGTCGAAGTTGAAGAAAAC AGAAACGCAA GAGAAAAATC CTCTGCCTTC AAAAGAAACA ATTGAACAAGAGAAGCAAGC TGGCGAATCG TAA – 3' (CDS, GenBank: AL731735.14)

Table 2.14: PCR conditions for Tβ4 amplification from cDNA.

Gene	**Recipe**	**Thermocycler conditions**	**Size of amplified fragment**
Thymosin β4	60 µL reaction: 5 µL *Pfx* Buffer (10x) 1 µL $MgSO_4$ 1.5 µL dNTP 5 µL Tβ4 primer mix (10µM each) 1 µL *Pfx* Polymerase (Invitrogen, Carlsbad, CA, USA, # 11708-013) 36.5 µL ddH_2O 5 µL Enhancer solution + 5 µL cDNA (	5 min at 95 °C 30 x 30 s at 95 °C 1 min at 55 °C 2 min at 72 °C 10 min at 72 °C ∞ 4 °C	135 bp

On ice, 1 µL standard Taq polymerase (Promega, Southampton, UK, # M8306) was added to the PCR product and the sample incubated at 72 °C for 10 min. This resulted in the addition of 3' adenine overhangs on the PCR products which was required for subsequent cloning. The presence of a single band indicating a specific reaction was assessed by agarose gel-electrophoresis.

2.13.1 Cloning of Tβ4

Tβ4 cDNA was cloned into vector pcDNA3.1/V5-His© TOPO® TA (Invitrogen, Carlsbad, CA, USA, # K4800-01, **Figure 2.13**).

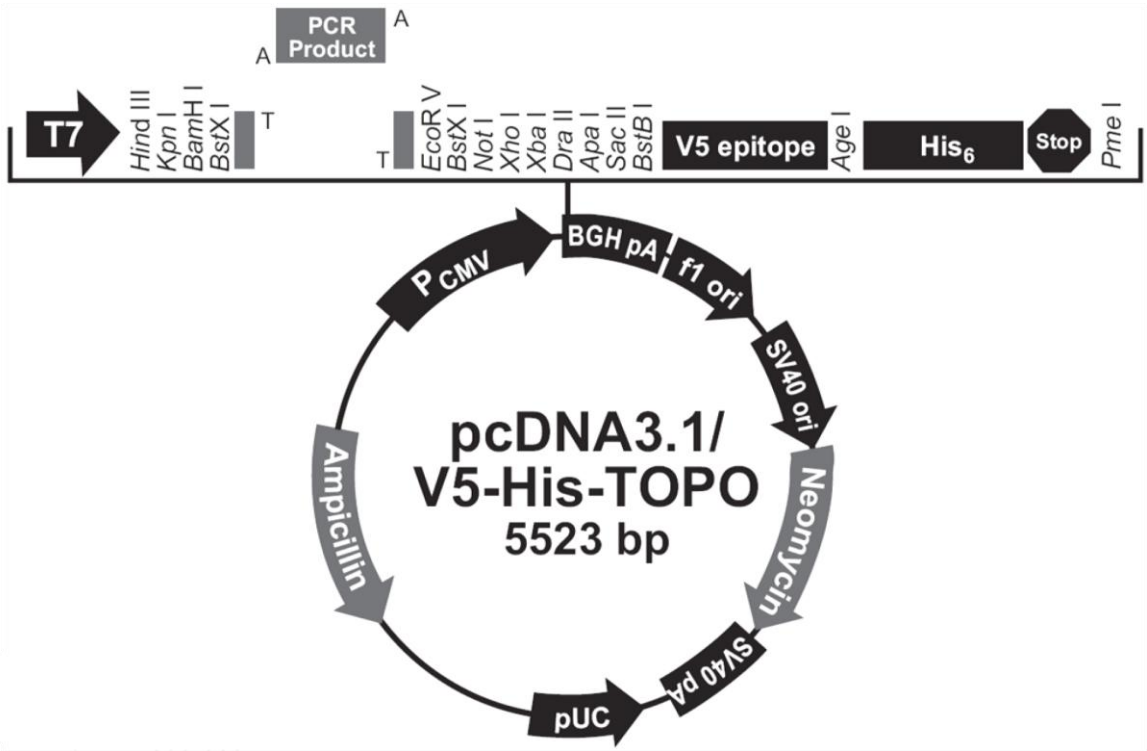


Figure 2.13: Vector used for the generation of recombinant Tβ4. *Tβ4* cDNA was cloned into the pcDNA3.1/V5-His-TOPO vector. (Invitrogen [Internet], Carlsbad, CA, pcDNA™3.1/V5-His TOPO® TA Expression Kit Manual 10/04/2009, ©2009, Cited 16/04/2012, Available from: http://tools.invitrogen.com/content/sfs/manuals/pcdna3.1topota_man.pdf).

Briefly, 3 µL undiluted PCR product were mixed with 1 µL salt solution (Invitrogen, Carlsbad, CA, USA, # 4800-01) and 1 µL vector. The 2 µL of this reaction mix were added to 50 µL DH5α™ Library Efficient® *Escherichia coli* suspension (*E. coli*, Invitrogen, Carlsbad, CA, USA, # 18263-012) and incubated for 30 min on ice, 30 s at 42 °C and 2 min again on ice. Control transformations were performed using the empty and a *LacZ* expressing control vectors. Transformed bacteria were incubated in 250 µL SOC medium (Invitrogen, Carlsbad, CA, USA, # 15544-034) at 37 °C for 1h. Volumes of 50 µL and 200 µL were streaked out on LB ampicillin agar plates (0.1 mg/mL ampicillin) and incubated at 37 °C overnight. The following morning 10 individual colonies were picked from the plates and grown in 4 mL Luria broth containing 4 µL ampicillin (100 mg/mL) overnight. The following day 150 µL glycerol were added to an aliquot of 850 µL LB culture and the sample stored at -80 °C. The remaining bacterial culture was used for DNA isolation using a QIAprep Spin Miniprep kit (QIAGEN, Crawley, UK, # 27104) according to manufacturer's instructions. This technique is based on alkaline lysis of bacteria with subsequent adsorption of DNA to a silica membrane, washing and elution in 10 mM TrisCl, pH 8.5 (Birnboim and Doly 1979). To control the transformation procedure *LacZ* control-plasmid transformed clones were tested by β-galactose activity assay. X-gal plates were prepared by covering regular LB ampicillin agar

plates with 40 µL X-gal solution (40 mg/mL in dimethylformamide) and drying for 15 min. *LacZ*-V5-His_6-transformed bacteria and clones containing the empty vector were streaked out on X-gal plates and incubated over night The *E. coli* strain used is deficient for LacZa, a β-galactosidase subunit, but expresses the complimentary LacZ∆M15 subunit. Together these peptides form the functional β-galactosidase enzyme. Active β-galactosidase is observable by blue coloured colonies on X-gal plates. This colour arises when X-gal is hydrolysed into an insoluble blue compound. This can be detected by eye and indicates successful transformation and LacZ expression.

2.13.2 Confirmation of positive clones

To confirm the presence and orientation of *Tβ4* cDNA within the vector, purified plasmid DNA was digested with *MfeI* endonuclease (New England BioLabs, Ipswitch, MA, USA, # R0598L) at 37 °C for 1 h. Plasmids containing the insert in the correct orientation yielded two fragments of 891 bp and 4767 bp after separation on 2% agarose gels. Bands of 826 bp and 4832 bp were observed for the inverse orientation. *MfeI*-digested control vectors yield bands of 8592 bp (linearised *LacZ* vector) and 5536 bp (linearised empty vector). DNA from positive *Tβ4* clones was sent for sequencing to the Imperial College Genomics Laboratory core facility using the following primers: T7 (forward) 5´ - TAA TAC GAC TCA CTA TAG GG - 3´ and BHG (reverse): 5´ - TAG AAG GCA CAG TCG AGG - 3´.

2.13.3 Tβ4-V5-His protein expression in *E. coli*

Bacterial stocks of positive clones were thawed and grown overnight in a 200 mL LB containing ampicillin (100 µg/mL). Aliquots were stored at -80 °C as described. 4 mL of the bacterial suspensions were used for DNA isolation using the Miniprep kit with subsequent *MfeI* digest to control continued presence of the correctly oriented insert. The remaining culture volumes were used for protein isolation using a Bacterial PE LB™ kit (G-Biosciences, Maryland Heights, MO, USA, # 786-176). Bacterial cells were pelleted by centrifugation at 5,000 g for 10 min, the supernatant discarded and the pellet dissolved in 5-10 volumes of proprietary Bacterial-*PE*-LB buffer. After homogenisation by vortexing and brief chilling of the sample (4 °C), lysozyme was added (5% v/v final) and the suspension incubated at 37 °C for 60 min. The sample was vortexed several times for 30 s each to complete lysis. Genomic DNA was sheared by passing the lysate 10 times through a 20 G needle. Finally, the sample was centrifuged at 20,000 g for 30 min at 4 °C and the clear supernatant collected.

In the event of protein aggregation as intracellular inclusion bodies, pellets were washed twice in 10x diluted Bacterial-*PE* LB buffer. For every 100 mg of pellet, 1 mL of proprietary IBS buffer and 1M DDT (to 20 mM final) were added and the pellets resuspended. Samples were agitated on a shaker for 1 h at 4 °C before centrifugation at 30,000 g for 15 min at 4 °C

and collection of protein-containing supernatant. Protein extracts were quantified and recombinant Tβ4-V5-His_6 expression analysed by immunoprecipitation and Western blotting using HRP conjugated anti-V5 antibodies (Invitrogen, Carlsbad, CA, USA, # R960-25).

2.13.4 Tβ4-V5-His protein expression in mammalian cells

HeLa cells were selected as the mammalian expression system due to their fast growth and ease of culture. Cells were grown in 10 cm^2 tissue culture dishes in standard cell culture medium consisting of high glucose DMEM (Sigma-Aldrich, Gillingham, UK, # D5671), 10% fetal bovine serum (FBS, Sigma-Aldrich, Gillingham, UK, # F6178), 1% L-glutamine (Sigma-Aldrich, Gillingham, UK, # G8540) and 1% penicillin/streptomycin (P/S) mix (Sigma-Aldrich, Gillingham, UK, # P4333). One day before transfection cells were washed with PBS to remove P/S which would exert cytotoxicity in combination with the transfection reagent. Cells were cultured in normal medium lacking P/S overnight. On the day of transfection, at 80-90% confluency, a transfection mix consisting of 100 µL opti-MEM (Invitrogen, Carlsbad, CA, USA, # 11058-021) containing 1-2 µg vector DNA was prepared. In a second reaction, 100 µL opti-MEM and 1-2 µL Lipofectamine (Invitrogen, Carlsbad, CA, USA, # 18324-012) were mixed. The two solutions were combined, gently mixed and incubated at RT for 30 min. Additional 600 µL opti-MEM were added. The total volume of 800 µL was combined with 3.2 mL transfection medium, which is normal growth medium without P/S and serum. The old medium was removed from the cells and the culture incubated with the 4 mL transfection solution for 6 h in a CO_2 incubator. The transfection medium was removed and the cells washed with PBS to remove residual Lipofectamine. Cells were allowed 2-3 days to recover in normal medium before harvest of proteins as described in Section 2.5.1. To generate a stable Tβ4-V5-His_6 overexpressing cell line, transfected HeLa cells were selected against G-418 for 1 week at 400 µg/ml and 2 weeks at 200 µg/mL. One day before harvesting G-418-containing medium was exchanged for normal growth medium.

2.13.5 Purification of His-tagged recombinant proteins

Isolation and purification of Tβ4-V5-His_6 was performed using the ProBond purification kit (Invitrogen, Carlsbad, CA, USA, # 45-0055) with modification to the original protocol (Invitrogen [Internet], Carlsbad, CA, ProBondTM Purification System Manual 02/09/2004, ©1997-2004, Cited 16/04/2012, Available from: http://tools.invitrogen.com/content/sfs/manuals/xprpur_man.pdf). Cells (bacteria or mammalian) were pelleted and resuspended in 8 mL guanidium lysis buffer (6 M guanidine HCl, 2 mM NaH_2PO_4, 500 mM NaCl) and agitated for 15-20 min. The suspension was pulsed 3 times for 10 s each using a sonicator, shock frozen in liquid nitrogen and warmed up to 37 °C. Homogenates were passed through a 16 G syringe to shear DNA and the samples

centrifuged at 3,000 g to pellet cell debris and the supernatant transferred. 2 mL nickel resin were used per column, which is sufficient to bind 10-20 mg of His_6-tagged protein. Binding was allowed for 30 min at RT. Since low expression levels were expected from previous experimentation the column was re-loaded with additional 8 mL lysates. After additional 30 min binding, columns were washed once with 4 mL denaturing binding buffer (8 M urea, 20 mM NaH_2PO_4 pH 7.8, 500 mM NaCl) and thrice with 4 mL denaturing wash buffer (8 M urea, 20 mM NaH_2PO_4, pH 6.0). This was followed by 4 washes using a more acidic denaturing wash buffer (pH 5.3). Finally, 4 mL denaturing elution buffer (8 M urea, 20 mM NaH_2PO_4 pH 4.0, 500 mM NaCl) were added and the solution eluted in ~1 mL fractions by gravity. To remove urea from the sample, fractions were dialysed against tris buffer (10 mM Tris pH 8.0, 0.1% Triton X-100) overnight at 4 °C using SnakeSkin Pleated Dialysis Tubing™ with a MWCO of 3.5 kDa (Thermo Fisher Scientific, Rockford, IL, USA, # 68035). Samples were stored at -80 °C until analysis by Tris-Tricine gel electrophoresis.

2.14 Immunoprecipitation

Day 1: Recombinant Tβ4-V5-His_6 was incubated with 2 mg cardiac protein extract in a total volume of 100 µL RIPA buffer for 2 h at RT. Pre-clearing was performed to remove substances that exhibit aspecific reactions with protein A/G from the protein mixture. Briefly, 20 µL Protein A/G beads (Santa Cruz Biotechnology, Santa Cruz, CA, USA, # sc-2003) were mixed with 100 µL protein sample and incubated on a rotor for 45 min at 4 °C. Samples were centrifuged at 600 g for 3 min and the supernatant transferred into fresh microcentrifuge tubes. 1.5 µL anti-V5 antibodies were added and the suspension incubated on a rotor overnight at 4 °C.

Day 2: 20 µL Protein A/G beads were added to sample. After 1 h incubation on a rotor at RT the samples were centrifuged at 600 g for 3 min and the supernatant aliquoted into a separate microcentrifuge tube. This supernatant was used as during Western blotting for quality control. The samples were washed by adding 500 µL RIPA buffer, mixing and centrifugation at 600 g for 3 min at RT. The supernatant was discarded and the procedure repeated once. A final wash was performed by adding 500 µL Tris (50 µM, pH 8.0), mixing and adding of 500 µL RIPA buffer. The sample was mixed again and a final centrifugation performed as for previous washes. The supernatant was discarded and pelleted beads re-suspended in 40 µL SDS sample buffer including β-mercaptoethanol in preparation for SDS PAGE analysis. Samples were boiled at 100 °C for 5 min and stored at -80 °C or used immediately. Prior to loading the gel, the samples were centrifuged to pellet the beads and only the supernatant was used for Western blotting analysis as described in section 2.6.2.

2.15 Thymosin β4 knockdown in neonatal cardiomyocyte preparations from mice

The culture of rodent neonatal cardiomyocytes (NCM) is a valuable technique in cardiac research from pharmacological safety testing to basic studies on CM function and molecular signalling. This technique exploits the resilience NCM retain during the first 1-2 days following birth (Porrello *et al.* 2011).

2.15.1 Neonatal cardiomyocyte preparation

This protocol is a modified version of the rat NCM protocol supplied with a kit of the same name by Worthington (Worthington Biochemical Corp., Lakewood, NJ, USA). Enzyme solutions were prepared in advance and stored at 4 °C (-20 °C for long term storage). Trypsin (~213 u/mg) was dissolved in 2 mL HBSS (Sigma-Aldrich, Gillingham, UK, # H6648), trypsin inhibitor in 1 mL HBSS and collagenase mix (1,085 u/mg) was reconstituted in 5 mL L-15 medium (all enzymes Worthington Biochemical Corp., Lakewood, NJ, USA). In preparation for plating the NCM on the following day, 6- or 12-well tissue culture plates were coated with fibronectin (Sigma-Aldrich, Gillingham, UK, # F0895). Briefly, fibronectin was dissolved in HBSS to a final concentration of 0.01 mg/mL using a total volume per well of 1 mL for 6-well plates and 400 µL for 12-well plates. After 12 h incubation at 4 °C most of the solution was aspirated leaving ~100 µL in the wells. Plates were dried in a cell culture hood and stored at 4 °C. Fibronectin was chosen since it resembles a physiological extracellular matrix component unlike digested gelatine preparations.

NCM prep day 1: A litter of 8-10 neonatal (P0 to P1) mouse pups was separated from their parents. After cervical dislocation the bodies were sprayed with 70% industrial methylated spirits (IMS) for sterilisation and placed in a tissue culture hood. Heads were removed and a ~ 5 mm anterior-posterior incision made into the thorax. Hearts were exteriorised by gentle lateral squeezing, excised and placed in approximately 10 mL HBSS in a 50mL Falcon tube on ice. Tools were sterilised between animals by spraying with 70% IMS. The tube containing the hearts was transferred on ice into a sterile tissue culture hood. Blood contaminated HBBS was aspirated and the hearts were washed twice with fresh, ice-cold HBSS. Following the last wash, 1 mL HBSS was added and the hearts transferred into a 10 cm^2 Petri dish. Atria were removed and discarded and the ventricular tissue finely minced using two sterile, disposable scalpels. Excess HBSS was aspirated. If significant blood contamination was still observed, the tissue was carefully washed by rinsing with HBSS. The homogenised tissue was transferred into a cm^2 Petri dish and 3 mL HBSS and 333 µL trypsin solution were added. Digestion was allowed for 12 h at 4 °C.

NCM prep day 2: The tissue was transferred into a 75 cm^2 cell culture flask using a plastic Pasteur pipette and at this point the homogenate should appear viscous indicating

successful pre-digestion. 166 µL trypsin inhibitor solution were added to the digest and the flask was placed in a 37 °C humidified CO_2 incubator for 15 minutes. After trypsin inhibition, 833 µL collagenase solution were added to the flask which was then placed in a shaking water bath. Digestion was checked after the first 30 minutes and every 5 minutes thereafter to prevent over-digestion. Once digestion was estimated to be 80-90% the flask was removed from the shaking waterbath. This was usually achieved within 45 min. Any residual chunks of tissue were further disrupted mechanically by pipetting the solution ten times up and down using a serological 10 mL pipette. A 70 µm mesh size cell strainer was pre-wetted with warm L-15 medium and placed on top of a new 50 mL falcon tube. Leaving any solid pieces of tissue in the flask, the suspension was carefully removed and filtered. The residual tissue was further disrupted by adding another 10 mL of L-15 medium and repeating the mechanical digestion. The resulting suspension was filtered, the suspensions pooled together and centrifuged at 1,000 g for 5 min to pellet the cells. The supernatant was aspirated and the cell pellet re-suspended in pre-warmed (37 °C) normal cell culture medium (as described in section 2.13.4).

Pre-plating: In order to separate cardiomyocytes from other cardiac cell populations, two to three pre-plating steps were performed. During these relatively short incubations, non-cardiomyocyte populations (mainly fibroblasts) attached to the tissue culture flask. Cardiomyocytes require more time to attach to plastic and were therefore retained in suspension and transferred. Repeating this step at least two times yielded a culture predominantly consisting of cardiomyocytes. *1st pre-plating:* The cell suspension was transferred into a 75 cm^2 tissue culture flask and placed in a CO_2 incubator for 30 min at 37 °C. The attached cells were rinsed twice with the supernatant to detach any cardiomyocytes that had started to attach and the suspension transferred to a 50 mL falcon tube. The plated cells were washed with additional 5 mL normal medium, the supernatant removed and both supernatants pooled together. Normal growth medium was added to the cells attached to the flask which was then placed in a CO_2 incubator and treated like a normal primary cell culture. These cultures consist mainly of fibroblasts and are used as experimental controls. The cells from the supernatants were pelleted by centrifugation as described in the previous steps. *2nd pre-plating:* The pre-plating procedure was repeated as described but allowing 40 min incubation time. *3rd pre-plating (optional):* A 3rd pre-plating was only performed if a large number of cells were observed to have attached to the tissue culture flask during the 2nd pre-plating indicative of considerable amounts of non-myocyte cells. In that case another re-plating for 30 min was performed.

NCM quantification: After pre-plating, the cardiomyocyte fraction was pelleted and re-suspended in 5 mL normal growth medium and the number of NCM was determined using a haemocytometer (VWR, Lutterworth, UK, # HECH47112). Briefly, 10 µL cell suspension were

mixed with 10 µL filtered Trypan Blue (Sigma-Aldrich, Gillingham, UK, # T8154) and 10 µL of the suspension transferred into the counting chamber of the haemocytometer.

Calculation to estimate the concentration of cells in suspension:

$N_{\text{cells counted in four squares}}$ /4 * 10,000 * dilution factor = n_{cells}/mL

Since 10 µL Trypan Blue were added to distinguish dead from living cells, the dilution factor is 2.

Example of an estimated cell concentration from a NCM preparation:

80 /4 * 10,000 * 2 = 10^5 cells/mL

Inherent inaccuracies of this cell quantification technique mean that the cell number is an estimate.

NCM plating: Since NCM are post-mitotic cells, it is important to plate total cell numbers that, once attached to the culture plate, will be near 100% confluency. Unoccupied space on the plate will be rapidly colonised by dividing fibroblasts that have escaped the purification procedure. For 12-well plates 6 * 10^5 NCM were plated per well in a total volume of 1 mL. NCM were used for experiments after 72 h incubation in a CO_2 incubator at 37 °C. At this point beating colonies were observed indicative of a healthy culture. Fibroblast cultures derived from the pre-platings were cultured until passage 2 (P_2) and plated in uncoated 6-well plates for experimental procedures.

2.15.2 Induction of Cre recombinase *in vitro*

The use of optimal concentrations of tamoxifen is crucial to induce sufficient nuclear translocation of the MerCreMer fusion-protein without cytotoxicity. The concentrations used in previous publications varied from 2 µM to 10 µM but different cell types were used (Furr and Jordan 1984). Lactate dehydrogenase (LDH) cytotoxicity assays (Promega, Southampton, UK, # G1780) were performed to determine a non-lethal dose of tamoxifen. This colorimetric assay is based on the indirect measurement of the release of LDH from dying cells at a wavelength of 490 nm. NCM and fibroblasts were isolated from litters of *Tβ4shRNAflox/MerCreMer* homozygous breedings, as described above. Control NCM preparations were derived from pure *αMHC/MerCreMer* breedings. The experiments were carried out in serum free culture conditions (medium changed on the day) to prevent binding and inactivation of tamoxifen by components of the serum. Tamoxifen was dissolved in 100%

EtOH and NCM and fibroblast cultures treated with 200 nM tamoxifen (Sigma-Aldrich, Gillingham, UK, # T5648) or with the same volume of 100% EtOH. After 24 h incubation at standard conditions, the medium was aspirated and the cells washed twice with cold PBS (4 °C). RNA was isolated as described in Section 2.7.1.

2.16 Isolation of adult cardiomyocytes

Mice were sacrificed by cervical dislocation. The thorax was opened and the sternum folded backwards over the head of the animal to expose the heart. Without touching the atria or ventricle, a pair of forceps was used to lift up the heart on the larger vessels, which were subsequently severed and the heart immediately placed in normal tyrodes including heparin (140 mM NaCl, 6mM KCl, 10 mM HEPES, 1 mM $MgCl_2$, pH 7.4, 1 mM $CaCl_2$) at RT. The heart had to be still contracting at this point which assisted in clearing blood from the tissue. The heparin in the solution prevented the blood from clotting which could otherwise have blocked the coronary vessels. After the heart had purified itself from blood for about 20 beats it was transferred into the dish containing the needle holder filled with perfusion buffer (120.4 mM NaCl, 14.7 mM KCl, 0.6 mM KH_2PO_4, 0.6 mM Na_2HPO_4, 1.2 mM $MgSO_4$-$7H_2O$, 10 mM HEPES, 4.6 mM $NaHCO_3$, 30 mM Taurine, 10 mM BDM, 5.5 mM Glucose, pH 7.0) and containing heparin (**Figure 2.14**). BDM was included in the buffer due to its cytoprotective properties during Ca^{2+} depletion (Thum and Borlak 2001). The aorta was cannulated and tied to the cannula with a 6/0 polypropylene suture (Ethicon, Johnson & Johnson, Brussels, Belgium). The cardiac chambers and coronary circulation were flushed with heparin-containing perfusion buffer.

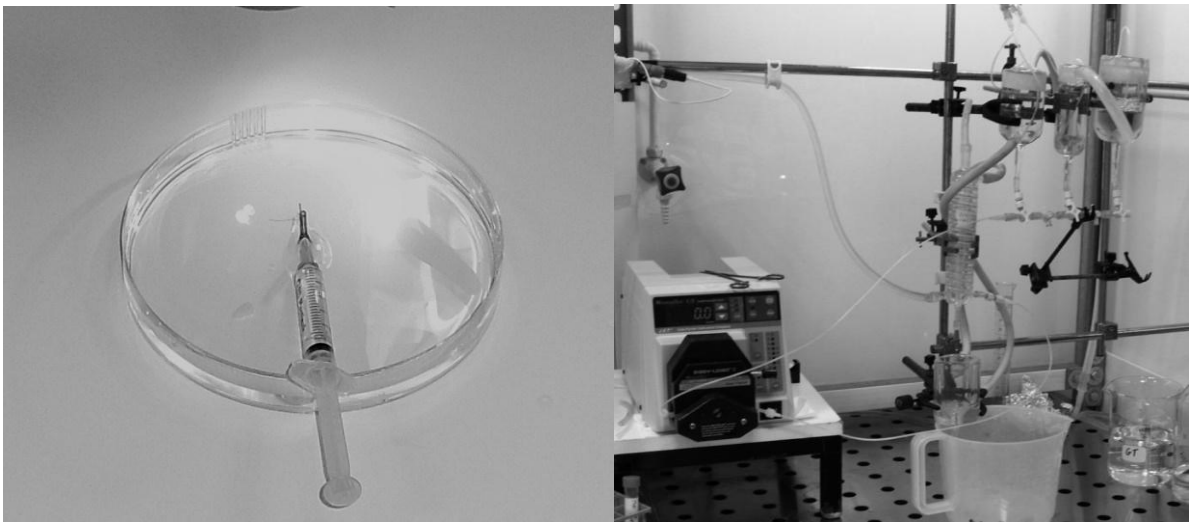


Figure 2.14: Langendorff setup required for adult cardiomyocyte isolation. Needle holder (left panel) and Langendorff perfusion system (right panel) used during adult cardiomyocyte isolation are shown.

The cannula was connected to the Langendorff perfusion system (**Figure 2.14**). The isolation procedure was performed at 37 °C and the temperature constantly monitored. All solutionas were continuously bubbled with O_2. The heart was washed with perfusion buffer for 4 min. Tissue digestion was initiated by perfusing the heart with myocyte perfusion buffer containing 2.4 mg/mL collagenase type II (Worthington Biochemical, Lakewood, NJ, USA) with an average activity of 340 u/mg for 3 min. The final digestion was performed using low Ca^{2+} myocyte digestion buffer (as above but containing 15 µL of 100 mM $CaCl_2$) for 6 min and 30 s. The heart was removed from the Langendorff apparatus and placed in 5 mL stopping solution (perfusion buffer, 10% (w/v) FCS, 12.5 µM $CaCl_2$) at RT. Venae cavae, aorta and atria were removed and the ventricles coarsely minced using scissors. The tissue was further disrupted using a plastic Pasteur pipette. Great care was taken to avoid creating air bubbles which could damage the cells. The cell suspension and any tissue fragments were transferred into a 15 mL reaction tube containing additional 5 mL stopping solution (RT) and further digested with a plastic Pasteur pipette. The sample was centrifuged for 3 min at 20 g and the supernatant discarded. The cells were washed in 10 mL additional stopping solution as above. Finally the cells were resuspended in perfusion buffer and a sample investigated by light microscopy to determine the percentage of viable cardiomyocyte. The cells were pelleted by centrifugation at 20 g for 3 min and frozen at -80 °C until RNA isolation.

2.17 Statistics

Statistical calculations were performed using Microsoft® Office Excel 2010 (Microsoft, Reading, UK) and GraphPad Prism® V.5 (GraphPad Software, LaJolla, USA). Comparison of 3 or more samples was performed by analysis of variance (ANOVA) and Bonferroni post-testing (compare all pairs of columns). * $p < 0.05$, ** $p < 0.01$, *** $p < 0.001$.

2.18 Real-time PCR probes

Table 2.15: Real-time PCR probes used during this study. All probes were purchased from Applied Biosystems, Carlsbad, CA, USA.

Species reactivity/Target	**Probe Code**	**Catalogue #**
Mouse CCL2	Mm00441242_m1	# 4331182
Mouse COL3A1	Mm01254476_m1	# 4331182
Mouse 18s rRNA	N/A	# 4310863E
Mouse TMSB4X	Mm01129684_g1	# 4331182
Mouse Nppa	Mm01255747_g1	# 4331182
Mouse Nppb	Mm01255770_g1	# 4331182
Mouse IL1β	Mm00434189_m1	# 4331182
Mouse IL6	Mm00446190_m1	# 4331182
Mouse IL10	Mm00439614_m1	# 4331182
Mouse IFNγ	Mm01168134_m1	# 4331182
Mouse TGFβ1	Mm01178820_m1	# 4331182
Mouse TNFα	Mm00443260_g	# 4331182
Rat IGF1	Rn00710306_m1	# 4331182
Cre	Mr00635245_cn	# 4400291

2.19 Antibodies

Table 2.16: Antibodies used during this study.

Target	Manufacturer	Product Number
α-synuclein	Cell Signaling, Danvers, MA, USA	# 4179
α-tubulin	Sigma-Aldrich, Gillingham, UK	# T6074
Bax	Cell Signaling, Danvers, MA, USA	# 2772
Bcl2	Cell Signaling, Danvers, MA, USA	# 2876
Beclin-1	Cell Signaling, Danvers, MA, USA	# 3495
Battenin	Abcam, Cambridge, UK	# ab75959
Caspase-3	Cell Signaling, Danvers, MA, USA	# 9662/9661
Cathepsin D (EM)	Merck Calbiochem, Nottingham, UK	# IM16
Cre	Merck Novagen, Darmstadt, Germany	# 69050-3
Cytochrome c	Cell Signaling, Danvers, MA, USA	# 4272
GAPDH	Cell Signaling, Danvers, MA, USA	# 2118
LAMP1	Novus Biologicals, Littleton, CO, USA	# NB110-82353
LC3	Abgent, San Diego, CA, USA	# AM1800A
LC3B	Cell Signaling, Danvers, MA, USA	# 2775
IGF-1	Sigma-Aldrich, Gillingham, UK	# I2157
Mouse IgG	GE Healthcare, Bucks, UK	# Na931V
Rabbit IgG	Cell Signaling, Danvers, MA, USA	# 7074
Rabbit IgG	GE Healthcare, Bucks, UK	# Na934V
Thymosin β4 (EM)	Santa Cruz Biotechnology, Santa Cruz, CA, USA	# sc-67114
Thymosin β4	Abcam, Cambridge, UK	# ab14334
Thymosin β4	Immundiagnostik, Bensheim, Germany	# A9522.1/A9522.2
Ubiquitin	Cell Signaling, Danvers, MA, USA	# 3933
V5	Invitrogen, Carlsbad, CA, USA	# R960-25

Chapter 3 - Tamoxifen-dependent Cardiomyocyte-specific Knockdown of Thymosin β4

3.1 Introduction

The importance of Tβ4 during development of the heart was demonstrated among others by the work of Paul Riley's group, who described a substantial cardiac phenotype and embryonic lethality after shRNA-mediated depletion of *Tβ4* mRNA during mouse development (Smart *et al.* 2007). This was attributed to a failure to induce inward migration of progenitor cells from the epicardium and ectopic EMT of EPDC in epicardial regions. The epicardium was also shown to be important in cardiac regeneration in zebrafish, a process dependent on EMT of an epicardial cell population and increased expression of a *Tβ4* ortholog (Lepilina *et al.* 2006; Lien *et al.* 2006).

In adult mammals, exogenous Tβ4 peptide, delivered intracardially or systemically after myocardial infarction, decreased scar volume and LV function in mouse and pig models highlighting its therapeutic potential (Bock-Marquette *et al.* 2004; Hinkel *et al.* 2008). Furthermore, Tβ4-priming mammalian hearts in the context of experimental MI reportedly induced epicardial cells positive for Wilm's tumour 1 (*Wt1*), a marker of adult cardiac progenitors underpinning the potential therapeutic potential of this peptide in stem cell-mediated cardiac regeneration (Smart *et al.* 2011).

With the focus of previous research on the role of Tβ4 during development and wound healing, the importance of *Tβ4* under physiological conditions and the consequences of an adult loss of function in the mammalian heart had not been previously addressed. The aim of the present study was to investigate the role of *Tβ4* in normal adult mouse heart and how this affects recovery after experimental MI. In order to understand the effects of downregulating Tβ4 in adult mammalian hearts under physiological and pathological conditions, the *Tβ4shRNAflox/MerCreMer* mouse strain was generated and analysed. The following chapter describes challenges of cardiomyocyte-specific conditional gene manipulation as well as three different approaches of determining the success of the inducible shRNA-mediated knockdown of *Tβ4* in cardiomyocytes. These approaches can be classified as *in vivo*, *in vitro* and *ex vivo*.

3.2 Thymosin *β4* knockdown by tamoxifen administration in the diet

In order to downregulate Tβ4 by *Tβ4shRNA* expression in the adult heart, 3-4 month old male *Tβ4shRNAflox/MerCreMer* mice were fed tamoxifen-containing diet. At baseline, cardiac function of these mice was unremarkable as analysed by transthoracic ECHO

(**Figure 3.1**). Left-ventricular (LV) ejection fraction (EF) and LV fractional shortening (FS) were normal across all experimental groups which consisted of *Tβ4shRNAflox/MerCreMer* mice (EF% 70.51 ± 5.95, FS% 34.92 ± 4.78) as well as *Tβ4shRNAflox* (EF% 64.26 ± 7.46, FS% 30.44 ± 5.20) and *MerCreMer*-single genotype (EF% 69.72 ± 6.11, FS% 34.81 ± 4.24) littermates.

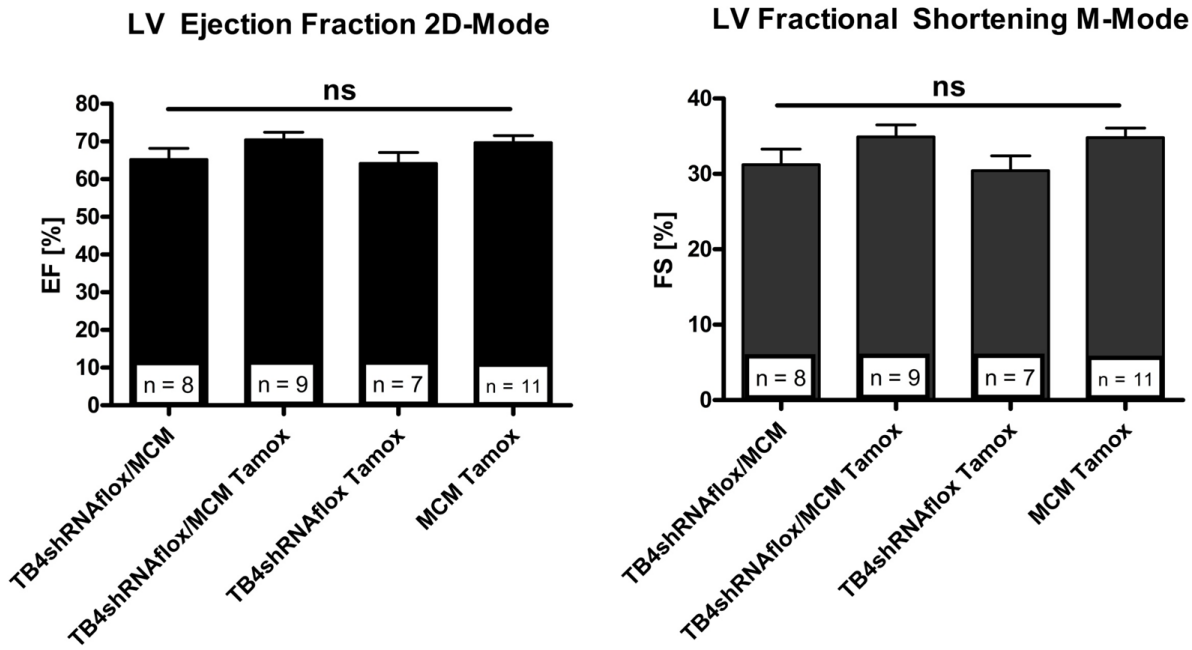


Figure 3.1: Baseline cardiac function of *Tβ4shRNAflox/MerCreMer* mice measured by transthoracic ECHO. Left-ventricular (LV) ejection fraction (EF) and LV fractional shortening (FS) were normal compared to controls prior to tamoxifen treatment. Groups labelled "Tamox" are animals on normal diet that were later subjected to tamoxifen treatment. Data are expressed as ± SD.

Following 14 days of tamoxifen diet, nuclear localisation of the MerCreMer fusion-protein was assessed in *Tβ4shRNAflox/MerCreMer* mice by immunofluorescence analysis of frozen cardiac sections. MerCreMer was frequently found localised to the nuclear compartment, but not in all cells, indicating a partial success of this mode of tamoxifen delivery (**Figure 3.2**).*Tβ4shRNAflox/MerCreMer* mice on normal diet did not show nuclear localisation of MerCreMer.

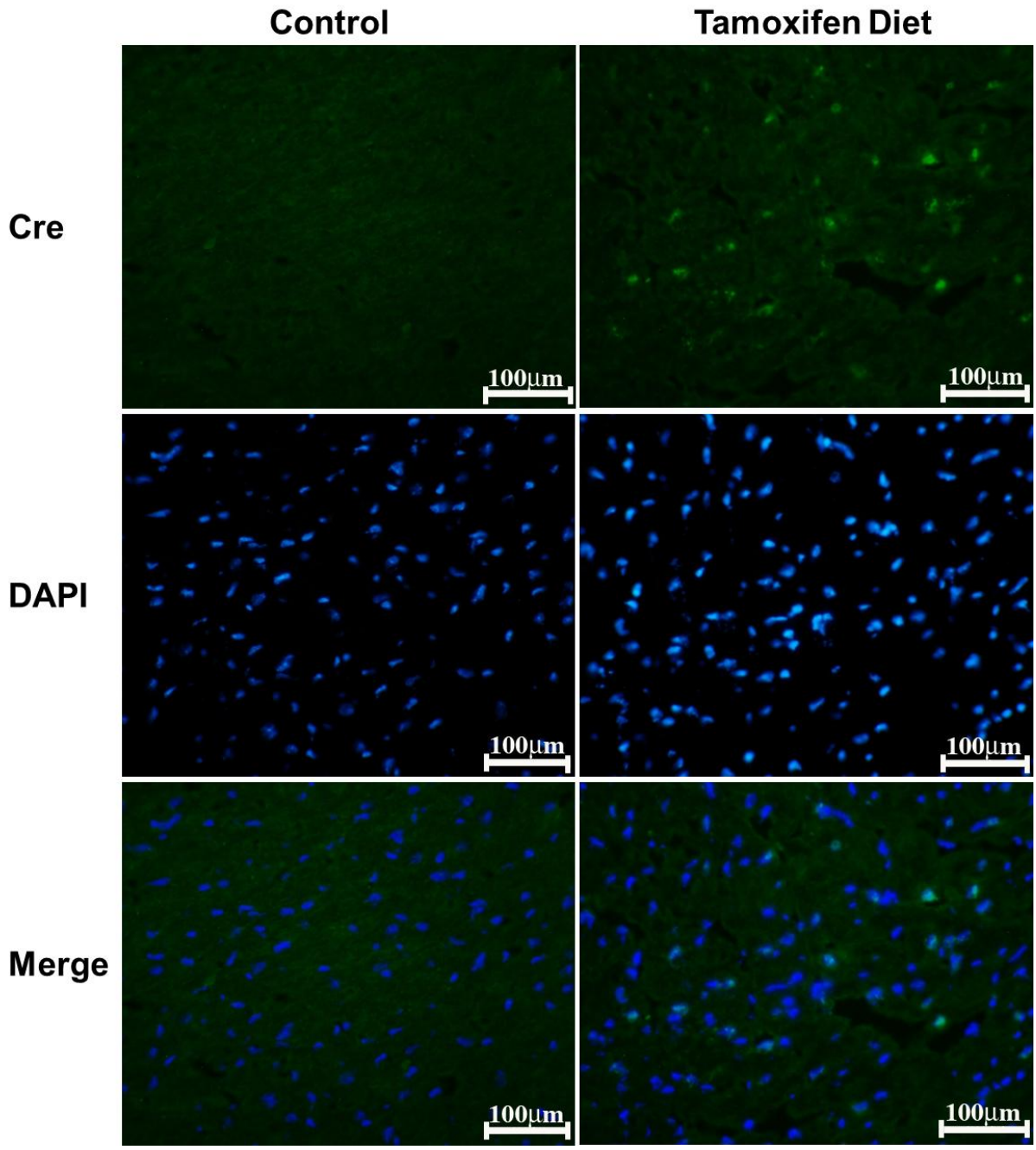


Figure 3.2: Immunofluorescence staining for Cre on cardiac cryosections. MerCreMer localisation is shown in left-ventricular cardiac tissue of *Tβ4shRNAflox/MerCreMer* mice after 14d of tamoxifen diet or normal diet (Control). Green – Anti-Cre, blue – DAPI. Scale bar 100 µm. n = 3 per group.

3.3 Cardiac function following tamoxifen diet

From approximately day 7 into tamoxifen treatment onwards, the animals displayed signs of poor health, such as weight loss and excessive urination. In addition, animals showed behavioural disturbances including aggression and apathy.

At day 14 post-treatment, ECHO analyses revealed high variability within experimental groups, with a large portion of the animals showing severe arrhythmia and depression of cardiac function, while the remaining mice appeared to be completely unaffected (data not shown). Considering the weight loss and excess urination, the observed phenotype suggested diet refusal in some of the mice or strong side effects of tamoxifen, since *Tβ4shRNAflox/MerCreMer* mice on normal diet were healthy. Animals were rested for 14 days on normal diet to allow for recovery from the effects of the supposed diet refusal and/or potential side effects of tamoxifen. After 14 days rest, cardiac function had normalised (%EF ~ 60, %FS ~30) and was similar across all experimental groups (**Figure 3.3**).

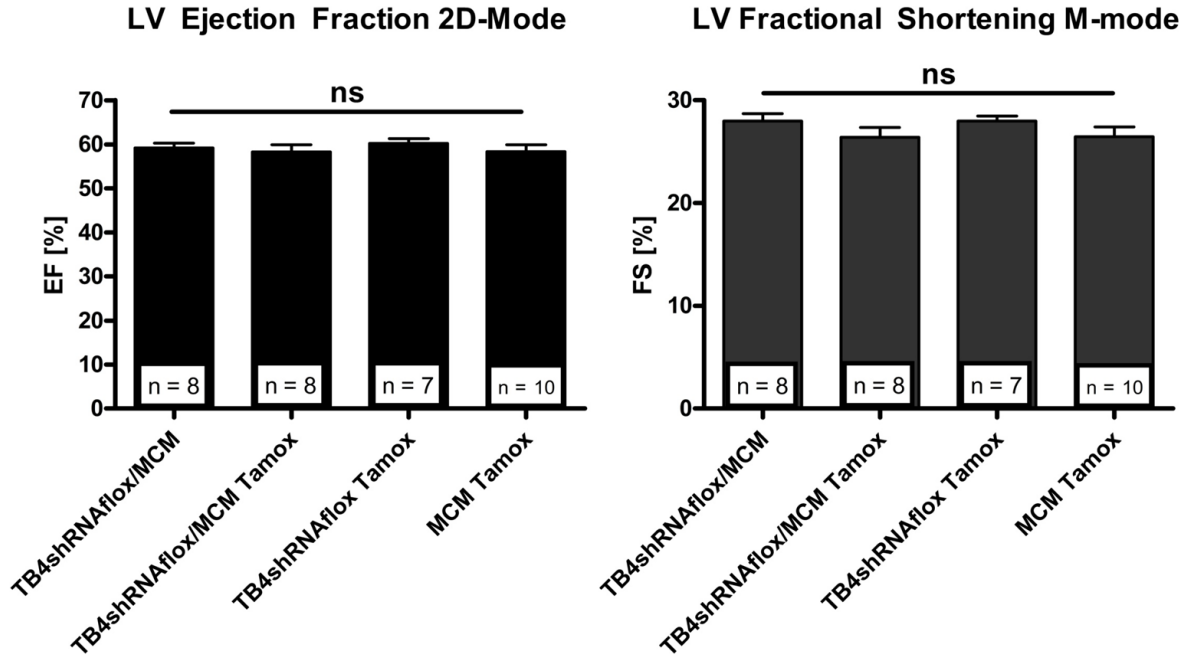


Figure 3.3: Cardiac function measured by transthoracic ECHO following tamoxifen delivery via diet. Normal LV EF and LV FS were observed in all groups following 14 days of tamoxifen diet and 14 days recovery on normal diet. Data presented as ± SD.

As expected, untreated *Tβ4shRNAflox/MerCreMer* mice showed a significantly higher body weight compared to tamoxifen-treated *Tβ4shRNAflox/MerCreMer*, *Tβ4shRNAflox* and *MerCreMer* littermates at sacrifice after 14 days of rest (**Figure 3.4 A**). Heart weights were similar across all groups, but the higher body weight of control-treated *Tβ4shRNAflox/MerCreMer* resulted in a significantly decreased heart-weight-to-body-weight (HW/BW) ratio in that group (**Figure 3.4 B, C**). HW/BW ratios between tamoxifen-treated *Tβ4shRNAflox/MerCreMer* and tamoxifen-treated control groups were comparable indicating no hypertrophy at this point. Lung weights were recorded as an indirect measure of cardiac insufficiency and pulmonary oedema, but were unchanged between experimental groups

(**Figure 3.4 D**). The lung-weight-to-body-weight (LuW/BW) ratio was altered as a consequence of decreased body weight in the tamoxifen-treated groups, as reported for the HW/BW ratio (**Figure 3.4 E**). Liver weights were recorded to assess the metabolic status of the animals and were found to be significantly reduced in tamoxifen-treated *Tβ4shRNAflox* and *MerCreMer* animals compared to *Tβ4shRNAflox/MerCreMer* mice on normal diet (**Figure 3.4 F, G**). This supports the hypothesis of food rejection in these animals. While overall liver weight loss suggested a similar effect in the tamoxifen-treated *Tβ4shRNAflox/MerCreMer* group, this change did not reach statistical significance.

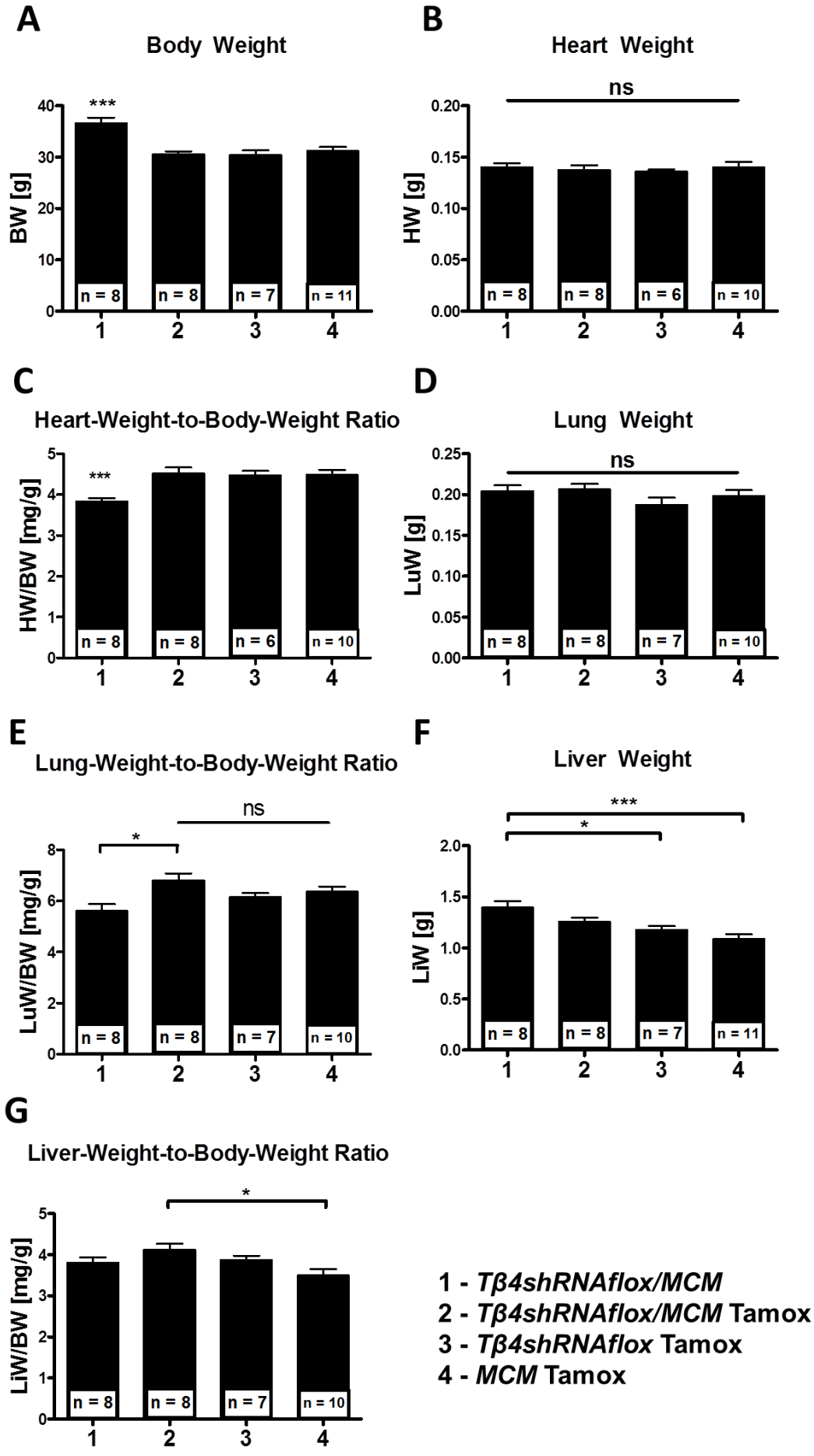

A
Body Weight
BW [g]
***
n = 8
n = 8
n = 7
n = 11
B
Heart Weight
HW [g]
ns
n = 8
n = 8
n = 6
n = 10
C
Heart-Weight-to-Body-Weight Ratio
HW/BW [mg/g]
***
n = 8
n = 8
n = 6
n = 10
D
Lung Weight
LuW [g]
ns
n = 8
n = 8
n = 7
n = 10
E
Lung-Weight-to-Body-Weight Ratio
LuW/BW [mg/g]
ns
*
n = 8
n = 8
n = 7
n = 10
F
Liver Weight
LiW [g]
***
*
n = 8
n = 8
n = 7
n = 11
G
Liver-Weight-to-Body-Weight Ratio
LiW/BW [mg/g]
*
n = 8
n = 8
n = 7
n = 10
1 - Tβ4shRNAflox/MCM
2 - Tβ4shRNAflox/MCM Tamox
3 - Tβ4shRNAflox Tamox
4 - MCM Tamox

Figure 3.4: Recordings of physiological parameters after tamoxifen delivery in the diet. (A) Body weights, (B) heart weights, (C) heart-weight-to-body-weight (HW/BW) ratios, (D) lung weights, (E) lung-weight-to-body-weight (LuW/BW) ratios, (F) liver weights and (G) liver-weight-to-body-weight (LiW/BW) ratios of *Tβ4shRNAflox/MerCreMer* and control mice after 14 days tamoxifen or normal diet and 14 days of rest. Data are expressed as ± SD.

Overall, *Tβ4shRNAflox/MerCreMer* mice on normal diet showed a natural weight increase over the treatment period while tamoxifen-treated groups lost weight (*Tβ4shRNAflox/MerCreMer, MerCreMer*) or maintained their weight (*Tβ4shRNAflox*) during that period (**Figure 3.5 A**). This effect did not stem from differences in starting weight, which was the same for all groups (**Figure 3.5 B**).

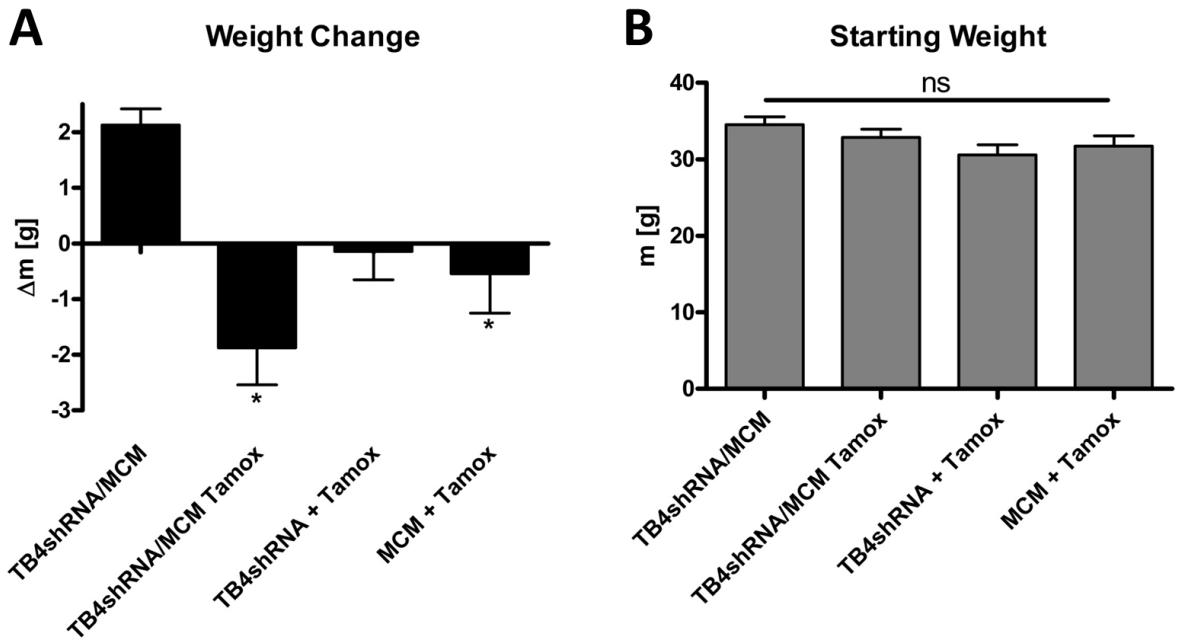


Figure 3.5: Body weight change of mice after one month of tamoxifen diet. (A) Significant loss of body weight was observed in *Tβ4shRNA/MerCreMer* and *MerCreMer* animals. *Tβ4shRNAflox/MerCreMer* mice on normal chow showed a normal increase of weight of ~2 g. Tamoxifen-treated *Tβ4shRNAflox* mice did not show a gain in weight and were not significantly different from untreated *Tβ4shRNAflox/MerCreMer* animals. (B) Body weights of all groups before start of treatment (n per group ≥ 7).

Despite concerns about the overall impact of the observed effects of the diet, the knockdown efficiency of *Tβ4shRNA* was assessed by rtPCR and Western blotting as a proof of principle. The PCR efficiency of the Tβ4 real-time probe was determined by preparation of standard curves for both PCR reactions and was found to be comparable (89%) to that of the 18s probe (85%) indicating its suitability for comparative ΔC_T analysis. Levels of *Tβ4* mRNA and protein were unaltered in tamoxifen-treated *Tβ4shRNAflox/MerCreMer* animals compared to

tamoxifen-treated *MerCreMer* littermates (**Figure 3.6 A, B**). The antibodies used showed substantial aspecific binding and the resulting blots were of poor quality indicating the superiority of rtPCR to determine the degree of Tβ4 knockdown in this model.

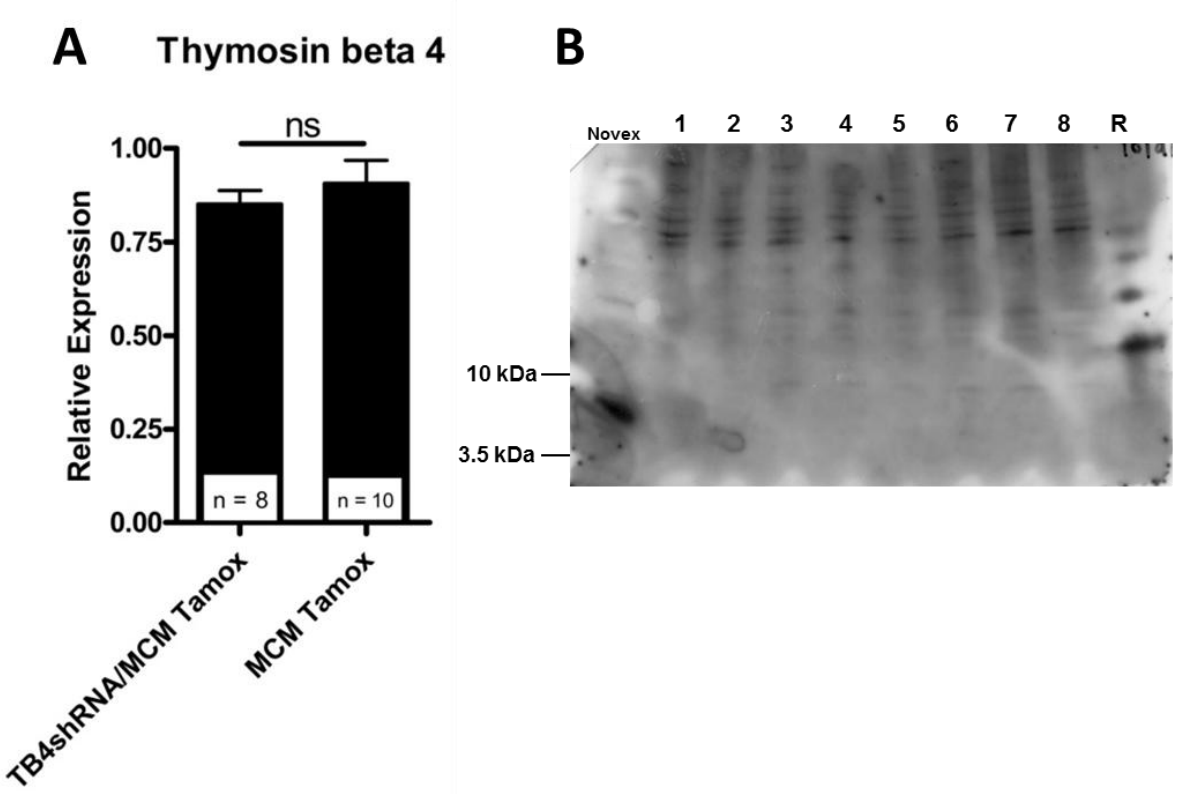


Figure 3.6: *Tβ4* mRNA and protein levels measured by real-time PCR and Western blotting. (A) Levels of *Tβ4* mRNA are unaltered in *Tβ4shRNAflox/MerCreMer* mice following 14 days of tamoxifen diet and 14 days of rest. (B) Changes in Tβ4 protein levels cannot be detected by Western blotting. Anti-Tβ4 antibodies (Abcam) show very limited specificity in Western blotting.

The overall negative effects of feeding tamoxifen diet on animal physiology and welfare, the fact that nuclear localisation of MerCreMer was only moderate and the failure of down-regulation cardiac *Tβ4* called for a change in tamoxifen delivery protocol. Since, oral tamoxifen delivery either involved the risk of rejection by the animals or considerable stress in the case of gavage, an IP injection protocol was the most feasible option. The original report on *αMHC/MerCreMer* mice described a 5 day injection regime of 20 mg/kg tamoxifen daily (Sohal *et al.* 2001). This protocol was adopted for the subsequent study.

3.4 *Thymosin β4* knockdown via intraperitoneal tamoxifen injections

3-4 month old *Tβ4shRNAflox/MerCreMer* and control mice were injected with tamoxifen or EtOH for 5 consecutive days (20 mg/kg daily). After 3-4 weeks of rest body, heart, lung and

liver weights and their respective ratios to body weight were unremarkable compared to controls (**Figure 3.7 A-G**).

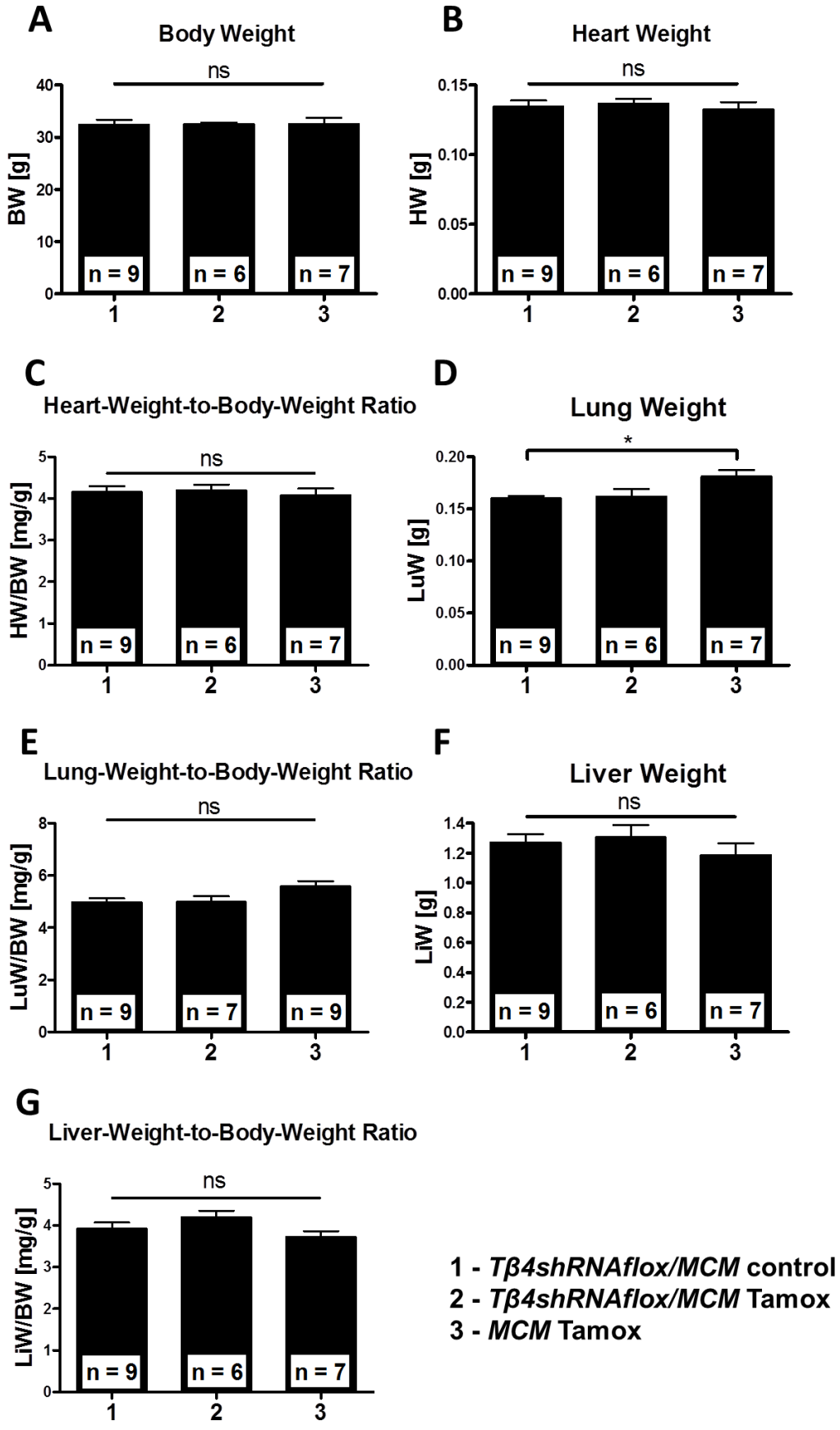


Figure 3.7: Recordings of physiological parameters after IP tamoxifen injections. (A) Body weights, (B) heart weights, (C) HW/BW ratios, (D) lung weights, (E) LuW/BW ratios, (F) liver weights and (G)

LiW/BW ratios of *Tβ4shRNAflox/MerCreMer* and control mice after 5 days tamoxifen (20 mg/kg daily) or control treatment and 3-4 weeks of rest.

3.4.1 MerCreMer localisation following tamoxifen injections

A separate batch of *Tβ4shRNAflox/MerCreMer* animals was sacrificed prematurely 3 days after completed injections and cardiac sections analysed for MerCreMer localisation. MerCreMer successfully translocated to nuclei of cardiomyocytes after tamoxifen but not after control injections (**Figure 3.8**).

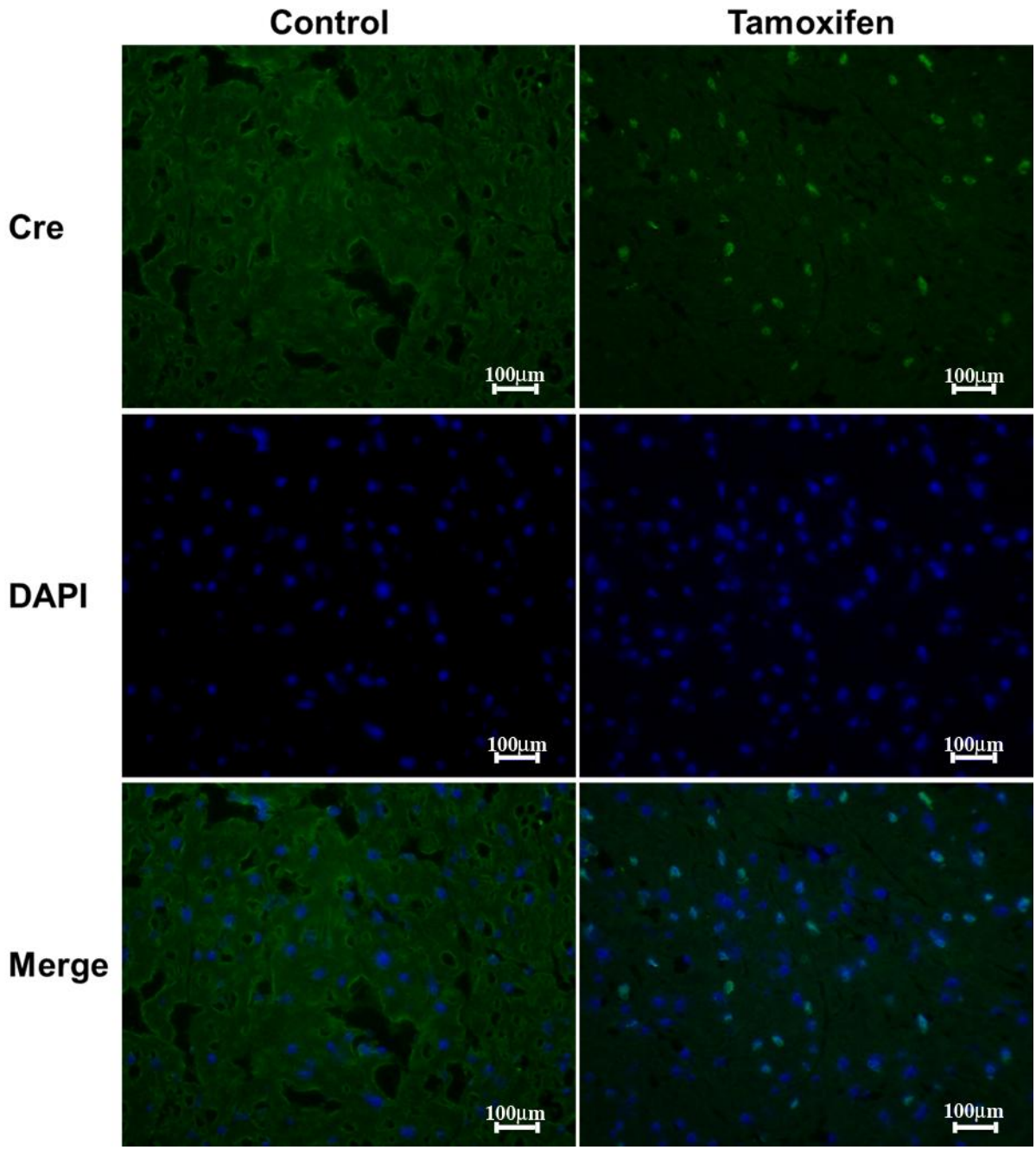


Figure 3.8: MerCreMer localisation in the left ventricle of *Tβ4shRNAflox/MerCreMer* animals. Cardiac frozen sections stained with anti-Cre antibody following 5 days tamoxifen (20 mg/kg IP) or EtOH control injections and 3 days of rest. Green – anti-Cre, blue – DAPI. Scale bar 200 µm. n = 3 per group.

3.4.2 Cardiac function and morphology 3-4 weeks following tamoxifen injections

Following 3-4 weeks of rest, LV function of tamoxifen-treated *Tβ4shRNAflox/MerCreMer* (%EF 58.93 ± 1.40, %FS 26.47 ± 2.02) animals measured by ECHO was unchanged compared to control-treated *Tβ4shRNAflox/MerCreMer* (%EF 61.25 ± 2.86, %FS 28.73 ±

2.48) or tamoxifen-treated *MerCreMer* single-genotype (%EF 61.44 ± 6.16, %FS 29.56 ± 3.94) animals (**Figure 3.9**).

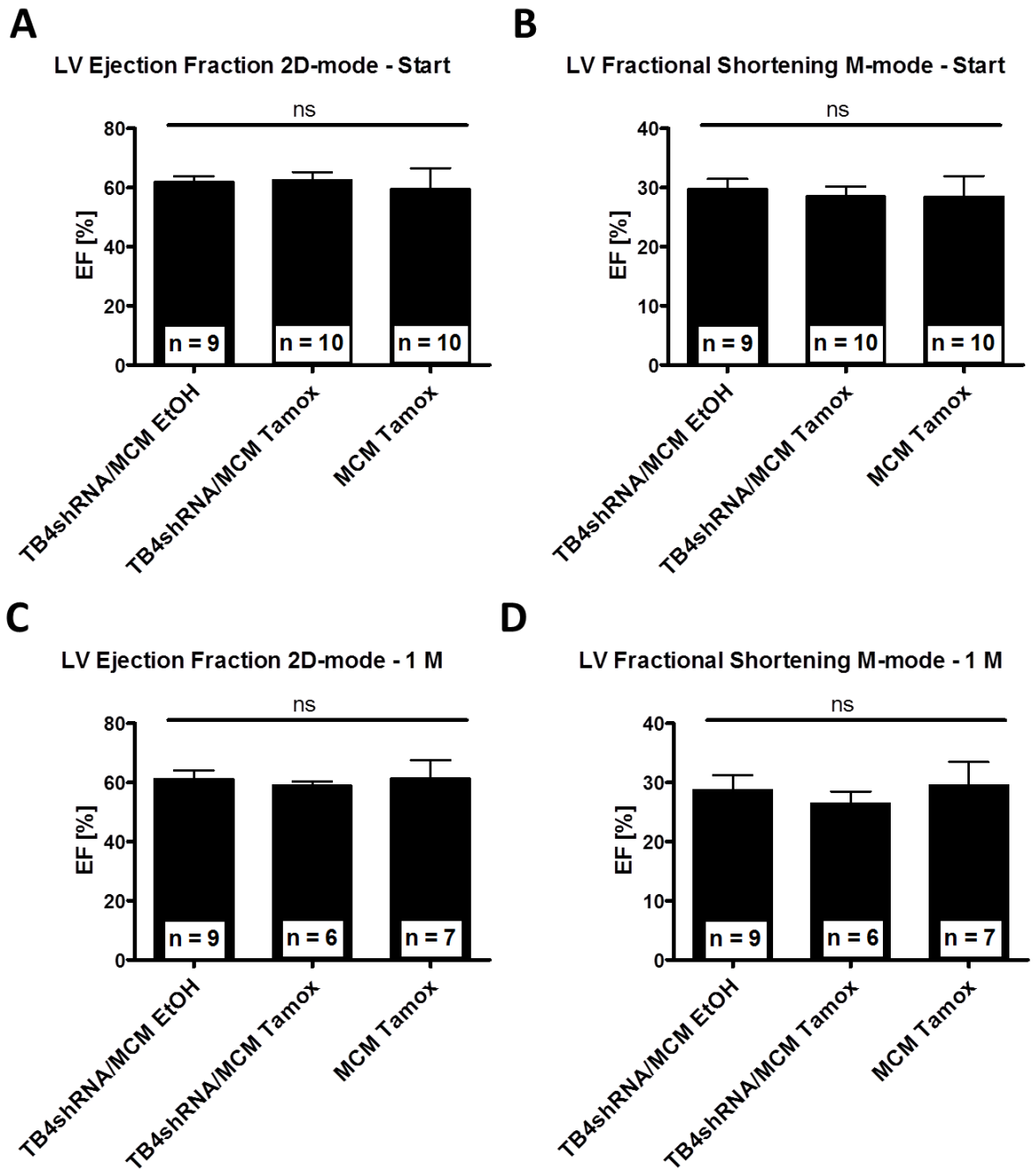


Figure 3.9: Cardiac function assessed by ECHO. Comparable LV function (EF, FS) at baseline was observed between all treatment groups. After 5 days of tamoxifen injections (20 mg/kg daily) and 3-4 weeks (1M) of rest, cardiac function of *Tβ4shRNAflox/MerCreMer* animals was unaltered.

To investigate potential changes of cardiac morphology following the putative downregulation of *Tβ4*, cardiac sections of tamoxifen or EtOH-treated *Tβ4shRNAflox/MerCreMer* and control mice were analysed by Masson's trichrome staining. This revealed interstitial fibrosis in a number of *Tβ4shRNAflox/MerCreMer* mice (**Figure 3.10**).

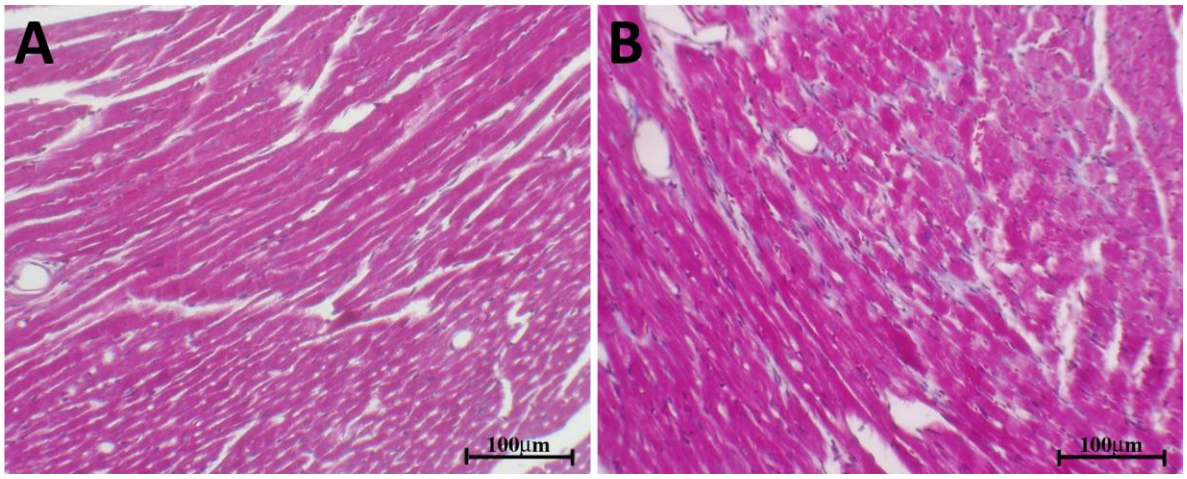


Figure 3.10: Masson's trichrome staining of cardiac sections. Overall morphology and fibrosis of the hearts of (A) control-treated *Tβ4shRNAflox/MerCreMer* and (B) tamoxifen-treated (20 mg/kg daily) *Tβ4shRNAflox/MerCreMer* 3-4 weeks following 5 days of injections. Tamoxifen-treated mice disply mild interstitial fibrosis. Scale bar 100 µm. n > 3 per group.

The incidence of fibrosis was not seen in relation to putative *Tβ4* downregulation, since it was also observed in tamoxifen-treated *αMHC/MerCreMer* mice lacking the floxed transgene. Since paraffinised tissue was only available of a subgroup of animals, this unexpected phenotype was analysed in a larger population of *Tβ4shRNAflox/MerCreMer*, *αMHC/MerCreMer* and *wt* mice.

3.4.3 Cardiac physiology and function of *Tβ4shRNAflox/MerCreMer* animals 6 weeks following tamoxifen treatment

Following the discovery of fibrosis in some tamoxifen-treated *MerCreMer* positive animals, a larger cohort was injected for 5 days with 20 mg/kg tamoxifen daily. To investigate the full extent of fibrosis and its longer term effect on cardiac function, animals were rested for 6 weeks before analysis by ECHO and histology. Body weights of treated animals were normal as for the previous study groups and the HW/BW ratio showed no increase in heart mass indicative of a cardiac hypertrophy (**Figure 3.11**).

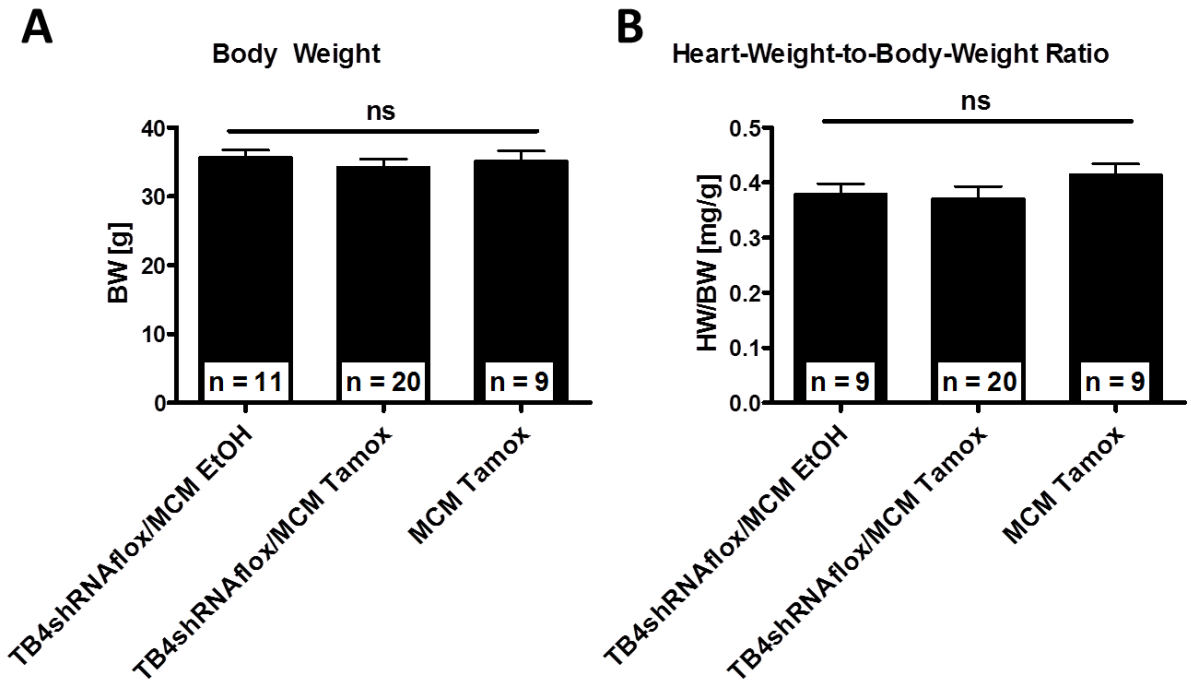


Figure 3.11: Physiological parameters following tamoxifen injections and 6 weeks of rest. (A) Body weights and (B) HW/BW ratios of animals subjected to 5 days of IP tamoxifen treatment (20 mg/kg daily).

However, after the prolonged resting phase of 6 weeks, a significant decrease in LV EF and FS was observed in tamoxifen-treated *Tβ4shRNAflox/MerCreMer* animals (%EF 55.90 ± 6.29, %FS 25.35 ± 3.57) compared to control-treated mice (%EF 62.36 ± 2.76, %FS 29.49 ± 1.93, **Figure 3.12**). In addition, the tamoxifen-treated *MerCreMer* control group also showed depressed cardiac function (%EF 55.52 ± 6.58, %FS 24.86 ± 3.93).

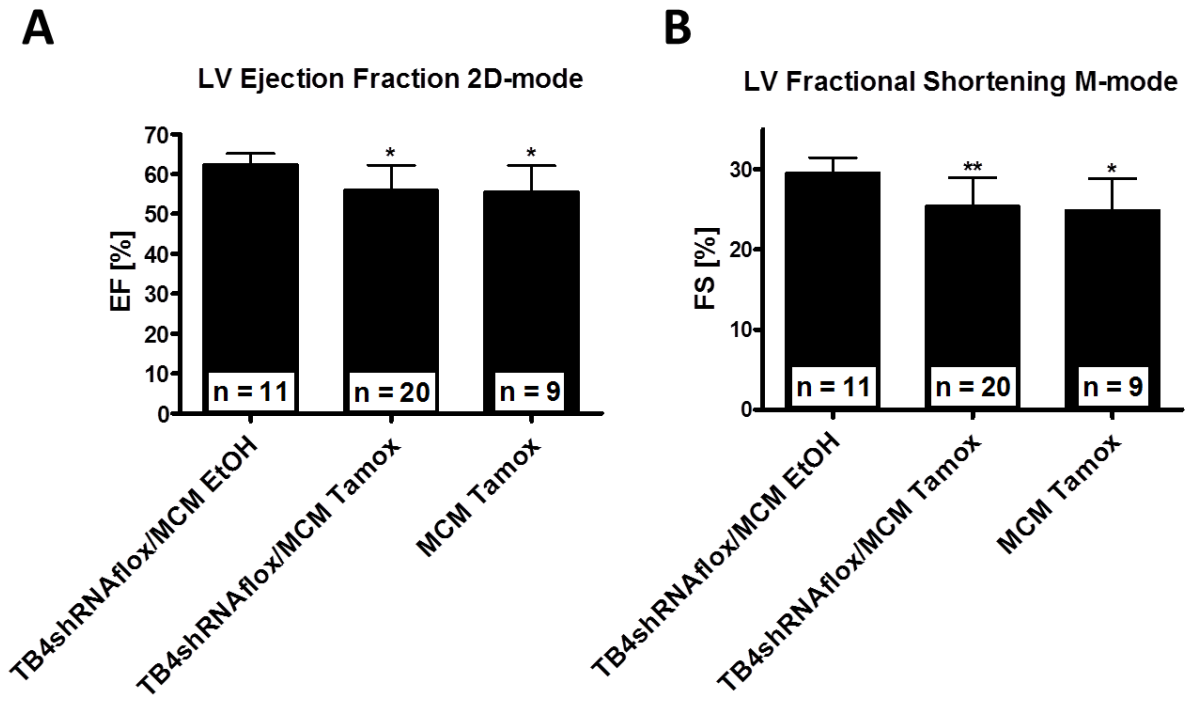


Figure 3.12: ECHO results after IP tamoxifen injections and 6 weeks rest. LV EF and FS of *Tβ4shRNAflox/MerCreMer* and *MerCreMer* animals following 5 days of tamoxifen (20 mg/kg daily) or control (EtOH) injections.

This depression of LV function and the associated fibrotic cardiac phenotype of *MerCreMer* control mice prompted more detailed investigations described in Chapter 4.

3.4.4 Assessment of *Thymosin* β4 knockdown following tamoxifen injections

Tβ4 knockdown efficiency following the 5 day tamoxifen injection protocol was assessed by rtPCR and Western blotting. Cardiac *Tβ4* mRNA and protein levels were unaltered after 6 weeks of rest (**Figure 3.13**).

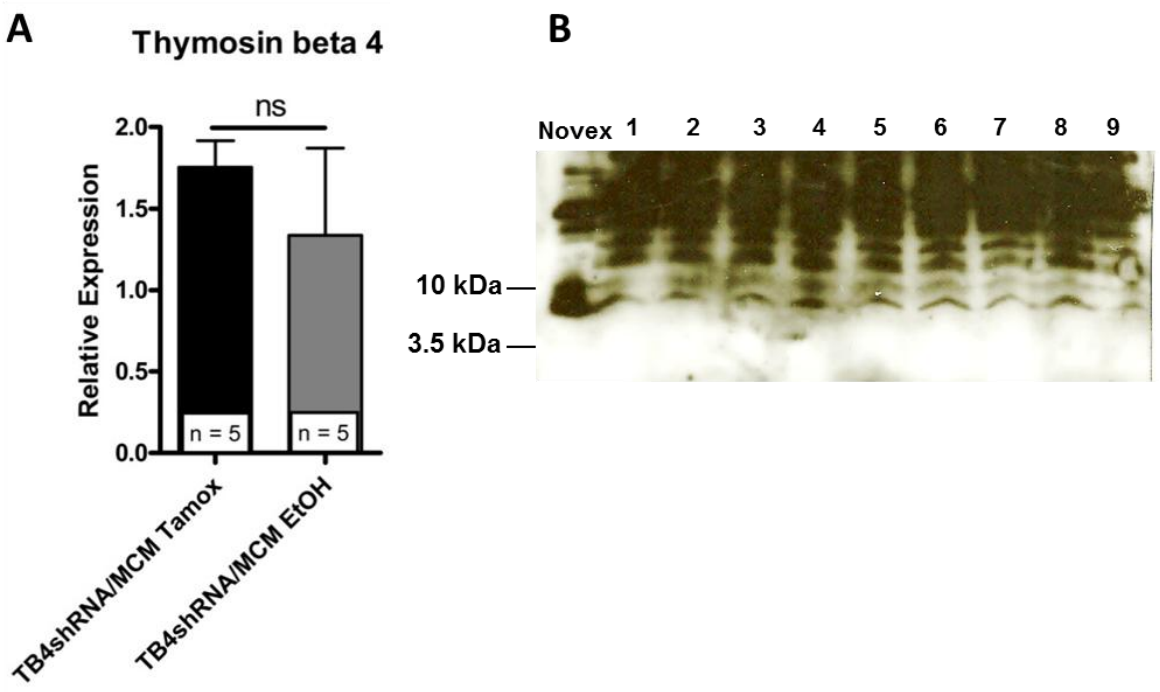


Figure 3.13: rtPCR and Western Blot for Tβ4 following 5 days of tamoxifen injections (20 mg/kg daily). (A) Levels of *Tβ4* mRNA were not changed in *Tβ4shRNAflox/MerCreMer* mouse hearts compared to control-treated *Tβ4shRNAflox/MerCreMer* animals after 6 weeks of rest. (B) Tβ4 Western blotting shows bands at the corresponding height and an abundance of aspecific bands. No changes are detectable between groups. Lanes 1-4 *Tβ4shRNAflox/MerCreMer* 5 days tamoxifen (20 mg/kg daily), 5-6 EtOH control-treated *Tβ4shRNAflox/MerCreMer*, 7-8 mouse thymus controls and lane 9 normal *wt* heart.

Immunofluorescence staining on cardiac sections of tamoxifen-treated *Tβ4shRNAflox/MerCreMer* mice revealed no differences in Tβ4 expression in the heart compared to controls (not shown). However, a strong signal was observed in cells lining the blood vessels (**Figure 3.14**).

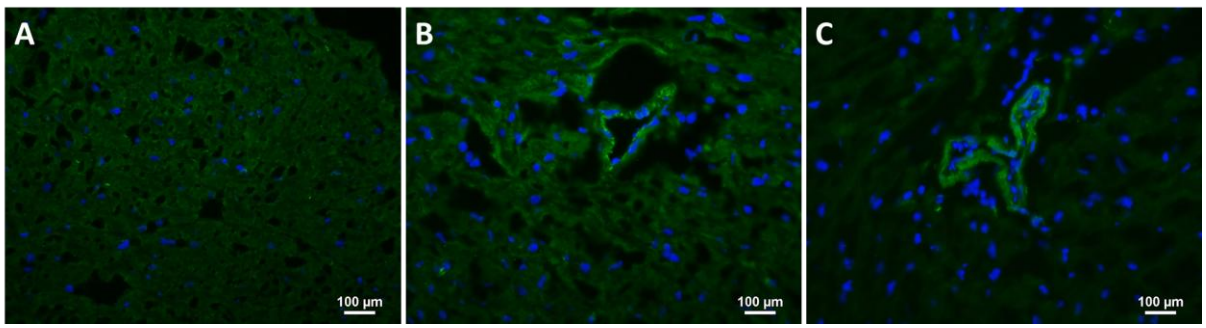


Figure 3.14: Immunofluorescence staining for Tβ4 on cardiac frozen sections. (A) Tβ4 was detected at basal levels in the left-ventricular myocardium. (B-C) Blood vessels of *Tβ4shRNAflox/MerCreMer* mice show a stronger signal. Sections shown are from EtOH control-treated *Tβ4shRNAflox/MerCreMer*. Scale bar 100 µm.

3.5 Thymosin β4 knockdown in vitro

Since a knockdown of *Tβ4* was not observed *in vivo* and Tβ4 immunofluorescence data suggested that other cardiac cell populations such as endothelial or smooth muscle cells express higher levels of Tβ4 than cardiomyocytes, alternative approaches to reduce the amount of contaminating cell types were considered. A more selective investigation of *Tβ4* knockdown was performed *in vitro* using neonatal cardiomyocytes (NCM) of *Tβ4shRNAflox/MerCreMer* mice.

3.5.1 Neonatal cardiomyocyte culture

The isolation procedure of mouse neonatal NCM removes endothelial cells, most fibroblasts and other contaminating cell types from the cell preparation. The aim of this experiment was to treat a purified culture with tamoxifen *in vitro* to obtain a more specific result of Tβ4 levels in cardiomyocytes. In the absence of a better reference, the initial range of suitable non-toxic tamoxifen concentrations for treatment *in vitro* was adopted from experiments involving MCF7 breast cancer cells, which showed that tamoxifen was effective at concentrations of 2 µM and 6 µM while 10 µM tamoxifen resulted in cell death within 48h (Furr and Jordan 1984). In the present setup, concentrations of 8 µM, 4 µM and 2 µM were found to be toxic for NCM cultures. After careful titration 200 nM tamoxifen were found to be the most suitable concentration.

To control for potential direct or indirect effects of tamoxifen-induced MerCreMer protein on Tβ4 expression (see Chapter 4), *MerCreMer* single-genotype NCM and fibroblast cultures were treated with 200 nm tamoxifen or equivalent EtOH control preparations. Tamoxifen-induced MerCreMer did not affect *Tβ4* mRNA levels which remained unchanged in *αMHC/MerCreMer* derived NCM and fibroblasts upon treatment (**Figure 3.15 A**).

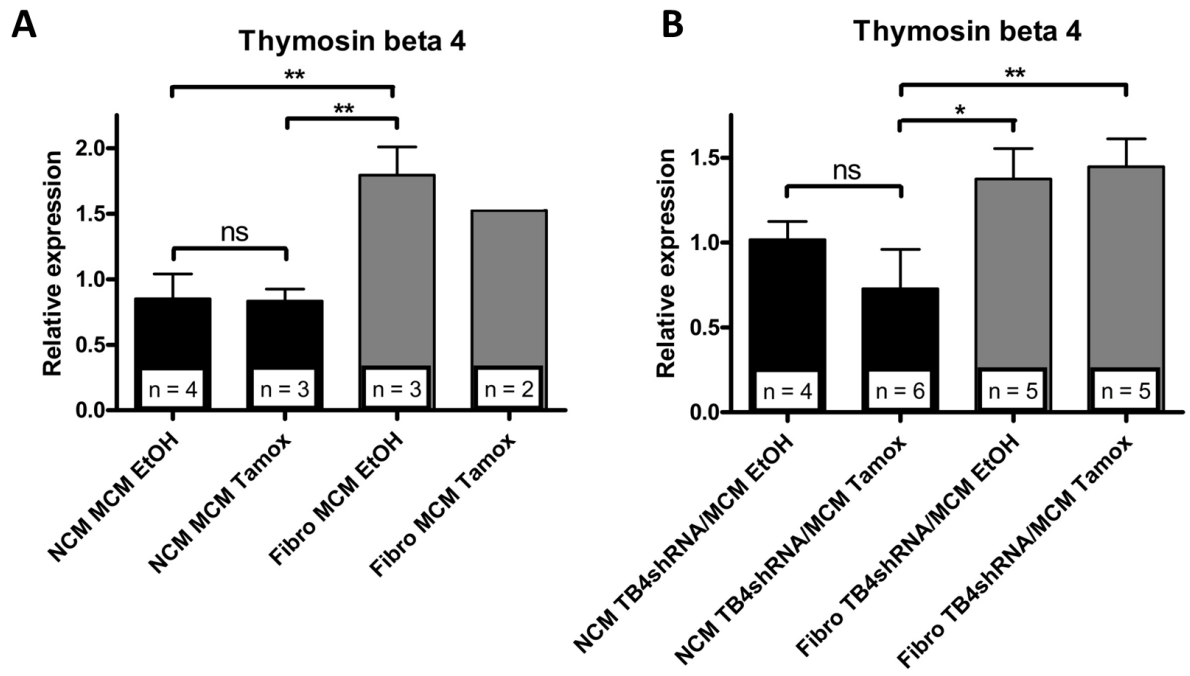


Figure 3.15: *Tβ4* mRNA levels after tamoxifen treatment of neonatal cardiomyocytes *in vitro* measured by rtPCR. (A) *Tβ4* mRNA levels in NCM and neonatal cardiac fibroblasts derived from *MerCreMer* single-transgenic littermates were analysed after tamoxifen treatment. (B) *Tβ4* mRNA levels in *Tβ4shRNAflox/MerCreMer* NCM and fibroblasts after tamoxifen treatment.

However, *Tβ4* mRNA was found to be significantly lower in *αMHC/MerCreMer* NCM compared to cardiac EtOH treated *αMHC/MerCreMer* fibroblasts. The loss of a tamoxifen-treated *MerCreMer* fibroblast sample meant that a sufficient number of samples was not available to include this group in the statistical analysis (n = 2). Tamoxifen treatment of *Tβ4shRNAflox/MerCreMer* NCM and fibroblasts resulted in a similar expression pattern, with higher *Tβ4* mRNA levels in neonatal cardiac fibroblasts compared to tamoxifen-treated NCM and no significant knockdown of *Tβ4* in NCM (**Figure 3.15 B**). Control-treated *Tβ4shRNAflox/MerCreMer* showed no significant change compared to fibroblast controls.

3.6 *Ex-vivo* investigation of *thymosin β4* knockdown in adult cardiomyocyte preparations isolated by Langendorff perfusion

One limitation of NCM cultures in terms of purity is the presence of cardiac fibroblasts. Even with relatively low starting counts following a good purification, the high proliferative potential of fibroblasts meant that a substantial contamination of up to estimated 10% was frequently observed at the end of each experiment. Eliminating all fibroblasts from the culture by prolonged pre-plating resulted in poor NCM cultures indicating the dependency of NCM on fibroblast-mediated conditioning of the culture likely by secretion of factors or extracellular

matrix. Since fibroblasts were shown to express higher concentrations of *Tβ4* mRNA than cardiomyocytes (**Figure 3.15**) the dilution of a putative knockdown (albeit small) and consequently the failure to reach a statistically significant result was conceivable. An additional confounding factor could comprise of the culture conditions which could have potentially induced changes in *Tβ4* mRNA expression. With the aim to limit these influences and to avoid dilution of the knockdown by *Tβ4*-expression of other cell types, adult cardiomyocytes were isolated from animals after 5 days tamoxifen injections (20 mg/kg). Since a separate line of experiments had established the formation of cardiac fibrosis and dysfunction in *αMHC/MerCreMer* animals following the 5 day injection protocol (see Chapter 4), a single injection protocol of 40 mg/kg tamoxifen was additionally tested in this study. The reduced total tamoxifen concentration was aimed at lowering the impact of the treatment on cardiomyocytes by limiting the time of MerCreMer in the nucleus. In order to determine the success of nuclear localisation of MerCreMer after a single tamoxifen injection (40 mg/kg), immunohistochemistry was performed on frozen sections of tamoxifen and control-treated *Tβ4shRNAflox/MerCreMer* mice three days after treatment. A single injection (40 mg/kg) was sufficient to induce nuclear localisation of MerCreMer although to a lesser degree than the 5 day injection protocol of 20 mg/kg daily (compare **Figure 3.8** and **Figure 3.16**).

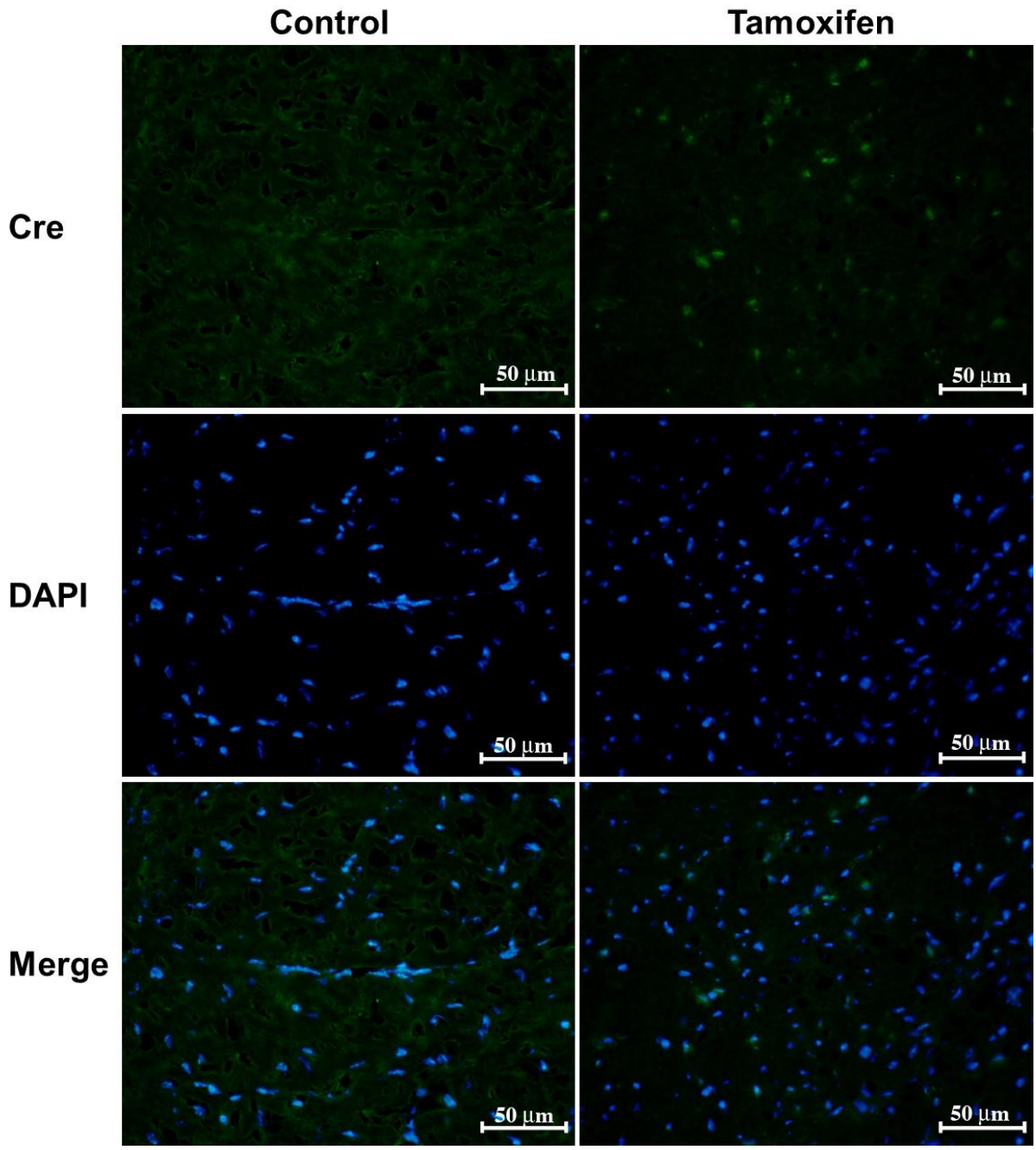


Figure 3.16: Immunofluorescence staining for Cre recombinase on left-ventricular cardiac tissue. Nuclear translocation of MerCreMer was shown in *Tβ4shRNAflox/MerCreMer* mice after 1d tamoxifen injection (40 mg/kg) but not after EtOH control injection. Green – anti-Cre, blue – DAPI. Scale bar 50 µm.

Following 5d/1d of tamoxifen injections and 1½ and 2½ months of rest respectively, hearts were harvested, Langendorff-perfused and adult cardiomyocytes enzymatically extracted from the tissue. Preparations typically yielded between 40% and 80% viable cardiac myocytes (**Figure 3.17**).

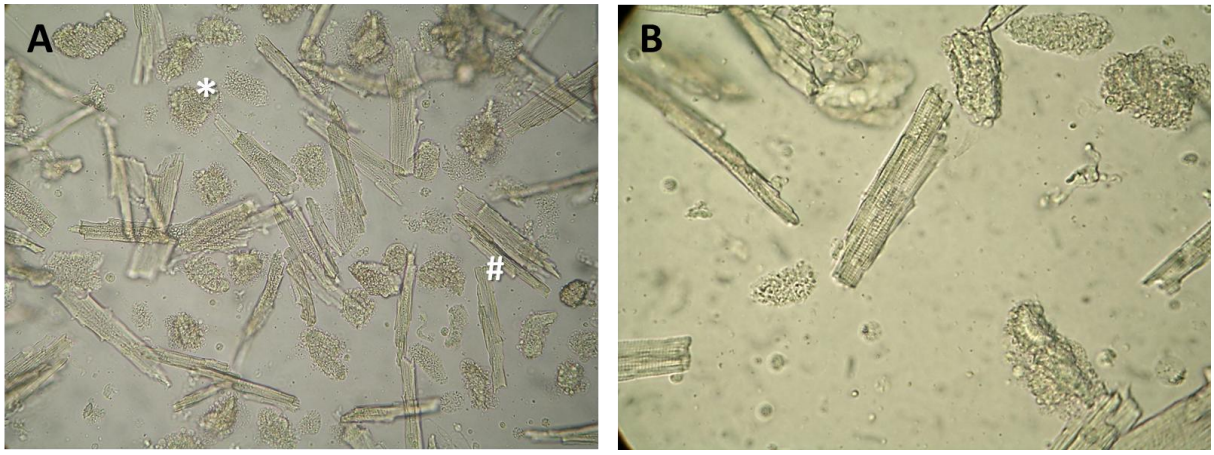


Figure 3.17: Morphology of adult cardiomyocytes isolated by Langendorff perfusion. (A) 10x magnification, (B) 20x magnification of adult cardiomyocytes in a Petri dish. * dead cardiomyocyte, # living and beating adult cardiomyocyte.

mRNA was extracted from the isolated NCM and rtPCR analysis revealed that *Tβ4* mRNA expression was unaltered compared to controls following 5 days of injections (20 mg/kg daily) and 1½ months of rest (**Figure 3.18**). In consequence, animals injected for 1 day (40 mg/kg) were maintained for 2 ½ months prior to analysis. Nevertheless, as for the 5-day-injected groups, this did not result in knockdown of *Tβ4* mRNA.

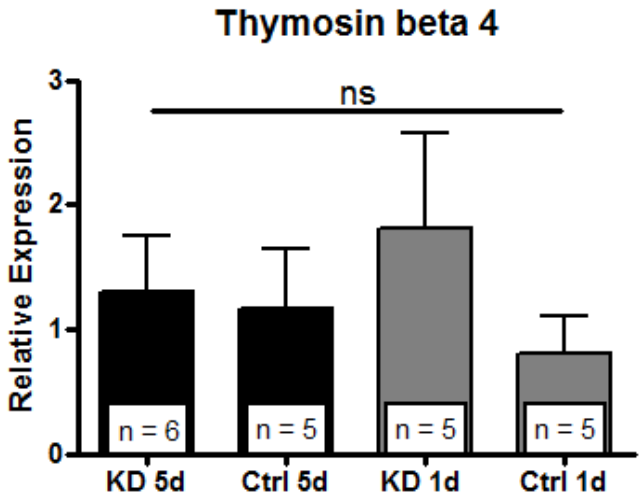


Figure 3.18: Determination of *Tβ4* mRNA levels in adult cardiomyocytes by real-time PCR. *Tβ4* mRNA levels were unaltered in adult cardiomyocytes from *Tβ4shRNA/MerCreMer* mice after 5d tamoxifen injections IP (20 mg/kg daily) and 1½ months of rest or 1d injection (40 mg/kg) and 2½ month of rest. Controls (Ctrl) consisted of a tamoxifen-treated, heterogeneous population of 2 *Tβ4shRNA* and 3 *MerCreMer* litter mates (5d) and 5 tamoxifen treated *wt* litter mates (1d) respectively.

3.7 Discussion

shRNA-mediated knockdown of *Tβ4* was evaluated after tamoxifen delivery in the diet, by IP injections, *in vitro* and *ex vivo*. In the following section strengths and limitations of each approach will be discussed and the overall suitability of a shRNA-mediated adult knockdown of cardiac *Tβ4* evaluated.

3.7.1 Tβ4 knockdown *in vivo*

Oral tamoxifen delivery: Delivering tamoxifen in the diet has caused unexpected changes in physiology and animal behaviour. The weight loss observed in mice on tamoxifen diet is likely a consequence of diet refusal since animals were age-matched and body mass was comparable at baseline across all groups (**Figure 3.4 A**, **Figure 3.5 B**). With reference to data presented in Chapter 4, it is however notable that the strongest decrease in body weight occurred in mice carrying the *MerCreMer* transgene potentially indicating a contribution of Cre. The observed reduction in liver weight can be explained by increased glucogenesis and concomitant depletion of hepatic intracellular glucose stores resulting in decreased hepatocyte size in response to fasting (**Figure 3.4 F**, Sokolovic *et al.* 2008). Relative lung weights in untreated *Tβ4shRNAflox/MerCreMer* mice were significantly lower compared to tamoxifen-treated *Tβ4shRNAflox/MerCreMer* mice, but since overall lung weights were similar across all groups this can be attributed to the physiological body weight gain in untreated mice, which was absent in the treated populations (**Figure 3.4 D, E**). Despite the fact that cardiac function was not chronically altered and normalised after 14 days of rest on normal diet oral delivery of tamoxifen via the diet proved to affect overall animal health and physiology to a degree that could certainly influence overall experimental outcomes (**Figure 3.3**). Since Cre localisation to nuclei of cardiomyocytes was only patchy and faint (**Figure 3.2**) and since no decrease in *Tβ4* mRNA levels was observed (**Figure 3.6**), concerns regarding the successful delivery of sufficient tamoxifen arose. In summary, refusal to ingest sufficient amounts of chow, indicated by total weight and liver weight loss, would explain the physiological and behavioural changes, as well as the failed knockdown of Tβ4. In addition, compensatory drinking indicated by excessive urination would have flushed out tamoxifen, thus further reducing tamoxifen levels in the body. To precisely control tamoxifen delivery and to avoid weight loss and the associated phenotypic changes, the IP injection protocol was adopted (Sohal *et al.* 2001).

IP tamoxifen injections: In addition to expected transitory cardiac dysfunction in *MerCreMer*-positive animals, cardiac interstitial fibrosis was discovered not only in tamoxifen-injected *Tβ4shRNAflox/MerCreMer* mice but also in tamoxifen-injected *αMHC/MerCreMer* animals (**Figure 3.10**, Buerger *et al.* 2006). Since these effects were not observed in control-treated *Tβ4shRNAflox/MerCreMer* mice, a causal relationship of tamoxifen-primed Cre or tamoxifen

alone was further investigated, as described in Chapter 4. Despite the longer resting period which allowed for more time of shRNA expression and its action, a decrease in *Tβ4* levels was not observed. The observation of higher levels of Tβ4 in blood vessel-associated cells by immunofluorescence compared to overall cardiac expression prompted the adoption of an *in vitro* approach using NCM.

3.7.2 Tβ4 knockdown *in vitro*

During NCM culture setup, pre-plating removes most fibroblasts adhering to the plastic of the cell culture dish and smaller cell types are excluded by sequential low speed centrifugation and medium changes. The resulting cultures contain low counts of fibroblasts and high concentrations of NCM. Near complete removal of fibroblasts from the culture by repeated pre-plating was observed to cause CM distress potentially caused by their dependence on basal levels of fibroblast-secreted factors (data not shown). Consequently, low levels of fibroblasts were allowed. Treating NCM with tamoxifen *in vitro* proved difficult due to the absence of protocols suitable for NCM in the literature. Concentrations used for other cell types proved to be cytotoxic for NCM and had to be lowered to sub-lethal levels. After finding changes in cardiac function in response to tamoxifen-primed MerCreMer in the *in vivo* knockdown study, the effects of tamoxifen-treating *αMHC/MerCreMer* NCM were evaluated. Tamoxifen treatment of *Tβ4shRNAflox/MerCreMer* NCM *in vitro* also showed no significant knockdown of *Tβ4* mRNA (**Figure 3.15 B**). The only other significant population of cells in the culture were cardiac fibroblasts in which a higher *Tβ4* mRNA expression was observed in comparison with NCM.

3.7.3 Assessment *ex-vivo*

The observation that fibroblasts express higher levels of Tβ4 compared to cardiomyocytes showed that more accurately defined experimental parameters were required to investigate the effects of adult loss of Tβ4 in cardiomyocytes. The use of highly purified adult cardiomyocytes cultures from *Tβ4shRNAflox/MerCreMer* mice following tamoxifen-treatment *in vivo* was considered to be a suitable additional approach since it removes contaminating cell types. Although FACS sorting and marker analysis by rtPCR were not performed, the isolation conditions were specifically designed for cardiomyocytes and final visual inspection did not reveal any living cell populations other than cardiomyocytes. RNA was isolated immediately following the isolation procedure, however as for the previous approaches, *ex vivo* investigation of adult cardiomyocytes did not show a knockdown of *Tβ4* (**Figure 3.18**).
While failure to observe *Tβ4* knockdown in any of the applied systems was unexpected and detrimental for the further conduct of this study, certain consideration need to be taken into account regarding each approach before judging the overall outcome.

3.7.4 Limitations *in vivo*

Despite the finding of fibrosis in tamoxifen-treated *αMHC/MerCreMer* mice (see also Chapter 4) there is uncertainty whether the amount of tamoxifen was sufficient to induce MerCreMer over a long enough period to activate shRNA expression. Although, MerCreMer was observed in nuclei following IP injections, others have reported that 5 days of 20 mg/kg tamoxifen IP is not sufficient to achieve significant reduction of their target gene (Koitabashi *et al.* 2009). Good recombination was reported at a dose of 80 mg/kg for 5 days but in this study resulted in 60% mortality after 7 days which would not have been acceptable in the UK following the Animals (Scientific Procedures) Act 1986. Furthermore, the side-effects in the surviving mice would have substantially influenced experimental outcomes. To distinguish between failed recombination and failed shRNA activity a direct investigation of genomic DNA by sequencing and analysis of *Tβ4shRNA* by Northern blotting respectively could have been performed and this should be considered for future shRNA-based depletion experiments (Hoess *et al.* 1982; Koscianska *et al.* 2011). An additional caveat constitutes the possibility that tamoxifen treatment alone modulates *Tβ4* expression. Recent reports have shown that tamoxifen can change approximately 10.9% of the transcriptome after 4 days of tamoxifen injections although at a higher dose of 40 mg/kg daily (Hougen *et al.* 2010). However, since no difference was detectable between tamoxifen-treated *Tβ4shRNAflox/MerCreMer* animals and EtOH control-treated *Tβ4shRNAflox/MerCreMer* mice, this was ruled out as a possible explanation for the failure to observe a knockdown. "Leaky" MerCreMer, i.e. its nuclear activity in the absence of tamoxifen, was reported *in vitro* and can result in failure to obtain changes in reference to the already affected baseline measurement (Buelow and Scharenberg 2008). However, this requires very high expression of MerCreMer. Furthermore, the authors suggest that a small cell size is important since their study investigated the relatively small DT-40B lymphocyte line. In addition, levels of non-tamoxifen primed nuclear MerCreMer would have been very low since nuclei of control-treated animals did not stain positive for Cre during IF (**Figure 3.1**).

While it is difficult to determine how much MerCreMer is expressed in our system and whether this is considered to be low enough to ensure tight regulation of Cre activity, cardiomyocytes are significantly larger than lymphocytes. That *Tβ4* mRNA levels were comparable between treated *Tβ4shRNAflox/MerCreMer* mice and *MerCreMer* littermates indicated that uninduced nuclear Cre activity does not account for the failed knockdown. While adjusted tamoxifen delivery approaches in terms of composition, route, concentration and timing are issues to be considered (see Chapter 4), a main limitation of this work has been the absence of a reliable expression profile of *Tβ4* in the adult heart. While there is some evidence that cardiomyocytes express higher levels of Tβ4 than the overall heart, I observed that vascular cells and fibroblasts are likely to contribute more significantly to the

cardiac Tβ4 pool than cardiomyocytes (Su *et al.* 2004). Since total cardiac RNA was investigated *in vivo*, this effect could have diluted the expected knockdown. In addition, macrophages, lymphocytes, and granulocytes were shown to express significant amounts of *Tβ4* (Xu *et al.* 1982; Gondo *et al.* 1987; Hannappel *et al.* 1989). While every effort was made to remove residual blood from the tissue before freezing, even low amounts of contaminating blood cells could have caused significant interference. For future investigations, careful expression profiling by *in situ* hybridisation should be performed in the respective model in advance to identify domains and cell types of high *Tβ4* expression. While levels in cardiomyocytes might be low, Tβ4 is a peptide with diverse functions and the role of basal Tβ4 expression and its importance for cardiac function especially after injury remain important questions to be answered.

3.7.5 Limitations *in vitro*

While experimentation *in vitro* had the described advantage of reducing contaminating cell populations a problem of the neonatal cell culture experiment was the genetic heterogeneity of the NCM. Whole litters of *Tβ4shRNAflox/MerCreMer* and *αMHC/MerCreMer* breedings were used for each NCM preparation, since genotyping individual embryos in advance was not feasible. Consequently, the cell population consisted predominantly of *Tβ4shRNAflox/MerCreMer* cells but also contained *MerCreMer* and *Tβ4shRNAflox* single-transgenic cardiomyocytes. This would have reduced the overall degree of knockdown observed within each pooled sample, especially if the level of knockdown was not high to start with. In addition, a general limitation of any cell culture experiment is the use of undefined serum. Growth factors and other molecules induce changes in cultured primary cells making them less comparable to cells *in vivo*. This also applies to the isolation of adult cardiomyocytes by Langendorff apparatus.

3.7.6 General considerations

It is indeed conceivable that the isolation conditions stimulated a survival signalling in cardiomyocytes involving upregulation of *Tβ4* (Bock-Marquette *et al.* 2004). Such an endogenous upregulation of Tβ4 as occurs in response to cardiac insult in zebrafish, mouse and pig heart could have been a source of substantial interference affecting all described *in vitro* experiments (Lien *et al.* 2006; Smart *et al.* 2007; Shah *et al.* 2011). *In vivo*, harvesting the heart for RNA extraction involved resection, weighing and dissected prior to freezing indicating that this limitation could extend to this part of study. To circumvent this potential caveat, freeze-clamping of beating hearts before cardiac resection and immediate storage in liquid N_2 would have been necessary. However, this would have limited the use of each heart to RNA analysis and would have doubled the amount of animals needed if other experiments

such as protein analysis and histology were to be performed as well. A final consideration should be given to the fact that standard mouse chow is soy-based and as such contains relatively high levels of phytoestrogens (Konhilas and Leinwand 2007). While the affinity of Mer for oestrogen is 1,000 times lower than for tamoxifen it is conceivable that in some settings this could result in unwanted MerCreMer activation (Zhang *et al.* 1996). However, as described previously, similar levels of *Tβ4* were observed in *Tβ4shRNAflox/MerCreMer* mice and single-genotype controls this can be discounted as a possible explanation.

Surprisingly, a very recent report showed that global knockout of *Tβ4* is not embryonic lethal and does not result in abnormal cardiac function or morphology (Banerjee *et al.* 2012). In general, global knockout mice can in some instances compensate for an early loss of function throughout their embryonic development by compensatory upregulation of functionally redundant or protective genes hence buffering the phenotype which would occur in an acute loss of function. However, Banerjee *et al.* included data from a conditional *Tβ4* knockout which showed no abnormalities following this sudden ablation of *Tβ4* during development. In the light of these new findings, it is evident that shRNA-mediated downregulation of Tβ4 as attempted here, is now obsolete since it is indirect, too complex and does not produce a significant cardiac phenotype. Conditional knockouts are more effective at depleting the target gene and do not suffer potential shRNA related pitfalls of limited knockdown efficiency and off target effects.

It is conceivable that the strong cardiac phenotype and embryonic lethality observed in *Tβ4shRNAflox/Nkx2.5-Cre* mice is the result of shRNA off-target effects or related to Cre toxicity (Chapter 4) or a combination of both (Smart *et al.* 2007). Regardless of these potential shortcomings of this developmental study, the beneficial effects of Tβ4 during wound healing and recovery have been well documented and it will remain an interesting candidate peptide for future gene or cell based therapy (Malinda *et al.* 1999; Philp *et al.* 2003; Bock-Marquette *et al.* 2004; Hinkel *et al.* 2008; Zhang *et al.* 2009). Besides its well characterised relationship with actin, only a limited number of Tβ4-interacting proteins have been identified (Safer *et al.* 1991; Didry *et al.* 2012). These include PINCH and ILK to facilitate complex formation with Akt1/2 (Fan *et al.* 2009), DNase helicase subunit II Ku80 (Bednarek *et al.* 2008), indirect or direct interaction with hMLH1 (Brieger *et al.* 2007) and more recently extracellular receptor F1-F0 ATP synthase (Freeman *et al.* 2011). However, how Tβ4 regulates the abundance of diverse functions described in the literature can currently not be explained mechanistically. Especially in the heart the absence of known binding partners necessitates future proteomic research into Tβ4-interacting proteins. An effective and popular approach to achieve this is the use of a tagged recombinant fusion proteins used to pulldown binding partners followed by 2D electrophoresis and mass spectrometry, as outlined in Chapter 5.

3.7.7 Summary

In summary, the presented work showed that *Tβ4* is expressed at higher levels in fibroblasts and potentially other cardiac cell types compared to cardiomyocytes. shRNA-mediated downregulation using a cardiomyocyte-specific tamoxifen-sensitive Cre driver is an overly complex approach of gene regulation since it requires excessive controlling and contains risks related to shRNA expression or functional failure. Furthermore, a recent publication has performed total ablation of *Tβ4* during development using a conditional knockout and observed no defects under physiological conditions. For future investigations into the function of Tβ4-depleted hearts during stress or injury, this model should be favoured over shRNA-based approaches.

Chapter 4 - Cardiac Fibrosis in Tamoxifen-treated *αMHC/MerCreMer* Mice

4.1 Introduction

Histological analyses of Chapter 3 showed interstitial cardiac fibrosis in the majority *MerCreMer*-positive mice (~60%) treated with tamoxifen for 5 days (20 mg/kg). *αMHC/MerCreMer* mice have become the most prominent tool of inducible cardiac gene regulation and a chronic defect such as fibrosis caused by the system itself would have significant implications for the interpretability of research past and present. This chapter describes the fibrotic phenotype discovered in tamoxifen-treated mice harbouring the *MerCreMer* transgene. The circumstances surrounding the appearance of the phenotype including the correlation between fibrosis and the abundance of *MerCreMer* in the genome were investigated in *Tβ4shRNAflox/MerCreMer* mice. The extent of the phenotype and molecular changes that contribute to it are characterised in the original *αMHC/MerCreMer* strain and the role of tamoxifen dose evaluated in this context.

4.2 Cardiac morphology of *Tβ4shRNAflox/MerCreMer* animals following tamoxifen treatment

Changes in cardiac function are often reflected in altered macroscopic or microscopic morphology of the heart. To investigate the cause of the observed decreased cardiac performance measured by ECHO, changes in cardiac morphology were analysed (Chapter 3, **Figure 3.12**). To assess the structure of *Tβ4shRNAflox/MerCreMer* hearts after tamoxifen-mediated induction of MerCreMer, paraffinised cardiac sections were stained by Masson's trichrome technique to visualise changes in extracellular matrix (ECM) expression and cellular architecture of the organ. After 5 days tamoxifen injections (20 mg/kg daily) and 3-4 weeks of rest, patchy interstitial and perivascular fibrosis was observed predominantly in the left ventricle, but also in the right ventricle and septum (**Figure 4.1**).

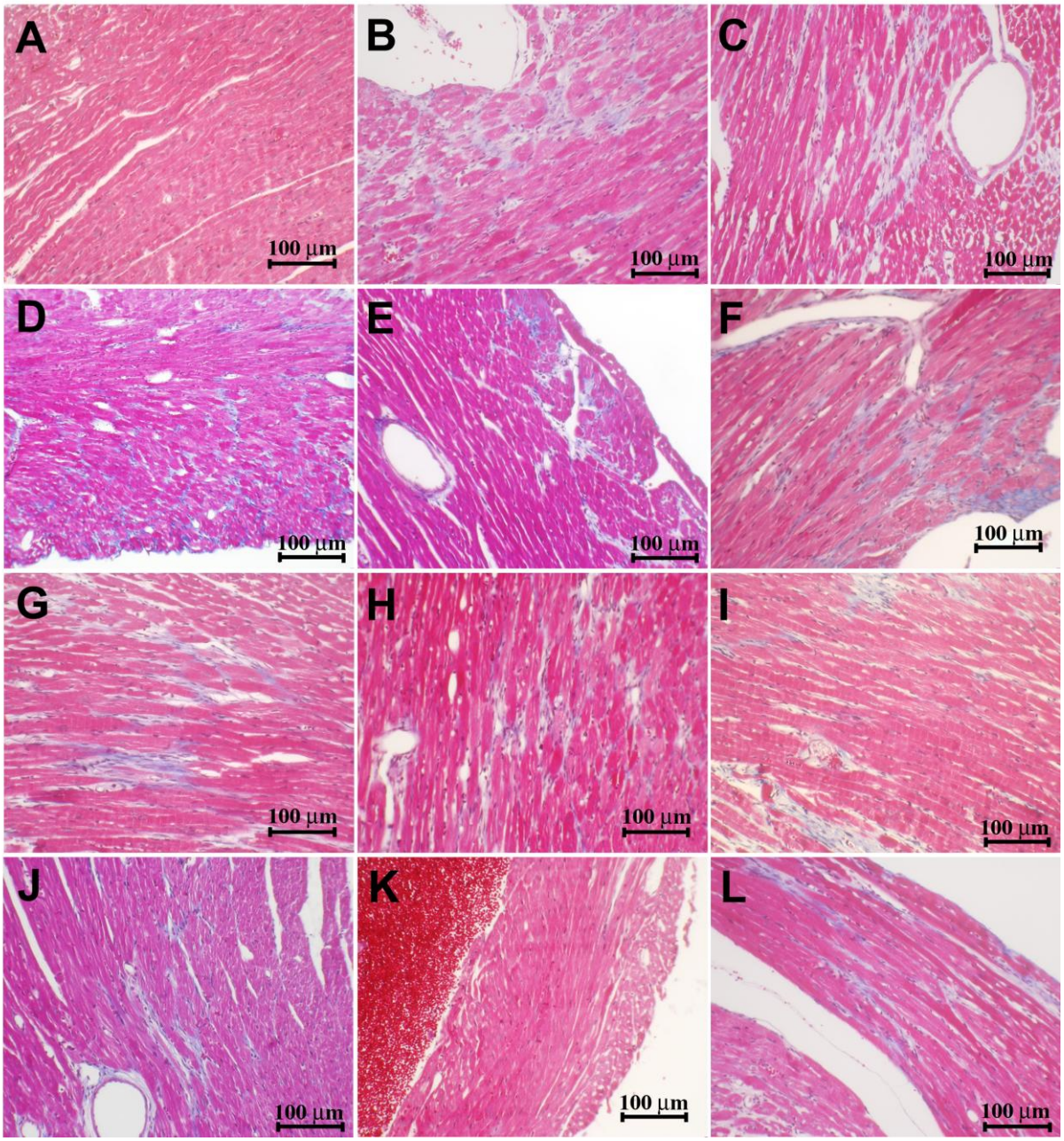


Figure 4.1: Masson's trichrome staining on cardiac sections following 5 days of tamoxifen injections and 3-4 weeks of rest. (A) Normal LV morphology observed in EtOH-treated *Tβ4shRNAflox/MerCreMer* mice. (B-E) Interstitial fibrosis observed in tamoxifen-treated *Tβ4shRNAflox/MerCreMer* mice and (F-I) tamoxifen-treated *MerCreMer* littermates. (J) Septum of tamoxifen-treated *Tβ4shRNAflox/MerCreMer* mouse. (K) RV observed in EtOH-treated and (L) in tamoxifen-treated *Tβ4shRNAflox/MerCreMer* mice. Scale bar 100 µm.

Fibrosis was accompanied by an infiltration of small cells in the proximity of blood vessels, which may relate to a strong inflammatory response. A larger study group was setup to specifically assess the distribution of fibrosis among mice of the different transgenic backgrounds used in this study. Animals were rested for 6-7 weeks after treatment to allow more time for the manifestation of the phenotype. To implicate tamoxifen in the disease

process, tamoxifen-treated *wt* and *Tβ4shRNAflox* animals as well as EtOH-treated *Tβ4shRNAflox/MerCreMer* mice were also included in this experiment. An incomplete penetrance of the fibrotic phenotype was observed, with only ~60% of tamoxifen-treated *MerCreMer*-positive mice affected (16/27, **Figure 4.2**, **Table 4.1**).

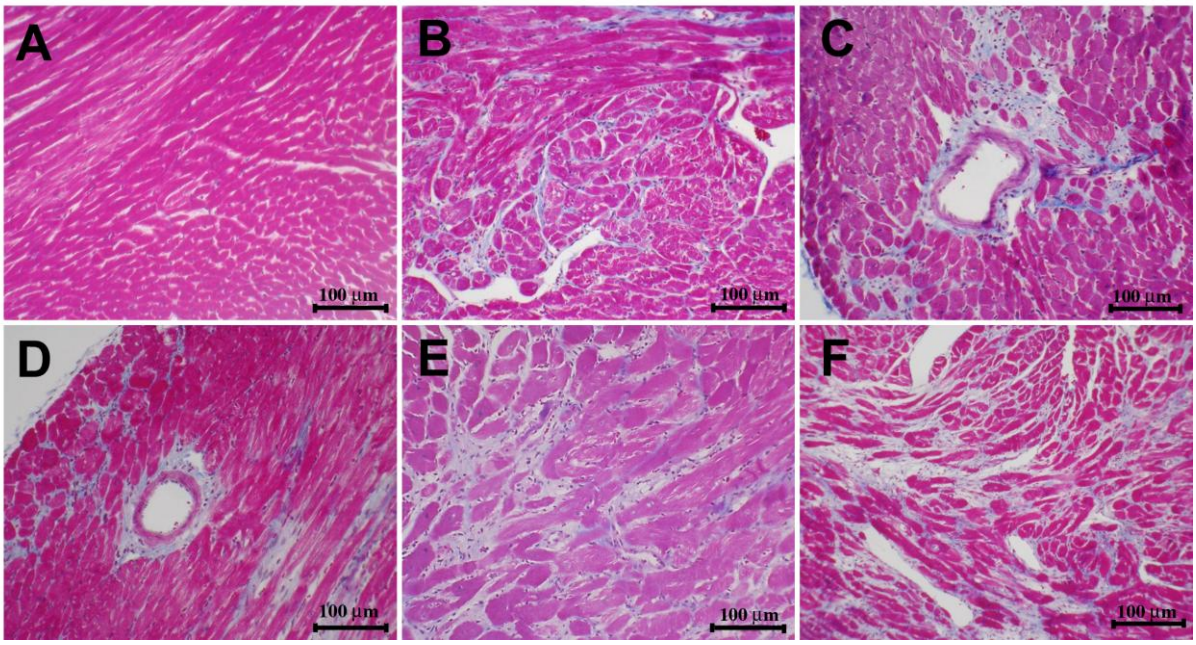


Figure 4.2: Masson's trichrome stain of cardiac sections of *Tβ4shRNAflox/MerCreMer* animals and controls following tamoxifen or control injections and 6-7 weeks of rest. (A) Normal cardiac morphology as observed in EtOH control treated *Tβ4shRNAflox/MerCreMer* mice and tamoxifen-treated *Tβ4shRNAflox* and *wt* animals. (B, C) *Tβ4shRNAflox/MerCreMer* animals and (D-F) *Tβ4shRNAflox*$^{-/-}$*/MerCreMer* animals display cardiac fibrosis after 5 days of daily tamoxifen injections (20 mg/kg). All images display LV tissue. Scale bars 100 µm.

Based on observations by Buerger and co-workers showing that high cellular levels of Cre driven by the *αMHC* promoter (*αMHC/Cre*) caused dilated cardiomyopathy, heart failure and death in mice in a copy number-dependent fashion, a potential correlation of the phenotype with *MerCreMer* gene copy number was investigated (Buerger *et al.* 2006). Since, *αMHC/MerCreMer* transgenic animals were generated by non-targeted insertion, detection of homo-/heterozygosity by means of normal genotyping PCR was not possible. Hence, a gene copy analysis was performed by rtPCR (**Table 4.1**).

Table 4.1: *Cre* gene copy number analysis. Genotype and correlating gene copy score indicating heterozygosity/low Cre (0.86 – 1.35), homozygosity/high Cre (1.80 – 2.62) and absence of a *Cre* transgene (~0). Presence and absence of cardiac fibrosis following tamoxifen injections for 5 days at 20mg/kg daily are indicated by + and – respectively.

Genotype	Gene copy score	Cardiac fibrosis	Cardiac fibrosis per group	Group classification
Tβ4shRNAflox/MerCreMer	0,97	+*	**9/14**	**Low Cre**
	1,05	+		
	1,08	+		
	1,09	+		
	0,95	+		
	1,01	+		
	0,93	+		
	1,04	+		
	0,96	+		
	0,86	-		
	0,96	-		
	0,99	-		
	1,05	-		
	1,35	-		
MerCreMer	0,92	+	**3/5**	**Low Cre**
	0,98	+		
	1,19	+		
	0,92	-		
	0,93	-		
	1,00 #	-		
Tβ4shRNAflox/MerCreMer	1,80	+*	**2/5**	**High Cre**
	1,98	+		
	2,23	-		
	2,44	-		
	2,62	-		
MerCreMer	2,18	+*	**3/3**	**High Cre**
	2,31	+		
	2,43	+		
Tβ4shRNAflox and *wt*	0,00	-	**0/5**	**Cre negative**
	0,00	-		
	0,00	-		
	0,00	-		
	0,04	-		

Reference sample, * Severe cardiac fibrosis

No correlation between cardiac fibrosis or its severity and gene copy number could be observed since both *MerCreMer* homo- and heterozygous mice of any background were affected by fibrosis. *Tβ4shRNAflox* and *wt* littermate controls had the expected gene copy score of 0 and served as negative controls in this experiment.

4.3 Abnormal cardiac function and morphology in *αMHC/MerCreMer* mice following tamoxifen treatment

Tβ4shRNAflox/MerCreMer animals used in Chapter 3 were of a mixed *129Ola/C57Bl/6J* background. To address the possibility of strain-specific effects of *MerCreMer* expression, 8 week old heterozygous *αMHC/MerCreMer* mice of the original *C57Bl/6J* background were examined at 4-5 weeks following standard tamoxifen treatment (5 days, 20 mg/kg daily). A significant depression of cardiac function (EF% 51.04 ± 2.10, FS% 23.40 ± 2.00) compared to *wt* mice (EF% 62.55 ± 3.00, FS% 29.35 ± 2.17), untreated *αMHC/MerCreMe*r mice of various ages (8w EF% 60.21 ± 3.64, FS% 28.36 ± 1.44, 7-8M EF% 59.27 ± 1.34, FS% 27.07 ± 1.35) and tamoxifen treated *Cre*-negative (*MerCreMer-/-*) littermates (EF% 59.31 ± 2.50, FS% 27.55 ± 2.37) was observed by ECHO (**Figure 4.3**).

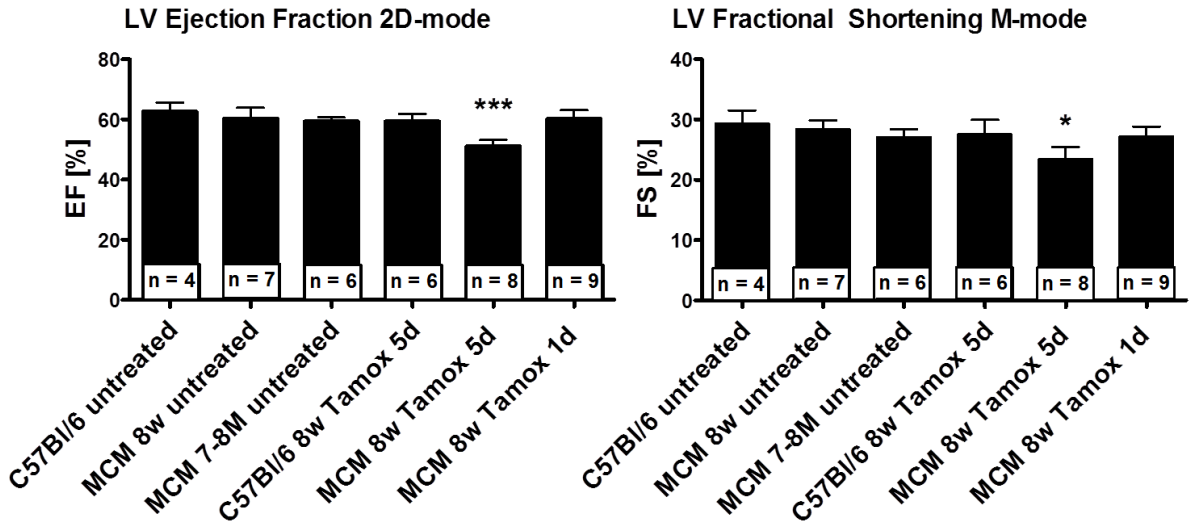


Figure 4.3: Cardiac function of *αMHC/MerCreMer* measured by ECHO. Animals were injected with tamoxifen for 1 day (40 mg/kg) or 5 days (20 mg/kg daily) and rested for 4-5 weeks. Left-ventricular ejection fraction measured in 2D-mode was significantly reduced after 5 days tamoxifen injections in *αMHC/MerCreMer* mice compared to *wt* or untreated littermates (*** $p < 0.001$). Injecting a single dose of tamoxifen (40 mg/kg) had no effect on function. Left-ventricular fractional shortening was significantly reduced in the 5 days-injected group compared to all other groups (* $p < 0.05$). Data is expressed as ± SD.

Since the original study was conducted in *Tβ4shRNAflox/MerCreMer* mice at 3-4 month of age, aged *αMHC/MerCreMer* mice were included in the analysis to rule out any age related occurrence of fibrosis as a consequence of chronic cytoplasmic levels of MerCreMer protein. Given that Hougen and co-workers reported that a single tamoxifen injection of 40 mg/kg is sufficient to induce recombination without impacting cardiac function, an additional *αMHC/MerCreMer* group using the 1 day injection protocol was assessed (Hougen *et al.*

2010). A single injection of tamoxifen (40 mg/kg) showed no detectable negative effect on cardiac function in the ECHO traces (EF% 60.14 ± 2.92, FS% 27.16 ± 1.62).

Histological analyses revealed that following the 5 day injection protocol, all samples of *MerCreMer*-positive animals displayed interstitial and perivascular cardiac fibrosis (5/5, **Figure 4.4**). As previously described for *Tβ4shRNAflox/MerCreMer* animals (**Figure 4.2**), increased ECM expression and replacement of cardiomyocytes with fibroblasts were observed in LV, RV and interventricular septum in this group. The single injection protocol did not result in any microscopic changes of heart morphology.

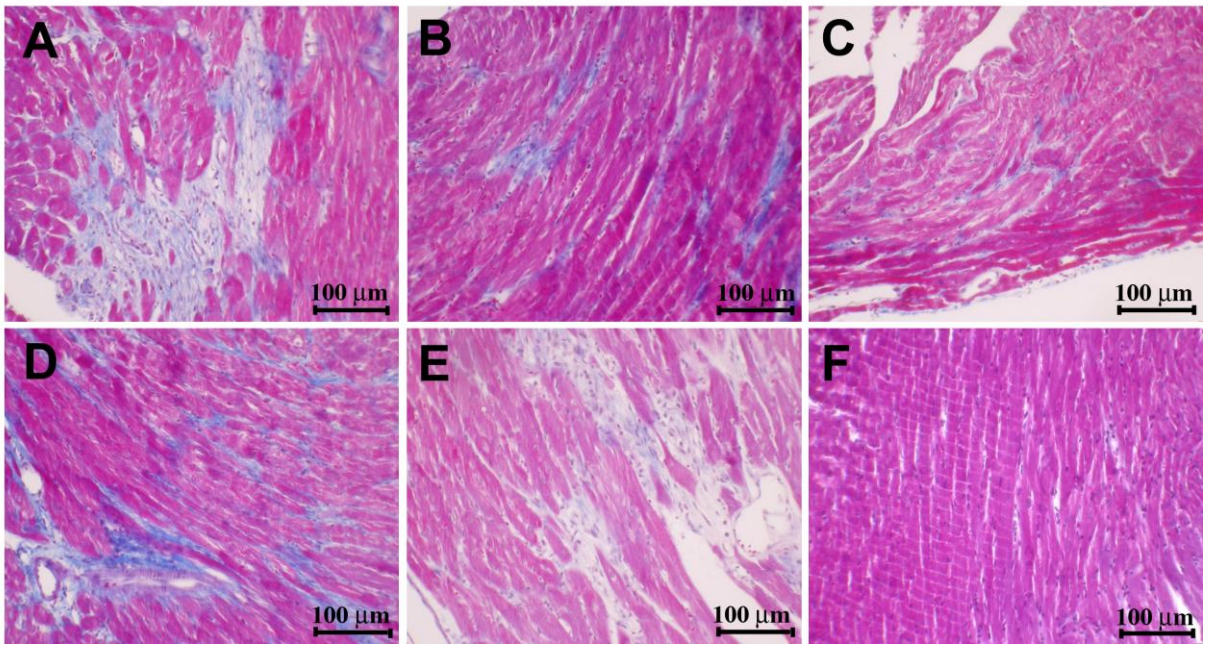


Figure 4.4: Masson's trichrome staining of cardiac sections of *αMHC/MerCreMer* animals after tamoxifen injections and 4-5 weeks of rest. (A-E) Interstitial and perivascular fibrosis in the LV of following 5 days of injections (20 mg/kg). (F) LV morphology after a single injection of tamoxifen (40 mg/kg). Scale bar 100 µm.

Gross cardiac morphology was normal with no thinning or thickening of myocardium in the affected group. This is in line with the ECHO data showing normal LV inner diameters (LVID) during diastole and systole (**Figure 4.5**). Untreated *αMHC/MerCreMer* animals of all ages (8 weeks, 7-8 months) were unaffected.

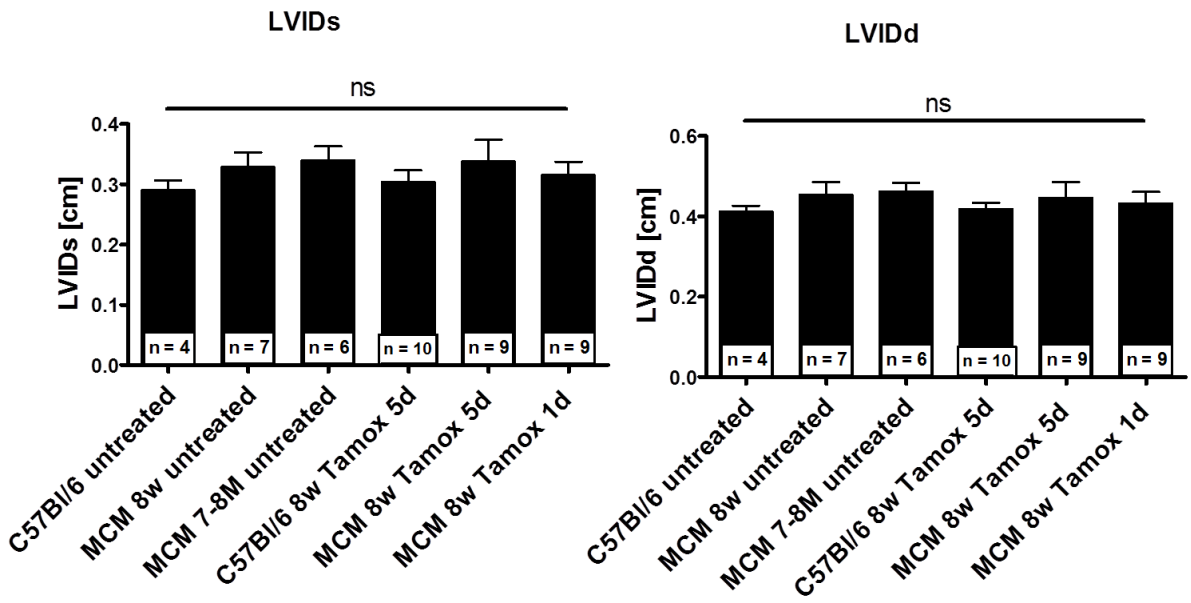


Figure 4.5: Left-ventricular inner diameters analysed by ECHO. Left-ventricular inner diameters of untreated *αMHC/MerCreMer* animals of various ages and tamoxifen-treated animals at 8 weeks of age were measured during diastole (LVIDd) and systole (LVIDs).

Following 1 day (40 mg/kg) or 5 days (20 mg/kg) tamoxifen treatment, normal BW, HW/BW and LuW/BW ratios and a healthy liver weight were observed in *αMHC/MerCreMer* and *C57BL/6J* mice compared to untreated *αMHC/MerCreMer* animals (**Figure 4.6**).

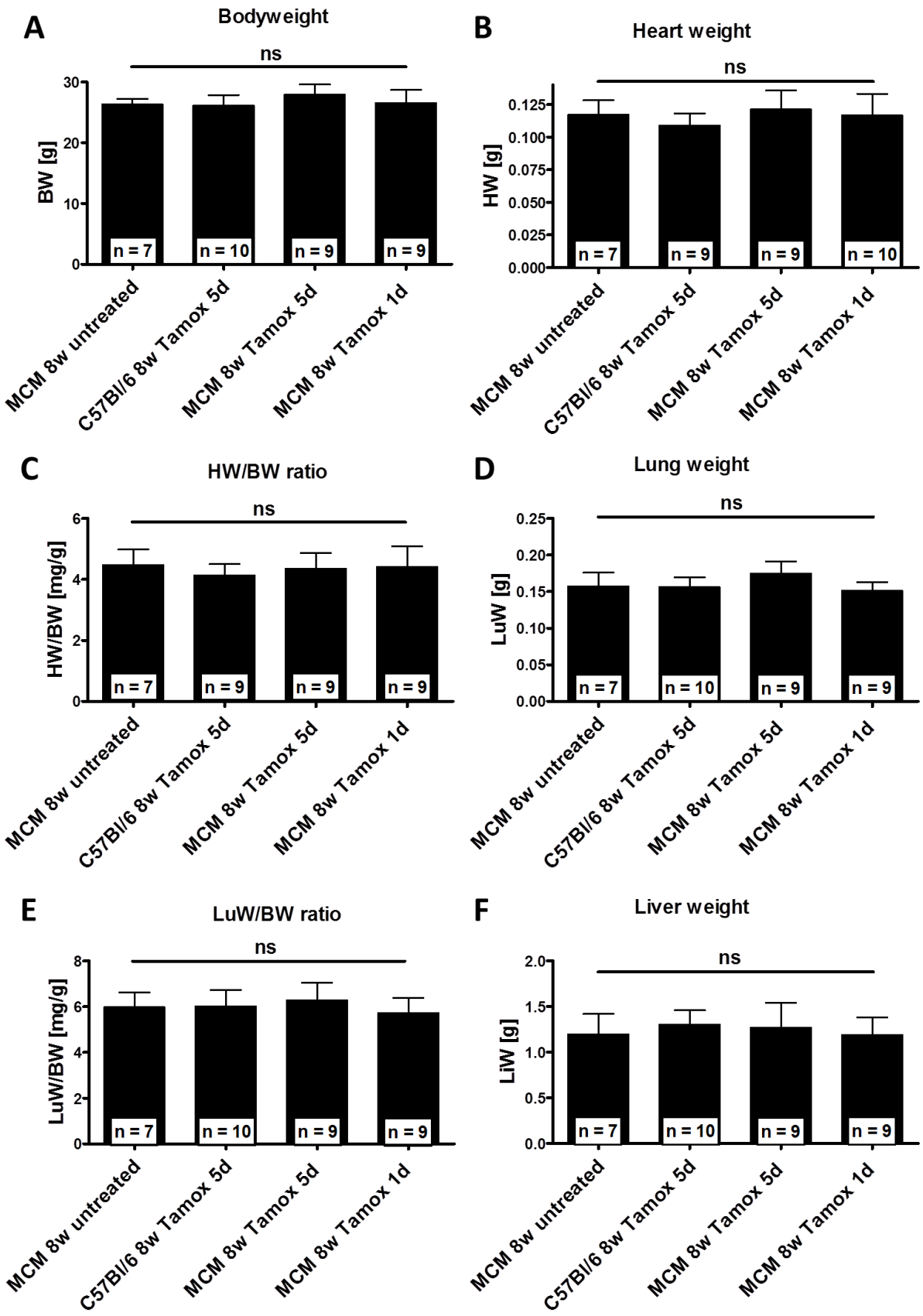


Figure 4.6: Physiological parameters of *αMHC/MerCreMer* mice measured after tamoxifen or control injections and 4-5 weeks of rest. (A) Body weight, (B) heart weight, (C) heart-weight-to-body-weight (HW/BW) ratio, (D) lung weight, (E) lung-weight-to-body-weight (LuW/BW) ratio and (F) liver weights

of *αMHC/MerCreMer* and *C57BL/6J* mice after 1d or 5d tamoxifen treatment (40 mg/kg, 20 mg/kg daily).

In summary, detailed analyses including histology and functional assessment showed that despite the fibrosis, dilated cardiomyopathy, hypertrophy or advanced heart failure were not present after 4-5 weeks of rest in animals treated with a single tamoxifen injection.

4.4 Mechanism of MerCreMer-induced fibrotic phenotype

To investigate the immediate response of the heart to 5 days tamoxifen exposure, animals were sacrificed 3 days after completing the treatment. At time of explant, the hearts of tamoxifen treated *αMHC/MerCreMer* animals showed clear signs of an inflammatory reaction, such as swelling and a deep red discoloration. Histology revealed cell infiltrates in the affected ventricles (**Figure 4.7**).

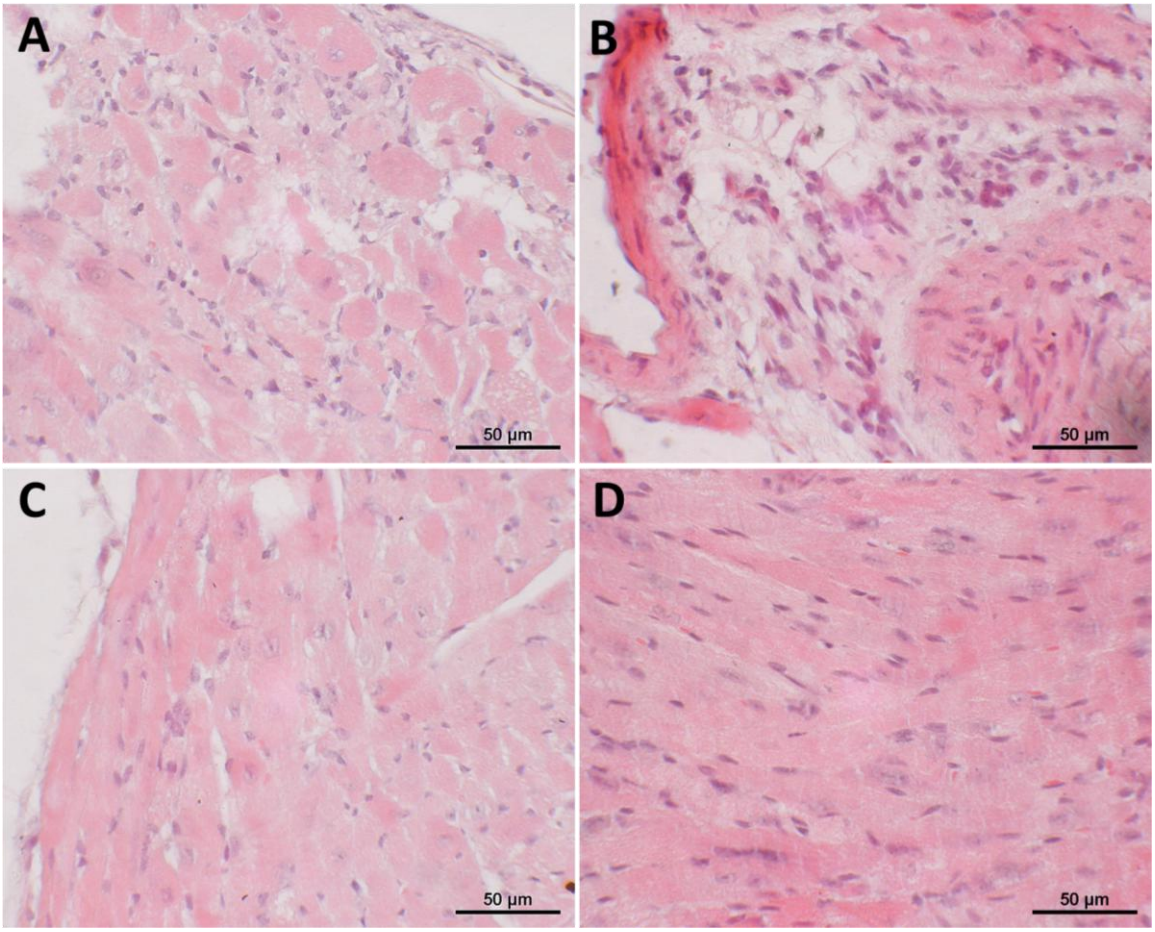


Figure 4.7: Cardiac sections of tamoxifen treated *αMHC/MerCreMer* mice 3 days after tamoxifen treatment. (A, B) Haematoxylin/Eosin staining showing cell infiltration, cardiomyocyte loss and beginning tissue replacement after 5 days of tamoxifen injections (20 mg/kg daily). (C, D) Normal cardiac morphology in unaffected areas of the same hearts. Scale bar 50 µm.

To further understand the mechanisms involved in the observed phenotype, rtPCR analysis for mediators of inflammation was performed. Pro-inflammatory cytokines *IL-1β*, *IL-6*, *TNFα*, *IFNγ* and *Ccl2* were significantly upregulated in tamoxifen-treated *αMHC/MerCreMer* mice compared to controls (**Figure 4.8**).

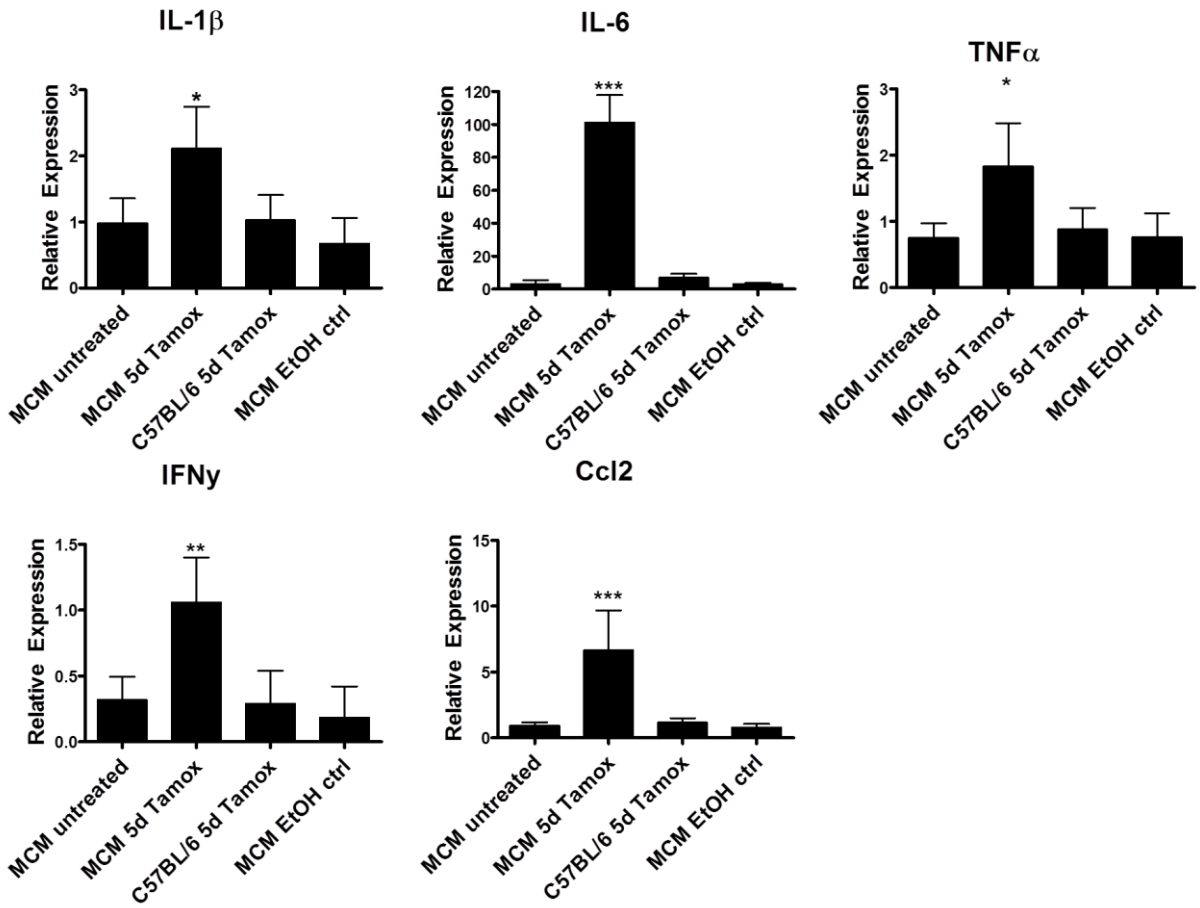


Figure 4.8: Cytokine expression analysis in tamoxifen treated *αMHC/MerCreMer* animals. rtPCR analysis at 3 days following 5d tamoxifen injections (20 mg/kg daily). *αMHC/MerCreMer* mice presented significant upregulation of pro-inflammatory *IL-1b*, *IL-6*, *TNFα*, *IFNγ* and *Ccl 2* mRNA. n = 7, 4, 4, 4 from left to right on the graph.

In addition, the expression of anti-inflammatory markers *IL-10* and *TGFβ1* was increased in this group (**Figure 4.9**).

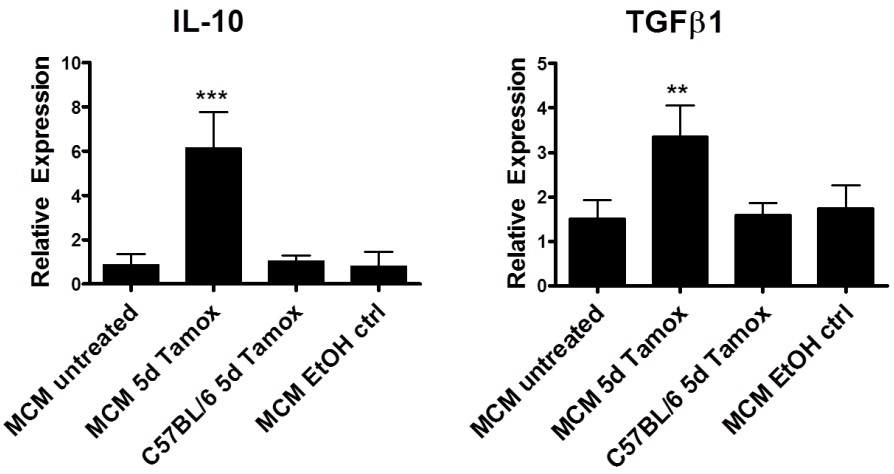


Figure 4.9: rtPCR cytokine expression analysis in tamoxifen treated *αMHC/MerCreMer* animals. Anti-inflammatory cytokines *TGFβ1* and *IL-10* are significantly upregulated 3 days after completion of 5 days tamoxifen (20 mg/kg daily). n = 7, 4, 4, 4 from left to right on the graph.

While functional and morphological analyses had not indicated cardiac hypertrophy or failure following 5 days tamoxifen treatment (20 mg/kg), *ANF, BNP* and *Col3A1*, hallmarks of cardiac remodelling, were expressed at significantly higher levels compared to controls (**Figure 4.10**, McMullen and Jennings 2007; Felkin *et al.* 2009).

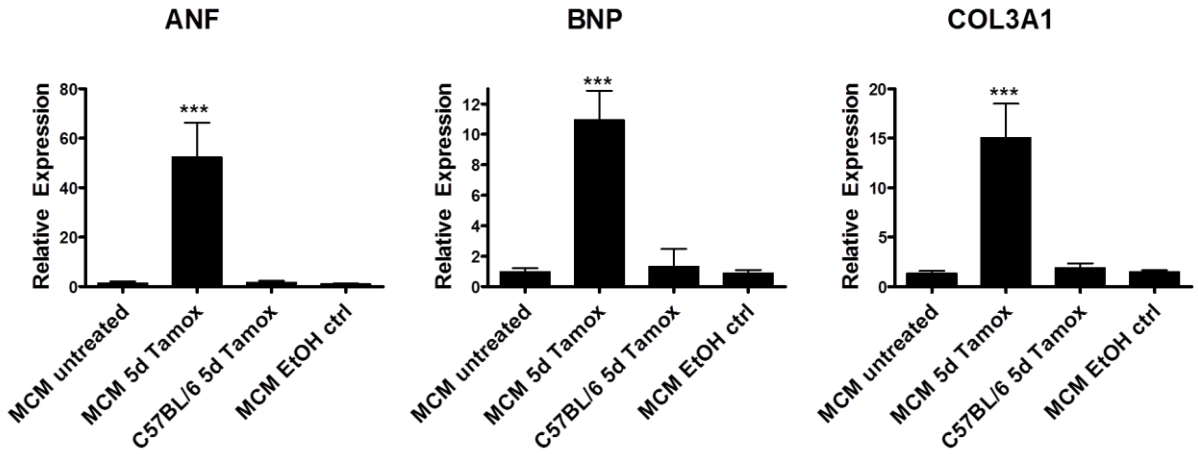


Figure 4.10: rtPCR for markers of cardiac remodelling 3 days after completion of 5 days tamoxifen (20 mg/kg daily). *αMHC/MerCreMer* mice express elevated levels of *ANF*, *BNP* and *Col3a1*. n = 7, 4, 4, 4 from left to right on the graph.

The extensive inflammatory response observed after treating *αMHC/MerCreMer* for 5 days (20 mg/kg daily) was not observed after a single injection of tamoxifen (40 mg/kg) and *IFNγ* expression was the same across all groups (**Figure 4.11**). However, *TNFα* was significantly

upregulated compared to all controls and levels of *IL-1β, IL-6* and *Ccl2* where elevated compared to untreated animals but not compared to tamoxifen-treated control mice.

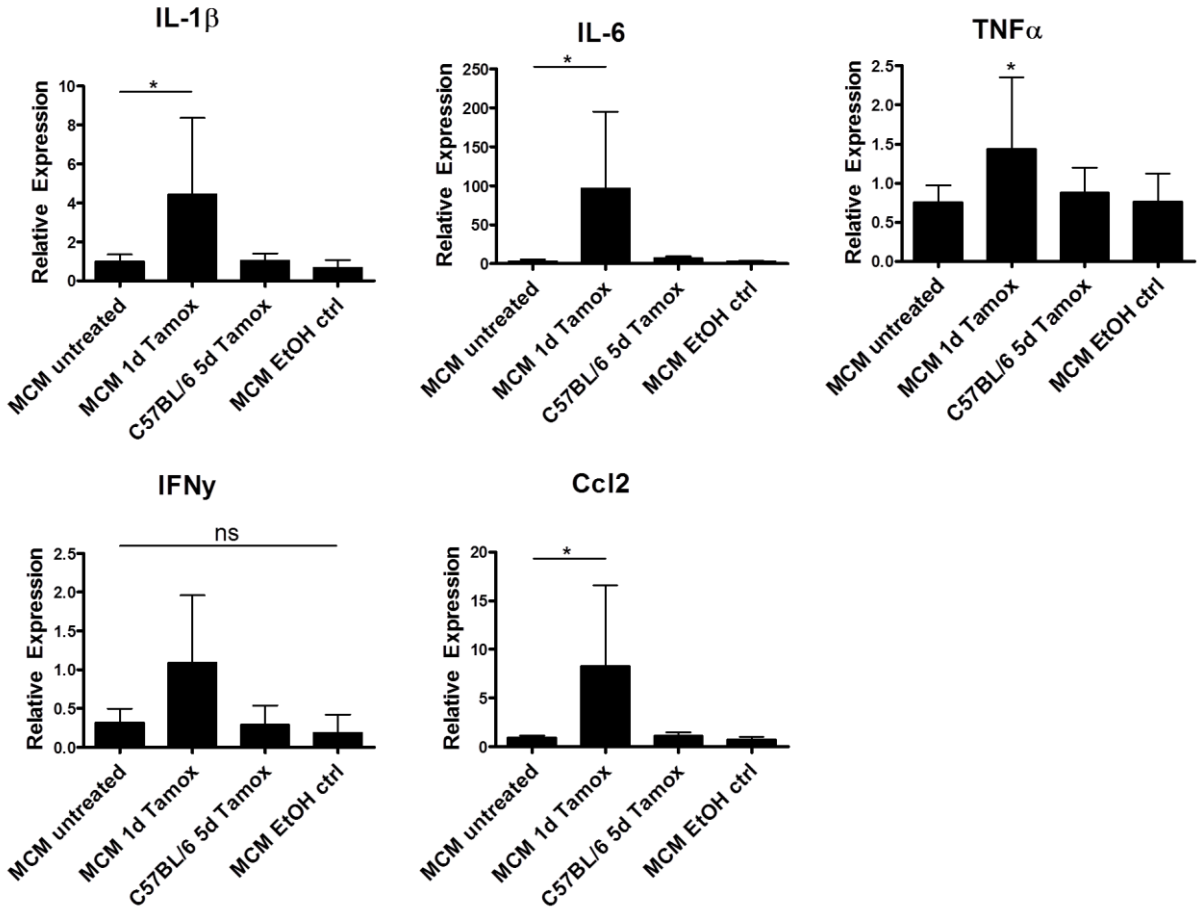


Figure 4.11: rt-PCR for pro-inflammatory makers in the heart of *αMHC/MerCreMer.* Following a single (1d) tamoxifen injection (40 mg/kg) differential expression of *IL-1β*, *IL-6*, *TNFα* and *Ccl2* was detected. n = 7, 4, 4, 4 from left to right on the graph.

Unlike after 5 days of tamoxifen treatment (20 mg/kg), mRNA levels of *IL-10* and *TGFβ1* were not upregulated 3 days following the single-injection protocol (40 mg/kg, **Figure 4.12**).

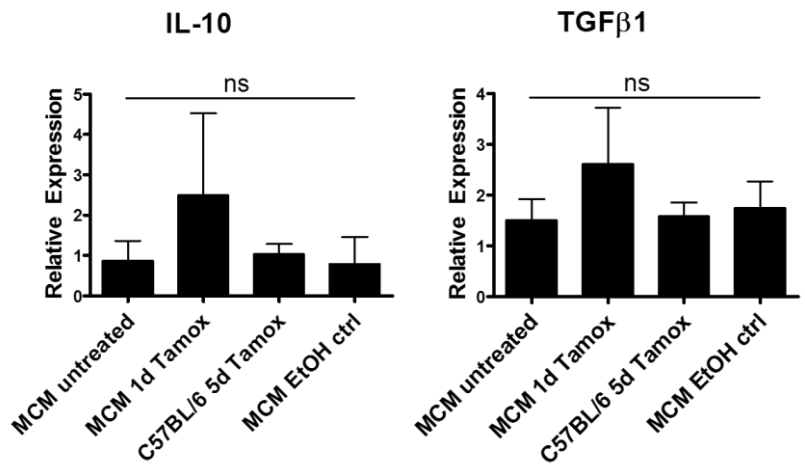


Figure 4.12: rtPCR analysis of anti-inflammatory markers following a single injection of tamoxifen (40 mg/kg). No difference in *IL-10* and *TGFβ1* mRNA levels were detected. n = 7, 4, 4, 4 from left to right on the graph.

While histological analysis of 1 day-treated *αMHC/MerCreMer* hearts had not revealed any morphological changes, markers of cardiac remodelling were upregulated in response to this reduced total tamoxifen dose and treatment period (**Figure 4.13**).

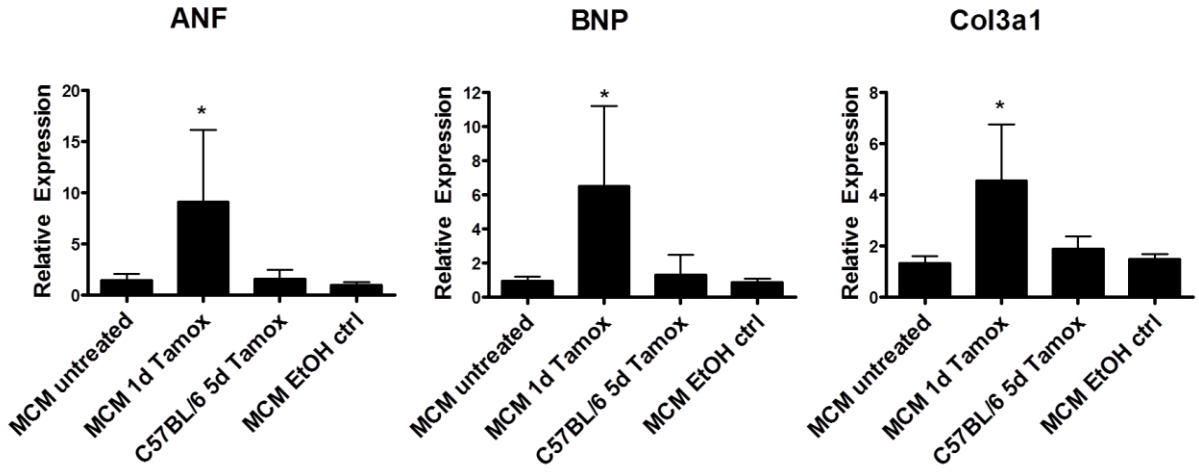


Figure 4.13: rtPCR analysis of markers of cardiac remodelling following a single injection of tamoxifen (40 mg/kg). Upregulation of *ANF*, *BNP* and *Col3a1* mRNA levels was detected following treatment. n = 7, 4, 4, 4 from left to right on the graph.

To evaluate the role of apoptosis in the pathological phenotype, proteins involved in apoptotic signalling were investigated by Western blotting 3 days following tamoxifen treatment (**Figure 4.14**).

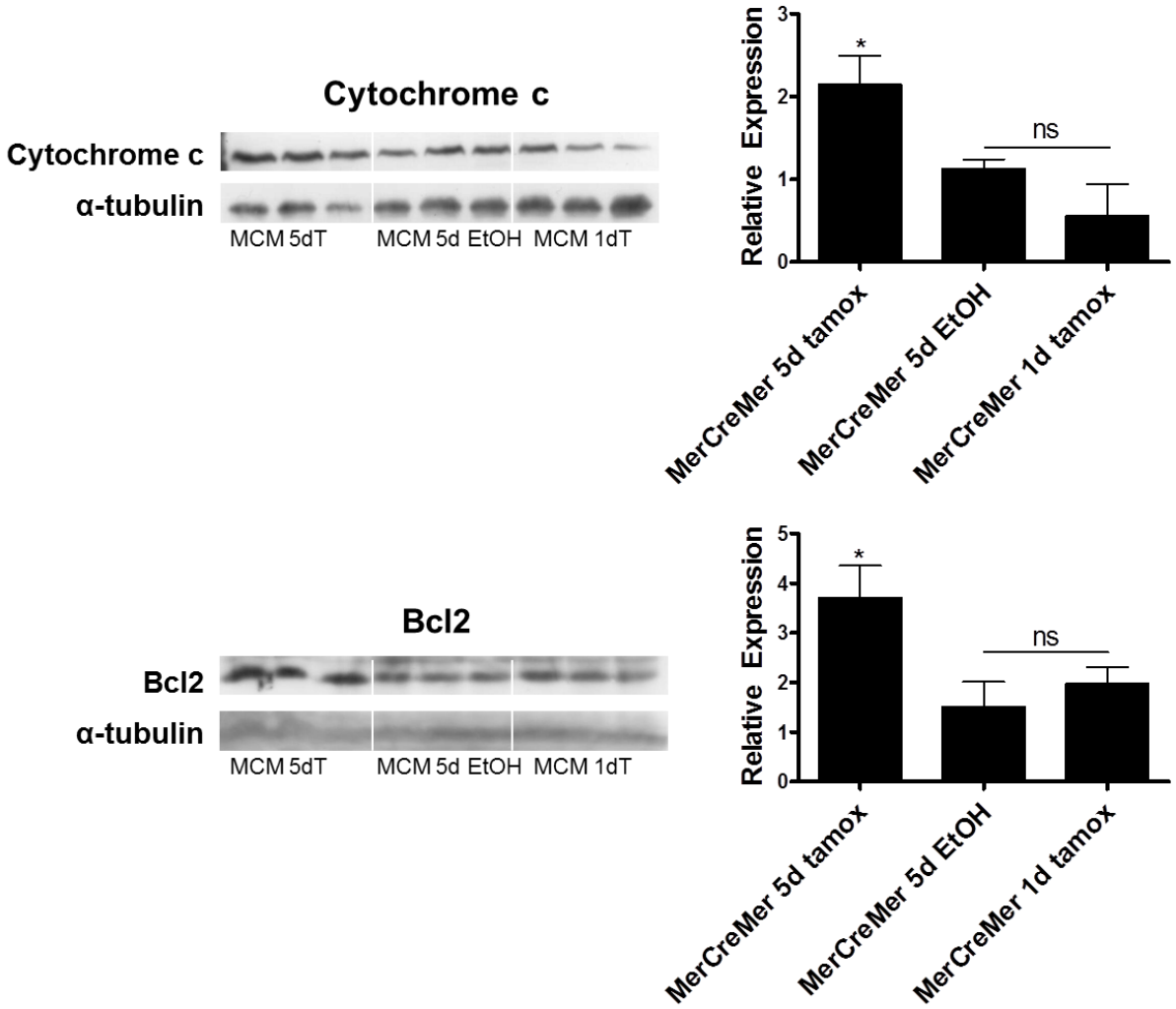


Figure 4.14: Western blots for markers of apoptosis. Cytochrome c and Bcl2 proteins are upregulated in *αMHC/MerCreMer* mice 3 days following 5 days of tamoxifen injections (20 mg/kg daily). Levels after one day of tamoxifen (40 mg/kg) are comparable to those in control-treated *αMHC/MerCreMer* mice.

This showed an upregulation of both cytochrome c and Bcl-2 in animals treated for 5 days (20 mg/kg daily), but not after a single injection of tamoxifen (40 mg/kg). Cleaved caspase 3 was not observed after tamoxifen treatment (**Figure 4.15**).

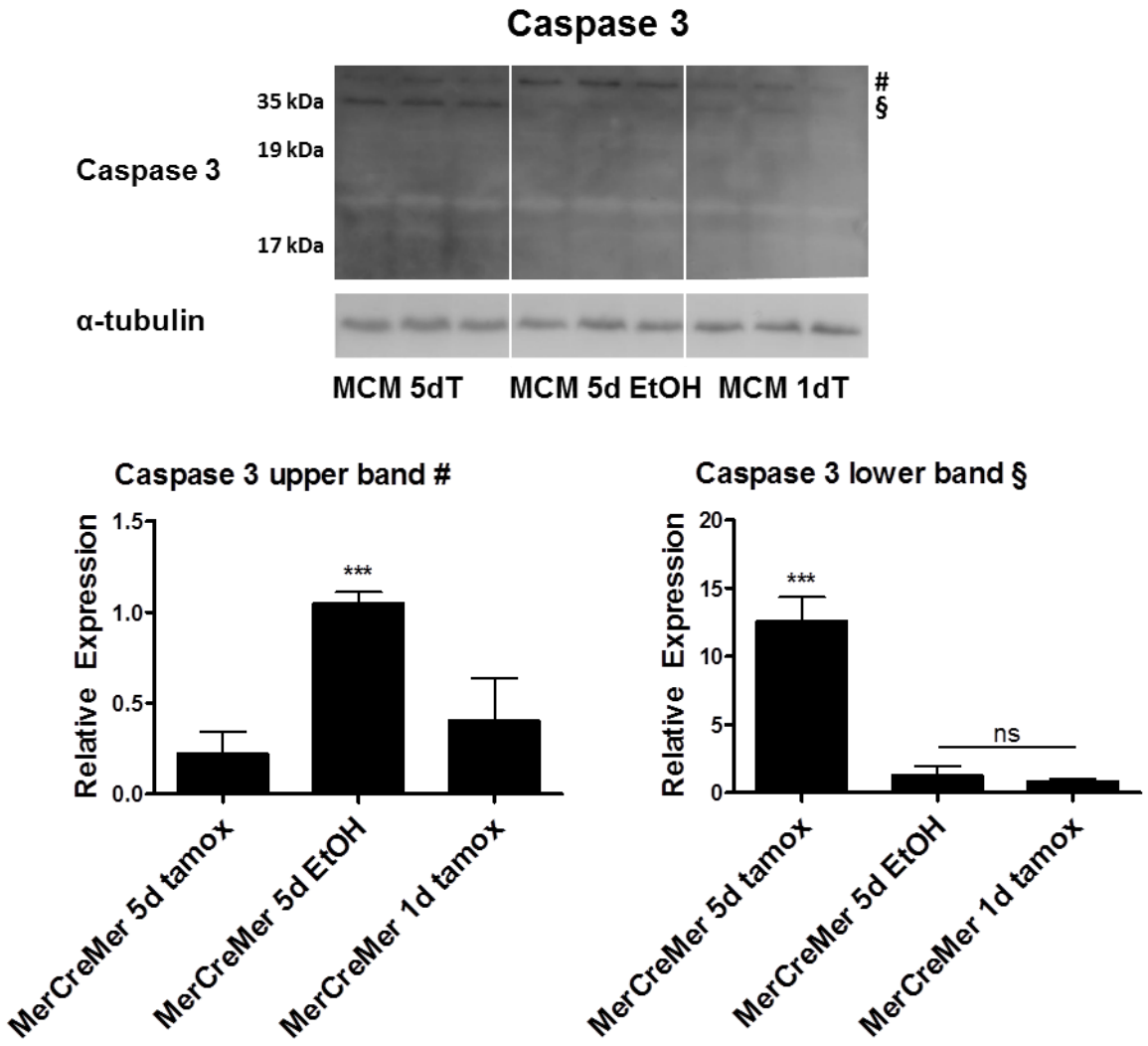


Figure 4.15: Western blot analysis for caspase 3. *αMHC/MerCreMer* mouse heart protein extracts were analysed for caspase-3 cleavage 3 days following tamoxifen treatment. No cleaved caspase 3 was observed in any group. Uncleaved pro-caspase-3 was detected at 35 kDa and ~40 kDa respectively. The upper band (#) is decreased in both tamoxifen treated groups. The lower band (§) is shows upregulation of this isoform after 5 days of tamoxifen exposure (20 mg/kg daily) but not after 1 day (40 mg/kg) of treatment.

However, a changed expression pattern was observed between two bands that appear to be different isoforms or differentially modified versions of pro-caspase-3 at 35 kDa and 40 kDa. Bax was not differentially regulated following tamoxifen treatment (**Figure 4.16**).

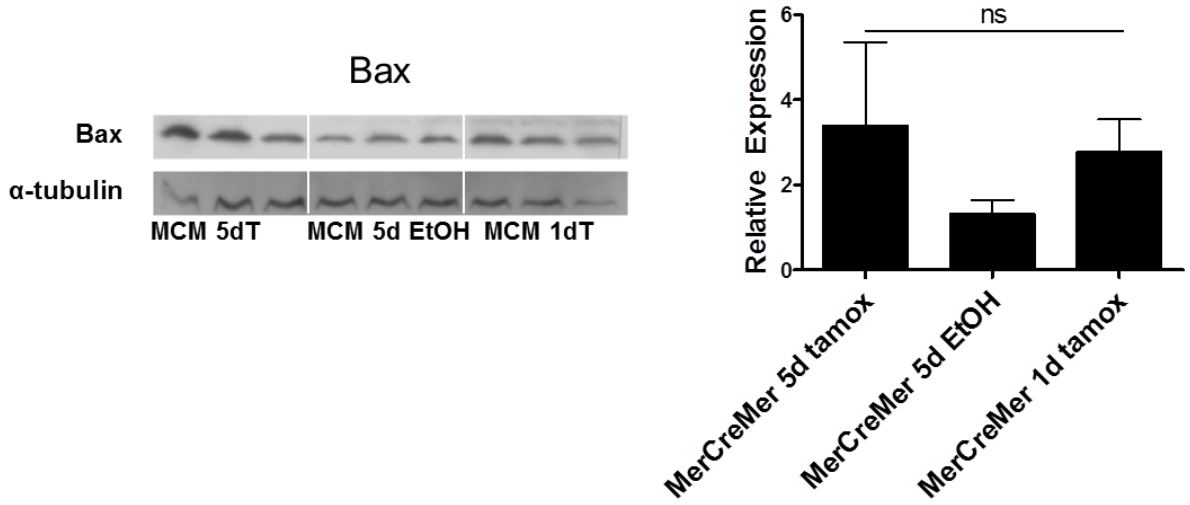


Figure 4.16: Western blotting analysis of Bax expression in *αMHC/MerCreMer* mice. Cardiac protein extracts were analysed 3 days following 5 days of tamoxifen (20 mg/kg daily), a single injection of tamoxifen (40 mg/kg) or control treatment.

Levels of apoptotic regulator Bax were not significantly changed between groups, but high variation within the 5 day-treated group was observed.

4.5 Discussion

The presented data shows that episodic tamoxifen-primed nuclear Cre recombinase accumulation in adult mouse hearts causes irreversible damage to the myocardium, reflected in decreased left-ventricular function. Since a single injection of tamoxifen (40 mg/kg) did not result in cardiac fibrosis, the observed phenotype is dose dependent and is caused by either the nuclear levels of MerCreMer protein or its duration in the nucleus, or a combination of both. While my results show that the single injection protocol is sufficient to induce nuclear localisation of MerCreMer in *αMHC/MerCreMer* cardiomyocytes, the nuclear signal was less pronounced compared to that after 5 days of injections (20 mg/kg), raising questions whether sufficient recombination is achieved by low tamoxifen exposure. That cytoplasmic MerCreMer in itself is not toxic was further supported by the observation of normal cardiac function and morphology in aged untreated animals (data not shown). Tamoxifen alone was also shown to have no effect in any *MerCreMer*-negative background. The toxicity of nuclear Cre could potentially stem from promiscuous aspecific genomic recombination at cryptic *loxP* sites on the genome (Loonstra *et al.* 2001; Semprini *et al.* 2007). This could lead to chromosomal aberration following DNA fragmentation and could be responsible for cell death and subsequent replacement of cardiac myocytes by fibroblasts resulting in the observed phenotypes. The observed cell infiltration and upregulation of various cytokines involved in

acute inflammation (*IL-1β*, *IL-6*, *TNFα*, *IFNγ* and *Ccl2*) in the tamoxifen treated *αMHC/MerCreMer* group, are a further indicators of the negative impact of excessive active MerCreMer in cardiac tissue (**Figure 4.7**, **Figure 4.9**). Although this response could be secondary to excessive tissue damage or necrosis, it is a further factor potentially compromising interpretation experimental outcomes, such as inflammation and cell death, which are frequently assessed in cardiac regeneration research studies. This also applies for markers of cardiac hypertrophy (*ANF, BNP, Col3a1*), frequently used as indicators of hypertrophy in cardiac-specific conditional knockout mice. Elevated pro-hypertrophic markers in tamoxifen-treated *αMHC/MerCreMer* mice have been reported previously, although higher doses of tamoxifen were used in these studies (40 mg/kg daily for 5 days, 200 mg total) (Andersson *et al.* 2010). The fact that *IL-10* and *TGFβ* mRNA levels were increased after 3 days is potentially attributable to a negative feedback response and indicating the end of the acute inflammatory phase following MerCreMer-mediated insult (**Figure 4.9**). A single injection of tamoxifen (40 mg/kg) resulted in a more heterogenic outcome. While pro-inflammatory *TNFα* was increased in the treated group, changes in *IL-1β*, *IL-6* and *Ccl2* were only statistically significant in comparison to the untreated *αMHC/MerCreMer* control group. mRNA levels of *IFNγ* were unchanged (**Figure 4.11**). While anti-inflammatory cytokines (*IL-10* and *TGFβ1*) were not elevated potentially due to the absence of a preceding inflammatory reaction, markers of cardiac remodelling (*ANF*, *BNP* and *Col3a1*) were shown to be increased, although to a lesser degree compared to the 5 days injection protocol (**Figure 4.12**, **Figure 4.13**). This indicated that while the single injection protocol was generally better tolerated, it still affected some parameters important for the assessment of cardiac health. To investigate the implication of apoptotic signalling in the observed phenotype, typical markers of programmed cell death were investigated by Western blotting. Increased cytochrome c expression indicated upregulated apoptosis, 3 days after 5 tamoxifen injections (20 mg/kg daily). The observation of elevated anti-apoptotic Bcl2, however, suggested that the resting period of 3 days was long enough to remove most damaged cells and the surviving tissue was counteracting sustained programmed cell death. This was supported by the fact that one of the key indicators of apoptosis, cleaved caspase-3, was not detected at this time point. Cleaved caspase-3 is rapidly activated and peaks around 30 h after insult in some tissues (Tyas *et al.* 2000; Ray *et al.* 2008). While there is no direct evidence for loss of an apoptotic signalling in the first 3 days following the treatment, the absence of cleaved caspase-3 could indicate excessively damaged cells have already completely undergone apoptosis in the damaged areas of the heart. In addition, pro-apoptotic Bax, a central regulator of all apoptotic pathways, was not expressed at increased levels 3 days after completed treatment, further supporting that apoptosis is either complete or the putative cell death follows a different mechanism such as necrosis (Wei *et al.* 2001).

Overall, the present findings are consistent with a recent parallel report, describing the chronic detrimental impact of MerCreMer and tamoxifen administration on cardiac physiology (Lexow *et al.* manuscript submitted, Kuhn *et al.* manuscript submitted).

4.5.1 *αMHC/*MerCreMer in the literature

Since *αMHC/MerCreMer* mice have been used in numerous cardiac research studies to date, I conducted a survey of the literature to determine previous reports of Cre mediated toxicity in the heart. A significant number of recent publications showed the use of this strain in conditional gene targeting without including tamoxifen treated *αMHC/MerCreMer* single-genotype experimental controls (**Table 4.2**).

Table 4.2: Publications using *αMHC/MerCreMer* mice in experiments without inclusion of tamoxifen-treated *αMHC/MerCreMer* controls (list not exhaustive).

Author	Journal	Year	Age of animals	Injection protocol	Reference
Birnbaum *et al.*	*Basic Res Cardiol*	2011	?	20 mg/kg * day^{-1}, 7d	(Birnbaum *et al.* 2011)
Agarwal *et al.*	*Circ Res*	2010	6w	40 mg/kg * day^{-1}, 5d	(Agarwal *et al.* 2010)
Ruan *et al.*	*J Mol Cell Cardiol*	2010	10-12w	20 mg/kg * day^{-1}, 7d	(Ruan *et al.* 2009)
Stokke *et al.*	*Cardiovasc Res*	2010	10w	40$^{\#}$ mg/kg * day^{-1}, 1d	(Stokke *et al.* 2010)
Andersson *et al.*	*J Mol Cell Cardiol*	2009	8-10w	40$^{\#}$ mg/kg * day^{-1}, 4d	(Andersson *et al.* 2009)
Wang *et al.*	*PNAS*	2009	?	100 mg/kg * day^{-1}, 5d	(Wang *et al.* 2009)
Martins *et al.*	*Circulation*	2008	3/8w	20 mg/kg * day^{-1}, 5d	(Martins *et al.* 2008)
Nakai *et al.*	*Nat Med*	2007	8w	80 mg/kg * day^{-1}, 7d	(Nakai *et al.* 2007)
Noh *et al.*	*Am J Physiol Endocrinol Metab*	2006	8-9w	20 mg/kg * day^{-1}, 2w	(Noh *et al.* 2006)
Zhou *et al.*	*Am J Physiol Heart Circ Physiol*	2006	3-4M	20 mg/kg * day^{-1}, 2w	(Zhou *et al.* 2007)
Parlakian *et al.*	*Circulation*	2005	2M	20 mg/kg * day^{-1}, 4d	(Parlakian *et al.* 2005)

M - month, w - week, d - day, $^{\#}$ - estimated

Noh *et al.*, Martins *et al.*, Parlakian *et al.*, Agarwal *et al.*, Ruan *et al.*, Andersson *et al.*, Nakai *et al.*, and Zhou *et al.* measured cardiac function by ECHO at different time points and reported varying degrees of impairment of cardiac function. Since tamoxifen-treated *αMHC/MerCreMer* controls were omitted, it is impossible to judge the contributions of the respective knockout and Cre-toxicity respectively to the reported functional (ECHO), histological (fibrosis) and molecular (*ANF* upregulation) phenotype. It is worth noting that many of these studies used far more extensive treatment regimen compared to that used in this project with some having used up to five times the tamoxifen dose or having extended the treatment to over 2 weeks. Among these publications, Noh *et al.*, Wang *et al.*, Martins *et al.* and Parlakian *et al.* observed cardiac fibrosis which they attributed to their conditional

knockout phenotype (Parlakian *et al.* 2005; Noh *et al.* 2006; Martins *et al.* 2008; Wang *et al.* 2009). Furthermore, Martins *et al.*, Andersson *et al.* and Nakai *et al.* claim that their respective conditional knockouts (*dicer*, *serca2a, atg5*) result in increased *ANF* expression (Nakai *et al.* 2007; Martins *et al.* 2008; Andersson *et al.* 2009). Nakai *et al.* and Ruan *et al.* also performed TUNEL assays to investigate cell death *in vivo* and in Langendorff perfused hearts (Ruan *et al.* 2009).

In the light of my results, the findings derived from these studies could have potentially been confounded by a Cre-mediated cardiomyopathy. We are grateful for the input of the authors Faqian Li, Vickas Patel, Garret Fitzgerald, Ira Goldberg, Mathis Stokke and Zhenlin Li who were open to discuss their use of *αMHC/MerCreMer* mice and the resulting data in personal communications. This confirmed that indeed in many cases, an unspecified number of control mice had been monitored during preliminary experiments, but were excluded from the main experiments that were later published due to the apparent absence of any remarkable phenotype. It is conceivable that the number of animals used during the setup phase was small and affected animals were not identified due to a low number being affected in the corresponding genetic background or discarded as irrelevant outliers.

Differences in genetic background are indeed likely a contributing factor to the observed variation in phenotypic penetrance. This is supported by the fact that we observed fibrosis in 60% of *Tβ4shRNAflox/MerCreMer* mice (*129Ola/C57Bl/6J*) and in 100% of *αMHC/MerCreMer* mice (*C57Bl/6J*), following tamoxifen treatment. This should be noted when considering that the majority of reports involving the *αMHC/MerCreMer* strain incorporated appropriate controls and some performed histological analyses, but did not report the detrimental phenotype observed here. For instance, studies by Xiong *et al.* and Di *et al.* measured fibrosis in tamoxifen treated *αMHC/MerCreMer* control mice, but did not report a fibrotic or otherwise adverse phenotype (Xiong *et al.* 2007; Di *et al.* 2010). Mice used in these studies were of *CD1/Balbc/C57Bl/6* and *C57Bl/6* backgrounds respectively. Since the phenotype appears less pronounced in certain genetic backgrounds, it is also conceivable that the fibrotic phenotype was missed where only a small number of animals were investigated. Regarding functional assessments by ECHO, it is evident that several measurements and a sufficiently large study group are required to identify significant outcomes when investigating small changes, as in the case of Cre-mediated cardiac damage.

4.5.2 Potential solutions to the problem of inducible Cre-mediated toxicity

Optimising the mode of tamoxifen administration: Temporary effects of tamoxifen exposure and nuclear MerCreMer accumulation on cardiac function have been well documented and methods have been proposed to reduce a transient cardiomyopathy (Hougen *et al.* 2010;

Hall *et al.* 2011). In addition to genetic background, the specific details of the injection protocol and the form of tamoxifen used may constitute parameters contributing to diverse outcomes. For instance Kiermayer *et al.* reported that oral tamoxifen citrate appears to be equally effective in terms of recombination and potentially safer compared to tamoxifen or its active metabolite 4-hydroxytamoxifen, while at the same time reducing stress and adverse effects associated with injections (Kiermayer *et al.* 2007). However, as the present study underlines, oral delivery is sensitive to diet refusal by the animals and can consequently result in insufficient recombination, weight loss and starvation-related phenotypes (see Chapter 3, Andersson *et al.* 2009).

These findings are in line with previous reports showing that administration of tamoxifen citrate pellets resulted in 10% weight loss regardless of genotype after 4 days as well as suboptimal recombination (< 50%) after 7 days (Andersson *et al.* 2010). Consequently, despite causing some stress to the animals, injecting tamoxifen citrate might be a good approach (Touvron *et al.* 2012 manuscript submitted). Regardless, there are a number of supportive arguments for delivery in the diet. It was demonstrated that tamoxifen absorption via the gut is as effective as via peritoneal cavity and changing the constitution of the chow could address diet refusal issues (Seibler *et al.* 2003). Indeed, Andersson *et al.* showed good acceptance of the chow and optimal recombination after feeding in the animals with self-made tamoxifen cakes (Andersson 2010). Others have shown that a mix of tamoxifen and soft chow over 7 days showed no mortality during oral delivery at concentrations (80 mg/kg) that were lethal during IP injections (Koitabashi *et al.* 2009). This is attributable to the fact that the LD_{50} of tamoxifen via the diet is 15-fold higher compared to IP injections (Seibler *et al.* 2003). The protocol proposed by Andersson *et al.* describes crushing standard chow and mixing it with drinking water and tamoxifen (Sigma T5648) at 0.5 mg/g (mass of dry chow, (Andersson *et al.* 2010). After drying, these pellets were administered for 4 days, which proved to be as effective as 2 days of tamoxifen in oil at 40 mg/kg via IP injections in terms of recombination. The oral delivery of raloxifene as a substitute for tamoxifen was also shown to be effective and to cause less short term cardiac side effects (Koitabashi *et al.* 2009). The potentially most potent composition is 4-hydroxytamoxifen which is now rarely used in adult studies. It remains however in use for genetic/lineage tracing. To achieve this, pregnant females are injected with 0.5 mg 4-hydroxytamoxifen daily over 14 days (Porrello *et al.* 2011).

It is evident that inducible genetic manipulations have become indispensable with hundreds of new Cre drivers currently generated as part of a large European consortium (EUCOMMTOOLS) and thousands of crosses to floxed alleles that are bound to follow from international initiatives (www.knockoutmouse.org, Skarnes *et al.* 2011). Conditional knockout approaches and cell lineage tracing have become to rely almost exclusively on the Cre/*loxP*

system, leaving two possible options to address the presented concern which will be discussed in detail below: 1) Elucidating mechanisms of Cre toxicity and defining the balance between satisfactory site-specific recombination in the various systems while carefully monitoring the effects of nuclear Cre or MerCreMer by use of meaningful controls and 2) Development and use of previously less popular alternatives available for gene targeting.

1) Optimisation Cre recombination: As indicated, it is not feasible to abandon MerCreMer-based systems immediately, given their current importance for developmental and regeneration research. Any experimentation involving the MerCreMer system, however, requires careful titration of tamoxifen to obtain maximal recombination with minimal side effects. Every step of this process should be controlled. Tamoxifen-primed MerCreMer localisation can be assessed by immunofluorescence (see Chapter 3) but ideally the ultimate outcome, *i.e*. gene activation or ablation must be assessed. The lowest possible tamoxifen dose to achieve a satisfying result must be established prior to experimentation. This approach was already successfully adopted by a recent study (Touvron *et al.* 2012). Most importantly, however, experimental design should take the toxic effects of nuclear Cre into consideration and controls should be included accordingly. In the light of the present findings, these controls are more relevant than tamoxifen-treated *flox/flox* single-genotype littermate controls, which to my knowledge have never been reported to produce any significant phenotype unless the construct itself was leaky. Leakiness of the construct, however, should be identified during generation of the respective floxed strain before establishing crosses with a Cre-driver strain.

2) Alternative means of gene targeting: Long term, there are number of approaches to manipulate gene expression that should be considered as alternatives to the Cre/*loxP* system. For example, the use of tetracycline-responsive promoters to externally activate gene expression has been used *in vitro* for decades and could constitute an alternative for certain experiments. The Tet-Off system which has found wide application in murine models relies on the presence of the tetracycline derivative doxycycline which binds a TetR/VP16 fusion protein (Gossen and Bujard 1992; Marongiu *et al.* 2012). This so-called tetracycline-responsive transcriptional activator (tTA) normally induces expression of transgenes by binding *Tet operator* (*TetO*) sequences, which activates the associated promoter. Upon doxycycline interaction the protein tTa is no longer bound to *TetO* and transcription is halted. The Tet-On system has an inverse working mechanism since tetracycline relieves transcriptional repression by binding the reverse tetracycline-responsive transcriptional activator (rtTA) fusion protein (Gossen *et al.* 1995). This is subsequently removed from *TetO* to allow target gene expression. There is some evidence that Tet-Off is superior to Tet-On in regulating gene expression following viral vector mediated delivery in mice (Mizuguchi and Hayakawa 2002). The reversibility of the Tet-mediated gene regulation is one of the key

strengths of this technique. Ironically however, this could pose a considerable disadvantage for long term *in vivo* experimentation. While recombinase-based techniques remove target sequences permanently there is a requirement for continuous doxycycline treatment in Tet-based experiments (Lai *et al.* 2012). Maintaining the necessary levels of this antibiotic could have side effects *in vivo* and requires meticulous controlling. In regenerative medicine, Tet was shown to be a well controllable regulator of gene overexpression in a pre-clinical animal model of MI (Lai *et al.* 2012). While the application of Tet in lineage tracing appears feasible, its future application for conditional gene downregulation is questionable. This is due to its incapacity to irreversibly remove DNA sequences, as discussed.

Despite being discovered almost simultaneously with Cre, another alternative molecule called FLP recombinase or flippase has not yet found wider application. Due to its ability of sequence specific DNA recombination, FLP has however received recent recognition for its use in cell lineage tracing experiments together with Cre in so called dual fate-mapping approaches (Schlake and Bode 1994; Engleka *et al.* 2012). Being a cleavage-dependent DNA ligase, FLPs mode of function is mechanistically similar to that of Cre. It is however of yeast origin (*Saccharomyces cerevisiae*) and has site specificity for *FLP recombination target* (*frt*) consisting of three 13 bp symmetry elements and surrounding the 8 bp core (Zhu and Sadowski 1995). Its yeast origin initially constituted the disadvantage that the native FLP had a temperature optimum at 30 °C (Buchholz *et al.* 1996). Using genetic engineering it has since been further developed into FLPe which shifted the effective working temperature to 37 °C (Buchholz *et al.* 1998). To date the most suitable FLP variant for use in mammalian systems is Flpo which shows recombination efficiencies comparable to Cre, with excellent expression characteristics and optimal activity at 37 °C (Raymond and Soriano 2007). The *frt* target site is more complex than the *loxp* site which consists of only two 13 bp repeats and the 8 bp core (Lee and Sadowski 2003). While this potentially implicates higher specificity of FLP-mediated recombination and subsequently a diminished risk of aspecific cleavage, caution should be exerted when using FLP since it has not been studied as extensively as Cre and similar problems in terms of concentration-dependent promiscuity of recombination could yet be uncovered. In the light of the current discourse surrounding Cre-mediated cytotoxicity, controls should be set up in a comparable fashion and data analysed with due vigilance.

The latest addition to the group of site-specific tyrosine recombinases developed for use in the mouse is Dre recombinase (Sauer and McDermott 2004; Anastassiadis *et al.* 2009). Dre targets *rox* sites, 32 bp sequence not recognised by Cre or FLP. Dre side-effects in mice have not yet been described. However, as for FLP the absence of adverse data is largely attributable to the fact that so far it has not found wide application, unlike Cre, which on its own or in fusion with Mer domains has been expressed in mice for more than a decade.

4.5.3 Summary

In summary, several conclusions can be drawn from the present study and literature survey. First of all, high levels of tamoxifen-induced MerCreMer can cause substantial cardiac phenotypes with short- and long-term effects. Secondly, the genetic background is most likely a determining factor of penetrance of the tamoxifen-induced MerCreMer phenotype. Thirdly, delivery methods have varying effectiveness in terms of tamoxifen bioavailability and will consequently affect concentration and duration of MerCreMer in the nucleus. The most appropriate delivery method for each model must be evaluated prior to extensive experimentation and the optimal dose of tamoxifen adjusted to the lowest concentration required for achieving sufficient recombination, as performed by Touvron *et al.* (Touvron *et al.* 2012). Given its potential to cause a substantial phenotype with regards to macrostructure, function and on the molecular level, the present findings support the call for inclusion of tamoxifen-treated *MerCreMer* single-genotype animals, particularly in experiments involving myocardial specific MerCreMer transgenes (reviewed in Anastassiadis *et al.* 2010). Since I showed that the observed phenotype is not related to cytoplasmic MerCreMer or the presence of a floxed transgene, tamoxifen-treated *αMHC/MerCreMer* animals should be chosen over *flox/flox* mice as negative controls where time and resources prohibit the inclusion of all control groups. Alternatively, FLP/*frt* and Dre/*rox* systems may provide suitable replacements for Cre recombinase in the future but have yet to be sufficiently developed and evaluated to seriously challenge the omnipresent *Cre/loxp* system.

Chapter 5 - Work in Progress: Alternative Approaches to Investigate the Role of Thymosin β4 in Cardiomyocytes

5.1 Introduction

Traditionally the main role of Tβ4 was considered to be binding of monomeric G-actin (Safer *et al.* 1991; Didry *et al.* 2012). This stabilises intracellular actin pools which serve as supplies for F-actin assembly for cytoskeletal rearrangement. However, Tβ4 has various intracellular and extracellular functions other than actin binding. Given its many diverse functions, the number of Tβ4-interacting proteins that have been identified over the decades seems surprisingly small. In endothelial cells, Tβ4 interacts directly with PINCH and ILK to facilitate complex formation with Akt1/2 and also binds extracellular receptor F1-F0 ATP synthase (Fan *et al.* 2009; Freeman *et al.* 2011). Also in endothelial cells, DNase helicase subunit II Ku80 was identified as a nuclear receptor for Tβ4 (Bednarek *et al.* 2008). In cancer cells, Tβ4 indirectly or directly interacts with hMLH1, a molecule involved in DNA mismatch repair (Brieger *et al.* 2007). Since previous research has focused on specific cell types *in vitro*, the scope of this part of the project was the identification of proteins interacting with Tβ4 specifically in the heart. To address this goal, the aim was to produce a tagged, recombinant Tβ4 fusion peptide to pull out interacting partners from total cardiac lysates or from protein preparations of cardiac subpopulations.

Historically, working with the Tβ4 peptide has been known to bear some technical challenges. For example, during filtration the behaviour of Tβ4 is anomalous. It appears 4-fold greater during gel filtration and during ultrafiltration is retained by a 10 kDa MWCO pore size despite having a theoretical molecular weight of 4.9 kDa (Haritos *et al.* 1989; Huff and Hannappel 1997). But even recent research has suffered from limited specificity of current Tβ4 antibodies and this poses a significant obstacle in Tβ4 research (from discussions with collaborators and other researchers, see also Chapter 3).

In the following study, two different expression systems namely prokaryotic and mammalian cells were used to produce a recombinant Tβ4 peptide that is fused to 6 histidine repeats (His_6) required for purification of the fusion peptide and a viral V5 epitope for improved detection. A similar proteomic procedure has been well described previously by Bednarek and co-workers in 2008 (Bednarek *et al.* 2008).

5.2 Proteomics – Identification of Tβ4-interacting proteins

Tβ4 cDNA was amplified from mouse cDNA using *Pfx* proofreading polymerase. Following electrophoresis, a single band of the predicted molecular weight was identified (**Figure 5.1**).

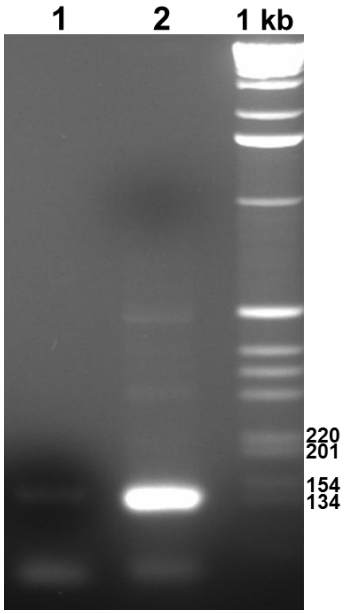


Figure 5.1: 2% Agarose gel showing the PCR product of *Tβ4* amplification. (1) PCR product using *Pfx* proofreading polymerase. (2) Positive control from standard *Taq* pol amplification of *Tβ4*. 1 kb DNA ladder was used as molecular weight marker (Invitrogen, Carlsbad, CA, USA).

Tβ4 cDNA was cloned into the pcDNA3.1 expression vector also containing the C-terminal V5-His_6 tag coding sequence (see Chapter 2: Methodology). *Tβ4-V5-His_6*, *LacZ-V5-His_6* plasmids and empty vector controls were transformed into *E. coli*. The success of transformation was controlled by monitoring LacZ protein expression on X-gal plates showing blue colonies for *LacZ-V5-His_6* but not control transformed cells (**Figure 5.2**).

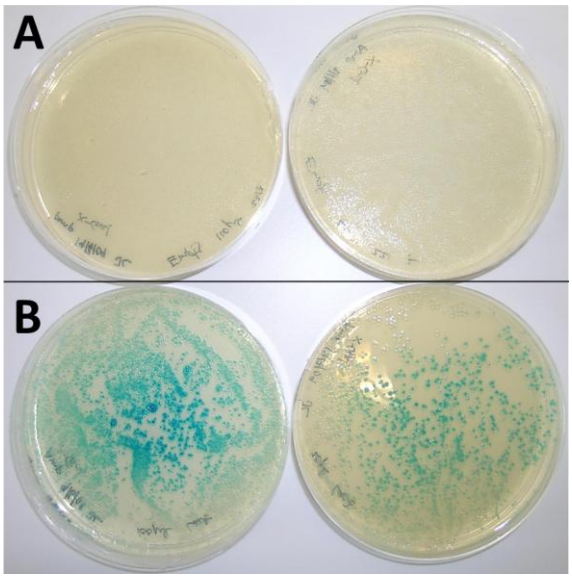


Figure 5.2: Transformation and protein expression control using β-galactosidase activity assay. (A) Colourless bacterial colonies transformed with the empty vector (B) *LacZ*-transformed bacteria metabolising X-gal shown by blue colouration of colonies.

Individual colonies of all three transformations were selected, expanded in liquid culture and DNA extracted. Correct insertion of *Tβ4* sequence in the plasmid was confirmed by *MfeI* endonuclease restriction digest and subsequent Agarose gel electrophoresis (**Figure 5.3**).

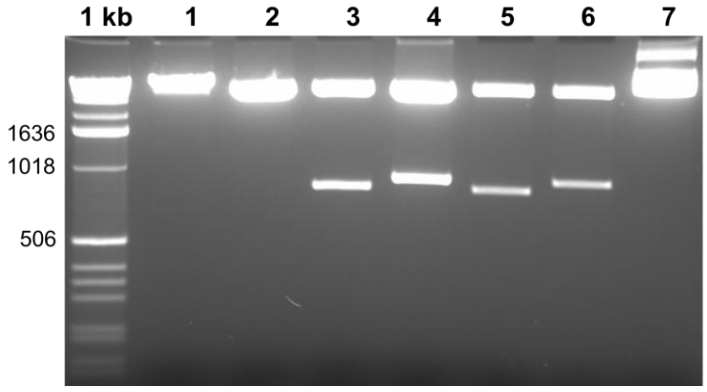


Figure 5.3: 2% Agarose gel of *MfeI*-digested vectors. Lane (1) linearised lacZ control plasmid, (2) linearised empty plasmid, (3) vector with inverted *Tβ4* sequence, (4) vector with correctly insert *Tβ4* sequence, (5) vector with inverted *Tβ4* sequence, (6) vector with correctly insert *Tβ4* sequence, (7) undigested control plasmid.

Two clones containing the vector with correct orientation of the *Tβ4* sequence were identified. Lanes 4 and 6 show the corresponding band of 891 bp (and 4767 bp). Examples of inverted *Tβ4* sequences can be seen in lanes 3 and 5 showing a band corresponding to 826 bp (and 4832 bp). Positive clones were sequenced using Imperial College Genomics Laboratory core facility and used for Tβ4-V5-His_6 protein production. In a separate experiment, plasmid DNA derived from sequence controlled clones was used to transiently transfect HeLa cells using Lipofectamine. Total protein was isolated from *E. coli* and HeLa cells and 100 µL of each sample used for precipitation of Tβ4-V5-His_6 and controls using protein A/G slurry and anti-V5 monoclonal antibodies. Precipitated protein was separated by SDS PAGE and evaluated by Western blotting (**Figure 5.4**).

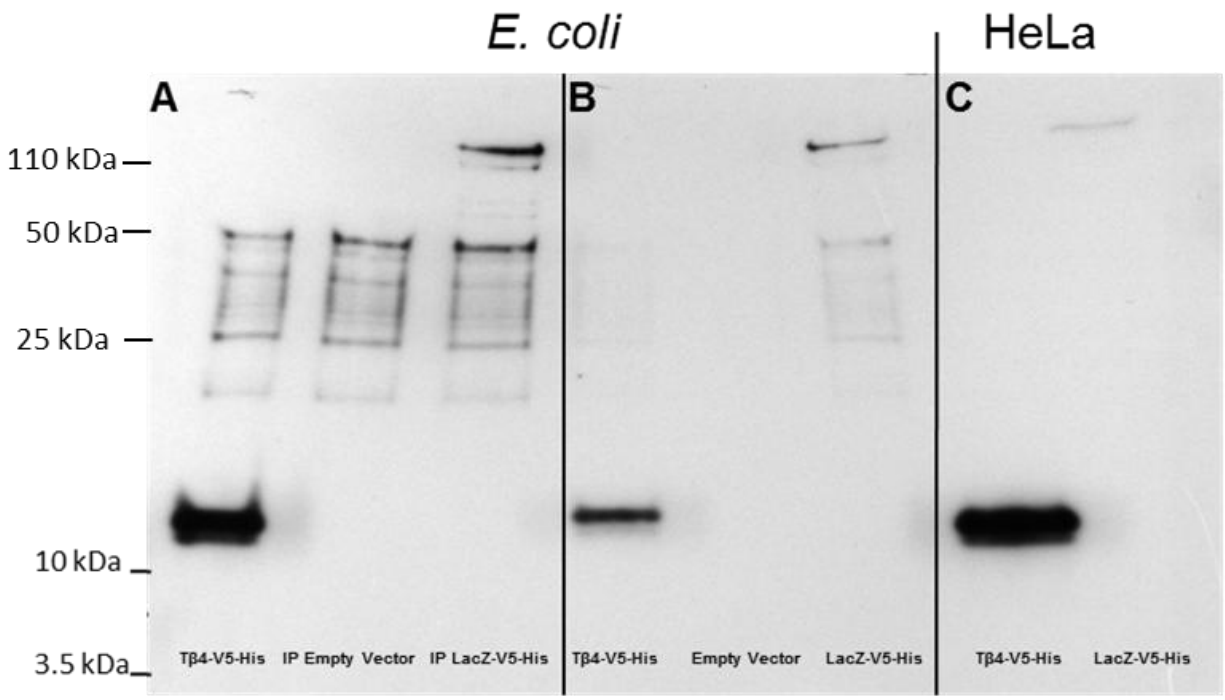


Figure 5.4: Western blot detection of V5 epitopes. (A) Immunoprecipitation of Tβ4-V5-His_6 and control peptides generated in *E. coli*. (B) Original unprocessed protein extract from *E. coli*. (C) Protein extracts from Tβ4-5-His_6 and LacZ-V5-His_6 HeLa cell lysates.

Band of the corresponding molecular weights of Tβ4-V5-His_6 at ~11 kDa (5 kDa + 6 kDa) and for LacZ-V5-His_6 at 122 kDa (116 kDa + 6 kDa) were identified. Two distinct bands at 25 kDa and 50 kDa stem from the denatured small and heavy chain of the IgG. For co-IP with subsequent mass spectrometry analysis, high purity recombinant protein is required. Protein extracts were therefore purified using ProBond His-affinity columns (Invitrogen, Carlsbad, CA, USA, # 45-0055). Although the recombinant protein had been identified in both *E. coli* and HeLa systems, expression in bacteria was selected over the mammalian system due to ease of handling and lower cost.

5.3 Pitfalls of recombinant protein production for proteomics

After His-affinity column purification, no clear band for Tβ4-V5-His_6 was detected in any fraction by coomassie staining (**Figure 5.5**).

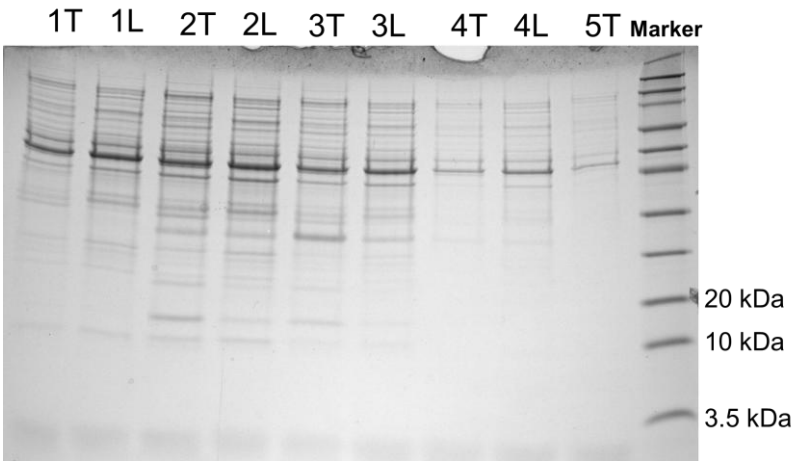


Figure 5.5: Fractions eluted after ProBond Ni^{2+}-affinity column purification. Protein lysates from *E. coli* were used. Arabic numerals indicate fractions (T – Tβ4-V5-His_6, L – LacZ-V5-His_6).

Although bands were found at low molecular weights potentially corresponding to the Tβ4 fusion protein, these bands were also detected in LacZ control preparations. To rule out the possibility of accidental wash out of the recombinant proteins, wash supernatants were investigated but did not show clear bands indicative of a robust overexpression. The experiment was repeated including a solubilisation step to address the possibility of inclusion body formation frequently occurring during bacterial overexpression, but no significant expression was observed (data not shown).

To investigate if HeLa cells were more suitable in producing sufficient protein amounts for His-affinity purification, a stable Tβ4-V5-His_6 cell line was generated. Stable transfection of HeLa cells did not produce a clear band on a coomassie gel after protein isolation and His-affinity purification (**Figure 5.6**).

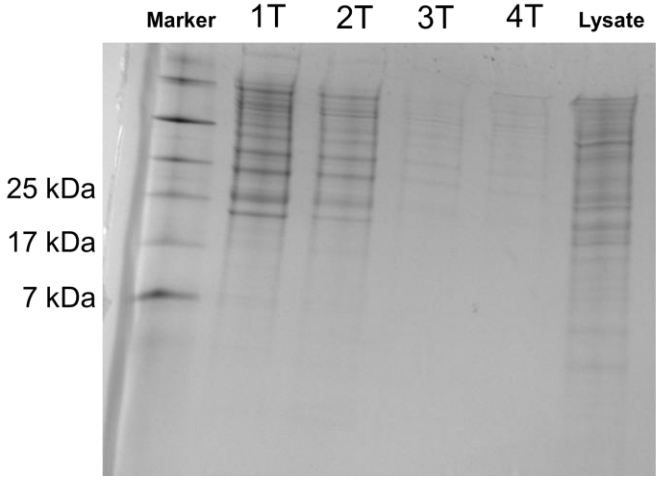


Figure 5.6: Coomassie stained gel of HeLa protein lysates after stable transfection and Ni^{2+}column purification. Eluted fractions: 1T-4T. Lysate = Unpurified cell lysate. NEB wide range pre-stained protein marker was used (New England Biolabs, Ipswich, MA, USA, # P7708V).

To investigate whether the recombinant protein was potentially secreted into the cell culture medium, supernatants were concentrated using 30 kDa and 3 kDa MWCO columns. Tβ4 passes 30 kDa MWCO pore sized filters but is retained by membranes with MWCO <10kDa (Huff and Hannappel 1997). As for previous attempts, no clear band for the Tβ4-V5-His_6 was identified in medium preparations (**Figure 5.7**).

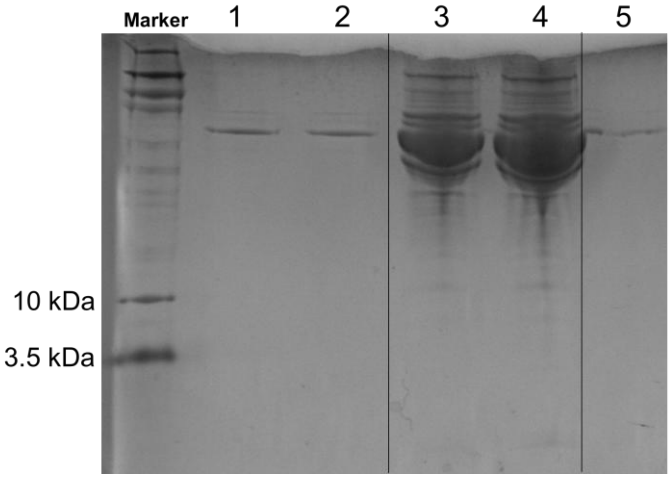


Figure 5.7: Medium from Tβ4-V5-His_6 transfected HeLa cells cultured under serum-free conditions. (1-2) Unpurified medium, (3-4) Concentrated medium MWCO 30 kDa, (5) concentrated medium with a MWCO of 3 kDa. Novex sharp (Invitrogen, Carlsbad, CA, USA) was used as molecular weight marker.

During this concentration approach the formation of dissoluble aggregates was observed. Re-diluting the purified and concentrated medium also showed irregular behaviour during electrophoresis, potentially indicating that it is not a concentration-dependent mechanism. Furthermore, Western blot analysis using anti-V5 antibodies to investigate basal levels of Tβ4-V5-His_6 in the medium was negative suggesting that it is not secreted even at low concentrations (not shown). Several modifications to the lysis protocol and isolation procedure as well as the inclusion of imidazole gradients to increase selectivity of His-affinity column interaction were attempted. Imidazole was added to the binding buffer at 5 mM, at 5 - 10 mM during washes and in a gradient from 10 - 500 during elution. While not solving the problem, it added complexity to the problem, since imidazole absorbs light making spectrophotometric protein quantification impossible. Subsequent Western blotting analysis using V5 antibodies on the unquantified fractions from the imidazole-assisted isolation only detected a Tβ4-V5-His_6 positive control from previous experiments but recombinant protein in the purified fractions (not shown).

5.4 Discussion

The aim of this chapter was to generate a polyhistidin and V5-epitope tagged recombinant protein to identify for the first time Tβ4 interacting proteins in the heart by co-immunoprecipitaion with subsequent mass spectrometry analysis. Problems resulting in poor purity and low levels of recombinant Tβ4-V5-His_6 were encountered and approaches to overcome these are discussed here.

Generally solubility problems during recombinant protein expression can stem from interactions of hydrophobic residues resulting in aggregates that require strong detergents or high concentrations of denaturants such as urea to re-dissolve proteins. However, Tβ4 is highly water-soluble and up to 100 mg/L Tβ4 can be dissolved in water (reviewed in Hannappel 2010). Given these hydrophilic properties and its disorganised structure in water, aggregation of the core peptide due to hydrophobic interactions is unlikely. In addition, the problems of low protein yield were also observed for LacZ-V5-His_6. To determine whether His_6 or V5 epitope interactions are underlying the putative protein aggregation, expression of the Tβ4 core without the tags could serve as a negative control for future experiments. Generally, bacteria can form inclusion bodies, intracellular aggregates mediated by heatshock proteins normally in response to thermal stress in order to compartmentalise poorly folded proteins (reviewed in Villaverde 2003). This is a frequently observed problem in bacterial overexpression settings. A commercially available kit was used to dissolve putative inclusion bodies but this did not significantly improve the outcome. Additionally, the observed failure to purify significant amounts of recombinant Tβ4-V5-His_6 could stem from low expression. This is supported by the lack of a clear band on coomassie stained gels, which are normally observed for robust overexpression (**Figure 5.5**, **Figure 5.6**). While the presence of the recombinant as well as LacZ-V5-His_6 was confirmed by Western blotting, this is a very sensitive technique able to detect very small amounts of protein. Secretion of the fusion peptide was ruled out as a possible explanation since the fusion peptide was not detected in the cell culture medium (**Figure 5.7**).

The failure to express significant amounts of recombinant protein in the stable HeLa cell line is most likely attributable to a loss of overexpression. This can happen as a result of gene silencing, but in this case is most likely attributable to the competitive disadvantage of highly expressing cells within the heterogeneous culture. To avoid this loss of expression, larger batches of cells could be transiently transfected to achieve a higher yield of recombinant protein. However, the high costs of Lipofectamine are prohibitive for this large scale transient transfection approach. A financially more feasible and much more elegant approach would be to select strongly expressing single clones of a freshly established stable cell line and expand these in culture. Strong monoclonal cultures could be selected for subsequent protein production.

In the bacterial system, inducible expression could be used to maximise recombinant protein yield while reducing the risk of gene silencing and protein aggregation. Commercially available options are vectors containing IPTG inducible *tac* promoters (GE Healthcare [Internet], Little Chalfont, UK, GST Gene Fusion System Handbook 10/2010, ©2009-2010, Cited 02/07/2012, Available from: https://www.gelifesciences.com/gehcls_images/GELS/Related%20Content/Files/1314807262343/litdoc18115758AB_20110831220904.pdf). These vectors allow optimisation of protein expression in bacteria by monitoring bacterial growth using photospectrometry and induction of protein expression during the exponential growth phase. The time point of harvest can be adjusted to ensure that sufficient protein has been produced without formation of dissoluble aggregates due to overloading of the bacterial cells. Furthermore reducing the culture temperature to 20 °C can reduce the formation of inclusion bodies.

Increasing the abundance of soluble protein could potentially address the problem of poor protein purification. Insufficient binding of residues of the Ni^{2+}-column allows for contaminants to attach to unoccupied binding sites and are subsequently eluted together with the recombinant protein resulting in multiple bands, as observed in this work (**Figure 5.5**). Consequently, it would be more feasible to optimise expression levels first and then address any prevailing purification issues.

5.4.1 Summary

Given the low yield and dissatisfying purity it was not possible at this stage to continue to 2D gel electrophoresis and mass-spectrometry to identify Tβ4-interacting proteins. Ultimately the unexpected complexity in terms of time and financial resources could justify outsourcing the whole production of the recombinant protein to an experienced company. Recombinant biotynilated Tβ4 peptides suitable for co-immunoprecipitation experiments are now commercially available (Freeman *et al.* 2011, Celtek Peptides, Nashville, TN, USA).

Chapter 6 - Work in Progress: Transmission Electron Microscope Analysis *αMHC/IGF-1Ea* Transgenic Hearts and the Role of IGF-1Ea in Cardiac Autophagy

6.1 Introduction

Along with Tβ4, insulin-like growth factor 1 (IGF-1) is another molecule that holds great potential for future therapeutic application to treat human heart disease. IGF-1 increases expression of antioxidant enzymes in blood vessels and inversely IGF-1 deficiency renders the blood vessels more prone to obesity-related vascular disease (Csiszar *et al.* 2008; Ungvari *et al.* 2010; Bailey-Downs *et al.* 2012). Overall IGF-1 is artheroprotective and promotes endothelial repair (reviewed in Higashi *et al.* 2010). In humans, promoter polymorphisms lowering the levels of IGF-1 decrease life expectancy after MI and low levels of circulating IGF-1 increase the risk of heart failure in elderly without previous MI (Vasan *et al.* 2003; Bleumink *et al.* 2004; Bleumink *et al.* 2005).

Several isoforms and pro-peptides have been identified including the locally acting IGF-1Ea isoform (reviewed in Musaro *et al.* 2001; Barton 2006). Muscle specific overexpression of IGF-1Ea in mice increases the number of myogenic progenitors, promotes healing after muscle injury and reduces muscle loss in cachexia and ageing (Musaro *et al.* 2001; Musaro *et al.* 2004). IGF-1Ea overexpression in the mouse heart decreases the inflammatory reaction and reduces scar formation following experimental MI which results in overall cardiac functional improvements compared to *wt* littermates (Santini *et al.* 2007). While macro- and microscopically these hearts have been well studied, a comprehensive analysis of their subcellular structure had not previously been performed. The following chapter details a transmission electron microscope (TEM) analysis of *αMHC/IGF-1Ea* hearts and focuses on newly discovered intracellular structures with potential implications in protein homeostasis and autophagy.

6.2 Large electron-dense structures in *αMHC/IGF-1Ea* cardiomyocytes

Normal 3-4 month old male *αMHC/IGF-1Ea* and *FVB* control mice were sacrificed and left-ventricular tissue prepared for microstructural investigation by TEM. Gross appearance of the myocardium was comparable between transgenic and *wt* animals. In *αMHC/IGF-1Ea* cardiomyocytes, previously not described large electron-dense structures were observed in in areas of high mitochondrial density (**Figure 6.1**).

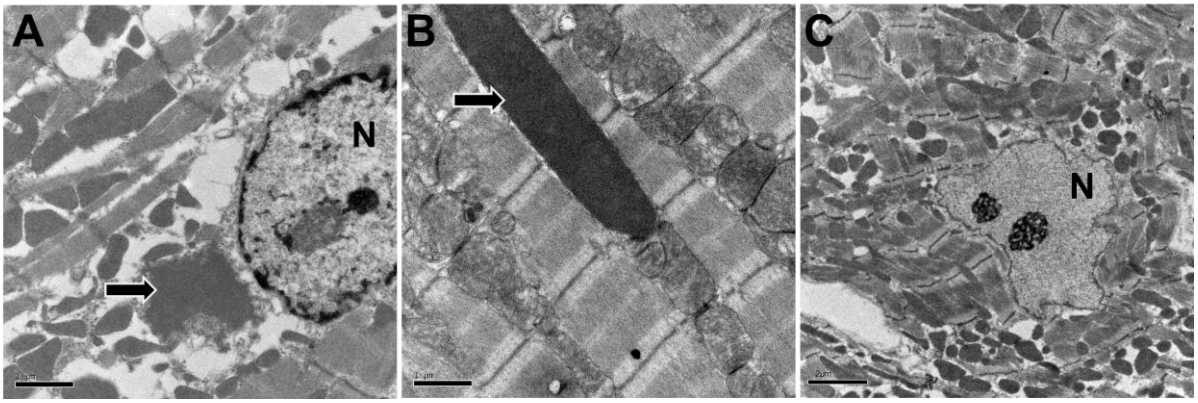


Figure 6.1: Electron micrographs of cardiac section from *αMHC/IGF-1Ea* transgenic mice. (A, B) Large electron-dense structures (arrows) were observed in the cytoplasm of cardiomyocytes. (C) Cardiomyocytes of *wt* littermates presented normal subcellular morphology. Scale bars A, B = 1µm, C = 2 µm.

The structures were mostly round or oval in shape and had smooth or slightly irregular outlines. In a few areas the structures were observed to be larger than the cell nucleus. The structures were not detectable in skeletal muscle (data not shown). A literature survey did not reveal any previous data on similar sized electron-dense structures in cardiomyocytes. The timing of the appearance of the structures in cardiac tissue was investigated by studying the hearts of juvenile mice. Six week old *αMHC/IGF-1Ea* mice presented normal intracellular morphology and the described electron-dense bodies were not observed (**Figure 6.2**).

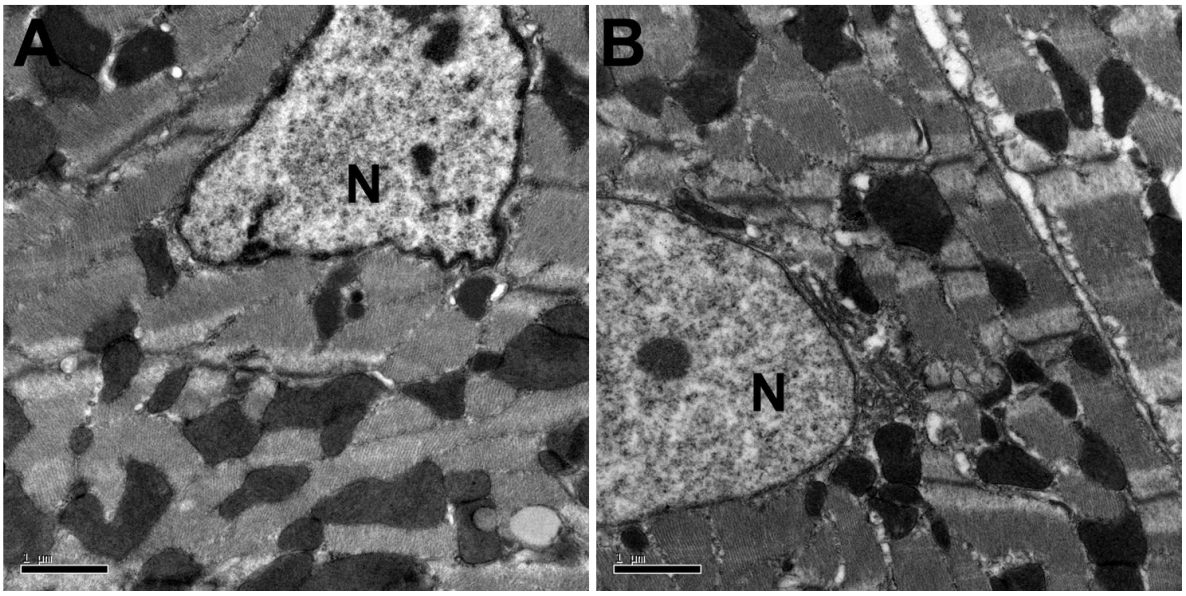


Figure 6.2: Electron micrographs of cardiac sections from 6 week old *αMHC/IGF-1Ea* mice. (A, B) Representative micrographs showing normal subcellular morphology of cardiomyocytes. (N – nucleus) Scale bar 1 µm.

Since *IGF-1Ea* expression is controlled by the strong *αMHC* promoter in these transgenic cardiomyocytes, the possibility that extensive protein overexpression results in overloaded intracellular degradation mechanisms such as proteasomal or autophagy pathways was considered. The accumulation of the final product of incomplete degradation of highly cross-linked proteins debris can lead to pathological aggregation in the form of lipofuscin (reviewed in Terman and Brunk 2004). Since lipofuscin accumulation can be aggravated over time and is found predominantly in aged post-mitotic tissues and since brain and heart are known to accumulate non-dissolvable, misfolded protein in mammals, we investigated whether lipofuscin aggregates were present in aged mice and whether they shared morphological resemblance with the observed electron-dense structures (Benavides *et al.* 2002). Electron-dense structures were identified in cardiac specimen from 2 year-old *αMHC/IGF-1Ea* mice but not *wt* mice and were of comparable size and abundance to those observed in 3-4 month old mice (**Figure 6.3**).

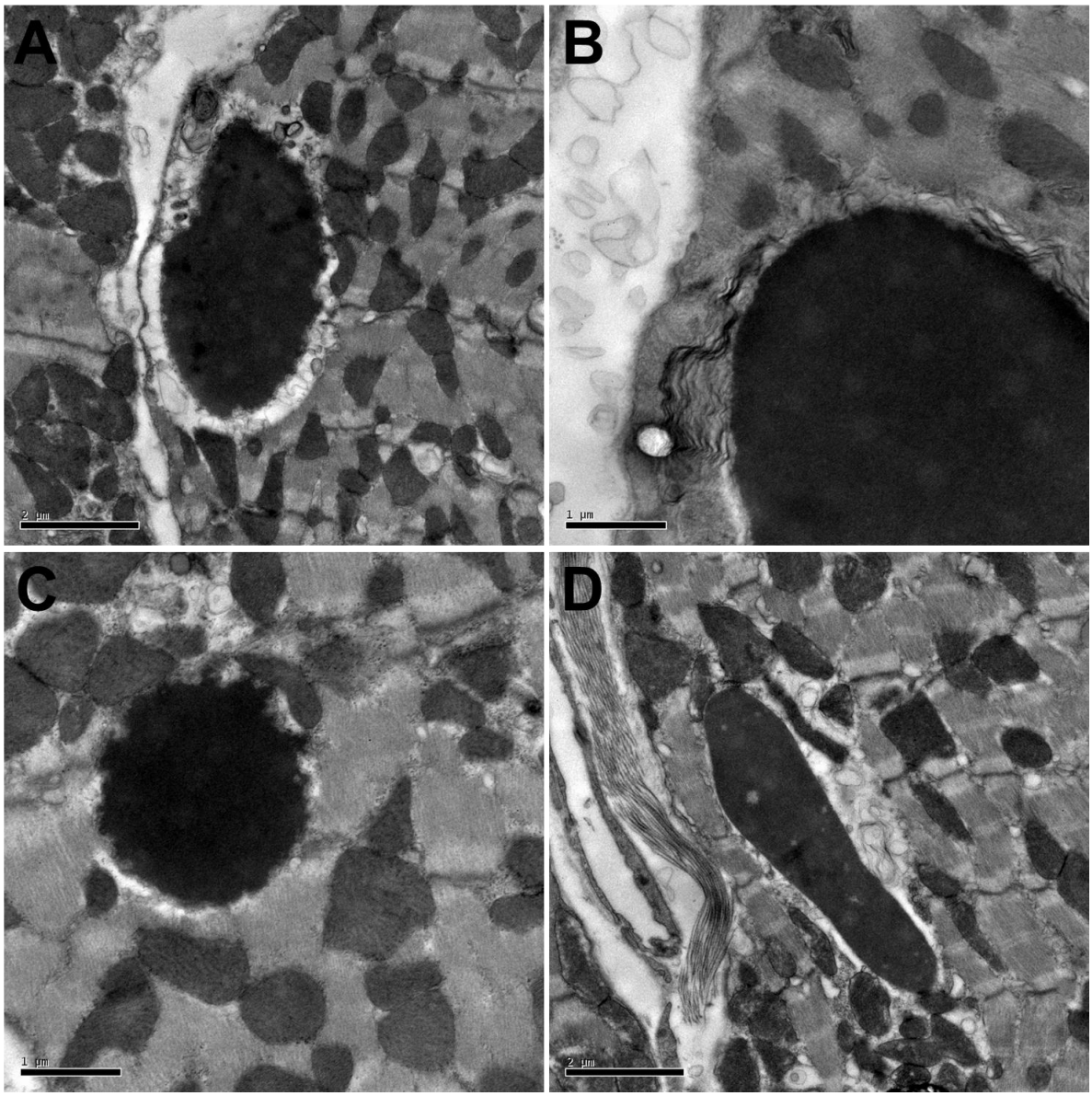


Figure 6.3: Electron micrographs of cardiac sections from 2 year old *αMHC/IGF-1Ea* mice. (A-D) Transmission electron micrographs showed electron-dense structures in similar size, abundance and morphology compared to those observed in 3-4 month old animals. Scale bars A, D = 2 µm, B, C = 1 µm.

In addition, lipofuscin granules, which were morphologically clearly distinguishable from the electron-dense structures and significantly smaller in size, were observed in aged cardiomyocytes of *αMHC/IGF-1Ea* and *wt* mice (**Figure 6.4**).

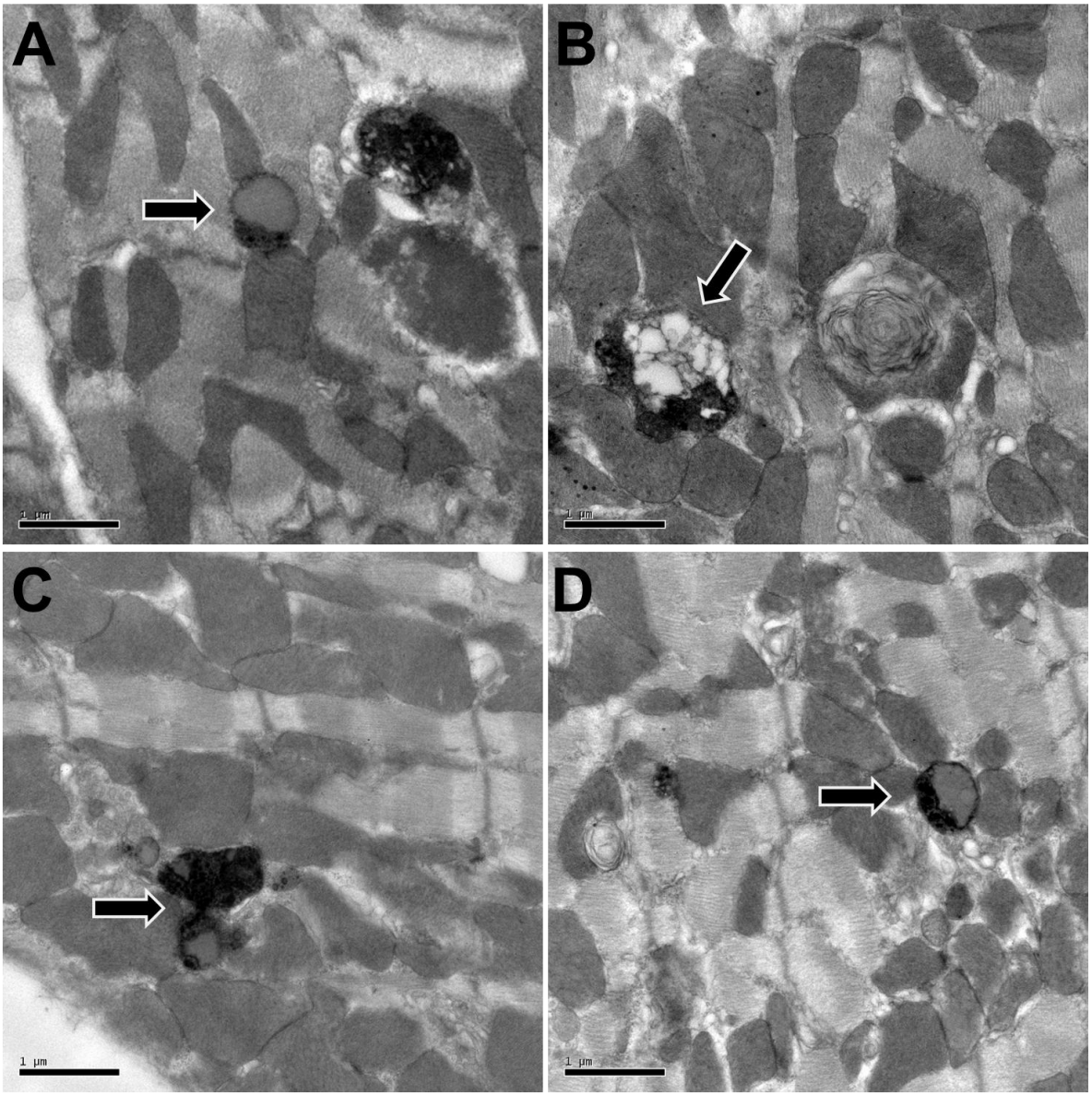


Figure 6.4: Electron micrographs of cardiac sections from 2 year old *αMHC/IGF-1Ea* and *wt* mice. (A, B) Lipofuscin granules (arrows) were observed in *αMHC/IGF-1Ea* and (C, D) *wt* cardiomyocytes. Scale bar 1 µm.

Processed cardiac tissue samples were transferred to our colleague Bart Wagner, Chief Biomedical Scientist at Northern General Hospital Sheffield to obtain an additional expert opinion. While no consensus was reached regarding the nature and origin of the structures, high quality images were obtained, clearly showing a membrane delineating the structures (**Figure 6.5**).

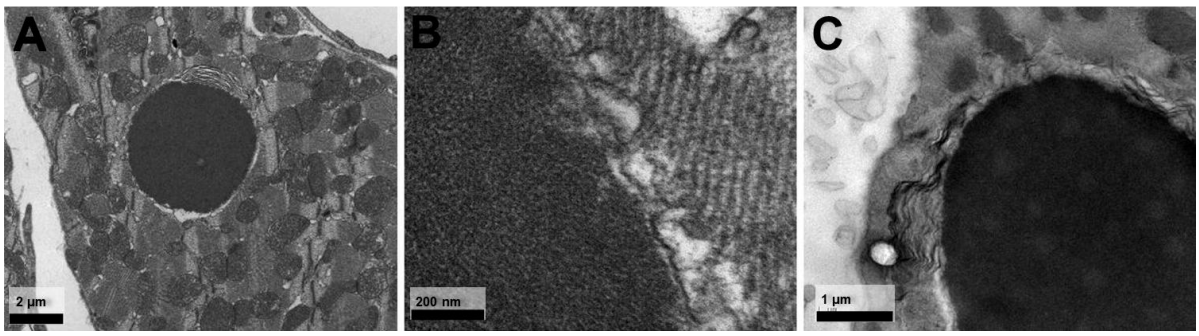


Figure 6.5: Transmission electron micrographs of cardiac sections from 3 month old *αMHC/IGF-1Ea* mice. (A-C) Electron-dense structures appear delineated by phospholipid bilayer (Images of panels A and B courtesy of Bart Wagner). Scale bars A = 2 µm, B, 200 nm, C = 1 µm.

Since the electron-dense structures did not appear to be any larger or more abundant in 2 year old mice compared to our previous findings, they were considered either remnants of an event occurring before the age of 3-4 months or were constantly turned over thus stabilising their size and abundance. Turnover of large intracellular structures mainly involves pathways that depend on lysosomal enzymes (Luzio *et al.* 2007). Since a lysosomal or endosomal origin would be in line with the phospholipid bilayer surrounding the structures, cardiac sections were analysed for lysosomal marker LAMP1 by immunogold labelling (**Figure 6.6**).

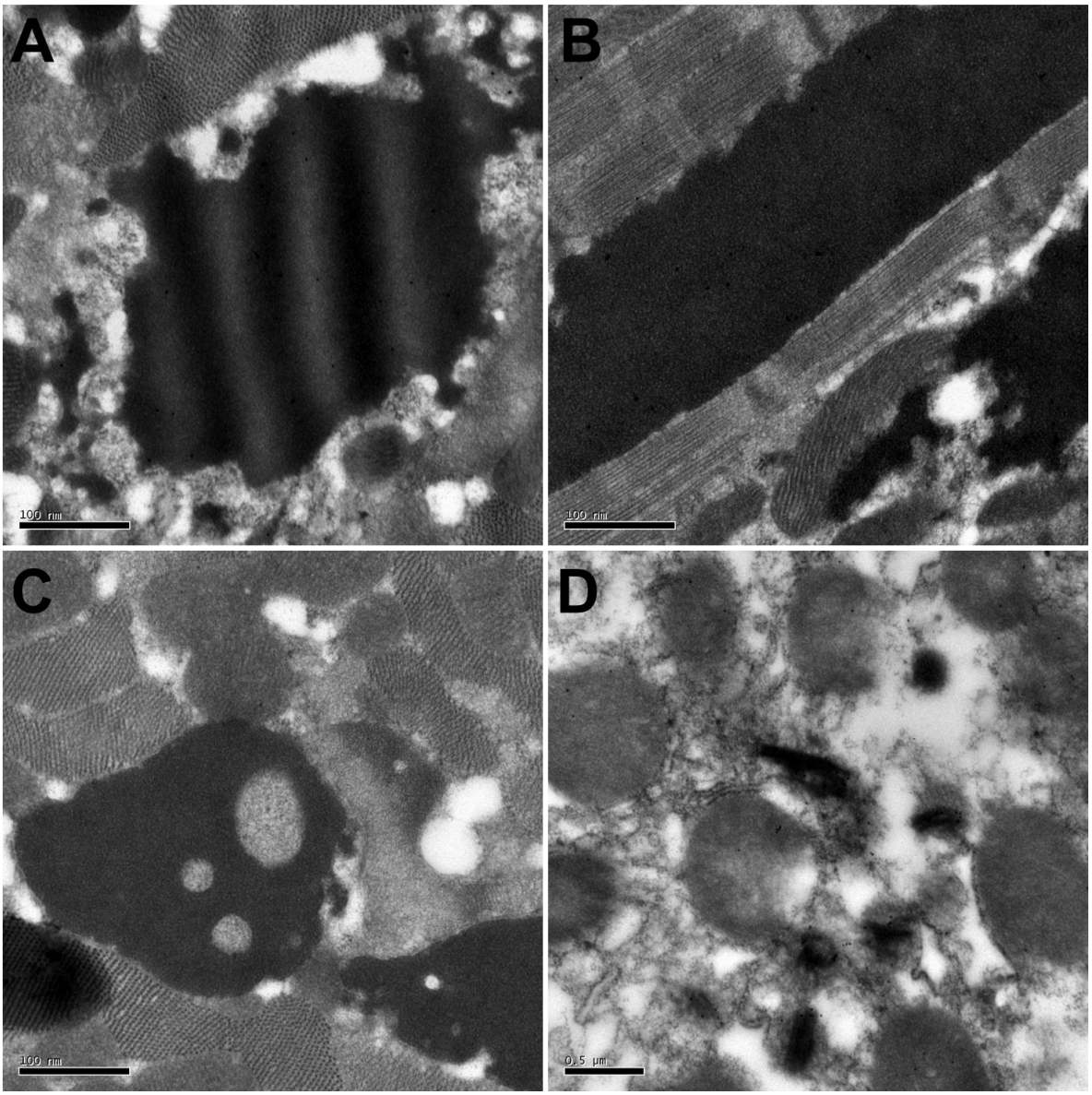


Figure 6.6: Immunogold staining of cardiac sections of *αMHC/IGF-1Ea* mice for LAMP1. (A-C) Electron micrographs showing LAMP1-negative electron-dense bodies in cardiomyocytes. (D) Liver tissue serving as positive control. Scale bars A, B, C = 100 nm, D = 500 nm.

The electron-dense structures were negative for LAMP1 and the positive control (liver tissue) showed only a small number of LAMP1-positive foci. Since the liver is considered a place of significant lysosomal activity, antibody specificity was questioned and a second lysosomal marker, cathepsin D, was used for further analysis (Erickson *et al.* 1981; Skop *et al.* 2012). While the electron-dense structures themselves did not stain positively for cathepsin D, positive signals were detected in vacuoles in the direct proximity of the structures (**Figure 6.7**).

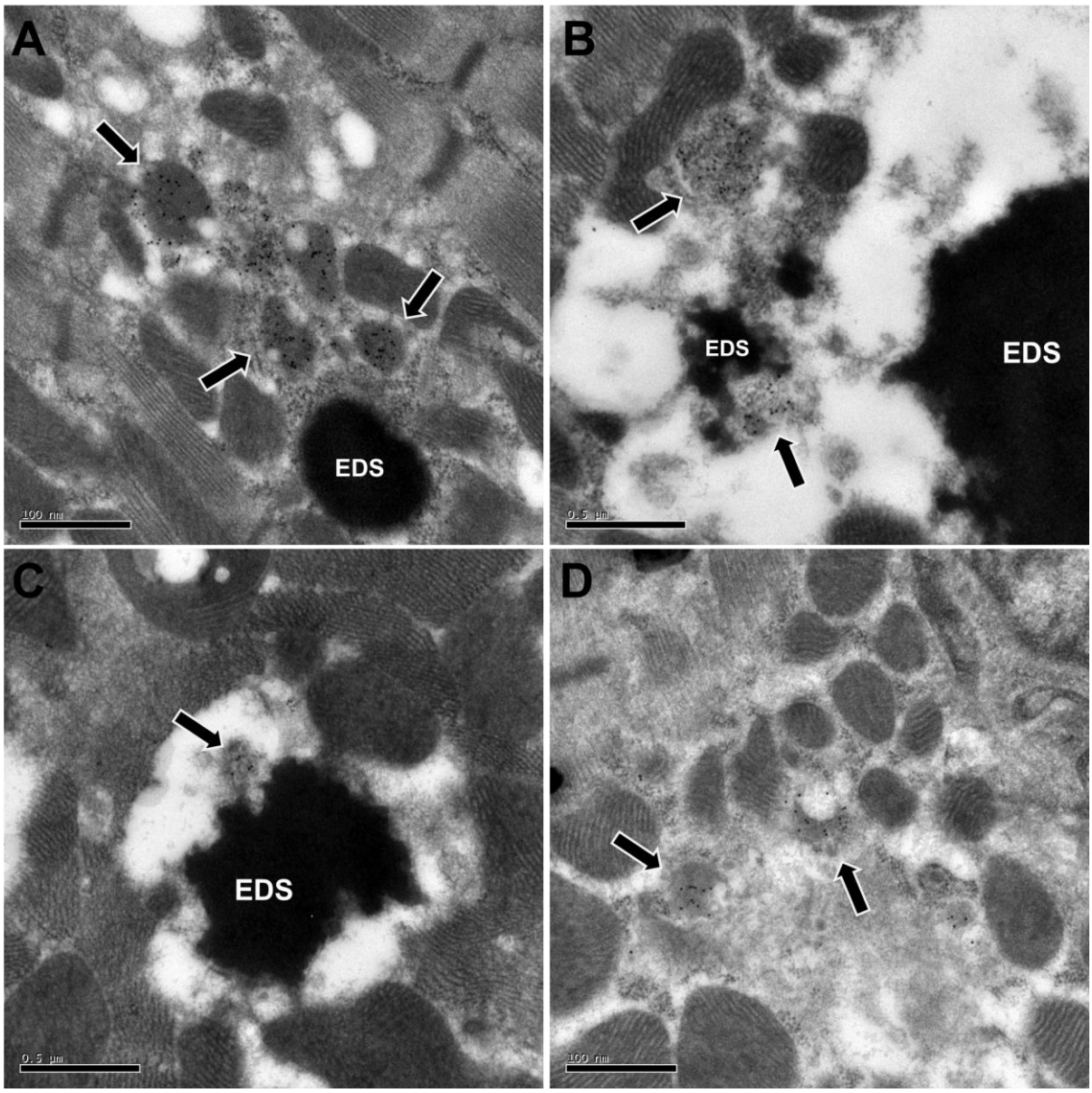


Figure 6.7: Immunogold staining for cathepsin D on cardiac sections of 3-4 month old αMHC/*IGF-1Ea* mice. (A-D) Vacuoles positive for cathepsin D (arrows) were discovered in the proximity of the electron-dense structures (EDS). Scale bars A, D = 100 nm, B, C = 500 nm.

This could indicate an intracellular attempt to dissolve the structures or could provide clues for a mechanism regulating their size. Since large organelles are degraded by a mechanism referred to as macroautophagy (or short autophagy), we investigated whether this pathway was involved in the formation or regulation of the structures.

6.3 The role of IGF-1Ea in cardiac autophagy

IGF-1 was previously shown to be involved in autophagy, the removal of old defective organelles and misfolded or excess proteins (reviewed in Klionsky and Emr 2000). Since the

electron-dense structures bear morphological resemblance to exceptionally large autophagosomes or autophagolysosomes, an analysis of markers of autophagy was carried out. The most prominent marker of autophagosomes is microtubule-associated protein 1 light chain 3 (LC3) and its isoforms (reviewed in Mizushima 2004). Consequently the presence of LC3 was analysed by immunogold labelling (**Figure 6.8**).

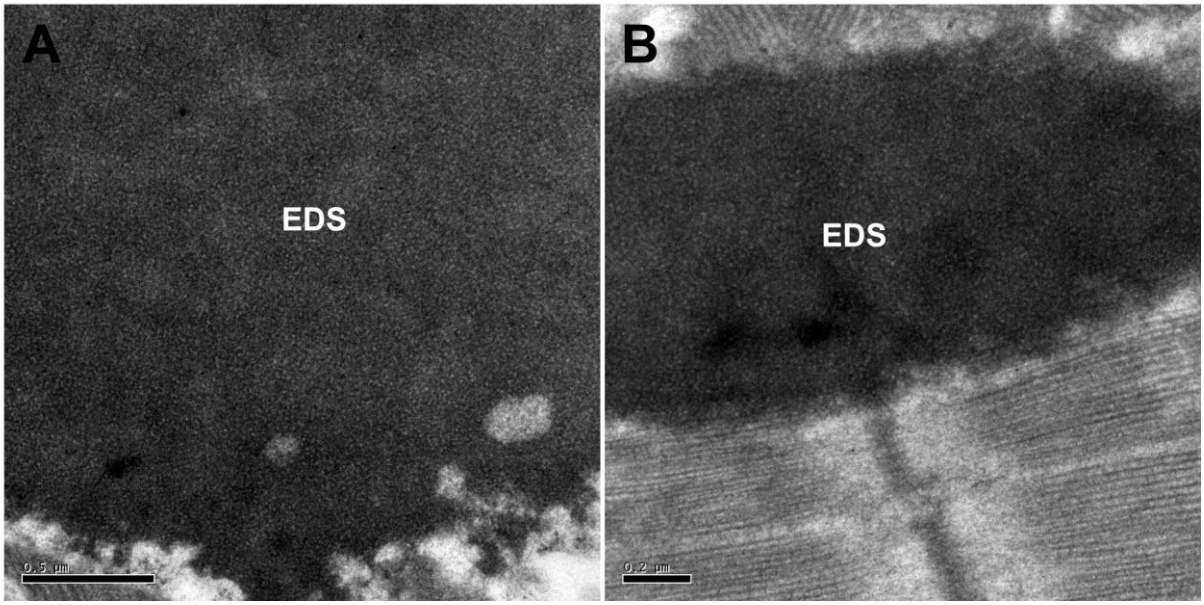


Figure 6.8: LC3 immunogold labelling of *αMHC/IGF-1Ea* cardiac sections. (A, B) Intracellular, large electron-dense structures (EDS) are negative for autophagosomal marker LC3. Scale bars A = 500 nm, B = 200 nm.

The electron-dense structures where negative for LC3. Since processing cardiac samples for TEM is extremely laborious, further investigations into differentially regulated markers of autophagy were performed by Western blotting and by PCR array using cardiac samples of 3-4 month old mice. Pro-autophagic protein Beclin-1 and LC3B II, the active form of the LC3B isoform, were not differentially regulated following IGF-1Ea overexpression (Liang *et al.* 1999, **Figure 6.9**).

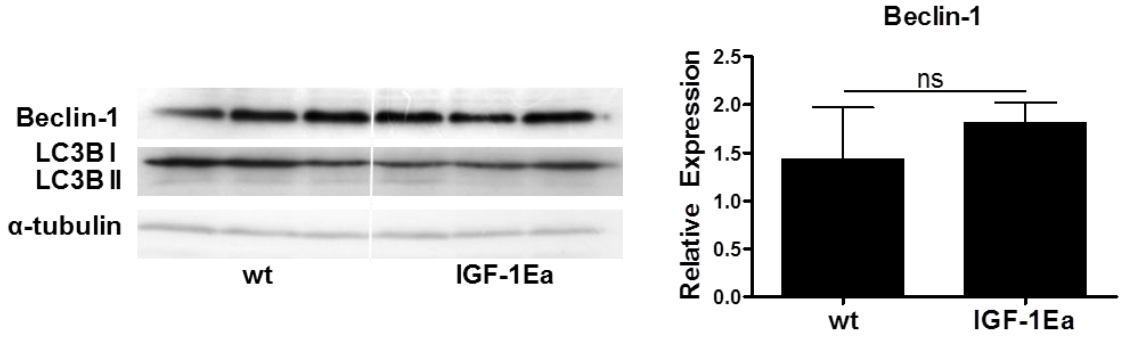


Figure 6.9: Western blot for markers of autophagy in adult mice. Cardiac protein extracts of 3 month old *αMHC/IGF-1Ea* and *wt* mice were analysed for Beclin-1 and LC3B. Beclin-1 was not differentially regulated. Active LC3B II was not quantifiable due low presence of the cleaved form but did not appear to be differentially regulated. Beclin-1 data expressed as standard deviation of the mean.

Since the analysis of these classical markers by immunogold and immunoblotting had not indicated a change in signalling, the broader approach of using a PCR array was considered to further elucidate the potential implication of autophagy signalling in the formation of electron-dense structures in *αMHC/IGF-1Ea* transgenic hearts.

6.3.1 Autophagy PCR array results

A more detailed analysis of the role of IGF-1Ea overexpression on autophagy signalling in the heart was performed using a PCR array covering 83 genes involved in autophagy (for full description see Chapter 2). Highly purified RNA extracts of 3 month old mouse hearts of *wt* and *αMHC/IGF-1Ea* mice were used. 7 genes were identified to be differentially regulated in *αMHC/IGF-1Ea* mice compared to *wt* (**Table 6.1**).

Table 6.1: Autophagy PCR array results. Statistically significant changes in gene expression are highlighted by bold fonts Experiments were performed in triplicate and analysed using the SABiosciences RT2 Profiler PCR Array Data Analysis version 3.5 online service (SABiosciences QIAGEN [Internet], Crawley, RT2 Profiler PCR Array Data Analysis version 3.5, ©2000-2010, Cited 24/06/2012, Available at: http://pcrdataanalysis.sabiosciences.com/pcr/arrayanalysis.php).

Symbol	Gene Name	Fold Change	p-value
Akt1	Thymoma viral proto-oncogene 1	1.0384	0.858282
Ambra1	Autophagy/beclin 1 regulator 1	1.0631	0.331051
App	Amyloid beta (A4) precursor protein	1.0694	0.338062
Arsa	Arylsulfatase A	1.0512	0.743929
Atg10	Autophagy-related 10 (yeast)	0.9961	0.932497

Atg12	Autophagy-related 12 (yeast)	1.1321	0.359769
Atg16l1	Autophagy-related 16-like 1 (yeast)	1.0218	0.680907
Atg16l2	Autophagy related 16 like 2 (S. cerevisiae)	0.8472	0.335553
Atg3	Autophagy-related 3 (yeast)	1.0701	0.40901
Atg4a	Autophagy-related 4A (yeast)	1.067	0.597124
Atg4b	Autophagy-related 4B (yeast)	1.0129	0.878001
Atg4c	Autophagy-related 4C (yeast)	1.0847	0.374467
Atg4d	Autophagy-related 4D (yeast)	1.1132	0.512934
Atg5	Autophagy-related 5 (yeast)	1.0256	0.827225
Atg7	Autophagy-related 7 (yeast)	1.0358	0.798985
Atg9a	Autophagy-related 9A (yeast)	0.9363	0.670983
Atg9b	ATG9 autophagy related 9 homolog B (S. cerevisiae)	1.0283	0.59055
Bad	BCL2-associated agonist of cell death	0.9568	0.269167
Bak1	BCL2-antagonist/killer 1	1.0515	0.616988
Bax	Bcl2-associated X protein	0.9496	0.636052
Bcl2	B-cell leukemia/lymphoma 2	0.8775	0.059786
Bcl2l1	Bcl2-like 1	1.3685	0.059459
Becn1	Beclin 1, autophagy related	1.0059	0.920936
Bid	BH3 interacting domain death agonist	1.2974	0.172133
Bnip3	BCL2/adenovirus E1B interacting protein 3	0.8609	0.136066
Casp3	Caspase 3	0.978	0.837968
Casp8	Caspase 8	1.053	0.728667
Cdkn1b	Cyclin-dependent kinase inhibitor 1B	1.031	0.858326
Cdkn2a	Cyclin-dependent kinase inhibitor 2A	0.7753	0.78705
Cln3	**Ceroid lipofuscinosis, neuronal 3, juvenile (Battenin)**	**0.8176**	**0.026159**
Ctsb	Cathepsin B	1.0235	0.702501
Ctss	Cathepsin S	1.2077	0.117806
Cxcr4	**Chemokine (C-X-C motif) receptor 4**	**0.6981**	**0.000787**
Dapk1	Death associated protein kinase 1	1.0568	0.988436
Dram1	**DNA-damage regulated autophagy modulator 1**	**1.4384**	**0.0169**
Eif2ak3	Eukaryotic translation initiation factor 2 alpha kinase 3	1.0188	0.840751
Eif4g1	Eukaryotic translation initiation factor 4, gamma 1	1.0096	0.896417
Esr1	**Estrogen receptor 1 α**	**1.592**	**0.024487**
Fadd	Fas (TNFRSF6)-associated via death domain	0.9062	0.496774
Fas	Fas (TNF receptor superfamily member 6	0.8941	0.656449
Gaa	Glucosidase, alpha, acid	0.9628	0.499632

Gabarap	Gamma-aminobutyric acid receptor associated protein	0.9328	0.272841
Gabarapl1	Gamma-aminobutyric acid (GABA) A receptor-associated protein-like 1	0.9693	0.501304
Gabarapl2	Gamma-aminobutyric acid (GABA) A receptor-associated protein-like 2	0.9621	0.611293
Hdac1	Histone deacetylase 1	1.3491	0.464767
Hgs	HGF-regulated tyrosine kinase substrate	0.8736	0.410567
Hsp90aa1	Heat shock protein 90, alpha (cytosolic), class A member 1	1.0234	0.88025
Hspa8	Heat shock protein 8	1.0208	0.721579
Htt	Huntingtin	0.9655	0.691381
Ifna2	Interferon alpha 2	1.0451	0.820517
Ifna4	Interferon alpha 4	0.9736	0.917096
Ifng	Interferon gamma	1.7311	0.366353
Igf1	**Insulin-like growth factor 1**	**1.3225**	**0.034521**
Ins2	Insulin II	1.3045	0.436792
Irgm1	Immunity-related GTPase family M member 1	1.1224	0.531918
Map1lc3a	Microtubule-associated protein 1 light chain 3 alpha	0.9765	0.786952
Map1lc3b	Microtubule-associated protein 1 light chain 3 beta	0.9728	0.626954
Mapk14	Mitogen-activated protein kinase 14	1.0692	0.512479
Mapk8	Mitogen-activated protein kinase 8	1.0951	0.441882
Nfkb1	Nuclear factor of kappa light polypeptide gene enhancer in B-cells 1, p105	0.9969	0.935844
Pik3c3	Phosphoinositide-3-kinase, class 3	0.9717	0.777134
Pik3cg	Phosphoinositide-3-kinase, catalytic, gamma polypeptide	1.1736	0.483422
Pik3r4	Phosphatidylinositol 3 kinase, regulatory subunit, polypeptide 4, p150	0.9813	0.745914
Prkaa1	Protein kinase, AMP-activated, alpha 1 catalytic subunit	1.0265	0.766799
Prkaa2	Protein kinase, AMP-activated, alpha 2 catalytic subunit	1.0381	0.716181
Pten	Phosphatase and tensin homolog	1.1721	0.171834
Rab24	RAB24, member RAS oncogene family	0.9833	0.630217
Rb1	Retinoblastoma 1	0.9933	0.879346
Rgs19	Regulator of G-protein signaling 19	1.0185	0.79704
Rps6kb1	Ribosomal protein S6 kinase, polypeptide 1	0.8669	0.349614
Snca	**Synuclein, alpha (α-synuclein)**	**2.9428**	**0.007024**
Sqstm1	Sequestosome 1	1.0339	0.570836

Tgfb1	Transforming growth factor, beta 1	0.9093	0.131689
Tgm2	Transglutaminase 2, C polypeptide	1.0585	0.525486
Fam176a	Family with sequence similarity 176, member A	0.8814	0.449408
Tmem74	Transmembrane protein 74	1.148	0.480341
Dram2	VDNA-damage regulated autophagy modulator 2	0.9764	0.499394
Tnf	Tumor necrosis factor	0.8022	0.437152
Tnfsf10	Tumor necrosis factor (ligand) superfamily, member 10	0.9444	0.561366
Trp53	**Transformation related protein 53 (p53)**	**0.8982**	**0.018938**
Trp73	Transformation related protein 73	1.0435	0.634059
Ulk1	Unc-51 like kinase 1 (C. elegans)	0.8947	0.36501
Ulk2	Unc-51 like kinase 2 (C. elegans)	1.0682	0.373641
Uvrag	UV radiation resistance associated gene	1.2278	0.154676

Expression data was derived using 4 of the 5 available reference genes: *Gusb*, *Hprt*, *Hsp90ab1*, *Gapdh*. The fifth control *Actb* was excluded since it appeared to be affected by *IGF-1Ea* overexpression. Due to the relatively low increase of *IGF-1* expression on the array, a separate rtPCR using Taqman® reagents was performed to confirm overexpression of the rat *IGF-1* isoform (**Figure 6.10**).

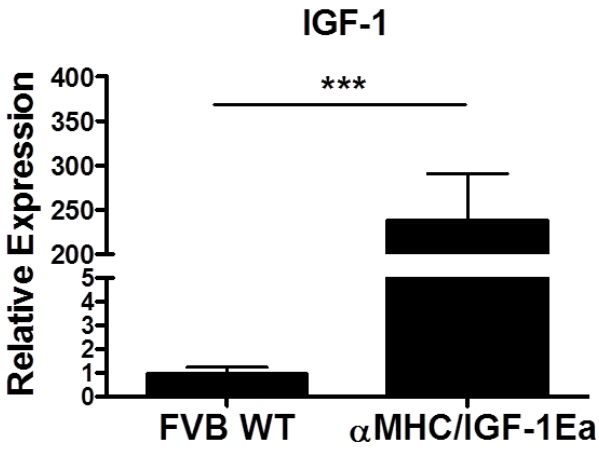


Figure 6.10: Real-time PCR for *IGF-1* in cardiac samples using Taqman® reagents. *FVB wt* (n = 3) and *αMHC/IGF-1Ea* (n = 4) cDNA was analysed using a rat *IGF-1* probe. Data is presented as standard deviation of the mean.

As expected from previous work, *IGF-1* was significantly upregulated around 300 fold in mice overexpressing cardiac *IGF-1Ea*. From the panel of differentially regulated genes, *α-synuclein* and *battenin* were selected for validation on the protein level. α-synuclein and battenin are known to play a role in intracellular amyloid/Lewy body formation and

lipofuscinosis respectively (reviewed in Lerner *et al.* 1995; Quinn *et al.* 2012). Elevated α-synuclein expression was confirmed on the protein level by Western blotting, showing a ~10-fold increase (**Figure 6.11**).

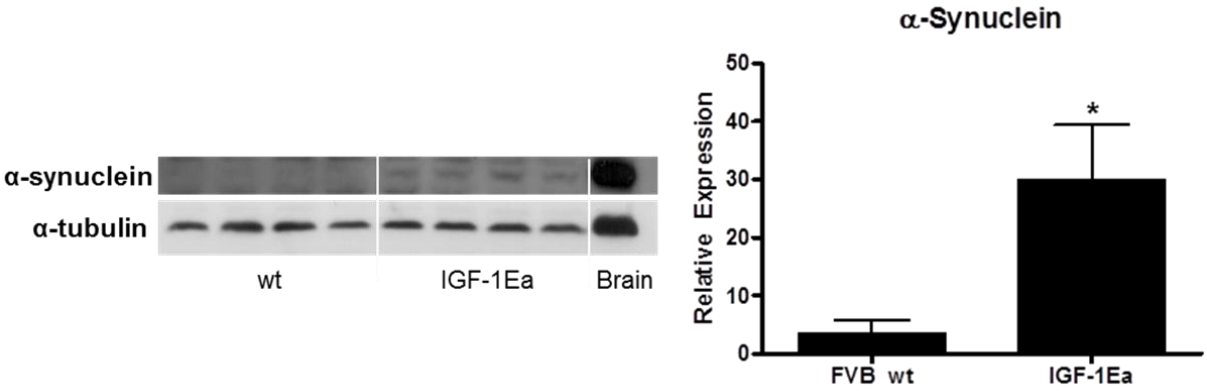


Figure 6.11: Western blot for α-synuclein using cardiac extracts from 3 month old *wt* and *αMHC/IGF-1Ea* mice. α-tubulin was used for normalisation and a brain sample served as positive control. Data presented as standard deviation of the mean.

Since α-synuclein immunofluorescence did not show a clear signal indicative of its presence in the large intracellular vacuoles in preliminary experiments, a detailed immunogold analysis for α-synuclein was not performed (data not shown). Despite a minor but significant downregulation on the mRNA level, battenin protein was not significantly downregulated in cardiac samples of *αMHC/IGF-1Ea* mice (**Figure 6.12**).

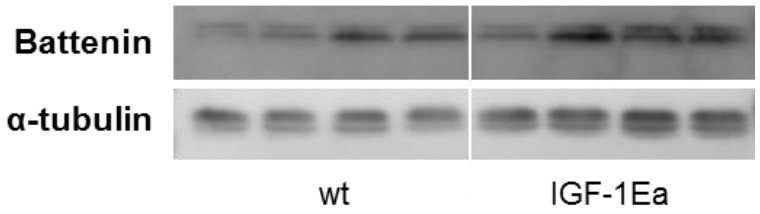


Figure 6.12: Western blot for battenin using cardiac protein samples of 3 month old *wt* and *αMHC/IGF-1Ea* mice. Bands normalised against α-tubulin. No statistical evaluation was possible due to high background and presence of an aspecific doublet.

The battenin Western blot showed high background staining and a potentially aspecific band at similar molecular weight which was prohibitive for quantification by ImageJ. Battenin bands appear to be slightly stronger in *αMHC/IGF-1Ea* but the α-tubulin revealed that also slightly larger amounts were loaded.

To further elucidate whether abnormal aggregation of protein destined for degradation may contribute to the formation of the large electron-dense structures, ubiquitination was investigated by Western blotting (**Figure 6.13**).

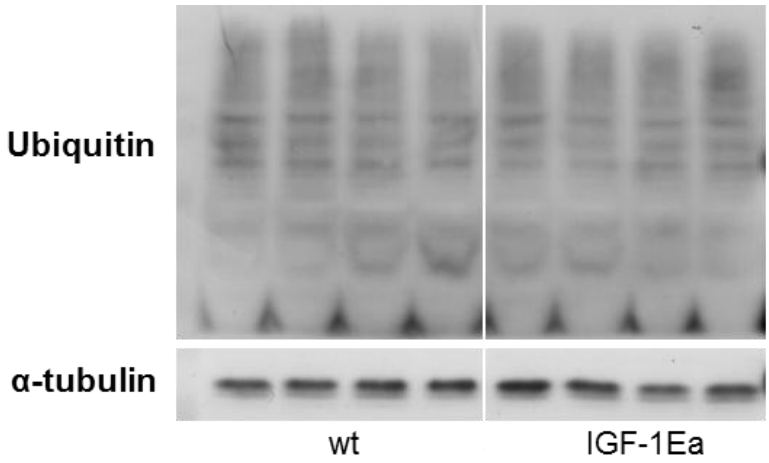


Figure 6.13: Western blot for ubiquitin using cardiac protein extracts of 3 month old *wt* and *αMHC/IGF-1Ea* mice. α-tubulin was used as control.

The overall level of ubiquitination appeared to be comparable between *αMHC/IGF-1Ea* and *wt* mice. Since not a single band but overall signal intensity was investigated, standard quantification using ImageJ was not possible.

The initial hypothesis was that IGF-1Ea could be mechanistically involved in the formation of the large vesicles or indirectly promote their formation by overloading protein production, storage or degradation mechanisms or even by depleting nutrients pushing the cells towards autophagy. Given the negative evidence for a role in autophagy, I considered that IGF-1Ea overexpression could lead to aggregation of this protein. To assess if IGF-1Ea was present within the structures, IGF-1 immunogold analysis was performed. This revealed that the electron-dense structures contained an abundance of IGF-1 protein (**Figure 6.14**).

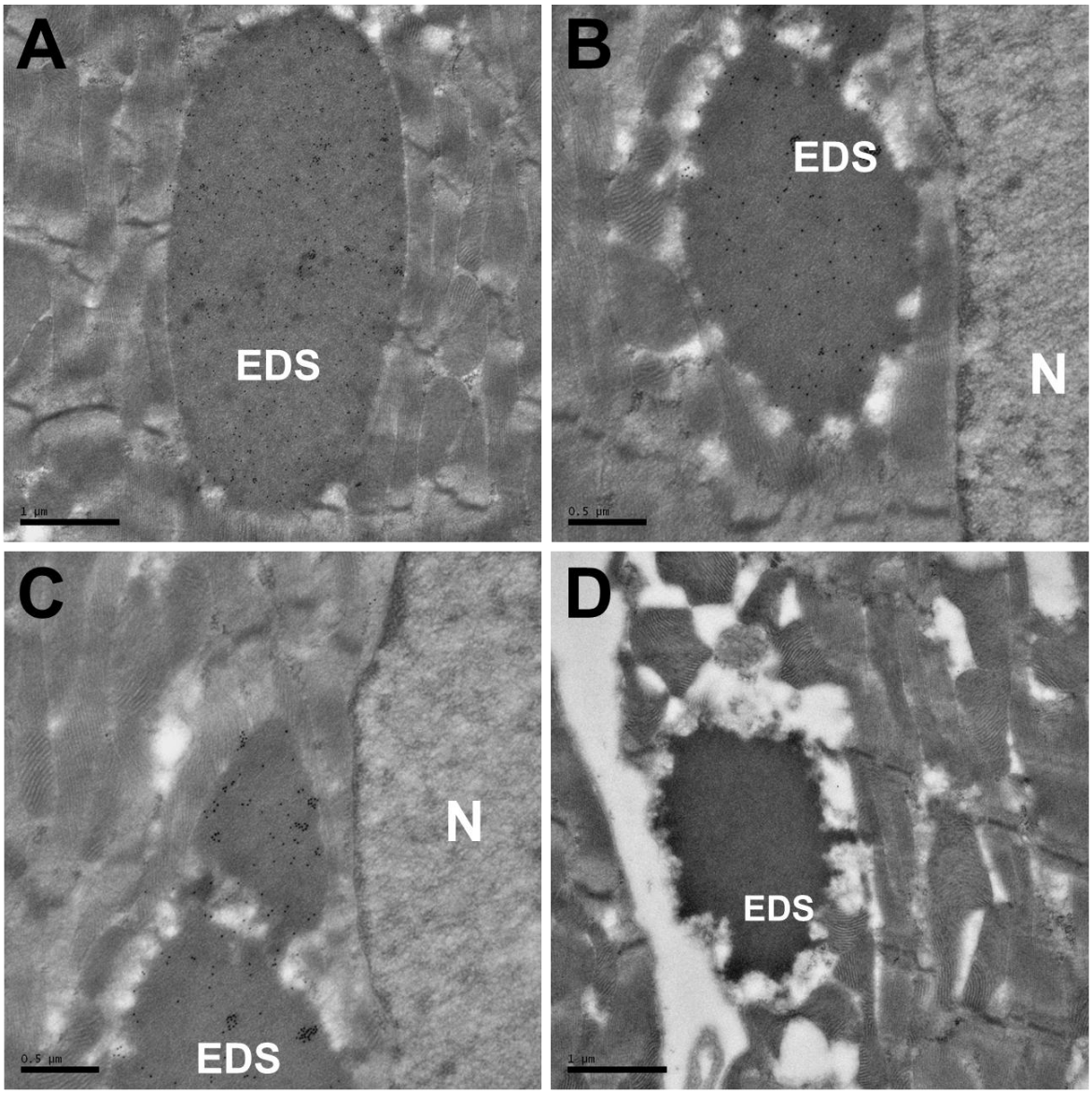


Figure 6.14: Immunogold staining for IGF-1 on cardiac section of 3 month *αMHC/IGF-1Ea* mice. (A-C) Transmission electron graphs showing positive signal for IGF-1 in electron-dense structures. (D) Negative control after incubation with secondary antibody only (EDS– Electron-dense structure, N – Nucleus). Scale bars A, D = 1 µm, B, C = 0.5 µm.

In addition to the presented data, paraffin sections of *αMHC/IGF-1Ea* or *wt* hearts were analysed for the presence of amyloid plaque (by congo red stain) and for iron deposits (by Pearl's Prussian blue), but neither were shown to aggregate in the myocardium (data not shown).

6.4 Discussion

This chapter describes the discovery of large electron-dense structures in the hearts of *αMHC/IGF-1Ea* transgenic mice. The fact that they arise between 6 weeks and 3 months of age and did not increase in size and abundance thereafter could be indicative of a compensatory adaption to high IGF-1Ea levels. The arrest in growth/formation is not caused by promoter silencing since high expression of *IGF-1* mRNA was detected (**Figure 6.10**). I investigated whether the structures could be lipofuscin, highly oxidised and cross-linked protein and organelle debris that cannot be removed by standard pathways, such as ubiquitin-proteasome degradation and autophagy (Powell *et al.* 2005). This was based on the knowledge that despite promoting preservation of bone and muscle tissue during ageing, elevated serum IGF-1 has indeed been linked increased oxidative stress/ROS production in skeletal muscle and IGF-1 treatment increased ROS production in adipose cells (Fukuoka *et al.* 2010; Elis *et al.* 2011). An intracellular mechanism to suppress ROS formation is the removal of defective mitochondria by autophagy (Gu *et al.* 2004). In the presence of IGF-1, however, autophagic degradation of mitochondria is reduced and this mechanism increases ROS-mediated protein crosslinking potentially resulting in their accumulation in the electron-dense structures. At the same time, knockdown of IGF-1 was shown to result in decreased oxidative stress tolerance in the liver and IGF-1 supplementation increases resistance to oxidative stress-induced apoptosis potentially explaining the absence of an adverse phenotype in *αMHC/IGF-1Ea* mice (Gu *et al.* 2004; Bailey-Downs *et al.* 2012). The local IGF-1Ea isoform in particular was found to reduce oxidative stress in cardiomyocytes via the protective molecule SirT1 (Alcendor *et al.* 2007; Vinciguerra *et al.* 2010). While it is conceivable that ROS plays a role in the formation of the structures, the distinct morphological difference between lipofuscin found in aged animals compared to the observed structures and disproved the lipofuscin hypothesis. Furthermore, increased lipofuscin formation is generally accompanied by a dramatic increase in ubiquitinated proteins, which was not observed in *αMHC/IGF-1Ea* mice (**Figure 6.13**, Powell *et al.* 2005). Given their morphological resemblance to large autophagosomes, further investigations focused on whether the electron-dense structures could resemble intermediates or arrested late stage components of autophagy signalling (**Figure 6.4**).

6.4.1 Autophagy in *αMHC/IGF-1Ea* hearts

Despite being much larger size, the structures resembled autophagosomes or later autophagolysosomes and I investigated this hypothesis given the implications of IGF-1 in autophagy regulation. Autophagy is a vital process that next to turnover of old organelles and proteins is mainly required to provide nutrition during starvation or following events that require large amounts of nutrients in a short period of time. While autophagy is critical to

overcome acute poor nutrient supply, excessive macroautophagy results in so called autophagic cell death and thus contributes to cardiomyocyte loss during human heart failure (reviewed in Kostin *et al.* 2003; Tsujimoto and Shimizu 2005). Ablation of autophagy on the other hand accelerates heart failure and increases mortality among patients indicating that pro and anti-autophagic stimuli have to be carefully balanced in a healthy cell (Tannous *et al.* 2008). IGF-1 is protecting the heart by preventing excessive autophagy and is reportedly balancing autophagy and apoptosis (Gu *et al.* 2004; Troncoso *et al.* 2012). It is thus not surprising to see apoptotic master regulator p53 downregulated on the autophagy PCR array (**Table 6.1**). In the rat, skeletal muscle protein production is reduced following major burn injury and hypercatalytic responses degrading protein and glucose are initiated (Clark *et al.* 1984; Fang *et al.* 1995). While this is normally accompanied by decreased protein production, IGF-1 supplementation was shown to increase protein production and prevent protein degradation in this model (Fang *et al.* 1997; Fang *et al.* 1998).

The role of IGF-1 to reduce the catabolic response to injury was further consolidated in the same burn injury model indicating that IGF-1 prevents lysosomal activity and the ubiquitin-proteasome pathway (Fang *et al.* 2002). If these findings could be extended to the IGF-1Ea propeptide, this would strongly support the hypothesis that the structures, though of unknown origin, could be accumulating due to reduced lysosomal activity. As such, it would have been interesting to investigate if overall protein content is increased in *αMHC/IGF-1Ea* cardiomyocytes, but limited time restricted further experimentation in this direction. Evidence *in vitro* showed that long-term IGF-1 exposure reduces autophagy and as a result increases the amount of depolarised mitochondria (Bitto *et al.* 2010). Conversely, mice with reduced IGF-1 activity due to hypomorphic *IGF-1* alleles showed increased autophagy shown by elevated levels of LC3 in the tissue.

Mechanistically, IGF-1 reduces autophagy via Akt signalling in vascular endothelial cells indicated by decreased abundance of Beclin-1 and LC3-positive vacuolated cells (Jia *et al.* 2006). This occurs in synergy with mTOR activation which has been implicated in autophagy suppression in yeast and mammals (Noda and Ohsumi 1998; Cutler *et al.* 1999; Sobolewska *et al.* 2009). This was confirmed in neonatal rat cardiomyocytes in which IGF-1 mediated inhibition of autophagy is achieved via the Akt/mTOR and AMPK/mTOR signalling axes (Troncoso *et al.* 2012). In relation to the electron-dense vesicles observed in *αMHC/IGF-1Ea* mice, it is noteworthy that experiments by Jia and colleagues showed that the overall number of vacuoles positive for autophagic markers was decreased in response to IGF-1 treatment (Jia *et al.* 2006). In line with the previously reported improved function of *αMHC/IGF-1Ea* hearts after injury, IGF-1 was also shown to rescue mitochondrial metabolism and to inhibit excessive autophagy in the heart thereby mitigating nutrient-related insult, as occurs during ischaemia (Santini *et al.* 2007; Troncoso *et al.* 2012).

In the current work, autophagy marker beclin-1 was not differentially regulated in the hearts of *αMHC/IGF-1Ea* mice and neither increased conversion of LC3BI into LC3BII, nor localisation of LC3 to the electron-dense structures was observed (**Figure 6.9**). However, beclin-1 is an early marker of autophagy involved in membrane nucleation and LC3 dissociates from the outer membrane after fusion of the autophagosome with the lysosome and is subsequently degraded on the inner membrane (Liang *et al.* 1999; Ropolo *et al.* 2007, Kabeya *et al.* 2000). Hence, neither would be expected to be present in late stage autophagolysosomes To determine if the electron-dense structures could resemble large arrested autophagolysosomes, the expression of a wider panel of genes involved in autophagy was analysed.

6.4.2 α-synuclein and battenin – Markers of neurological disease

Robust overexpression of *IGF-1Ea* was confirmed by rtPCR (**Figure 6.10**). Apart from IGF-1, six further genes were found to be differentially regulated on the autophagy PCR array (**Table 6.1**). Out of these, *α-synuclein* (*Snca*) and *battenin* (*Cln3*) were selected due to their implication in storage diseases of post-mitotic tissues.

α-synuclein is a natively unfolded protein and lacks a defined structure but can assume a more organised shape if bound to other proteins (Weinreb *et al.* 1996). While the function of α-synuclein is poorly characterised, it is recognised for its pathological accumulation in so called Lewy bodies in brain cells during Parkinson's disease (Spillantini *et al.* 1997). An Ala30Pro point mutation has been identified to contribute to this pathology (Kruger *et al.* 1998). Since proline is involved in secondary protein structure acquisition this could lead to aberrant folding making the protein prone to aggregation. Along point mutations α-synuclein accumulation is frequently caused by triplications of the α-synuclein gene (Kruger *et al.* 1998; Singleton *et al.* 2003). This indicates neuronal storage disease can be caused by α-synuclein in a qualitative and quantitative manner.

α-synuclein is found predominantly cytosolic but is present in mitochondria as well (Shavali *et al.* 2008). Mitochondria are affected in Parkinson's disease displaying a swollen and rounded morphology in brain tissues (Trimmer *et al.* 2000). Since α-synuclein was upregulated both on mRNA and protein levels, a retrospective analysis of the TEM data was performed. This revealed that mitochondria appeared slightly enlarged in *αMHC/IGF-1Ea* hearts compared to *wt* but retained an otherwise normal structure (data not shown). It remains unclear whether there is a connection between this observation and elevated α-synuclein levels. With regards to the presence of the electron-dense structures, it is noteworthy that α-synuclein predisposes cells to proteasomal dysfunction (Sun *et al.* 2005). Furthermore, α-synuclein and Akt were shown to directly interact to regulate IGF-1 (Chung *et al.* 2011). α-synuclein translational regulation is controlled in part by intracellular iron and the expression of ferritins,

proteins that convert Fe(II) into Fe(III), is in turn regulated by IGF-1 signalling in nematodes, indicating further possible links between the two molecules (Lawson *et al.* 1989; Ackerman and Gems 2012; Febbraro *et al.* 2012). However, iron deposition was not observed in the electron-dense structures or in *αMHC/IGF-1Ea* cardiac tissue in general. While α-synuclein was increased on both mRNA and protein level, a direct link with IGF-1Ea overexpression and the electron-dense structures was not established. It is furthermore remarkable that despite the presence of the large structures and elevated α-synuclein, cardiac function was normal in these mice compared to *wt* and even superior under pathological conditions (Santini *et al.* 2007). This could be explained by the ability of IGF isoforms to rescue α-synuclein toxicity (Kao 2009). This analysis potentially indicates that the increase in α-synuclein is an effect not directly related to IGF-1Ea function, but could rather be a secondary response mechanism, which does not result in a pathologic phenotype on the organ level due to the protective effects of IGF-1Ea counteracting its toxicity.

The second marker selected from the PCR array for further analysis was battenin, which was reduced in *αMHC/IGF-1Ea* hearts (**Table 6.1**). Battenin, or CLN3, has been researched in the context of a lipofuscinosis called Batten disease, which is caused by reduction of battenin expression due to genetic mutations (Lerner *et al.* 1995). It is a multipass transmembrane protein found on lysosomes and endosomes and plays a role in late endosomal/lysosomal membrane transport (reviewed in Phillips *et al.* 2005; Uusi-Rauva *et al.* 2012). Low IGF-1 levels in cerebrospinal fluid have previously been associated with neuropathology in infantile CLN1 disease due to its role in regulating apoptosis via PI3K signalling and an ex-vivo canine model of related CLN8 NCF showed that IGF-1 was improving outgrowth of neurons (Dunn *et al.* 1994; Riikonen *et al.* 2000; Katz *et al.* 2005). However, an analysis of cerebrospinal fluid showed that levels of IGF-1 are normal in CLN3-type neuronal ceroid lipofuscinosis/Battens disease in humans and sheep (Kay *et al.* 2009). While the role of battenin in juvenile lipofuscinosis and the associated reduction of autophagy and accumulation of storage vesicles have been well documented, the present study was unable to link the large intracellular vesicles to reduction in battenin. The downregulation on the mRNA levels on the autophagy PCR array was not confirmed on the protein level. (Cao *et al.* 2006).

It is important to highlight that the majority of published work on IGF-1 has involved the analysis of fully processed IGF-1 protein and did not consider the unique action of propeptide precursors such as IGF-1Ea. On a case-by-case basis the signalling pathways of IGF-1 and IGF-1Ea differ significantly and the full spectrum mechanisms regulated by either form remains to be elucidated (Grounds 2002; Santini *et al.* 2007). In the presented work, neither changes in LC3B conversion or beclin-1 levels nor in the expression of classical markers of autophagy were observed. This is in line with previous work showing that mTOR is not

differentially regulated *αMHC/IGF-1Ea* mouse hearts and potentially indicates that there is no direct involvement of IGF-1Ea in the regulation of autophagy (Santini *et al.* 2007). Finally, the possibility that the structures could be the product of an overloaded protein degradation mechanism was considered since ribosomal subunit S6 activity is induced in *αMHC/IGF-1Ea* hearts under physiological conditions. When investigating overall ubiquitination of proteins in *αMHC/IGF-1Ea* hearts, we observed no increase compared to *wt* under physiological conditions it possible that a change would be observed following cardiac MI (**Figure 6.13**).

To understand whether the electron-dense vesicles relate to an abnormal IGF-1Ea accumulation simply as a consequence of overexpression we compared electron micrographs of *αMHC/IGF-1Ea* to those of Fstl1 overexpressing mice of our collaborator Enrique Lara-Pezzi. Comparable structures were not identified indicating that overexpression of proteins *per se* does not result in the formation of the observed electron-dense structures in cardiomyocytes. This could indicate either a direct role of IGF-1Ea in the formation of these structures or that the specific biochemical attributes of IGF-1Ea render it more prone to aggregation compared to other overexpressed proteins.

6.4.3 Summary

The current work describes the morphology and timing of appearance of large, IGF-1-containing, electron-dense structures in cardiomyocytes of *αMHC/IGF-1Ea* mice, but does not come to a final conclusion as to the origin of the structures and whether they comprise a pathological aggregation, are beneficial as storage vesicles or prime the cells to respond to starvation or other challenges. While storage diseases have been researched predominantly in diseases of the nervous system, they are not exclusively confined to this environment but found in post-mitotic tissues in general (Nakano and Gotoh 1992; Zhou *et al.* 2006). An exploratory characterisation of the biochemical properties was performed and showed an involvement of lysosomes, but not of the autophagy pathway. To further characterise the vesicles, the remaining positive hits of the autophagy PCR array could be validated, but these are not strong classical markers and it is therefore not feasible to continue this line of investigation. Further analyses by molecular biology and histology techniques are neither cost nor time effective and broader analytical techniques should be considered. Laser dissection and subsequent digestion and mass spectrometry analysis could provide information on the composition of the structures which could then be followed up by appropriate, more educated experimental approaches.

Final Conclusion

The original aim of this thesis was the investigation of a knock-down of Tβ4 in adult mouse hearts. This was based on the previous finding that shRNA-mediated cardiac-specific depletion of Tβ4 resulted in a severe, embryonic lethal cardiac phenotype in mouse embryos. My work has demonstrated that shRNA-mediated knockdown of Tβ4 in cardiomyocytes using a tamoxifen-sensitive Cre driver strain does not result in a measurable reduction of *Tβ4 in vivo*, *in vitro* or in isolated adult cardiomyocytes. In addition, recent results from another laboratory have indicated that complete *Tβ4* knockout as well as adult cardiac-specific conditional knockout do not result in any significant cardiac phenotype. These findings show that even if a sufficient knock-down of *Tβ4* mRNA would have been achieved, this would not have resulted in a significant phenotype at least under physiological conditions and implies that the previously observed embryonic phenotype is likely attributable to off-target effects of the shRNA rather than reduction of Tβ4. While Tβ4 depletion in adult mouse hearts proved unsuccessful and in the light of more recent data redundant, I uncovered an important perturbation in tamoxifen-treated *αMHC/MerCreMer* mice. Treatment using standard protocols not only resulted in a transient cardiomyopathy but also in a previously not described chronic fibrotic phenotype altering cardiac function. This was furthermore characterised to stimulate inflammatory processes and to elevate expression of pathological hypertrophy markers, both of which are frequently used as readouts in cardiac regeneration experiments. Overall these findings raised concerns about the use of appropriate controls in a number of recent publications in the field and emphasises the importance of using appropriate controls for complex genetic manipulations.

The proteomic investigation to further study Tβ4-interacting proteins was hampered by technical difficulties and resulted in the conclusion that dedicated proteomic support services should be used where local infrastructure, resources and time are limited.

In *αMHC/IGF-1Ea* mice, I characterised novel electron-dense structures the nature of which was not conclusively resolved at the end of this study. While they appeared morphologically similar to autophagolysosomes a detailed marker analysis did not reveal any implication of autophagy in their formation. However, the fact that they were co-localising with lysosomes could imply a role in turnover of intracellular macromolecules but this will need to be addressed by more focused research in this direction.

Given the urgency to develop novel approaches to treat cardiac disease, the research into novel molecules and their mechanisms is critical but should be performed to the highest standards. Critical reflection and diligence should be exercised to ascertain that the most

robust data is obtained. While being essentially good scientific practice and preserving vital resources this is also crucial to avoid unnecessary use of animals in laboratory research.

Publications and Presentations

Publications

Santini, M. P., **Lexow J**., *et al.* (2011). "IGF-1Ea induces vessel formation after injury and mediates bone marrow and heart cross-talk through the expression of specific cytokines." Biochem Biophys Res Commun 410(2):201-7.

Lexow J.; Poggioli T.; *et al.* (2013). Combinatorial Therapies for Cardiac Regeneration. Rec Pat Regen Med. Vol. 3, No.1.

Lexow J., Sarathchandra P.; *et al.* (submitted). Cardiac fibrosis in mice expressing an inducible myocardial-specific Cre driver.

Presentations

- Keystone Symposium, Taos, New Mexico 2012 – Poster: Cardiac fibrosis in tamoxifen-treated *αMHC/MerCreMer* mice
- NHLI Postgraduate Research Day 2011 – Talk: Cardiac fibrosis in “healthy” *MerCreMer* transgenic mice – The importance of good controlling
- Heart Science Centre Seminar – Talk: 07/2011
- Oxford University Seminar – Talk: 04/2011
- Keystone Symposium, Keystone, Colorado, 2010 – Poster: Enlarged autophagolysosomes in mIGF´-1 transgenic hearts: a better way to regenerate?

Awards

- NHBLI Scholarship for the Keystone Cardiovascular Development and Repair Meeting 2010
- Laboratory Animal Science Association (LASA) Conference Travel Bursary for the Keystone Cardiovascular Development and Regeneration Meeting 2012

References

Ackerman, D. and D. Gems (2012). "Insulin/IGF-1 and Hypoxia Signaling Act in Concert to Regulate Iron Homeostasis in Caenorhabditis elegans." Plos Genetics **8**(3).

Adamopoulos, S., J. T. Parissis and D. T. Kremastinos (2001). "A glossary of circulating cytokines in chronic heart failure." European Journal of Heart Failure **3**(5): 517-526.

Afonina, I., M. Zivarts, I. Kutyavin, E. Lukhtanov, H. Gamper and R. B. Meyer (1997). "Efficient priming of PCR with short oligonucleotides conjugated to a minor groove binder." Nucleic Acids Research **25**(13): 2657-2660.

Agarwal, U., W. Ghalayini, F. Dong, K. Weber, Y.-R. Zou, S. Y. Rabbany, S. Rafii and M. S. Penn (2010). "Role of Cardiac Myocyte CXCR4 Expression in Development and Left Ventricular Remodeling After Acute Myocardial Infarction." Circulation Research **107**(5): 667-U236.

Aharinejad, S., M. Salama, S. Roedler, M. Ehrlich, A. Zuckermann and G. Laufer (2012). "Low Serum IGF-1 Is a Risk Factor for Cardiac Allograft Vasculopathy in Cardiac Transplant Recipients." Transplantation **93**(3): 309-313.

Al-Nedawi, K. N., M. Czyz, R. Bednarek, J. Szemraj, M. Swiatkowska, A. Cierniewska-Cieslak, J. Wyczolkowska and C. S. Cierniewski (2004). "Thymosin beta 4 induces the synthesis of plasminogen activator inhibitor 1 in cultured endothelial cells and increases its extracellular expression." Blood **103**(4): 1319-24.

Alcendor, R. R., S. Gao, P. Zhai, D. Zablocki, E. Holle, X. Yu, B. Tian, T. Wagner, S. F. Vatner and J. Sadoshima (2007). "Sirt1 regulates aging and resistance to oxidative stress in the heart." Circulation Research **100**(10): 1512-1521.

Alessi, D. R., M. Andjelkovic, B. Caudwell, P. Cron, N. Morrice, P. Cohen and B. A. Hemmings (1996). "Mechanism of activation of protein kinase B by insulin and IGF-1." EMBO J **15**(23): 6541-51.

Anastassiadis, K., J. Fu, C. Patsch, S. Hu, S. Weidlich, K. Duerschke, F. Buchholz, F. Edenhofer and A. F. Stewart (2009). "Dre recombinase, like Cre, is a highly efficient site-specific recombinase in E-coli, mammalian cells and mice." Disease Models & Mechanisms **2**(9-10): 508-515.

Anastassiadis, K., S. Glaser, A. Kranz, K. Berhardt and A. F. Stewart (2010). A PRACTICAL SUMMARY OF SITE-SPECIFIC RECOMBINATION, CONDITIONAL MUTAGENESIS, AND TAMOXIFEN INDUCTION OF CREERT2. Methods in Enzymology, Vol 477: Guide to Techniques in Mouse Development, Part B: Mouse Molecular Genetics, Second Edition. **477:** 109-123.

Anderson, J. L., C. D. Adams, E. M. Antman, C. R. Bridges, R. M. Califf, D. E. Casey Jr, W. E. Chavey Ii, F. M. Fesmire, J. S. Hochman, T. N. Levin, A. M. Lincoff, E. D. Peterson, P. Theroux, N. K. Wenger, R. S. Wright, S. C. Smith Jr, A. K. Jacobs, J. L. Halperin, S. A. Hunt, H. M. Krumholz, F. G. Kushner, B. W. Lytle, R. Nishimura, J. P. Ornato, R. L. Page and B. Riegel (2007). "ACC/AHA 2007 Guidelines for the Management of Patients With Unstable Angina/Nonâ€“ST-Elevation Myocardial Infarction: A Report of the American College of Cardiology/American Heart Association Task Force on Practice Guidelines (Writing Committee to Revise the 2002 Guidelines for the Management of Patients With Unstable Angina/Nonâ€“ST-Elevation Myocardial Infarction) Developed in Collaboration with the American College of Emergency Physicians, the Society for Cardiovascular Angiography and Interventions, and the Society of Thoracic Surgeons Endorsed by the American Association of Cardiovascular and Pulmonary Rehabilitation and the Society for Academic Emergency Medicine." Journal of the American College of Cardiology **50**(7): e1-e157.

Andersson, K. B., J. A. K. Birkeland, A. V. Finsen, W. E. Louch, I. Sjaastad, Y. Wang, J. Chen, J. D. Molkentin, K. R. Chien, O. M. Sejersted and G. Christensen (2009). "Moderate heart dysfunction in mice with inducible cardiomyocyte-specific excision of the Serca2 gene." Journal of Molecular and Cellular Cardiology **47**(2): 180-187.

Andersson, K. B., L. H. Winer, H. K. Mork, J. D. Molkentin and F. Jaisser (2010). "Tamoxifen administration routes and dosage for inducible Cre-mediated gene disruption in mouse hearts." Transgenic Research **19**(4): 715-725.

Aoyama, T., T. Matsui, M. Novikov, J. Park, B. Hemmings and A. Rosenzweig (2005). "Serum and glucocorticoid-responsive kinase-1 regulates cardiomyocyte survival and hypertrophic response." Circulation **111**(13): 1652-9.

Asakura, M., M. Kitakaze, S. Takashima, Y. Liao, F. Ishikura, T. Yoshinaka, H. Ohmoto, K. Node, K. Yoshino, H. Ishiguro, H. Asanuma, S. Sanada, Y. Matsumura, H. Takeda, S. Beppu, M. Tada, M. Hori and S. Higashiyama (2002). "Cardiac hypertrophy is inhibited by antagonism of ADAM12 processing of HB-EGF: metalloproteinase inhibitors as a new therapy." Nat Med **8**(1): 35-40.

Aukrust, P., T. Ueland, E. Lien, K. Bendtzen, F. Muller, A. K. Andreassen, I. Nordoy, H. Aass, T. Espevik, S. Simonsen, S. S. Froland and L. Gullestad (1999). "Cytokine network in congestive heart failure secondary to ischemic or idiopathic dilated cardiomyopathy." Am J Cardiol **83**(3): 376-82.

Aukrust, P., T. Ueland, F. Muller, A. K. Andreassen, I. Nordoy, H. Aas, J. Kjekshus, S. Simonsen, S. S. Froland and L. Gullestad (1998). "Elevated circulating levels of C-C chemokines in patients with congestive heart failure." Circulation **97**(12): 1136-43.

Badamchian, M., M. O. Fagarasan, R. L. Danner, A. F. Suffredini, H. Damavandy and A. L. Goldstein (2003). "Thymosin beta(4) reduces lethality and down-regulates inflammatory mediators in endotoxin-induced septic shock." International Immunopharmacology **3**(8): 1225-1233.

Bailey-Downs, L. C., D. Sosnowska, P. Toth, M. Mitschelen, T. Gautam, J. C. Henthorn, P. Ballabh, A. Koller, J. A. Farley, W. E. Sonntag, A. Csiszar and Z. Ungvari (2012). "Growth Hormone and IGF-1 Deficiency Exacerbate High-Fat Diet-Induced Endothelial Impairment in Obese Lewis Dwarf Rats: Implications for Vascular Aging." Journals of Gerontology Series a-Biological Sciences and Medical Sciences **67**(6): 553-564.

Baker, J., J. P. Liu, E. J. Robertson and A. Efstratiadis (1993). "ROLE OF INSULIN-LIKE GROWTH-FACTORS IN EMBRYONIC AND POSTNATAL-GROWTH." Cell **75**(1): 73-82.

Banerjee, I., J. Zhang, T. Moore-Morris, S. Lange, T. Shen, N. D. Dalton, Y. Gu, K. L. Peterson, S. M. Evans and J. Chen (2012). "Thymosin Beta 4 Is Dispensable for Murine Cardiac Development and Function." Circulation Research **110**(3): 456-U188.

Banyard, J., L. M. Hutchinson and B. R. Zetter (2007). Thymosin beta-NB is the human isoform of rat thymosin beta 15. Thymosins in Health and Disease: First International Symposium. **1112:** 286-296.

Bao, L. R., M. Loda, P. A. Janmey, R. Stewart, B. AnandApte and B. R. Zetter (1996). "Thymosin beta 15: A novel regulator of tumor cell motility upregulated in metastatic prostate cancer." Nature Medicine **2**(12): 1322-1328.

Bartling, B., H. Milting, H. Schumann, D. Darmer, L. Arusoglu, M. M. Koerner, A. El-Banayosy, R. Koerfer, J. Holtz and H. R. Zerkowski (1999). "Myocardial gene expression of regulators of myocyte apoptosis and myocyte calcium homeostasis during hemodynamic unloading by ventricular assist devices in patients with end-stage heart failure." Circulation **100**(19 Suppl): II216-23.

Barton, E. R. (2006). "The ABCs of IGF-I isoforms: impact on muscle hypertrophy and implications for repair." Applied Physiology Nutrition and Metabolism-Physiologie Appliquee Nutrition Et Metabolisme **31**(6): 791-797.

Bednarek, R., J. Boncela, K. Smolarczyk, A. Cierniewska-Cieslak, E. Wyroba and C. S. Cierniewski (2008). "Ku80 as a novel receptor for thymosin beta4 that mediates its intracellular activity different from G-actin sequestering." J Biol Chem **283**(3): 1534-44.

Beltrami, A. P., L. Barlucchi, D. Torella, M. Baker, F. Limana, S. Chimenti, H. Kasahara, M. Rota, E. Musso, K. Urbanek, A. Leri, J. Kajstura, B. Nadal-Ginard and P. Anversa (2003). "Adult Cardiac Stem Cells Are Multipotent and Support Myocardial Regeneration." Cell **114**(6): 763-776.

Beltrami, A. P., K. Urbanek, J. Kajstura, S. M. Yan, N. Finato, R. Bussani, B. Nadal-Ginard, F. Silvestri, A. Leri, C. A. Beltrami and P. Anversa (2001). "Evidence that human cardiac myocytes divide after myocardial infarction." N Engl J Med **344**(23): 1750-7.

Benavides, S. H., A. J. Monserrat, S. Farina and E. A. Porta (2002). "Sequential histochemical studies of neuronal lipofuscin in human cerebral cortex from the first to the ninth decade of life." Archives of Gerontology and Geriatrics **34**(3): 219-231.

Bergmann, O., R. D. Bhardwaj, S. Bernard, S. Zdunek, F. Barnabe-Heider, S. Walsh, J. Zupicich, K. Alkass, B. A. Buchholz, H. Druid, S. Jovinge and J. Frisen (2009). "Evidence for Cardiomyocyte Renewal in Humans." Science **324**(5923): 98-102.

Bernstein, E., A. A. Caudy, S. M. Hammond and G. J. Hannon (2001). "Role for a bidentate ribonuclease in the initiation step of RNA interference." Nature **409**(6818): 363-366.

Bersell, K., M. Mollova, S. Choudhury, B., D. Polizzotti, B. Ganapathy, S. Walsh, B. Wadugu, S. Arab and B. Kühn (2012). “Moderate and high amounts of tamoxifen in α-MHC-MerCreMer mice induce a DNA damage response, leading to heart failure and death.” DMM submitted.

Bersell, K., S. Arab, B. Haring and B. Kuehn (2009). "Neuregulin1/ErbB4 Signaling Induces Cardiomyocyte Proliferation and Repair of Heart Injury." Cell **138**(2): 257-270.

Bicer, A., O. Karakurt, R. Akdemir, G. Erden, A. Yildiz, O. Ozcan, Y. Sezen, S. Acikel, H. Kilic and R. Demirbag (2011). "Thymosin beta 4 is associated with collateral development in coronary artery disease." Scandinavian Journal of Clinical & Laboratory Investigation **71**(8): 625-630.

Birks, E. J., R. S. George, A. Firouzi, G. Wright, T. Bahrami, M. H. Yacoub and A. Khaghani (2012). "Long-term outcomes of patients bridged to recovery versus patients bridged to transplantation." Journal of Thoracic and Cardiovascular Surgery **144**(1): 190-196.

Birks, E. J., P. D. Tansley, J. Hardy, R. S. George, C. T. Bowles, M. Burke, N. R. Banner, A. Khaghani and M. H. Yacoub (2006). "Left ventricular assist device and drug therapy for the reversal of heart failure." New England Journal of Medicine **355**(18): 1873-1884.

Birnbaum, Y., B. Long, J. Qian, J. R. Perez-Polo and Y. Ye (2011). "Pioglitazone limits myocardial infarct size, activates Akt, and upregulates cPLA2 and COX-2 in a PPAR-gamma-independent manner." Basic Research in Cardiology **106**(3): 431-446.

Birnboim, H. C. and J. Doly (1979). "RAPID ALKALINE EXTRACTION PROCEDURE FOR SCREENING RECOMBINANT PLASMID DNA." Nucleic Acids Research **7**(6): 1513-1523.

Bitto, A., C. Lerner, C. Torres, M. Roell, M. Malaguti, V. Perez, A. Lorenzini, S. Hrelia, Y. Ikeno, M. E. Matzko, R. McCarter and C. Sell (2010). "Long-Term IGF-I Exposure Decreases Autophagy and Cell Viability." Plos One **5**(9).

Bleumink, G. S., I. Rietveld, J. Janssen, E. F. C. van Rossum, J. W. Deckers, A. Hofman, J. C. M. Witteman, C. M. van Duijn and B. H. C. Stricker (2004). "Insulin-like growth factor-I gene polymorphism and risk of heart failure (the Rotterdam study)." American Journal of Cardiology **94**(3): 384-386.

Bleumink, G. S., A. F. C. Schut, M. Sturkenboom, J. Janssen, J. C. M. Witteman, C. M. van Duijn, A. Hofman and B. H. C. Stricker (2005). "A promoter polymorphism of the insulin-like growth factor-I gene is associated with left ventricular hypertrophy." Heart **91**(2): 239-240.

Bock-Marquette, I., A. Saxena, M. D. White, J. M. Dimaio and D. Srivastava (2004). "Thymosin beta4 activates integrin-linked kinase and promotes cardiac cell migration, survival and cardiac repair." Nature **432**(7016): 466-72.

Bolli, R., A. R. Chugh, D. D'Amario, J. H. Loughran, M. F. Stoddard, S. Ikram, G. M. Beache, S. G. Wagner, A. Leri, T. Hosoda, F. Sanada, J. B. Elmore, P. Goichberg, D. Cappetta, N. K. Solankhi, I. Fahsah, D. G. Rokosh, M. S. Slaughter, J. Kajstura and P. Anversa (2011). "Cardiac stem cells in patients with ischaemic cardiomyopathy (SCIPIO): initial results of a randomised phase 1 trial." Lancet **378**(9806): 1847-1857.

Bollini, S., K. K. Cheung, J. Riegler, X. Dong, N. Smart, M. Ghionzoli, S. P. Loukogeorgakis, P. Maghsoudlou, K. N. Dube, P. R. Riley, M. F. Lythgoe and P. De Coppi (2011). "Amniotic Fluid Stem Cells Are Cardioprotective Following Acute Myocardial Infarction." Stem Cells and Development **20**(11): 1985-1994.

Boncela, J., K. Smolarczyk, E. Wyroba and C. S. Cierniewski (2006). "Binding of PAI-1 to endothelial cells stimulated by thymosin beta4 and modulation of their fibrinolytic potential." J Biol Chem **281**(2): 1066-72.

Brieger, A., G. Plotz, S. Zeuzem and J. Trojan (2007). "Thymosin beta 4 expression and nuclear transport are regulated by hMLH1." Biochem Biophys Res Commun **364**(4): 731-6.

Bristow, M. R., K. F. Adams, Jr., J. L. Bauman, A. M. Feldman, T. D. Giles, S. Goldstein, D. L. Mann and R. L. Talbert (2005). "The COMET trial." Congestive heart failure (Greenwich, Conn.) **11**(1): 39-47.

British Heart Foundation (2005). British Heart Foundation Statistics 2005.

Brodie, B. R. (2008). "What anti-thrombotic therapy is best with primary PCI for acute ST elevation myocardial infarction: How should the HORIZONS trial change current practice?" Catheterization and Cardiovascular Interventions **71**(6): 816-821.

Brunet, A., J. Park, H. Tran, L. S. Hu, B. A. Hemmings and M. E. Greenberg (2001). "Protein kinase SGK mediates survival signals by phosphorylating the forkhead transcription factor FKHRL1 (FOXO3a)." Mol Cell Biol **21**(3): 952-65.

Buchholz, F., P. O. Angrand and A. F. Stewart (1998). "Improved properties of FLP recombinase evolved by cycling mutagenesis." Nature Biotechnology **16**(7): 657-662.

Buchholz, F., L. Ringrose, P. O. Angrand, F. Rossi and A. F. Stewart (1996). "Different thermostabilities of FLP and Cre recombinases: Implications for applied site-specific recombination." Nucleic Acids Research **24**(21): 4256-4262.

Buelow, B. and A. M. Scharenberg (2008). "Characterization of Parameters Required for Effective Use of Tamoxifen-Regulated Recombination." Plos One **3**(9).

Buerger, A., O. Rozhitskaya, M. C. Sherwood, A. L. Dorfman, E. Bisping, E. D. Abel, W. T. Pu, S. Izumo and P. Y. Jay (2006). "Dilated cardiomyopathy resulting from high-level myocardial expression of Cre-recombinase." Journal of Cardiac Failure **12**(5): 392-398.

Burnette, W. N. (1981). "WESTERN BLOTTING - ELECTROPHORETIC TRANSFER OF PROTEINS FROM SODIUM DODECYL SULFATE-POLYACRYLAMIDE GELS TO UNMODIFIED

NITROCELLULOSE AND RADIOGRAPHIC DETECTION WITH ANTIBODY AND RADIOIODINATED PROTEIN-A." Analytical Biochemistry **112**(2): 195-203.

Buse, P., S. H. Tran, E. Luther, P. T. Phu, G. W. Aponte and G. L. Firestone (1999). "Cell cycle and hormonal control of nuclear-cytoplasmic localization of the serum- and glucocorticoid-inducible protein kinase, Sgk, in mammary tumor cells. A novel convergence point of anti-proliferative and proliferative cell signaling pathways." J Biol Chem **274**(11): 7253-63.

Buss, F., C. Temm-Grove, S. Henning and B. M. Jockusch (1992). "Distribution of profilin in fibroblasts correlates with the presence of highly dynamic actin filaments." Cell Motil Cytoskeleton **22**(1): 51-61.

Caldarella, J., G. J. Goodall, A. M. Felix, E. P. Heimer, S. B. Salvin and B. L. Horecker (1983). "THYMOSIN-ALPHA-11 - A PEPTIDE RELATED TO THYMOSIN-ALPHA-1 ISOLATED FROM CALF THYMOSIN FRACTION-5." Proceedings of the National Academy of Sciences of the United States of America-Biological Sciences **80**(24): 7424-7427.

Cao, Y., J. A. Espinola, E. Fossale, A. C. Massey, A. M. Cuervo, M. E. MacDonald and S. L. Cotman (2006). "Autophagy is disrupted in a knock-in mouse model of juvenile neuronal ceroid lipofuscinosis." Journal of Biological Chemistry **281**(29): 20483-20493.

Capecchi, M. R. (1989). "ALTERING THE GENOME BY HOMOLOGOUS RECOMBINATION." Science **244**(4910): 1288-1292.

Care, A., D. Catalucci, F. Felicetti, D. Bonci, A. Addario, P. Gallo, M.-L. Bang, P. Segnalini, Y. Gu, N. D. Dalton, L. Elia, M. V. G. Latronico, M. Hoydal, C. Autore, M. A. Russo, G. W. Dorn, II, O. Ellingsen, P. Ruiz-Lozano, K. L. Peterson, C. M. Croce, C. Peschle and G. Condorelli (2007). "MicroRNA-133 controls cardiac hypertrophy." Nature Medicine **13**(5): 613-618.

Carpintero, P., R. Anadon, F. F. Delamo and J. Gomezmarquez (1995). "THE THYMOSIN BETA(4) GENE IS STRONGLY ACTIVATED IN NEURAL TISSUES DURING EARLY POSTIMPLANTATION MOUSE DEVELOPMENT." Neuroscience Letters **184**(1): 63-66.

Carpintero, P., F. F. delAmo, R. Anadon and J. GomezMarquez (1996). "Thymosin beta(10) mRNA expression during early postimplantation mouse development." Febs Letters **394**(1): 103-106.

Cavasin, M. A., T. D. Liao, X. P. Yang, J. J. Yang and O. A. Carretero (2007). "Decreased endogenous levels of Ac-SDKP promote organ fibrosis." Hypertension **50**(1): 130-6.

Cavasin, M. A., N. E. Rhaleb, X. P. Yang and O. A. Carretero (2004). "Prolyl oligopeptidase is involved in release of the antifibrotic peptide Ac-SDKP." Hypertension **43**(5): 1140-5.

Cha, H. J., M. J. Jeong and H. K. Kleinman (2003). "Role of thymosin beta4 in tumor metastasis and angiogenesis." J Natl Cancer Inst **95**(22): 1674-80.

Chevrier, M., N. Brakch, C. Lesueur, D. Genty, Y. Ramdani, S. Moll, M. Djavaheri-Mergny, C. Brasse-Lagnel, A. Laquerriere, F. Barbey and S. Bekri (2010). "Autophagosome maturation is impaired in Fabry disease." Autophagy **6**(5): 589-599.

Chisalita, S. I., U. Dahlstrom, H. J. Arnqvist and U. Alehagen (2011). "Increased IGF1 levels in relation to heart failure and cardiovascular mortality in an elderly population: impact of ACE inhibitors." European Journal of Endocrinology **165**(6): 891-898.

Choi, H. M., Y.-A. Lee, H.-I. Yang, M. C. Yoo and K. S. Kim (2011). "Increased levels of thymosin beta 4 in synovial fluid of patients with rheumatoid arthritis: association of thymosin beta 4 with other factors that are involved in inflammation and bone erosion in joints." International Journal of Rheumatic Diseases **14**(4): 320-324.

Chung, J.-Y., S.-J. Lee, S.-H. Lee, Y. S. Jung, N.-C. Ha, W. Seol and B.-J. Park (2011). "Direct Interaction of alpha-Synuclein and AKT Regulates IGF-1 Signaling: Implication of Parkinson Disease." Neurosignals **19**(2): 86-96.

Chung, J., T. C. Grammer, K. P. Lemon, A. Kazlauskas and J. Blenis (1994). "PDGF- and insulin-dependent pp70S6k activation mediated by phosphatidylinositol-3-OH kinase." Nature **370**(6484): 71-5.

Chung, J., C. J. Kuo, G. R. Crabtree and J. Blenis (1992). "Rapamycin-FKBP specifically blocks growth-dependent activation of and signaling by the 70 kd S6 protein kinases." Cell **69**(7): 1227-36.

Clark, A. S., R. A. Kelly and W. E. Mitch (1984). "SYSTEMIC RESPONSE TO THERMAL-INJURY IN RATS - ACCELERATED PROTEIN-DEGRADATION AND ALTERED GLUCOSE-UTILIZATION IN MUSCLE." Journal of Clinical Investigation **74**(3): 888-897.

Clark, E. A., T. R. Golub, E. S. Lander and R. O. Hynes (2000). "Genomic analysis of metastasis reveals an essential role for RhoC." Nature **406**(6795): 532-535.

Cleutjens, J. P. and E. E. Creemers (2002). "Integration of concepts: cardiac extracellular matrix remodeling after myocardial infarction." J Card Fail **8**(6 Suppl): S344-8.

Corr, P. B., F. X. Witkowski and B. E. Sobel (1978). "MECHANISMS CONTRIBUTING TO MALIGNANT DYSRHYTHMIAS INDUCED BY ISCHEMIA IN CAT." Journal of Clinical Investigation **61**(1): 109-119.

Cowen, T., A. J. Haven and G. Burnstock (1985). "PONTAMINE SKY BLUE - A COUNTERSTAIN FOR BACKGROUND AUTOFLUORESCENCE IN FLUORESCENCE AND IMMUNOFLUORESCENCE HISTOCHEMISTRY." Histochemistry **82**(3): 205-208.

Csiszar, A., N. Labinskyy, V. Perez, F. A. Recchia, A. Podlutsky, P. Mukhopadhyay, G. Losonczy, P. Pacher, S. N. Austad, A. Bartke and Z. Ungvari (2008). "Endothelial function and vascular oxidative stress in long-lived GH/IGF-deficient Ames dwarf mice." American Journal of Physiology-Heart and Circulatory Physiology **295**(5): H1882-H1894.

Cutler, N. S., J. Heitman and M. E. Cardenas (1999). "TOR kinase homologs function in a signal transduction pathway that is conserved from yeast to mammals." Molecular and Cellular Endocrinology **155**(1-2): 135-142.

D'Amario, D., M. C. Cabral-Da-Silva, H. Zheng, C. Fiorini, P. Goichberg, E. Steadman, J. Ferreira-Martins, F. Sanada, M. Piccoli, D. Cappetta, D. A. D'Alessandro, R. E. Michler, T. Hosoda, L. Anastasia, M. Rota, A. Leri, P. Anversa and J. Kajstura (2011). "Insulin-Like Growth Factor-1 Receptor Identifies a Pool of Human Cardiac Stem Cells With Superior Therapeutic Potential for Myocardial Regeneration." Circulation Research **108**(12): 1467-U178.

D'Ercole, A. J., A. D. Stiles and L. E. Underwood (1984). "Tissue concentrations of somatomedin C: further evidence for multiple sites of synthesis and paracrine or autocrine mechanisms of action." Proc Natl Acad Sci U S A **81**(3): 935-9.

Damas, J. K., L. Gullestad, T. Ueland, N. O. Solum, S. Simonsen, S. S. Froland and P. Aukrust (2000). "CXC-chemokines, a new group of cytokines in congestive heart failure--possible role of platelets and monocytes." Cardiovasc Res **45**(2): 428-36.

Danielian, P. S., R. White, S. A. Hoare, S. E. Fawell and M. G. Parker (1993). "IDENTIFICATION OF RESIDUES IN THE ESTROGEN-RECEPTOR THAT CONFER DIFFERENTIAL SENSITIVITY TO ESTROGEN AND HYDROXYTAMOXIFEN." Molecular Endocrinology **7**(2): 232-240.

Davies, M. J., N. Woolf and W. B. Robertson (1976). "Pathology of acute myocardial infarction with particular reference to occlusive coronary thrombi." Br Heart J **38**(7): 659-64.

DeBosch, B., I. Treskov, T. S. Lupu, C. Weinheimer, A. Kovacs, M. Courtois and A. J. Muslin (2006). "Akt1 is required for physiological cardiac growth." Circulation **113**(17): 2097-2104.

Delcayre, C. and B. Swynghedauw (2002). "Molecular mechanisms of myocardial remodeling. The role of aldosterone." J Mol Cell Cardiol **34**(12): 1577-84.

Dhaese, S., V. Jonckheere, M. Goethals, D. Waltregny, J. Vandekerckhove, C. Ampe and M. Van Troys (2007). "Functional and profiling studies prove that prostate cancer upregulated neuroblastoma thymosin beta is the true human homologue of rat thymosin beta 15." Febs Letters **581**(25): 4809-4815.

Dhaese, S., K. Vandepoele, D. Waterschoot, B. Vanloo, J. Vandekerckhove, C. Ampe and M. Van Troys (2009). "The Mouse Thymosin Beta15 Gene Family Displays Unique Complexity and Encodes A Functional Thymosin Repeat." Journal of Molecular Biology **387**(4): 809-825.

Di, R.-m., Q.-t. Feng, Z. Chang, Q. Luan, Y.-y. Zhang, J. Huang, X.-l. Li and Z.-z. Yang (2010). "PDK1 plays a critical role in regulating cardiac function in mice and human." Chinese Medical Journal **123**(17): 2358-2363.

Didry, D., F.-X. Cantrelle, C. Husson, P. Roblin, A. M. E. Moorthy, J. Perez, C. Le Clainche, M. Hertzog, E. Guittet, M.-F. Carlier, C. van Heijenoort and L. Renault (2012). "How a single residue in individual beta-thymosin/WH2 domains controls their functions in actin assembly." Embo Journal **31**(4): 1000-1013.

Dobrowolny, G., C. Giacinti, L. Pelosi, C. Nicoletti, N. Winn, L. Barberi, M. Molinaro, N. Rosenthal and A. Musaro (2005). "Muscle expression of a local Igf-1 isoform protects motor neurons in an ALS mouse model." J Cell Biol **168**(2): 193-9.

Ducharme, A., S. Frantz, M. Aikawa, E. Rabkin, M. Lindsey, L. E. Rohde, F. J. Schoen, R. A. Kelly, Z. Werb, P. Libby and R. T. Lee (2000). "Targeted deletion of matrix metalloproteinase-9 attenuates left ventricular enlargement and collagen accumulation after experimental myocardial infarction." Journal of Clinical Investigation **106**(1): 55-62.

Dunn, W. A., M. K. Raizada, E. S. Vogt and E. A. Brown (1994). "GROWTH FACTOR-INDUCED NEURITE GROWTH IN PRIMARY NEURONAL CULTURES OF DOGS WITH NEURONAL CEROID-LIPOFUSCINOSIS." International Journal of Developmental Neuroscience **12**(3): 185-196.

Elbashir, S. M., W. Lendeckel and T. Tuschl (2001). "RNA interference is mediated by 21-and 22-nucleotide RNAs." Genes & Development **15**(2): 188-200.

Elis, S., Y. Wu, H.-W. Courtland, D. Cannata, H. Sun, M. Beth-On, C. Liu, H. Jasper, H. Domene, L. Karabatas, C. Guida, J. Basta-Pljakic, L. Cardoso, C. J. Rosen, J. Frystyk and S. Yakar (2011). "Unbound (bioavailable) IGF1 enhances somatic growth." Disease Models & Mechanisms **4**(5): 649-658.

Ellison, G. M., D. Torella, S. Dellegrottaglie, C. Perez-Martinez, A. Perez de Prado, C. Vicinanza, S. Purushothaman, V. Galuppo, C. Iaconetti, C. D. Waring, A. Smith, M. Torella, C. Cuellas Ramon, J. Manuel Gonzalo-Orden, V. Agosti, C. Indolfi, M. Galinanes, F. Fernandez-Vazquez and B. Nadal-Ginard (2011). "Endogenous Cardiac Stem Cell Activation by Insulin-Like Growth Factor-1/Hepatocyte Growth Factor Intracoronary Injection Fosters Survival and Regeneration of the Infarcted Pig Heart." Journal of the American College of Cardiology **58**(9): 977-986.

Engel, F. B., P. C. H. Hsieh, R. T. Lee and M. T. Keating (2006). "FGF1/p38 MAP kinase inhibitor therapy induces cardiomyocyte mitosis, reduces scarring, and rescues function after myocardial infarction." Proceedings of the National Academy of Sciences of the United States of America **103**(42): 15546-15551.

Engleka, K. A., L. J. Manderfield, R. D. Brust, L. Li, A. Cohen, S. M. Dymecki and J. A. Epstein (2012). "Islet1 Derivatives in the Heart Are of Both Neural Crest and Second Heart Field Origin." Circulation Research **110**(7): 922-U47.

Enoki, C., H. Otani, D. Sato, T. Okada, R. Hattori and H. Imamura (2010). "Enhanced mesenchymal cell engraftment by IGF-1 improves left ventricular function in rats undergoing myocardial infarction." International Journal of Cardiology **138**(1): 9-18.

Erickson, A. H., G. E. Conner and G. Blobel (1981). "BIOSYNTHESIS OF A LYSOSOMAL-ENZYME - PARTIAL STRUCTURE OF 2 TRANSIENT AND FUNCTIONALLY DISTINCT NH2-TERMINAL SEQUENCES IN CATHEPSIN-D." Journal of Biological Chemistry **256**(21): 1224-1231.

Fan, Y., Y. Gong, P. K. Ghosh, L. M. Graham and P. L. Fox (2009). "Spatial coordination of actin polymerization and ILK-Akt2 activity during endothelial cell migration." Dev Cell **16**(5): 661-74.

Fang, C. H., H. J. James, C. Ogle, J. E. Fischer and P. O. Hasselgren (1995). "INFLUENCE OF BURN INJURY ON PROTEIN-METABOLISM IN DIFFERENT TYPES OF SKELETAL-MUSCLE AND THE ROLE OF GLUCOCORTICOIDS." Journal of the American College of Surgeons **180**(1): 33-42.

Fang, C. H., B. G. Li, J. J. Wang, J. E. Fischer and P. O. Hasselgren (1997). "Insulin-like growth factor 1 stimulates protein synthesis and inhibits protein breakdown in muscle from burned rats." Journal of Parenteral and Enteral Nutrition **21**(5): 245-251.

Fang, C. H., B. G. Li, J. J. Wang, J. E. Fischer and P. O. Hasselgren (1998). "Treatment of burned rats with insulin-like growth factor I inhibits the catabolic response in skeletal muscle." American Journal of Physiology-Regulatory Integrative and Comparative Physiology **275**(4): R1091-R1098.

Fang, C. H., B. G. Li, C. J. Wray and P. O. Hasselgren (2002). "Insulin-like growth factor-I inhibits lysosomal and proteasome-dependent proteolysis in skeletal muscle after burn injury." Journal of Burn Care & Rehabilitation **23**(5): 318-325.

Favaloro, R. G., D. B. Effler, C. Cheanvechai, R. A. Quint and F. M. Sones, Jr. (1971). "Acute coronary insufficiency (impending myocardial infarction and myocardial infarction): surgical treatment by the saphenous vein graft technique." Am J Cardiol **28**(5): 598-607.

Febbraro, F., M. Giorgi, S. Caldarola, F. Loreni and M. Romero-Ramos (2012). "alpha-Synuclein expression is modulated at the translational level by iron." Neuroreport **23**(9): 576-580.

Feil, R., J. Brocard, B. Mascrez, M. LeMeur, D. Metzger and P. Chambon (1996). "Ligand-activated site-specific recombination in mice." Proceedings of the National Academy of Sciences of the United States of America **93**(20): 10887-10890.

Felkin, L. E., E. Lara-Pezzi, R. George, M. H. Yacoub, E. J. Birks and P. J. R. Barton (2009). "Expression of Extracellular Matrix Genes During Myocardial Recovery From Heart Failure After Left Ventricular Assist Device Support." Journal of Heart and Lung Transplantation **28**(2): 117-122.

Ferrari, S. and G. Thomas (1994). "S6 phosphorylation and the p70s6k/p85s6k." Crit Rev Biochem Mol Biol **29**(6): 385-413.

Fire, A., S. Q. Xu, M. K. Montgomery, S. A. Kostas, S. E. Driver and C. C. Mello (1998). "Potent and specific genetic interference by double-stranded RNA in Caenorhabditis elegans." Nature **391**(6669): 806-811.

Förster, T. (1948). "Zwischenmolekulare Energiewanderung und Fluoreszenz." Annalen der Physik **437**(1-2): 55-75.

Frazier, O. H., E. A. Rose, P. McCarthy, N. A. Burton, A. Tector, H. Levin, H. L. Kayne, V. L. Poirier and K. A. Dasse (1995). "Improved mortality and rehabilitation of transplant candidates treated with a long-term implantable left ventricular assist system." Ann Surg **222**(3): 327-36; discussion 336-8.

Freeman, K. W., B. R. Bowman and B. R. Zetter (2011). "Regenerative protein thymosin beta-4 is a novel regulator of purinergic signaling." Faseb Journal **25**(3): 907-915.

Froesch, E. R., H. Buergi, E. B. Ramseier, P. Bally and A. Labhart (1963). "Antibody-Suppressible and Nonsuppressible Insulin-Like Activities in Human Serum and Their Physiologic Significance. An Insulin Assay with Adipose Tissue of Increased Precision and Specificity." J Clin Invest **42**: 1816-34.

Frohm, M., H. Gunne, A. C. Bergman, B. Agerberth, T. Bergman, A. Boman, S. Liden, H. Jornvall and H. G. Boman (1996). "Biochemical and antibacterial analysis of human wound and blister fluid." European Journal of Biochemistry **237**(1): 86-92.

Fujio, Y., T. Nguyen, D. Wencker, R. N. Kitsis and K. Walsh (2000). "Akt promotes survival of cardiomyocytes in vitro and protects against ischemia-reperfusion injury in mouse heart." Circulation **101**(6): 660-7.

Fukuoka, H., K. Iida, H. Nishizawa, M. Imanaka, R. Takeno, G. Iguchi, M. Takahashi, Y. Okimura, H. Kaji, K. Chihara and Y. Takahashi (2010). "IGF-I stimulates reactive oxygen species (ROS) production and inhibits insulin-dependent glucose uptake via ROS in 3T3-L1 adipocytes." Growth Hormone & Igf Research **20**(3): 212-219.

Furr, B. J. A. and V. C. Jordan (1984). "THE PHARMACOLOGY AND CLINICAL USES OF TAMOXIFEN." Pharmacology & Therapeutics **25**(2): 127-205.

Gail, M. H., J. P. Costantino, J. Bryant, R. Croyle, L. Freedman, K. Helzlsouer and V. Vogel (1999). "Weighing the risks and benefits of tamoxifen treatment for preventing breast cancer." Journal of the National Cancer Institute **91**(21): 1829-1846.

Gamper, N., S. Fillon, S. M. Huber, Y. Feng, T. Kobayashi, P. Cohen and F. Lang (2002). "IGF-1 up-regulates K+ channels via PI3-kinase, PDK1 and SGK1." Pflugers Arch **443**(4): 625-34.

Gao, C., W. Ye and L. Li (2010). "Three-dimension structure of ventricular myocardial fibers after myocardial infarction." Journal of Cardiothoracic Surgery **5**.

Gardin, J. M., F. Siri, R. N. Kitsis and L. Leinwand (1996). "Intravascular ultrasound catheter evaluation of the left ventricle in mice: A feasibility study." Echocardiography-a Journal of Cardiovascular Ultrasound and Allied Techniques **13**(6): 609-612.

Gerhard, D. S., L. Wagner, E. A. Feingold, C. M. Shenmen, L. H. Grouse, G. Schuler, S. L. Klein, S. Old, R. Rasooly, P. Good, M. Guyer, A. M. Peck, J. G. Derge, D. Lipman, F. S. Collins, W. Jang, S. Sherry, M. Feolo, L. Misquitta, E. Lee, K. Rotmistrovsky, S. F. Greenhut, C. F. Schaefer, K. Buetow, T. I. Bonner, D. Haussler, J. Kent, M. Kiekhaus, T. Furey, M. Brent, C. Prange, K. Schreiber, N. Shapiro, N. K. Bhat, R. F. Hopkins, F. Hsie, T. Driscoll, M. B. Soares, T. L. Casavant, T. E. Scheetz, M. J. Brown-stein, T. B. Usdin, S. Toshiyuki, P. Carninci, Y. Piao, D. B. Dudekula, M. S. Ko, K. Kawakami, Y. Suzuki, S. Sugano, C. E. Gruber, M. R. Smith, B. Simmons, T. Moore, R. Waterman, S. L. Johnson, Y. Ruan, C. L. Wei, S. Mathavan, P. H. Gunaratne, J. Wu, A. M. Garcia, S. W. Hulyk, E. Fuh, Y. Yuan, A. Sneed, C. Kowis, A. Hodgson, D. M. Muzny, J. McPherson, R. A. Gibbs, J. Fahey, E. Helton, M. Ketteman, A. Madan, S. Rodrigues, A. Sanchez, M. Whiting, A. Madari, A. C. Young, K. D. Wetherby, S. J. Granite, P. N. Kwong, C. P. Brinkley, R. L. Pearson, G. G. Bouffard, R. W. Blakesly, E. D. Green, M. C. Dickson, A. C. Rodriguez, J. Grimwood, J. Schmutz, R. M. Myers, Y. S. Butterfield, M. Griffith, O. L. Griffith, M. I. Krzywinski, N. Liao, R. Morin, D. Palmquist, A. S. Petrescu, U. Skalska, D. E. Smailus, J. M. Stott, A. Schnerch, J. E. Schein, S. J. Jones, R. A. Holt, A. Baross, M. A. Marra, S. Clifton, K. A. Makowski, S. Bosak and J. Malek (2004). "The status, quality, and expansion of the NIH full-length cDNA project: the Mammalian Gene Collection (MGC)." Genome Res **14**(10B): 2121-7.

Gnecchi, M., Z. Zhang, A. Ni and V. J. Dzau (2008). "Paracrine Mechanisms in Adult Stem Cell Signaling and Therapy." Circulation Research **103**(11): 1204-1219.

Goetz, R. H., M. Rohman, J. D. Haller, R. Dee and S. S. Rosenak (1961). "Internal mammary-coronary artery anastomosis. A nonsuture method employing tantalum rings." The Journal of thoracic and cardiovascular surgery **41**: 378-86.

Goldstein, A. L., A. Guha, M. M. Zatz, M. A. Hardy and A. White (1972). "Purification and biological activity of thymosin, a hormone of the thymus gland." Proc Natl Acad Sci U S A **69**(7): 1800-3.

Goldstein, A. L., E. Hannappel, G. Sosne and H. K. Kleinman (2012). "Thymosin beta(4): a multi-functional regenerative peptide. Basic properties and clinical applications." Expert Opinion on Biological Therapy **12**(1): 37-51.

Goldstein, A. L., T. L. K. Low, M. McAdoo, J. McClure, G. B. Thurman, J. Rossio, C. Y. Lai, D. Chang, S. S. Wang, C. Harvey, A. H. Ramel and J. Meienhofer (1977). "THYMOSIN-ALPHA-1 - ISOLATION AND SEQUENCE-ANALYSIS OF AN IMMUNOLOGICALLY ACTIVE THYMIC POLYPEPTIDE." Proceedings of the National Academy of Sciences of the United States of America **74**(2): 725-729.

Goldstein, D. J. and M. C. Oz (2000). "Mechanical support for postcardiotomy cardiogenic shock." Seminars in thoracic and cardiovascular surgery **12**(3): 220-8.

Gomez-Marquez, J., M. Dosil, F. Segade, X. R. Bustelo, J. G. Pichel, F. Dominguez and M. Freire (1989). "Thymosin-beta 4 gene. Preliminary characterization and expression in tissues, thymic cells, and lymphocytes." J Immunol **143**(8): 2740-4.

Gomez-Marquez, J., F. Franco del Amo, P. Carpintero and R. Anadon (1996). "High levels of mouse thymosin beta4 mRNA in differentiating P19 embryonic cells and during development of cardiovascular tissues." Biochim Biophys Acta **1306**(2-3): 187-93.

Gondo, H., J. Kudo, J. W. White, C. Barr, P. Selvanayagam and G. F. Saunders (1987). "DIFFERENTIAL EXPRESSION OF THE HUMAN THYMOSIN-BETA-4 GENE IN LYMPHOCYTES, MACROPHAGES, AND GRANULOCYTES." Journal of Immunology **139**(11): 3840-3848.

Gossen, M. and H. Bujard (1992). "TIGHT CONTROL OF GENE-EXPRESSION IN MAMMALIAN-CELLS BY TETRACYCLINE-RESPONSIVE PROMOTERS." Proceedings of the National Academy of Sciences of the United States of America **89**(12): 5547-5551.

Gossen, M., S. Freundlieb, G. Bender, G. Muller, W. Hillen and H. Bujard (1995). "TRANSCRIPTIONAL ACTIVATION BY TETRACYCLINES IN MAMMALIAN-CELLS." Science **268**(5218): 1766-1769.

Grant, D. S., J. L. Kinsella, M. C. Kibbey, S. Laflamme, P. D. Burbelo, A. L. Goldstein and H. K. Kleinman (1995). "MATRIGEL INDUCES THYMOSIN BETA-4 GENE IN DIFFERENTIATING ENDOTHELIAL-CELLS." Journal of Cell Science **108**: 3685-3694.

Grant, D. S., W. Rose, C. Yaen, A. Goldstein, J. Martinez and H. Kleinman (1999). "Thymosin beta4 enhances endothelial cell differentiation and angiogenesis." Angiogenesis **3**(2): 125-35.

Grant, S. G. N. and A. J. Silva (1994). "TARGETING LEARNING." Trends in Neurosciences **17**(2): 71-75.

Grounds, M. D. (2002). "Reasons for the degeneration of ageing skeletal muscle: a central role for IGF-1 signalling." Biogerontology **3**(1-2): 19-24.

Grube, E., S. Silber, K. E. Hauptmann, R. Mueller, L. Buellesfeld, U. Gerckens and M. E. Russell (2003). "Six- and twelve-month results from a randomized, double-blind trial on a slow-release paclitaxel-eluting stent for de novo coronary lesions." Circulation **107**(1): 38-42.

Gruntzig, A. and H. J. Schneider (1977). "PERCUTANEOUS DILATATION OF CHRONIC CORONARY STENOSIS - EXPERIMENT AND MORPHOLOGY." Schweizerische Medizinische Wochenschrift **107**(44): 1588-1588.

Gu, Y. P., C. J. Wang and A. Cohen (2004). "Effect of IGF-1 on the balance between autophagy of dysfunctional mitochondria and apoptosis." Febs Letters **577**(3): 357-360.

Gulick, J., A. Subramaniam, J. Neumann and J. Robbins (1991). "ISOLATION AND CHARACTERIZATION OF THE MOUSE CARDIAC MYOSIN HEAVY-CHAIN GENES." Journal of Biological Chemistry **266**(14): 9180-9185.

Guo, W., S. Schafer, M. L. Greaser, M. H. Radke, M. Liss, T. Govindarajan, H. Maatz, H. Schulz, S. Li, A. M. Parrish, V. Dauksaite, P. Vakeel, S. Klaassen, B. Gerull, L. Thierfelder, V. Regitz-Zagrosek, T. A. Hacker, K. W. Saupe, G. W. Dec, P. T. Ellinor, C. A. MacRae, B. Spallek, R. Fischer, A. Perrot, C. Oezcelik, K. Saar, N. Hubner and M. Gotthardt (2012). "RBM20, a gene for hereditary cardiomyopathy, regulates titin splicing." Nature Medicine **18**(5): 766-U162.

Haider, H. K., S. Jiang, N. M. Idris and M. Ashraf (2008). "IGF-1-Overexpressing Mesenchymal Stem Cells Accelerate Bone Marrow Stem Cell Mobilization via Paracrine Activation of SDF-1 alpha/CXCR4 Signaling to Promote Myocardial Repair." Circulation Research **103**(11): 1300-1308.

Hall, M. E., G. Smith, J. E. Hall and D. E. Stec (2011). "Systolic dysfunction in cardiac-specific ligand-inducible MerCreMer transgenic mice." American Journal of Physiology-Heart and Circulatory Physiology **301**(1): H253-H260.

Hamacher, J., M. Arras, F. Bootz, M. Weiss, R. Schramm and U. Moehrlen (2008). "Microscopic wire guide-based orotracheal mouse intubation: description, evaluation and comparison with transillumination." Laboratory Animals **42**(2): 222-230.

Han, J. J., Y. Lee, K. H. Yeom, J. W. Nam, I. Heo, J. K. Rhee, S. Y. Sohn, Y. J. Cho, B. T. Zhang and V. N. Kim (2006). "Molecular basis for the recognition of primary microRNAs by the Drosha-DGCR8 complex." Cell **125**(5): 887-901.

Hannappel, E. (2010). Thymosin beta(4) and its posttranslational modifications. Thymosins in Health and Disease. **1194:** 27-35.

Hannappel, E., F. Wartenberg and X. R. Bustelo (1989). "ISOLATION AND CHARACTERIZATION OF THYMOSIN BETA-9MET FROM PORK SPLEEN." Archives of Biochemistry and Biophysics **273**(2): 396-402.

Hannappel, E., G. J. Xu, J. Morgan, J. Hempstead and B. L. Horecker (1982). "THYMOSIN-BETA-4 - A UBIQUITOUS PEPTIDE IN RAT AND MOUSE-TISSUES." Proceedings of the National Academy of Sciences of the United States of America-Biological Sciences **79**(7): 2172-2175.

Haritos, A. A., G. J. Goodall and B. L. Horecker (1984). "PROTHYMOSIN-ALPHA - ISOLATION AND PROPERTIES OF THE MAJOR IMMUNOREACTIVE FORM OF THYMOSIN-ALPHA-1 IN RAT THYMUS." Proceedings of the National Academy of Sciences of the United States of America-Biological Sciences **81**(4): 1008-1011.

Haritos, A. A., P. P. Yialouris, E. P. Heimer, A. M. Felix, E. Hannappel and M. A. Rosemeyer (1989). "EVIDENCE FOR THE MONOMERIC NATURE OF THYMOSINS." Febs Letters **244**(2): 287-290.

Haskell, J. F. and D. C. Tucker (1994). "BINDING OF INSULIN-LIKE GROWTH-FACTORS (IGF-I AND IGF-II) TO THE IGF-II MANNOSE 6-PHOSPHATE RECEPTOR IN FETAL-RAT MYOCARDIUM." Endocrinology **135**(1): 231-239.

Hepler, J. E., J. J. Van Wyk and P. K. Lund (1990). "Different half-lives of insulin-like growth factor I mRNAs that differ in length of 3' untranslated sequence." Endocrinology **127**(3): 1550-2.

Hers, I. (2007). "Insulin-like growth factor-1 potentiates platelet activation via the IRS/PI3K alpha pathway." Blood **110**(13): 4243-4252.

Hertzog, M., C. van Heijenoort, D. Didry, M. Gaudier, J. Coutant, B. Gigant, G. Didelot, T. Preat, M. Knossow, E. Guittet and M. F. Carlier (2004). "The beta-thymosin/WH2 domain: Structural basis for the switch from inhibition to promotion of actin assembly." Cell **117**(5): 611-623.

Hertzog, M., E. G. Yarmola, D. Didry, M. R. Bubb and M. F. Carlier (2002). "Control of actin dynamics by proteins made of beta-thymosin repeats - The actobindin family." Journal of Biological Chemistry **277**(17): 14786-14792.

Higashi, Y., S. Sukhanov, A. Anwar, S.-Y. Shai and P. Delafontaine (2010). "IGF-1, oxidative stress and atheroprotection." Trends in Endocrinology and Metabolism **21**(4): 245-254.

Hill, M. and G. Goldspink (2003). "Expression and splicing of the insulin-like growth factor gene in rodent muscle is associated with muscle satellite (stem) cell activation following local tissue damage." J Physiol **549**(Pt 2): 409-18.

Hinkel, R., C. El-Aouni, T. Olson, J. Horstkotte, S. Mayer, S. Muller, M. Willhauck, C. Spitzweg, F. J. Gildehaus, W. Munzing, E. Hannappel, I. Bock-Marquette, J. M. DiMaio, A. K. Hatzopoulos, P. Boekstegers and C. Kupatt (2008). "Thymosin beta4 is an essential paracrine factor of embryonic endothelial progenitor cell-mediated cardioprotection." Circulation **117**(17): 2232-40.

Hoess, R. H., M. Ziese and N. Sternberg (1982). "P1 SITE-SPECIFIC RECOMBINATION - NUCLEOTIDE-SEQUENCE OF THE RECOMBINING SITES." Proceedings of the National Academy of Sciences of the United States of America-Biological Sciences **79**(11): 3398-3402.

Hougen, K., J. M. Aronsen, M. K. Stokke, U. Enger, S. Nygard, K. B. Andersson, G. Christensen, O. M. Sejersted and I. Sjaastad (2010). "Cre-loxP DNA recombination is possible with only minimal unspecific transcriptional changes and without cardiomyopathy in Tg(alpha MHC-MerCreMer) mice." American Journal of Physiology-Heart and Circulatory Physiology **299**(5): H1671-H1678.

Hoyt, E. C., J. E. Hepler, J. J. Van Wyk and P. K. Lund (1992). "Structural characterization of exon 6 of the rat IGF-I gene." DNA Cell Biol **11**(6): 433-41.

Hu, S. K., T. L. K. Low and A. L. Goldstein (1981). "MODULATION OF TERMINAL DEOXYNUCLEOTIDYL TRANSFERASE-ACTIVITY BY THYMOSIN." Molecular and Cellular Biochemistry **41**(DEC): 49-58.

Hua, Y., Y. Zhang and J. Ren (2012). "IGF-1 deficiency resists cardiac hypertrophy and myocardial contractile dysfunction: role of microRNA-1 and microRNA-133a." Journal of Cellular and Molecular Medicine **16**(1): 83-95.

Huang, H. C., C. H. Hu, M. C. Tang, W. S. Wang, P. M. Chen and Y. Su (2007). "Thymosin beta 4 triggers an epithelial-mesenchymal transition in colorectal carcinoma by upregulating integrin-linked kinase." Oncogene **26**(19): 2781-2790.

Huff, T., E. Ballweber, A. Humeny, T. Bonk, C. M. Becker, C. S. G. Muller, H. G. Mannherz and E. Hannappel (1999). "Thymosin beta(4) serves as a glutaminyl substrate of transglutaminase. Labeling with fluorescent dansylcadaverine does not abolish interaction with G-actin." Febs Letters **464**(1-2): 14-20.

Huff, T. and E. Hannappel (1997). "Oxidation and reduction of thymosin beta(4) and its influence on the interaction with G-actin studied by reverse-phase HPLC and post-column derivatization with fluorescamine." Analytica Chimica Acta **352**(1-3): 249-255.

Huff, T., C. S. Muller, A. M. Otto, R. Netzker and E. Hannappel (2001). "beta-Thymosins, small acidic peptides with multiple functions." Int J Biochem Cell Biol **33**(3): 205-20.

Huff, T., A. M. Otto, C. S. G. Muller, M. Meier and E. Hannappel (2002). "Thymosin beta(4) is released from human blood platelets and attached by factor XIIIa (transglutaminase) to fibrin and collagen." Faseb Journal **16**(7).

Huff, T., O. Rosorius, A. M. Otto, C. S. Muller, E. Ballweber, E. Hannappel and H. G. Mannherz (2004). "Nuclear localisation of the G-actin sequestering peptide thymosin beta4." J Cell Sci **117**(Pt 22): 5333-41.

Husson, C., F.-X. Cantrelle, P. Roblin, D. Didry, K. H. D. Le, J. Perez, E. Guittet, C. Van Heijenoort, L. Renault and M.-F. Carlier (2010). Multifunctionality of the beta-thymosin/WH2 module: G-actin sequestration, actin filament growth, nucleation, and severing. Thymosins in Health and Disease. **1194:** 44-52.

Huynh, K., J. R. McMullen, T. L. Julius, J. W. Tan, J. E. Love, N. Cemerlang, H. Kiriazis, X.-J. Du and R. H. Ritchie (2010). "Cardiac-Specific IGF-1 Receptor Transgenic Expression Protects Against Cardiac Fibrosis and Diastolic Dysfunction in a Mouse Model of Diabetic Cardiomyopathy." Diabetes **59**(6): 1512-1520.

Ikeda, S., A. He, S. W. Kong, J. Lu, R. Bejar, N. Bodyak, K.-H. Lee, Q. Ma, P. M. Kang, T. R. Golub and W. T. Pu (2009). "MicroRNA-1 Negatively Regulates Expression of the Hypertrophy-Associated Calmodulin and Mef2a Genes." Molecular and Cellular Biology **29**(8): 2193-2204.

Ince, H., M. Petzsch, H. D. Kleine, H. Eckard, T. Rehders, D. Burska, S. Kische, M. Freund and C. A. Nienaber (2005). "Prevention of left ventricular remodeling with granulocyte colony-stimulating factor after acute myocardial infarction: final 1-year results of the Front-Integrated Revascularization and Stem Cell Liberation in Evolving Acute Myocardial Infarction by Granulocyte Colony-Stimulating Factor (FIRSTLINE-AMI) Trial." Circulation **112**(9 Suppl): I73-80.

Inoue, K., A. Ikemura, Y. Tsuruta, K. Watanabe, K. Tsutsumiuchi, T. Hino and H. Oka (2011). "Quantification of N-acetyl-seryl-aspartyl-lysyl-proline in hemodialysis patients administered angiotensin-converting enzyme inhibitors by stable isotope dilution liquid chromatography-tandem mass spectrometry." Journal of Pharmaceutical and Biomedical Analysis **54**(4): 765-771.

Isotani, S., K. Hara, C. Tokunaga, H. Inoue, J. Avruch and K. Yonezawa (1999). "Immunopurified mammalian target of rapamycin phosphorylates and activates p70 S6 kinase alpha in vitro." J Biol Chem **274**(48): 34493-8.

Jacob, R., E. Barrett, G. Plewe, K. D. Fagin and R. S. Sherwin (1989). "ACUTE EFFECTS OF INSULIN-LIKE GROWTH FACTOR-I ON GLUCOSE AND AMINO-ACID METABOLISM IN THE AWAKE FASTED RAT - COMPARISON WITH INSULIN." Journal of Clinical Investigation **83**(5): 1717-1723.

Jansen, M., F. M. van Schaik, A. T. Ricker, B. Bullock, D. E. Woods, K. H. Gabbay, A. L. Nussbaum, J. S. Sussenbach and J. L. Van den Brande (1983). "Sequence of cDNA encoding human insulin-like growth factor I precursor." Nature **306**(5943): 609-11.

Jia, G., G. Cheng, D. M. Gangahar and D. K. Agrawal (2006). "Insulin-like growth factor-1 and TNF-alpha regulate autophagy through c-jun N-terminal kinase and Akt pathways in human atherosclerotic vascular smooth cells." Immunology and Cell Biology **84**(5): 448-454.

Jo, J.-O., S.-R. Kim, M.-K. Bae, Y.-J. Kang, M. S. Ock, H. K. Kleinman and H.-J. Cha (2010). "Thymosin beta 4 induces the expression of vascular endothelial growth factor (VEGF) in a hypoxia-inducible factor (HIF)-1 alpha-dependent manner." Biochimica Et Biophysica Acta-Molecular Cell Research **1803**(11): 1244-1251.

Johnson, W. B., S. Katugampola, S. Able, C. Napier and S. E. Harding (2012). "Profiling of cAMP and cGMP phosphodiesterases in isolated ventricular cardiomyocytes from human hearts: Comparison with rat and guinea pig." Life Sciences **90**(9-10): 328-336.

Jopling, C., G. Sune, C. Morera and J. C. Izpisua Belmonte (2012). "p38 alpha MAPK regulates myocardial regeneration in zebrafish." Cell Cycle **11**(6): 1195-1201.

Kabeya, Y., N. Mizushima, T. Ueno, A. Yamamoto, T. Kirisako, T. Noda, E. Kominami, Y. Ohsumi and T. Yoshimori (2000). "LC3, a mammalian homologue of yeast Apg8p, is localized in autophagosome membranes after processing." EMBO J **19**(21): 5720-8.

Kalka, C., H. Masuda, T. Takahashi, R. Gordon, O. Tepper, E. Gravereaux, A. Pieczek, H. Iwaguro, S. I. Hayashi, J. M. Isner and T. Asahara (2000). "Vascular endothelial growth factor(165) gene transfer augments circulating endothelial progenitor cells in human subjects." Circulation Research **86**(12): 1198-1202.

Kang, Y.-J., J.-O. Jo, M.-K. Cho, H.-S. Yu, M. S. Ock and H.-J. Cha (2011). "Trichinella spiralis infection induces angiogenic factor thymosin beta 4 expression." Veterinary Parasitology **181**(2-4): 222-228.

Kao, S.-Y. (2009). "Rescue of alpha-synuclein cytotoxicity by insulin-like growth factors." Biochemical and Biophysical Research Communications **385**(3): 434-438.

Kapuscinski, J. (1995). "DAPI - A DNA-SPECIFIC FLUORESCENT-PROBE." Biotechnic & Histochemistry **70**(5): 220-233.

Karey, K. P. and D. A. Sirbasku (1989). "HUMAN PLATELET-DERIVED MITOGENS .2. SUBCELLULAR-LOCALIZATION OF INSULINLIKE GROWTH FACTOR-I TO THE ALPHA-GRANULE AND RELEASE IN RESPONSE TO THROMBIN." Blood **74**(3): 1093-1100.

Kato, H., T. N. Faria, B. Stannard, C. T. Roberts, Jr. and D. LeRoith (1994). "Essential role of tyrosine residues 1131, 1135, and 1136 of the insulin-like growth factor-I (IGF-I) receptor in IGF-I action." Mol Endocrinol **8**(1): 40-50.

Katz, M. L., S. Khan, T. Awano, S. A. Shahid, A. N. Siakotos and G. S. Johnson (2005). "A mutation in the CLN8 gene in English Setter dogs with neuronal ceroid-lipofuscinosis." Biochemical and Biophysical Research Communications **327**(2): 541-547.

Kaur, H., R. Heeney, R. Carriveau, G. Sosne and B. Mutus (2010). "Whole blood, flow-chamber studies in real-time indicate a biphasic role for thymosin beta-4 in platelet adhesion." Biochimica Et Biophysica Acta-General Subjects **1800**(12): 1256-1261.

Kay, G. W., M. M. Verbeek, J. M. Furlong, M. A. A. P. Willemsen and D. N. Palmer (2009). "Neuropeptide changes and neuroactive amino acids in CSF from humans and sheep with neuronal ceroid lipofuscinoses (NCLs, Batten disease)." Neurochemistry International **55**(8): 783-788.

Kiermayer, C., M. Conrad, M. Schneider, J. Schmidt and M. Brielmeier (2007). "Optimization of spatiotemporal gene inactivation in mouse heart by oral application of tamoxifen citrate." Genesis **45**(1): 11-16.

Kim, A., M. Son, K. Il Kim, Y. Yang, E. Y. Song, H. G. Lee and J.-S. Lim (2009). "Elevation of intracellular cyclic AMP inhibits NF-kappa B-mediated thymosin beta 4 expression in melanoma cells." Experimental Cell Research **315**(19): 3325-3335.

Kim, N. S., Y.-J. Kang, J.-O. Jo, H. Y. Kim, Y. R. Oh, Y.-O. Kim, M. H. Jung, M. S. Ock and H.-J. Cha (2011). "Elevated Expression of Thymosin beta 4, Vascular Endothelial Growth Factor (VEGF), and Hypoxia Inducible Factor (HIF)-1 alpha in Early-Stage Cervical Cancers." Pathology & Oncology Research **17**(3): 493-502.

Kim, V. N. (2005). "Small RNAs: Classification, biogenesis, and function." Molecules and Cells **19**(1): 1-15.

Klein, J. J., A. L. Goldstein and A. White (1965). "Enhancement of in Vivo Incorporation of Labeled Precursors into DNA and Total Protein of Mouse Lymph Nodes after Administration of Thymic Extracts." Proc Natl Acad Sci U S A **53**: 812-7.

Klionsky, D. J. and S. D. Emr (2000). "Cell biology - Autophagy as a regulated pathway of cellular degradation." Science **290**(5497): 1717-1721.

Knecht, E., C. Aguado, S. Sarkar, V. I. Korolchuk, O. Criado-Garcia, S. Vernia, P. Boya, P. Sanz, S. Rodriguez de Cordoba and D. C. Rubinsztein (2010). "Impaired autophagy in Lafora disease." Autophagy **6**(7): 991-993.

Kobayashi, T. and P. Cohen (1999). "Activation of serum- and glucocorticoid-regulated protein kinase by agonists that activate phosphatidylinositide 3-kinase is mediated by 3-phosphoinositide-dependent protein kinase-1 (PDK1) and PDK2." Biochem J **339 (Pt 2)**: 319-28.

Kocanova, S., M. Mazaheri, S. Caze-Subra and K. Bystricky (2010). "Ligands specify estrogen receptor alpha nuclear localization and degradation." Bmc Cell Biology **11**.

Koerner, C., T. Guan, L. Gerace and G. Cingolani (2003). "Synergy of silent and hot spot mutations in importin beta reveals a dynamic mechanism for recognition of a nuclear localization signal." Journal of Biological Chemistry **278**(18): 16216-16221.

Koitabashi, N., D. Bedja, A. L. Zaiman, Y. M. Pinto, M. Zhang, K. L. Gabrielson, E. Takimoto and D. A. Kass (2009). "Avoidance of Transient Cardiomyopathy in Cardiomyocyte-Targeted Tamoxifen-Induced MerCreMer Gene Deletion Models." Circulation Research **105**(1): 12-U38.

Konhilas, J. P. and L. A. Leinwand (2007). "The effects of biological sex and diet on the development of heart failure." Circulation **116**(23): 2747-2759.

Koscianska, E., J. Starega-Roslan, L. J. Sznajder, M. Olejniczak, P. Galka-Marciniak and W. J. Krzyzosiak (2011). "Northern blotting analysis of microRNAs, their precursors and RNA interference triggers." Bmc Molecular Biology **12**.

Kostin, S., L. Pool, A. Elsasser, S. Hein, H. C. A. Drexler, E. Arnon, Y. Hayakawa, R. Zimmermann, E. Bauer, W. P. Klovekorn and J. Schaper (2003). "Myocytes die by multiple mechanisms in failing human hearts." Circulation Research **92**(7): 715-724.

Koutrafouri, V., L. Leondiadis, N. Ferderigos, K. Avgoustakis, E. Livaniou, G. P. Evangelatos and D. S. Ithakissios (2003). "Synthesis and angiogenetic activity in the chick chorioallantoic membrane model of thymosin beta-15." Peptides **24**(1): 107-115.

Kraehenbuehl, T. P., L. S. Ferreira, A. M. Hayward, M. Nahrendorf, A. J. van der Vlies, E. Vasile, R. Weissleder, R. Langer and J. A. Hubbell (2011). "Human embryonic stem cell-derived microvascular grafts for cardiac tissue preservation after myocardial infarction." Biomaterials **32**(4): 1102-1109.

Kruger, R., W. Kuhn, T. Muller, D. Woitalla, M. Graeber, S. Kosel, H. Przuntek, J. T. Epplen, L. Schols and O. Riess (1998). "Ala30Pro mutation in the gene encoding alpha-synuclein in Parkinson's disease." Nature Genetics **18**(2): 106-108.

Kuhn, B., F. del Monte, R. J. Hajjar, Y.-S. Chang, D. Lebeche, S. Arab and M. T. Keating (2007). "Periostin induces proliferation of differentiated cardiomyocytes and promotes cardiac repair." Nature Medicine **13**(8): 962-969.

Kumar, S. and S. Gupta (2011). "Thymosin beta 4 prevents oxidative stress by targeting antioxidant and anti-apoptotic genes in cardiac fibroblasts." Plos One **6**(10): e26912.

Kupatt, C., J. Horstkotte, G. A. Vlastos, A. Pfosser, C. Lebherz, M. Semisch, M. Thalgott, K. Buttner, C. Browarzyk, J. Mages, R. Hoffmann, A. Deten, M. Lamparter, F. Muller, H. Beck, H. Buning, P. Boekstegers and A. K. Hatzopoulos (2005). "Embryonic endothelial progenitor cells expressing a broad range of proangiogenic and remodeling factors enhance vascularization and tissue recovery in acute and chronic ischemia." FASEB J **19**(11): 1576-8.

Kutyavin, I. V., E. A. Lukhtanov, H. B. Gamper and R. B. Meyer (1997). "Oligonucleotides with conjugated dihydropyrroloindole tripeptides: base composition and backbone effects on hybridization." Nucleic Acids Research **25**(18): 3718-3723.

Lagerqvist, B., S. K. James, U. Stenestrand, J. Lindback, T. Nilsson and L. Wallentin (2007). "Long-term outcomes with drug-eluting stents versus bare-metal stents in Sweden." N Engl J Med **356**(10): 1009-19.

Lai, N. C., T. Tang, M. H. Gao, M. Saito, A. Miyanohara and H. K. Hammond (2012). "Improved Function of the Failing Rat Heart by Regulated Expression of Insulin-Like Growth Factor I via Intramuscular Gene Transfer." Human Gene Therapy **23**(3): 255-261.

Lang, F. and P. Cohen (2001). "Regulation and physiological roles of serum- and glucocorticoid-induced protein kinase isoforms." Sci STKE **2001**(108): re17.

Lauffenburger, D. A. and A. F. Horwitz (1996). "Cell migration: a physically integrated molecular process." Cell **84**(3): 359-69.

Lawson, D. M., A. Treffry, P. J. Artymiuk, P. M. Harrison, S. J. Yewdall, A. Luzzago, G. Cesareni, S. Levi and P. Arosio (1989). "IDENTIFICATION OF THE FERROXIDASE CENTER IN FERRITIN." Febs Letters **254**(1-2): 207-210.

Lee, H.-r., S. Y. Yoon, S. B. Song, Y. Park, T. S. Kim, S. Kim, D. Y. Hur, H. K. Song, H. Park and D. Cho (2011). "Interleukin-18-mediated interferon-gamma secretion is regulated by thymosin beta 4 in human NK cells." Immunobiology **216**(10): 1155-1162.

Lee, L. and P. D. Sadowski (2003). "Sequence of the loxP site determines the order of strand exchange by the Cre recombinase." Journal of Molecular Biology **326**(2): 397-412.

Lenfant, M., K. Itoh, H. Sakoda, D. Sotty, N. A. Sasaki, J. Wdzieczakbakala and K. J. Mori (1989). "ENHANCEMENT OF THE ADHERENCE OF HEMATOPOIETIC STEM-CELLS TO MOUSE BONE MARROW-DERIVED STROMAL CELL-LINE MS-1-T BY A TETRAPEPTIDE ACETYL-N-SER-ASP-LYS-PRO." Experimental Hematology **17**(8): 898-902.

Lepilina, A., A. N. Coon, K. Kikuchi, J. E. Holdway, R. W. Roberts, C. G. Burns and K. D. Poss (2006). "A dynamic epicardial injury response supports progenitor cell activity during zebrafish heart regeneration." Cell **127**(3): 607-619.

Lerner, T. J., R. M. N. Boustany, J. W. Anderson, K. L. Darigo, K. Schlumpf, A. J. Buckler, J. F. Gusella, J. L. Haines, G. Kremmidiotis, I. L. Lensink, G. R. Sutherland, D. F. Callen, P. E. M. Taschner, N. Devos, G. J. B. Vanommen, M. H. Breuning, N. A. Doggett, L. J. Meincke, Z. Y. Liu, L. A. Goodwin, J. G. Tesmer, H. M. Mitchison, A. M. Orawe, P. B. Munroe, I. E. Jarvela, R. M. Gardiner and S. E. Mole (1995). "ISOLATION OF A NOVEL GENE UNDERLYING BATTEN-DISEASE, CLN3." Cell **82**(6): 949-957.

Levine, B., J. Kalman, L. Mayer, H. M. Fillit and M. Packer (1990). "ELEVATED CIRCULATING LEVELS OF TUMOR-NECROSIS-FACTOR IN SEVERE CHRONIC HEART-FAILURE." New England Journal of Medicine **323**(4): 236-241.

Levine, B. and G. Kroemer (2008). "Autophagy in the pathogenesis of disease." Cell **132**(1): 27-42.

Lexow, J., P. Sarathchandra; M. P. Santini, T. Poggioli and N. Rosenthal (2012). “Cardiac fibrosis in mice expressing an inducible myocardial-specific Cre driver.” DMM submitted.

Li, Q., B. S. Li, X. W. Wang, A. Leri, K. P. Jana, Y. Liu, J. Kajstura, R. Baserga and P. Anversa (1997). "Overexpression of insulin-like growth factor-1 in mice protects from myocyte death after infarction, attenuating ventricular dilation, wall stress, and cardiac hypertrophy." Journal of Clinical Investigation **100**(8): 1991-1999.

Li, X., A. Zimmerman, N. G. Copeland, D. J. Gilbert, N. A. Jenkins and H. L. Yin (1996). "The mouse thymosin beta 4 gene: structure, promoter identification, and chromosome localization." Genomics **32**(3): 388-94.

Liang, X. H., S. Jackson, M. Seaman, K. Brown, B. Kempkes, H. Hibshoosh and B. Levine (1999). "Induction of autophagy and inhibition of tumorigenesis by beclin 1." Nature **402**(6762): 672-676.

Liao, J. K. (2002). "Shedding growth factors in cardiac hypertrophy." Nat Med **8**(1): 20-21.

Lien, C.-L., M. Schebesta, S. Makino, G. J. Weber and M. T. Keating (2006). "Gene expression analysis of zebrafish heart regeneration." Plos Biology **4**(8): 1386-1396.

Lin, S., H. Yokoyama, V. E. Rac and S. C. Brooks (2012). "Novel biomarkers in diagnosing cardiac ischemia in the emergency department: A systematic review." Resuscitation **83**(6): 684-691.

Liu, J. L., A. Grinberg, H. Westphal, B. Sauer, D. Accili, M. Karas and D. LeRoith (1998). "Insulin-like growth factor-I affects perinatal lethality and postnatal development in a gene dosage-dependent manner: Manipulation using the Cre/loxP system in transgenic mice." Molecular Endocrinology **12**(9): 1452-1462.

Liu, J. M., F. Lawrence, M. Kovacevic, J. Bignon, E. Papadimitriou, J. Y. Lallemand, P. Katsoris, P. Potier, Y. Fromes and J. Wdzieczak-Bakala (2003). "The tetrapeptide AcSDKP, an inhibitor of primitive hematopoietic cell proliferation, induces angiogenesis in vitro and in vivo." Blood **101**(8): 3014-20.

Liu, Y.-H., M. D'Ambrosio, T.-d. Liao, H. Peng, N.-E. Rhaleb, U. Sharma, S. Andre, H.-J. Gabius and O. A. Carretero (2009). "N-acetyl-seryl-aspartyl-lysyl-proline prevents cardiac remodeling and dysfunction induced by galectin-3, a mammalian adhesion/growth-regulatory lectin." American Journal of Physiology-Heart and Circulatory Physiology **296**(2): H404-H412.

Lloyd, J. (2010). "Heart Disease and Stroke Statistics-2010 Update: A Report From the American Heart Association (vol 121, pg e46, 2010)." Circulation **124**(16): E425-E425.

Loonstra, A., M. Vooijs, H. B. Beverloo, B. Al Allak, E. van Drunen, R. Kanaar, A. Berns and J. Jonkers (2001). "Growth inhibition and DNA damage induced by Cre recombinase in mammalian cells." Proceedings of the National Academy of Sciences of the United States of America **98**(16): 9209-9214.

Low, T. L. and A. L. Goldstein (1982). "Chemical characterization of thymosin beta 4." J Biol Chem **257**(2): 1000-6.

Low, T. L. K. and A. L. Goldstein (1984). "THYMOSINS - STRUCTURE, FUNCTION AND THERAPEUTIC APPLICATIONS." Thymus **6**(1-2): 27-42.

Low, T. L. K., S. K. Hu and A. L. Goldstein (1981). "COMPLETE AMINO-ACID-SEQUENCE OF BOVINE THYMOSIN-BETA-4 - A THYMIC HORMONE THAT INDUCES TERMINAL DEOXYNUCLEOTIDYL TRANSFERASE-ACTIVITY IN THYMOCYTE POPULATIONS." Proceedings of the National Academy of Sciences of the United States of America-Biological Sciences **78**(2): 1162-1166.

Lowry, O. H., N. J. Rosebrough, A. L. Farr and R. J. Randall (1951). "Protein measurement with the Folin phenol reagent." The Journal of biological chemistry **193**(1): 265-75.

Luzio, J. P., P. R. Pryor and N. A. Bright (2007). "Lysosomes: fusion and function." Nature Reviews Molecular Cell Biology **8**(8): 622-632.

Ma, Q.-l., T.-l. Yang, J.-y. Yin, Z.-y. Peng, M. Yu, Z.-q. Liu and F.-p. Chen (2009). "Role of insulin-like growth factor-1 (IGF-1) in regulating cell cycle progression." Biochemical and Biophysical Research Communications **389**(1): 150-155.

Maiuri, M. C., G. Le Toumelin, A. Criollo, J.-C. Rain, F. Gautier, P. Juin, E. Tasdemir, G. Pierron, K. Troulinaki, N. Tavernarakis, J. A. Hickman, O. Geneste and G. Kroemer (2007). "Functional and physical interaction between Bcl-X-L and a BH3-like domain in Beclin-1." Embo Journal **26**(10): 2527-2539.

Makkar, R. R., R. R. Smith, K. Cheng, K. Malliaras, L. E. J. Thomson, D. Berman, L. S. C. Czer, L. Marban, A. Mendizabal, P. V. Johnston, S. D. Russell, K. H. Schuleri, A. C. Lardo, G. Gerstenblith and E. Marban (2012). "Intracoronary cardiosphere-derived cells for heart regeneration after myocardial infarction (CADUCEUS): a prospective, randomised phase 1 trial." Lancet **379**(9819): 895-904.

Makogonenko, E., A. L. Goldstein, P. D. Bishop and L. Medved (2004). "Factor XIIIa incorporates thymosin beta(4) preferentially into the fibrin(ogen) alpha C-domains." Biochemistry **43**(33): 10748-10756.

Malinda, K. M., A. L. Goldstein and H. K. Kleinman (1997). "Thymosin beta(4) stimulates directional migration of human umbilical vein endothelial cells." Faseb Journal **11**(6): 474-481.

Malinda, K. M., G. S. Sidhu, H. Mani, K. Banaudha, R. K. Maheshwari, A. L. Goldstein and H. K. Kleinman (1999). "Thymosin beta4 accelerates wound healing." J Invest Dermatol **113**(3): 364-8.

Mannherz, H. G. and E. Hannappel (2009). "The beta-Thymosins: Intracellular and Extracellular Activities of a Versatile Actin Binding Protein Family." Cell Motility and the Cytoskeleton **66**(10): 839-851.

Marongiu, M. F., D. Poddie, S. Porcu, M. F. Manchinu, M. P. Castelli, V. Sogos, V. Bini, R. Frau, E. Caredda, M. Collu and M. S. Ristaldi (2012). "Reversible Disruption of Pre-Pulse Inhibition in Hypomorphic-Inducible and Reversible CB1(-/-) Mice." Plos One **7**(4).

Martin, S. E. and N. J. Caplen (2007). Applications of RNA interference in mammalian systems. Annual Review of Genomics and Human Genetics. **8:** 81-108.

Martins, P. A. d. C., M. Bourajjaj, M. Gladka, M. Kortland, R. J. van Oort, Y. M. Pinto, J. D. Molkentin and L. J. De Windt (2008). "Conditional Dicer gene deletion in the postnatal myocardium provokes spontaneous cardiac remodeling." Circulation **118**(15): 1567-1576.

Matranga, C., Y. Tomari, C. Shin, D. P. Bartel and P. D. Zamore (2005). "Passenger-strand cleavage facilitates assembly of siRNA into Ago2-containing RNAi enzyme complexes." Cell **123**(4): 607-620.

Matsui, T., L. Li, F. del Monte, Y. Fukui, T. F. Franke, R. J. Hajjar and A. Rosenzweig (1999). "Adenoviral gene transfer of activated phosphatidylinositol 3'-kinase and Akt inhibits apoptosis of hypoxic cardiomyocytes in vitro." Circulation **100**(23): 2373-9.

Maures, T., S. J. Chan, B. Xu, H. Sun, J. Ding and C. M. Duan (2002). "Structural, biochemical, and expression analysis of two distinct insulin-like growth factor I receptors and their ligands in zebrafish." Endocrinology **143**(5): 1858-1871.

McMullen, J. R. and G. L. Jennings (2007). "Differences between pathological and physiological cardiac hypertrophy: novel therapeutic strategies to treat heart failure." Clin Exp Pharmacol Physiol **34**(4): 255-62.

Meyer, G. P., K. C. Wollert, J. Lotz, J. Steffens, P. Lippolt, S. Fichtner, H. Hecker, A. Schaefer, L. Arseniev, B. Hertenstein, A. Ganser and H. Drexler (2006). "Intracoronary bone marrow cell transfer after myocardial infarction - Eighteen months' follow-up data from the randomized, controlled BOOST (BOne marrOw transfer to enhance ST-elevation infarct regeneration) trial." Circulation **113**(10): 1287-1294.

Michael, L. H., M. L. Entman, C. J. Hartley, K. A. Youker, J. Zhu, S. R. Hall, H. K. Hawkins, K. Berens and C. M. Ballantyne (1995). "Myocardial ischemia and reperfusion: A murine model." American Journal of Physiology-Heart and Circulatory Physiology **269**(6): H2147-H2154.

Minamisawa, S., M. Hoshijima, G. Chu, C. A. Ward, K. Frank, Y. Gu, M. E. Martone, Y. Wang, J. Ross, Jr., E. G. Kranias, W. R. Giles and K. R. Chien (1999). "Chronic phospholamban-sarcoplasmic reticulum calcium ATPase interaction is the critical calcium cycling defect in dilated cardiomyopathy." Cell **99**(3): 313-22.

Mizuguchi, H. and T. Hayakawa (2002). "The tet-off system is more effective than the tet-on system for regulating transgene expression in a single adenovirus vector." Journal of Gene Medicine **4**(3): 240-247.

Mizushima, N. (2004). "Methods for monitoring autophagy." International Journal of Biochemistry & Cell Biology **36**(12): 2491-2502.

Mizushima, N., T. Yoshimori and Y. Ohsumi (2003). "Role of the Apg12 conjugation system in mammalian autophagy." International Journal of Biochemistry & Cell Biology **35**(5): 553-561.

Morice, M., P. W. Serruys, J. E. Sousa, J. Fajadet, E. B. Hayashi, M. Perin, A. Colombo, G. Schuler, P. Barragan, G. Guagliumi, F. Molnar and R. Falotico (2002). "A randomized comparison of a sirolimus-eluting stent with a standard stent for coronary revascularization." New England Journal of Medicine **346**(23): 1773-1780.

Morris, D. C., M. Chopp, L. Zhang, M. Lu and Z. G. Zhang (2010). "THYMOSIN beta 4 IMPROVES FUNCTIONAL NEUROLOGICAL OUTCOME IN A RAT MODEL OF EMBOLIC STROKE." Neuroscience **169**(2): 674-682.

Muller, J., G. Wallukat, Y. G. Weng, M. Dandel, S. Spiegelsberger, S. Semrau, K. Brandes, V. Theodoridis, M. Loebe, R. Meyer and R. Hetzer (1997). "Weaning from mechanical cardiac support in patients with idiopathic dilated cardiomyopathy." Circulation **96**(2): 542-549.

Musaro, A., C. Giacinti, G. Borsellino, G. Dobrowolny, L. Pelosi, L. Cairns, S. Ottolenghi, G. Cossu, G. Bernardi, L. Battistini, M. Molinaro and N. Rosenthal (2004). "Stem cell-mediated muscle regeneration is enhanced by local isoform of insulin-like growth factor 1." Proc Natl Acad Sci U S A **101**(5): 1206-10.

Musaro, A., K. McCullagh, A. Paul, L. Houghton, G. Dobrowolny, M. Molinaro, E. R. Barton, H. L. Sweeney and N. Rosenthal (2001). "Localized Igf-1 transgene expression sustains hypertrophy and regeneration in senescent skeletal muscle." Nat Genet **27**(2): 195-200.

Musaro, A. and N. Rosenthal (2002). "The Role of local Insulin-like Growth Factor-1 Isoforms in the Pathophysiology of Skeletal Muscle." Current Genomics **3**: 149-162.

Myers, M. G., Jr., X. J. Sun and M. F. White (1994). "The IRS-1 signaling system." Trends Biochem Sci **19**(7): 289-93.

Myohanen, T. T., J. Tenorio-Laranga, B. Jokinen, R. Vazquez-Sanchez, M. J. Moreno-Baylach, J. A. Garcia-Horsman and P. T. Mannisto (2010). "Prolyl oligopeptidase induces angiogenesis both in vitro and in vivo in a novel regulatory manner." British Journal of Pharmacology **163**(8): 1666-1678.

Nakai, A., O. Yamaguchi, T. Takeda, Y. Higuchi, S. Hikoso, M. Taniike, S. Omiya, I. Mizote, Y. Matsumura, M. Asahi, K. Nishida, M. Hori, N. Mizushima and K. Otsu (2007). "The role of autophagy in cardiomyocytes in the basal state and in response to hemodynamic stress." Nature Medicine **13**(5): 619-624.

Nakano, M. and S. Gotoh (1992). "ACCUMULATION OF CARDIAC LIPOFUSCIN DEPENDS ON METABOLIC-RATE OF MAMMALS." Journals of Gerontology **47**(4): B126-B129.

Ng, W. A., I. L. Grupp, A. Subramaniam and J. Robbins (1991). "CARDIAC MYOSIN HEAVY-CHAIN MESSENGER-RNA EXPRESSION AND MYOCARDIAL-FUNCTION IN THE MOUSE HEART." Circulation Research **68**(6): 1742-1750.

Noda, N. N., K. Satoo, Y. Fujioka, H. Kumeta, K. Ogura, H. Nakatogawa, Y. Ohsumi and F. Inagaki (2011). "Structural Basis of Atg8 Activation by a Homodimeric E1, Atg7." Molecular Cell **44**(3): 462-475.

Noh, H.-L., K. Okajima, J. D. Molkentin, S. Homma and I. J. Goldberg (2006). "Acute lipoprotein lipase deletion in adult mice leads to dyslipidemia and cardiac dysfunction." American Journal of Physiology-Endocrinology and Metabolism **291**(4): E755-E760.

Novoyatleva, T., F. Diehl, M. J. van Amerongen, C. Patra, F. Ferrazzi, R. Bellazzi and F. B. Engel (2009). "TWEAK is a positive regulator of cardiomyocyte proliferation." Cardiovasc Res **85**(4): 681-90.

Ohki, S., T. Kaneko, Y. Satoh, H. Inaba, N. Kaki, T. Yamagishi and Y. Morishita (2002). "[Coronary artery bypass grafting in octogenarian]." Kyobu geka. The Japanese journal of thoracic surgery **55**(10): 829.

Orlic, D., J. Kajstura, S. Chimenti, I. Jakoniuk, S. M. Anderson, B. Li, J. Pickel, R. McKay, B. Nadal-Ginard, D. M. Bodine, A. Leri and P. Anversa (2001). "Bone marrow cells regenerate infarcted myocardium." Nature **410**(6829): 701-5.

Padin-Iruegas, M. E., Y. Misao, M. E. Davis, V. F. M. Segers, G. Esposito, T. Tokunou, K. Urbanek, T. Hosoda, M. Rota, P. Anversa, A. Leri, R. T. Lee and J. Kajstura (2009). "Cardiac Progenitor Cells and Biotinylated Insulin-Like Growth Factor-1 Nanofibers Improve Endogenous and Exogenous Myocardial Regeneration After Infarction." Circulation **120**(10): 876-887.

Pantaloni, D. and M. F. Carlier (1993). "How profilin promotes actin filament assembly in the presence of thymosin beta 4." Cell **75**(5): 1007-14.

Panteghini, M., W. Gerhardt, F. S. Apple, F. Dati, J. Ravkilde and A. H. Wu (2001). "Quality specifications for cardiac troponin assays." Clin Chem Lab Med **39**(2): 175-9.

Park, J., M. L. Leong, P. Buse, A. C. Maiyar, G. L. Firestone and B. A. Hemmings (1999). "Serum and glucocorticoid-inducible kinase (SGK) is a target of the PI 3-kinase-stimulated signaling pathway." EMBO J **18**(11): 3024-33.

Parker, J. S. and D. Barford (2006). "Argonaute: a scaffold for the function of short regulatory RNAs." Trends in Biochemical Sciences **31**(11): 622-630.

Parlakian, A., C. Charvet, B. Escoubet, M. Mericskay, J. D. Molkentin, G. Gary-Bobo, L. J. De Windt, M. A. Ludosky, D. Paulin, D. Daegelen, D. Tuil and Z. L. Li (2005). "Temporally controlled onset of dilated cardiomyopathy through disruption of the SRF gene in adult heart." Circulation **112**(19): 2930-2939.

Peng, H., O. A. Carretero, D. R. Brigstock, N. Oja-Tebbe and N. E. Rhaleb (2003). "Ac-SDKP reverses cardiac fibrosis in rats with renovascular hypertension." Hypertension **42**(6): 1164-70.

Peng, H., O. A. Carretero, E. L. Peterson and N.-E. Rhaleb (2010). "Ac-SDKP inhibits transforming growth factor-beta 1-induced differentiation of human cardiac fibroblasts into myofibroblasts." American Journal of Physiology-Heart and Circulatory Physiology **298**(5): H1357-H1364.

Peterson, G. L. (1979). "REVIEW OF THE FOLINE PHENOL PROTEIN QUANTITATION METHOD OF LOWRY, ROSEBROUGH, FARR AND RANDALL." Analytical Biochemistry **100**(2): 201-220.

Petiot, A., E. Ogier-Denis, E. F. C. Blommaart, A. J. Meijer and P. Codogno (2000). "Distinct classes of phosphatidylinositol 3 '-kinases are involved in signaling pathways that control macroautophagy in HT-29 cells." Journal of Biological Chemistry **275**(2): 992-998.

Pfeffer, M. A. and E. Braunwald (1990). "VENTRICULAR REMODELING AFTER MYOCARDIAL-INFARCTION - EXPERIMENTAL-OBSERVATIONS AND CLINICAL IMPLICATIONS." Circulation **81**(4): 1161-1172.

Phillips, S. N., J. W. Benedict, J. M. Weimer and D. A. Pearce (2005). "CLN3, the protein associated with batten disease: Structure, function and localization." Journal of Neuroscience Research **79**(5): 573-583.

Philp, D., M. Badamchian, B. Scheremeta, M. Nguyen, A. L. Goldstein and H. K. Kleinman (2003). "Thymosin beta 4 and a synthetic peptide containing its actin-binding domain promote dermal wound repair in db/db diabetic mice and in aged mice." Wound Repair Regen **11**(1): 19-24.

Philp, D., T. Huff, Y. S. Gho, E. Hannappel and H. K. Kleinman (2003). "The actin binding site on thymosin beta(4) promotes angiogenesis." Faseb Journal **17**(12): 2103-+.

Philp, D., M. Nguyen, B. Scheremeta, S. St-Surin, A. M. Villa, A. Orgel, H. K. Kleinman and M. Elkin (2004). "Thymosin beta4 increases hair growth by activation of hair follicle stem cells." FASEB J **18**(2): 385-7.

Philp, D., B. Scheremeta, K. Sibliss, M. Zhou, E. L. Fine, M. Nguyen, L. Wahl, M. P. Hoffman and H. K. Kleinman (2006). "Thymosin beta4 promotes matrix metalloproteinase expression during wound repair." J Cell Physiol **208**(1): 195-200.

Pi, Y., M. J. Goldenthal and J. Marin-Garcia (2007). "Mitochondrial involvement in IGF-1 induced protection of cardiomyocytes against hypoxia/reoxygenation injury." Molecular and Cellular Biochemistry **301**(1-2): 181-189.

Pitchford, S. C., R. C. Furze, C. P. Jones, A. M. Wengner and S. M. Rankin (2009). "Differential mobilization of subsets of progenitor cells from the bone marrow." Cell Stem Cell **4**(1): 62-72.

Podzuweit, T., D. J. Els and J. McCarthy (1981). "CYCLIC-AMP MEDIATED ARRHYTHMIAS INDUCED IN THE ISCHEMIC PIG-HEART." Basic Research in Cardiology **76**(4): 443-448.

Polgar, L. (2002). "The prolyl oligopeptidase family." Cell Mol Life Sci **59**(2): 349-62.

Pollard, T. D. and G. G. Borisy (2003). "Cellular motility driven by assembly and disassembly of actin filaments." Cell **112**(4): 453-65.

Popoli, P., R. Pepponi, A. Martire, M. Armida, A. Pezzola, M. Galluzzo, M. R. Domenici, R. L. Potenza, M. T. Tebano, C. Mollinari, D. Merlo and E. Garaci (2007). Neuroprotective effects of thymosin beta(4) in experimental models of excitotoxicity. Thymosins in Health and Disease: First International Symposium. **1112:** 219-224.

Porrello, E. R., A. I. Mahmoud, E. Simpson, J. A. Hill, J. A. Richardson, E. N. Olson and H. A. Sadek (2011). "Transient Regenerative Potential of the Neonatal Mouse Heart." Science **331**(6020): 1078-1080.

Powell, S. R., P. Wang, A. Divald, S. Teichberg, V. Haridas, T. W. McCloskey, K. J. A. Davies and H. Katzeff (2005). "Aggregates of oxidized proteins (lipofuscin) induce apoptosis through proteasome inhibition and dysregulation of proapoptotic proteins." Free Radical Biology and Medicine **38**(8): 1093-1101.

Pullen, N., P. B. Dennis, M. Andjelkovic, A. Dufner, S. C. Kozma, B. A. Hemmings and G. Thomas (1998). "Phosphorylation and activation of p70s6k by PDK1." Science **279**(5351): 707-10.

Qin, J. Y., L. Zhang, K. L. Clift, I. Hulur, A. P. Xiang, B.-Z. Ren and B. T. Lahn (2010). "Systematic Comparison of Constitutive Promoters and the Doxycycline-Inducible Promoter." Plos One **5**(5).

Qiu, P., M. Kurpakus-Wheater and G. Sosne (2007). "Matrix metalloproteinase activity is necessary for thymosin beta 4 promotion of epithelial cell migration." J Cell Physiol **212**(1): 165-73.

Qiu, P., M. K. Wheater, Y. Qiu and G. Sosne (2011). "Thymosin beta(4) inhibits TNF-alpha-induced NF-kappa B activation, IL-8 expression, and the sensitizing effects by its partners PINCH-1 and ILK." Faseb Journal **25**(6): 1815-1826.

Quinn, J. G., D. T. R. Coulson, S. Brockbank, N. Beyer, R. Ravid, J. Hellemans, G. B. Irvine and J. A. Johnston (2012). "alpha-Synuclein mRNA and soluble alpha-synuclein protein levels in post-mortem brain from patients with Parkinson's disease, dementia with Lewy bodies, and Alzheimer's disease." Brain Research **1459**: 71-80.

Ray, P., A. De, M. Patel and S. S. Gambhir (2008). "Monitoring caspase-3 activation with a multimodality Imaging sensor in living subjects." Clinical Cancer Research **14**(18): 5801-5809.

Raymond, C. S. and P. Soriano (2007). "High-Efficiency FLP and Phi C31 Site-Specific Recombination in Mammalian Cells." Plos One **2**(1).

Rhaleb, N. E., H. M. Peng, X. P. Yang, Y. H. Liu, D. Mehta, E. Ezan and O. A. Carretero (2001). "Long-term effect of N-acetyl-seryl-aspartyl-lysyl-proline on left ventricular collagen deposition in rats with 2-kidney, 1-clip hypertension." Circulation **103**(25): 3136-3141.

Richard, S., F. Leclercq, S. Lemaire, C. Piot and J. Nargeot (1998). "Ca2+ currents in compensated hypertrophy and heart failure." Cardiovascular Research **37**(2): 300-311.

Richeson, J. F., C. Paulshock and P. N. Yu (1982). "NON-HYDROSTATIC PULMONARY-EDEMA AFTER CORONARY-ARTERY LIGATION IN DOGS - PROTECTIVE EFFECT OF INDOMETHACIN." Circulation Research **50**(2): 301-309.

Riikonen, R., S. L. Vanhanen, J. Tyynela, P. Santavuori and U. Turpeinen (2000). "CSF insulin-like growth factor-1 in infantile neuronal ceroid lipofuscinosis." Neurology **54**(9): 1828-1832.

Rinderknecht, E. and R. E. Humbel (1976). "Amino-terminal sequences of two polypeptides from human serum with nonsuppressible insulin-like and cell-growth-promoting activities: evidence for structural homology with insulin B chain." Proc Natl Acad Sci U S A **73**(12): 4379-81.

Risau, W. and I. Flamme (1995). "Vasculogenesis." Annual Review of Cell and Developmental Biology **11**: 73-91.

Robinson, S. P., S. M. Langanfahey, D. A. Johnson and V. C. Jordan (1991). "METABOLITES, PHARMACODYNAMICS, AND PHARMACOKINETICS OF TAMOXIFEN IN RATS AND MICE COMPARED TO THE BREAST-CANCER PATIENT." Drug Metabolism and Disposition **19**(1): 36-43.

Ropolo, A., D. Grasso, R. Pardo, M. L. Sacchetti, C. Archange, A. Lo Re, M. Seux, J. Nowak, C. D. Gonzalez, J. L. Iovanna and M. I. Vaccaro (2007). "The pancreatitis-induced vacuole membrane protein 1 triggers autophagy in mammalian cells." Journal of Biological Chemistry **282**(51): 37124-37133.

Rosenblatt-Velin, N., S. Ogay, A. Felley, W. L. Stanford and T. Pedrazzini (2012). "Cardiac dysfunction and impaired compensatory response to pressure overload in mice deficient in stem cell antigen-1." Faseb Journal **26**(1): 229-239.

Roth, J., M. Bendayan and L. Orci (1978). "Ultrastructural localization of intracellular antigens by the use of protein A-gold complex." J Histochem Cytochem **26**(12): 1074-81.

Rother, K. I., Y. Imai, M. Caruso, F. Beguinot, P. Formisano and D. Accili (1998). "Evidence that IRS-2 phosphorylation is required for insulin action in hepatocytes." J Biol Chem **273**(28): 17491-7.

Rousseau, A., A. Michaud, M. T. Chauvet, M. Lenfant and P. Corvol (1995). "THE HEMOREGULATORY PEPTIDE N-ACETYL-SER-ASP-LYS-PRO IS A NATURAL AND SPECIFIC SUBSTRATE OF THE N-TERMINAL ACTIVE-SITE OF HUMAN ANGIOTENSIN-CONVERTING ENZYME." Journal of Biological Chemistry **270**(8): 3656-3661.

Ruan, H., J. Li, S. Ren, J. Gao, G. Li, R. Kim, H. Wu and Y. Wang (2009). "Inducible and cardiac specific PTEN inactivation protects ischemia/reperfusion injury." Journal of Molecular and Cellular Cardiology **46**(2): 193-200.

Ruff, D., D. Crockford, G. Girardi and Y. Zhang (2010). A randomized, placebo-controlled, single and multiple dose study of intravenous thymosin beta 4 in healthy volunteers. Thymosins in Health and Disease. **1194:** 223-229.

Ruidavets, J. B., G. Luc, E. Machez, A. L. Genoux, F. Kee, D. Arveiler, P. Morange, J. V. Woodside, P. Amouyel, A. Evans, P. Ducimetiere, A. Bingham, J. Ferrieres and B. Perret (2011). "Effects of insulin-like growth factor 1 in preventing acute coronary syndromes: The PRIME study." Atherosclerosis **218**(2): 464-469.

Ruvinov, E., J. Leor and S. Cohen (2011). "The promotion of myocardial repair by the sequential delivery of IGF-1 and HGF from an injectable alginate biomaterial in a model of acute myocardial infarction." Biomaterials **32**(2): 565-578.

Safer, D., M. Elzinga and V. T. Nachmias (1991). "Thymosin beta 4 and Fx, an actin-sequestering peptide, are indistinguishable." J Biol Chem **266**(7): 4029-32.

Safer, D., R. Golla and V. T. Nachmias (1990). "Isolation of a 5-kilodalton actin-sequestering peptide from human blood platelets." Proc Natl Acad Sci U S A **87**(7): 2536-40.

Salto-Tellez, M., S. Yung Lim, R. M. El-Oakley, T. P. Tang, A. L. ZA and S. K. Lim (2004). "Myocardial infarction in the C57BL/6J mouse: a quantifiable and highly reproducible experimental model." Cardiovasc Pathol **13**(2): 91-7.

Santini, M. P., L. Tsao, L. Monassier, C. Theodoropoulos, J. Carter, E. Lara-Pezzi, E. Slonimsky, E. Salimova, P. Delafontaine, Y. H. Song, M. Bergmann, C. Freund, K. Suzuki and N. Rosenthal (2007). "Enhancing repair of the mammalian heart." Circ Res **100**(12): 1732-40.

Sauer, B. and N. Henderson (1988). "SITE-SPECIFIC DNA RECOMBINATION IN MAMMALIAN-CELLS BY THE CRE RECOMBINASE OF BACTERIOPHAGE-P1." Proceedings of the National Academy of Sciences of the United States of America **85**(14): 5166-5170.

Sauer, B. and J. McDermott (2004). "DNA recombination with a heterospecific Cre homolog identified from comparison of the pac-c1 regions of P1-related phages." Nucleic Acids Research **32**(20): 6086-6095.

Savagner, P. (2001). "Leaving the neighborhood: molecular mechanisms involved during epithelial-mesenchymal transition." Bioessays **23**(10): 912-923.

Schlake, T. and J. Bode (1994). "USE OF MUTATED FLP RECOGNITION TARGET (FRT) SITES FOR THE EXCHANGE OF EXPRESSION CASSETTES AT DEFINED CHROMOSOMAL LOCI." Biochemistry **33**(43): 12746-12751.

Schober, M. E., X. Ke, B. Xing, B. P. Block, D. F. Requena, R. McKnight and R. H. Lane (2012). "Traumatic Brain Injury Increased IGF-1B mRNA and Altered IGF-1 Exon 5 and Promoter Region Epigenetic Characteristics in the Rat Pup Hippocampus." Journal of neurotrauma **29**(11): 2075-85.

Schroeder, A., O. Mueller, S. Stocker, R. Salowsky, M. Leiber, M. Gassmann, S. Lightfoot, W. Menzel, M. Granzow and T. Ragg (2006). "The RIN: an RNA integrity number for assigning integrity values to RNA measurements." Bmc Molecular Biology **7**.

Schuldt, A. J. T., M. R. Rosen, G. R. Gaudette and I. S. Cohen (2008). "Repairing damaged myocardium: evaluating cells used for cardiac regeneration." Current treatment options in cardiovascular medicine **10**(1): 59-72.

Seibler, J., B. Zevnik, B. Kuter-Luks, S. Andreas, H. Kern, T. Hennek, A. Rode, C. Heimann, N. Faust, G. Kauselmann, M. Schoor, R. Jaenisch, K. Rajewsky, R. Kuhn and F. Schwenk (2003). "Rapid generation of inducible mouse mutants." Nucleic Acids Research **31**(4).

Sekulic, A., C. C. Hudson, J. L. Homme, P. Yin, D. M. Otterness, L. M. Karnitz and R. T. Abraham (2000). "A direct linkage between the phosphoinositide 3-kinase-AKT signaling pathway and the mammalian target of rapamycin in mitogen-stimulated and transformed cells." Cancer Res **60**(13): 3504-13.

Semprini, S., T. J. Troup, N. Kotelevtseva, K. King, J. R. E. Davis, L. J. Mullins, K. E. Chapman, D. R. Dunbar and J. J. Mullins (2007). "Cryptic loxP sites in mammalian genomes: genome-wide distribution and relevance for the efficiency of BAC/PAC recombineering techniques." Nucleic Acids Research **35**(5): 1402-1410.

Shah, A. P., S. T. Youngquist, C. D. McClung, E. Tzvetkova, M. A. Hanif, J. P. Rosborough and J. T. Niemann (2011). "Markers of Progenitor Cell Recruitment and Differentiation Rise Early During Ischemia and Continue During Resuscitation in a Porcine Model of Acute Ischemia." Circulation **124**(21).

Shavali, S., H. M. Brown-Borg, M. Ebadi and J. Porter (2008). "Mitochondrial localization of alpha-synuclein protein in alpha-synuclein overexpressing cells." Neuroscience Letters **439**(2): 125-128.

Sherr, C. J. and J. M. Roberts (1995). "INHIBITORS OF MAMMALIAN G(1) CYCLIN-DEPENDENT KINASES." Genes & Development **9**(10): 1149-1163.

Shih, H., B. Lee, R. J. Lee and A. J. Boyle (2010). "The Aging Heart and Post-Infarction Left Ventricular Remodeling." Journal of the American College of Cardiology **57**(1): 9-17.

Shimatsu, A. and P. Rotwein (1987). "Sequence of two rat insulin-like growth factor I mRNAs differing within the 5' untranslated region." Nucleic Acids Res **15**(17): 7196.

Shintani, T., N. Mizushima, Y. Ogawa, A. Matsuura, T. Noda and Y. Ohsumi (1999). "Apg10p, a novel protein-conjugating enzyme essential for autophagy in yeast." Embo Journal **18**(19): 5234-5241.

Shioi, T., P. M. Kang, P. S. Douglas, J. Hampe, C. M. Yballe, J. Lawitts, L. C. Cantley and S. Izumo (2000). "The conserved phosphoinositide 3-kinase pathway determines heart size in mice." EMBO J **19**(11): 2537-48.

Sigwart, U., J. Puel, V. Mirkovitch, F. Joffre and L. Kappenberger (1987). "INTRAVASCULAR STENTS TO PREVENT OCCLUSION AND RESTENOSIS AFTER TRANS-LUMINAL ANGIOPLASTY." New England Journal of Medicine **316**(12): 701-706.

Simmons, J. G., J. J. Van Wyk, E. C. Hoyt and P. K. Lund (1993). "Multiple transcription start sites in the rat insulin-like growth factor-I gene give rise to IGF-I mRNAs that encode different IGF-I precursors and are processed differently in vitro." Growth Factors **9**(3): 205-21.

Singleton, A. B., M. Farrer, J. Johnson, A. Singleton, S. Hague, J. Kachergus, M. Hulihan, T. Peuralinna, A. Dutra, R. Nussbaum, S. Lincoln, A. Crawley, M. Hanson, D. Maraganore, C. Adler, M. R. Cookson, M. Muenter, M. Baptista, D. Miller, J. Blancato, J. Hardy and K. Gwinn-Hardy (2003). "alpha-synuclein locus triplication causes Parkinson's disease." Science **302**(5646): 841-841.

Skarnes, W. C., B. Rosen, A. P. West, M. Koutsourakis, W. Bushell, V. Iyer, A. O. Mujica, M. Thomas, J. Harrow, T. Cox, D. Jackson, J. Severin, P. Biggs, J. Fu, M. Nefedov, P. J. de Jong, A. F. Stewart and A. Bradley (2011). "A conditional knockout resource for the genome-wide study of mouse gene function." Nature **474**(7351): 337-U361.

Skop, V., M. Cahova, Z. Papackova, E. Palenickova, H. Dankova, M. Baranowski, P. Zabielski, J. Zdychova, J. Zidkova and L. Kazdova (2012). "Autophagy-Lysosomal Pathway Is Involved in Lipid Degradation in Rat Liver." Physiological Research **61**(3): 287-297.

Smart, N., S. Bollini, K. N. Dube, J. M. Vieira, B. Zhou, S. Davidson, D. Yellon, J. Riegler, A. N. Price, M. F. Lythgoe, W. T. Pu and P. R. Riley (2011). "De novo cardiomyocytes from within the activated adult heart after injury." Nature **474**(7353): 640-U117.

Smart, N., A. A. Hill, J. C. Cross and P. R. Riley (2002). "A differential screen for putative targets of the bHLH transcription factor Hand1 in cardiac morphogenesis." Mech Dev **119 Suppl 1**: S65-71.

Smart, N., C. A. Risebro, A. A. Melville, K. Moses, R. J. Schwartz, K. R. Chien and P. R. Riley (2007). "Thymosin beta4 induces adult epicardial progenitor mobilization and neovascularization." Nature **445**(7124): 177-82.

Smart, N., A. Rossdeutsch and P. R. Riley (2007). "Thymosin beta4 and angiogenesis: modes of action and therapeutic potential." Angiogenesis **10**(4): 229-41.

So, A., J. Hsieh, J.-Y. Li, J. Hadway, H.-F. Kong and T.-Y. Lee (2012). "Quantitative myocardial perfusion measurement using CT Perfusion: a validation study in a porcine model of reperfused acute myocardial infarction." International Journal of Cardiovascular Imaging **28**(5): 1237-1248.

Sobolewska, A., M. Gajewska, J. Zarzynska, B. Gajkowska and T. Motyl (2009). "IGF-I, EGF, and sex steroids regulate autophagy in bovine mammary epithelial cells via the mTOR pathway." European Journal of Cell Biology **88**(2): 117-130.

Sohal, D. S., M. Nghiem, M. A. Crackower, S. A. Witt, T. R. Kimball, K. M. Tymitz, J. M. Penninger and J. D. Molkentin (2001). "Temporally regulated and tissue-specific gene manipulations in the adult and embryonic heart using a tamoxifen-inducible Cre protein." Circ Res **89**(1): 20-5.

Sokolovic, M., A. Sokolovic, D. Wehkamp, E. V. L. van Themaat, D. R. de Waart, L. A. Gilhuijs-Pederson, Y. Nikolsky, A. H. C. van Kampen, T. B. M. Hakvoort and W. H. Lamers (2008). "The transcriptomic signature of fasting murine liver." Bmc Genomics **9**.

Song, J. J., S. K. Smith, G. J. Hannon and L. Joshua-Tor (2004). "Crystal structure of argonaute and its implications for RISC slicer activity." Science **305**(5689): 1434-1437.

Soonpaa, M. H. and L. J. Field (1998). "Survey of studies examining mammalian cardiomyocyte DNA synthesis." Circ Res **83**(1): 15-26.

Sopko, N., Y. Qin, A. Finan, A. Dadabayev, S. Chigurupati, J. Qin, M. S. Penn and S. Gupta (2011). "Significance of Thymosin beta 4 and Implication of PINCH-1-ILK-alpha-Parvin (PIP) Complex in Human Dilated Cardiomyopathy." Plos One **6**(5).

Sosne, G., C. C. Chan, K. Thai, M. Kennedy, E. A. Szliter, L. D. Hazlett and H. K. Kleinman (2001). "Thymosin beta 4 promotes corneal wound healing and modulates inflammatory mediators in vivo." Exp Eye Res **72**(5): 605-8.

Sosne, G., P. Qiu, P. L. Christopherson and M. K. Wheater (2007). "Thymosin beta 4 suppression of corneal NF kappa B: A potential anti-inflammatory pathway." Experimental Eye Research **84**(4): 663-669.

Sosne, G., E. A. Szliter, R. Barrett, K. A. Kernacki, H. Kleinman and L. D. Hazlett (2002). "Thymosin beta 4 promotes corneal wound healing and decreases inflammation in vivo following alkali injury." Experimental Eye Research **74**(2): 293-299.

Spillantini, M. G., M. L. Schmidt, V. M. Y. Lee, J. Q. Trojanowski, R. Jakes and M. Goedert (1997). "alpha-synuclein in Lewy bodies." Nature **388**(6645): 839-840.

Stephan, J. P., N. Melaine, E. Ezan, H. Hakovirta, S. Maddocks, J. Toppari, D. H. Garnier, J. Wdzieczak-Bakala and B. Jegou (2000). "Source, catabolism and role of the tetrapeptide N-Acetyl-Ser-Asp-Lys-Pro within the testis." Journal of Cell Science **113**(1): 113-121.

Sternberg, N. and D. Hamilton (1981). "BACTERIOPHAGE-P1 SITE-SPECIFIC RECOMBINATION .1. RECOMBINATION BETWEEN LOXP SITES." Journal of Molecular Biology **150**(4): 467-486.

Stewart, C. E. and P. Rotwein (1996). "Growth, differentiation, and survival: multiple physiological functions for insulin-like growth factors." Physiol Rev **76**(4): 1005-26.

Stokke, M. K., K. Hougen, I. Sjaastad, W. E. Louch, S. J. Briston, U. H. Enger, K. B. Andersson, G. Christensen, D. A. Eisner, O. M. Sejersted and A. W. Trafford (2010). "Reduced SERCA2 abundance decreases the propensity for Ca2+ wave development in ventricular myocytes." Cardiovascular Research **86**(1): 63-71.

Stoll, R., W. Voelter and T. A. Holak (1997). "Conformation of thymosin beta(9) in water/fluoroalcohol solution determined by NMR spectroscopy." Biopolymers **41**(6): 623-634.

Stone, G. W., B. T. McLaurin, D. A. Cox, M. E. Bertrand, A. M. Lincoff, J. W. Moses, H. D. White, S. J. Pocock, J. H. Ware, F. Feit, A. Colombo, P. E. Aylward, A. R. Cequier, H. Darius, W. Desmet, R. Ebrahimi, M. Hamon, L. H. Rasmussen, H. J. Rupprecht, J. Hoekstra, R. Mehran and E. M. Ohman (2006). "Bivalirudin for patients with acute coronary syndromes." N Engl J Med **355**(21): 2203-16.

Stoye, J. P. and J. M. Coffin (1987). "THE 4 CLASSES OF ENDOGENOUS MURINE LEUKEMIA-VIRUS - STRUCTURAL RELATIONSHIPS AND POTENTIAL FOR RECOMBINATION." Journal of Virology **61**(9): 2659-2669.

Su, A. I., T. Wiltshire, S. Batalov, H. Lapp, K. A. Ching, D. Block, J. Zhang, R. Soden, M. Hayakawa, G. Kreiman, M. P. Cooke, J. R. Walker and J. B. Hogenesch (2004). "A gene atlas of the mouse and human protein-encoding transcriptomes." Proceedings of the National Academy of Sciences of the United States of America **101**(16): 6062-6067.

Sugden, P. H. (1999). "Signaling in myocardial hypertrophy: life after calcineurin?" Circ Res **84**(6): 633-46.

Sun, F., V. Anantharam, C. Latchoumycandane, A. Kanthasamy and A. G. Kanthasamy (2005). "Dieldrin induces ubiquitin-proteasome dysfunction in alpha-synuclein overexpressing dopaminergic neuronal cells and enhances susceptibility to apoptotic cell death." Journal of Pharmacology and Experimental Therapeutics **315**(1): 69-79.

Sun, H., B. G. Kerfant, D. L. Zhao, M. G. Trivieri, G. Y. Oudit, J. M. Penninger and P. H. Backx (2006). "Insulin-like growth factor-1 and PTEN deletion enhance cardiac L-type Ca2+ currents via increased PI3K alpha/PKB signaling." Circulation Research **98**(11): 1390-1397.

Suzuki, Y., H. Itoh, F. Katagiri, F. Sato, K. Kawasaki, Y. Sato, H. Mimata and M. Takeyama (2012). "Establishment and clinical application of a highly sensitive enzyme immunoassay for determination of N-acetyl-seryl-aspartyl-lysyl-proline." Journal of Peptide Science **18**(4): 276-281.

Tai, D. J., C. C. Su, Y. L. Ma and E. H. Lee (2009). "SGK1 phosphorylation of IkappaB Kinase alpha and p300 Up-regulates NF-kappaB activity and increases N-Methyl-D-aspartate receptor NR2A and NR2B expression." J Biol Chem **284**(7): 4073-89.

Tanaka, S., T. Ito and J. R. Wands (1996). "Neoplastic transformation induced by insulin receptor substrate-1 overexpression requires an interaction with both Grb2 and Syp signaling molecules." J Biol Chem **271**(24): 14610-6.

Tang, Y. Q., M. R. Yeaman and M. E. Selsted (2002). "Antimicrobial peptides from human plateletst." Infection and Immunity **70**(12): 6524-6533.

Tannous, P., H. Zhu, J. L. Johnstone, J. M. Shelton, N. S. Rajasekaran, I. J. Benjamin, L. Nguyen, R. D. Gerard, B. Levine, B. A. Rothermel and J. A. Hill (2008). "Autophagy is an adaptive response in desmin-related cardiomyopathy." Proceedings of the National Academy of Sciences of the United States of America **105**(28): 9745-9750.

Terman, A. and U. T. Brunk (2004). "Lipofuscin." The International Journal of Biochemistry & Cell Biology **36**(8): 1400-1404.

Testa, M., M. Yeh, P. Lee, R. Fanelli, F. Loperfido, J. W. Berman and T. H. LeJemtel (1996). "Circulating levels of cytokines and their endogenous modulators in patients with mild to

severe congestive heart failure due to coronary artery disease or hypertension." J Am Coll Cardiol **28**(4): 964-71.

Thiele, H., R. W. Smalling and G. C. Schuler (2007). "Percutaneous left ventricular assist devices in acute myocardial infarction complicated by cardiogenic shock." Eur Heart J **28**(17): 2057-63.

Thum, T. and J. Borlak (2001). "Butanedione monoxime increases the viability and yield of adult cardiomyocytes in primary cultures." Cardiovascular toxicology **1**(1): 61-72.

Thygesen, K., J. S. Alpert and H. D. White (2007). "Universal definition of myocardial infarction." Eur Heart J **28**(20): 2525-38.

Tokura, Y., Y. Nakayama, S.-i. Fukada, N. Nara, H. Yamamoto, R. Matsuda and T. Hara (2011). "Muscle injury-induced thymosin beta 4 acts as a chemoattractant for myoblasts." Journal of Biochemistry **149**(1): 43-48.

Touvron, M., B. Escoubet, M. Mericskay, A. Angelini, L. Lamotte, M. P. Santini, N. Rosenthal, D. Daegelen, D. Tuil and J.-F. Decaux (2012). "Locally expressed IGF1 propeptide improves mouse heart function in induced dilated cardiomyopathy by blocking myocardial fibrosis and SRF-dependent CTGF induction." Disease Models & Mechanisms **5**(4): 481-491.

Trimmer, P. A., R. H. Swerdlow, J. K. Parks, P. Keeney, J. P. Bennett, S. W. Miller, R. E. Davis and W. D. Parker (2000). "Abnormal mitochondrial morphology in sporadic Parkinson's and Alzheimer's disease cybrid cell lines." Experimental Neurology **162**(1): 37-50.

Troncoso, R., J. Miguel Vicencio, V. Parra, A. Nemchenko, Y. Kawashima, A. del Campo, B. Toro, P. K. Battiprolu, P. Aranguiz, M. Chiong, S. Yakar, T. G. Gillette, J. A. Hill, E. D. Abel, D. LeRoith and S. Lavandero (2012). "Energy-preserving effects of IGF-1 antagonize starvation-induced cardiac autophagy." Cardiovascular Research **93**(2): 320-329.

Tsujimoto, Y. and S. Shimizu (2005). "Another way to die: autophagic programmed cell death." Cell Death and Differentiation **12**: 1528-1534.

Tu, J. V., J. Bowen, M. Chiu, D. T. Ko, P. C. Austin, Y. He, R. Hopkins, J. E. Tarride, G. Blackhouse, C. Lazzam, E. A. Cohen and R. Goeree (2007). "Effectiveness and safety of drug-eluting stents in Ontario." N Engl J Med **357**(14): 1393-402.

Tuschl, T., P. D. Zamore, R. Lehmann, D. P. Bartel and P. A. Sharp (1999). "Targeted mRNA degradation by double-stranded RNA in vitro." Genes & Development **13**(24): 3191-3197.

Tyas, L., V. A. Brophy, A. Pope, A. J. Rivett and J. M. Tavare (2000). "Rapid caspase-3 activation during apoptosis revealed using fluorescence-resonance energy transfer." Embo Reports **1**(3): 266-270.

Tzehoval, E., M. B. Sztein and A. L. Goldstein (1989). "THYMOSINS ALPHA-1 AND BETA-4 POTENTIATE THE ANTIGEN-PRESENTING CAPACITY OF MACROPHAGES." Immunopharmacology **18**(2): 107-113.

Ungvari, Z., T. Gautam, P. Koncz, J. C. Henthorn, J. T. Pinto, P. Ballabh, H. Yan, M. Mitschelen, J. Farley, W. E. Sonntag and A. Csiszar (2010). "Vasoprotective Effects of Life Span-Extending Peripubertal GH Replacement in Lewis Dwarf Rats." Journals of Gerontology Series a-Biological Sciences and Medical Sciences **65**(11): 1145-1156.

Uusi-Rauva, K., A. Kyttala, R. van der Kant, J. Vesa, K. Tanhuanpaa, J. Neefjes, V. M. Olkkonen and A. Jalanko (2012). "Neuronal ceroid lipofuscinosis protein CLN3 interacts with motor proteins and modifies location of late endosomal compartments." Cellular and Molecular Life Sciences **69**(12): 2075-2089.

Van Troys, M., D. Dewitte, M. Goethals, M. F. Carlier, J. Vandekerckhove and C. Ampe (1996). "The actin binding site of thymosin beta 4 mapped by mutational analysis." EMBO J **15**(2): 201-10.

Vartiainen, M. K., S. Guettler, B. Larijani and R. Treisman (2007). "Nuclear actin regulates dynamic subcellular localization and activity of the SRF cofactor MAL." Science **316**(5832): 1749-1752.

Vasan, R. S., L. M. Sullivan, R. B. D'Agostino, R. Roubenoff, T. Harris, D. B. Sawyer, D. Levy and P. W. F. Wilson (2003). "Serum insulin-like growth factor I and risk for heart failure in elderly individuals without a previous myocardial infarction: The Framingham Heart Study." Annals of Internal Medicine **139**(8): 642-648.

Vernon, A. E. and C. LaBonne (2004). "Tumor metastasis: A new twist on epithelial-mesenchymal transitions." Current Biology **14**(17): R719-R721.

Vinciguerra, M., M. P. Santini, W. C. Claycomb, A. G. Ladurner and N. Rosenthal (2010). "Local IGF-1 isoform protects cardiomyocytes from hypertrophic and oxidative stresses via SirT1 activity." Aging-Us **2**(1): 43-62.

Wang, D., V. V. Patel, E. Ricciotti, R. Zhou, M. D. Levin, E. Gao, Z. Yu, V. A. Ferrari, M. M. Lu, J. Xu, H. Zhang, Y. Hui, Y. Cheng, N. Petrenko, Y. Yu and G. A. FitzGerald (2009). "Cardiomyocyte cyclooxygenase-2 influences cardiac rhythm and function." Proceedings of the National Academy of Sciences of the United States of America **106**(18): 7548-7552.

Wang, L., W. Q. Ma, R. Markovich, J. W. Chen and P. H. Wang (1998). "Regulation of cardiomyocyte apoptotic signaling by insulin-like growth factor I." Circulation Research **83**(5): 516-522.

Wang, W. S., P. M. Chen, H. L. Hsiao, S. Y. Ju and Y. Su (2003). "Overexpression of the thymosin beta-4 gene is associated with malignant progression of SW480 colon cancer cells." Oncogene **22**(21): 3297-3306.

Wang, W. S., P. M. Chen, H. L. Hsiao, H. S. Wang, W. Y. Liang and Y. Su (2004). "Overexpression of the thymosin beta-4 gene is associated with increased invasion of SW480 colon carcinoma cells and the distant metastasis of human colorectal carcinoma." Oncogene **23**(39): 6666-6671.

Wang, Z. Y., F. Q. Zeng, Z. H. Zhu, G. S. Jiang, L. Lv, F. Wan, R. Dong, X. Y. Xiao and S. A. Xing (2012). "Evaluation of thymosin beta 4 in the regulation of epithelial-mesenchymal transformation in urothelial carcinoma." Urologic Oncology-Seminars and Original Investigations **30**(2): 167-176.

Waterston, R. H., K. Lindblad-Toh, E. Birney, J. Rogers, J. F. Abril, P. Agarwal, R. Agarwala, R. Ainscough, M. Alexandersson, P. An, S. E. Antonarakis, J. Attwood, R. Baertsch, J. Bailey, K. Barlow, S. Beck, E. Berry, B. Birren, T. Bloom, P. Bork, M. Botcherby, N. Bray, M. R. Brent, D. G. Brown, S. D. Brown, C. Bult, J. Burton, J. Butler, R. D. Campbell, P. Carninci, S. Cawley, F. Chiaromonte, A. T. Chinwalla, D. M. Church, M. Clamp, C. Clee, F. S. Collins, L. L. Cook, R. R. Copley, A. Coulson, O. Couronne, J. Cuff, V. Curwen, T. Cutts, M. Daly, R. David, J. Davies, K. D. Delehaunty, J. Deri, E. T. Dermitzakis, C. Dewey, N. J. Dickens, M. Diekhans, S. Dodge, I. Dubchak, D. M. Dunn, S. R. Eddy, L. Elnitski, R. D. Emes, P. Eswara, E. Eyras, A. Felsenfeld, G. A. Fewell, P. Flicek, K. Foley, W. N. Frankel, L. A. Fulton, R. S. Fulton, T. S. Furey, D. Gage, R. A. Gibbs, G. Glusman, S. Gnerre, N. Goldman, L. Goodstadt, D. Grafham, T. A. Graves, E. D. Green, S. Gregory, R. Guigo, M. Guyer, R. C. Hardison, D. Haussler, Y. Hayashizaki, L. W. Hillier, A. Hinrichs, W. Hlavina, T. Holzer, F. Hsu, A. Hua, T. Hubbard, A. Hunt, I. Jackson, D. B. Jaffe, L. S. Johnson, M. Jones, T. A. Jones, A. Joy, M. Kamal, E. K. Karlsson, D. Karolchik, A. Kasprzyk, J. Kawai, E. Keibler, C. Kells, W. J. Kent, A. Kirby, D. L. Kolbe, I. Korf, R. S. Kucherlapati, E. J. Kulbokas, D. Kulp, T. Landers, J. P. Leger, S. Leonard, I. Letunic, R. Levine, J. Li, M. Li, C. Lloyd, S. Lucas, B. Ma, D. R. Maglott, E. R. Mardis, L. Matthews, E. Mauceli, J. H. Mayer, M. McCarthy, W. R. McCombie, S. McLaren, K. McLay, J. D. McPherson, J. Meldrim, B. Meredith, J. P. Mesirov, W. Miller, T. L. Miner, E. Mongin, K. T. Montgomery, M. Morgan, R. Mott, J. C. Mullikin, D. M. Muzny, W. E. Nash, J. O. Nelson, M. N. Nhan, R. Nicol, Z. Ning, C. Nusbaum, M. J. O'Connor, Y. Okazaki, K. Oliver, E. Overton-Larty, L. Pachter, G. Parra, K. H. Pepin, J. Peterson, P. Pevzner, R. Plumb, C. S. Pohl, A. Poliakov, T. C. Ponce, C. P. Ponting, S. Potter, M. Quail, A. Reymond, B. A. Roe, K. M. Roskin, E. M. Rubin, A. G. Rust, R. Santos, V. Sapojnikov, B. Schultz, J. Schultz, M. S. Schwartz, S. Schwartz, C. Scott, S. Seaman, S. Searle, T. Sharpe, A. Sheridan, R. Shownkeen, S. Sims, J. B. Singer, G. Slater, A. Smit, D. R. Smith, B. Spencer, A. Stabenau, N. Stange-Thomann, C. Sugnet, M. Suyama, G. Tesler, J. Thompson, D. Torrents, E. Trevaskis, J. Tromp, C. Ucla, A. Ureta-Vidal, J. P. Vinson, A. C. Von Niederhausern, C. M. Wade, M. Wall, R. J. Weber, R. B. Weiss, M. C. Wendl, A. P. West, K. Wetterstrand, R. Wheeler, S. Whelan, J. Wierzbowski, D. Willey, S. Williams, R. K. Wilson, E. Winter, K. C. Worley, D. Wyman, S. Yang, S. P. Yang, E. M. Zdobnov, M. C. Zody and E. S. Lander (2002). "Initial sequencing and comparative analysis of the mouse genome." Nature **420**(6915): 520-62.

Wei, M. C., W. X. Zong, E. H. Y. Cheng, T. Lindsten, V. Panoutsakopoulou, A. J. Ross, K. A. Roth, G. R. MacCregor, C. B. Thompson and S. J. Korsmeyer (2001). "Proapoptotic BAX and BAK: A requisite gateway to mitochondrial dysfunction and death." Science **292**(5517): 727-730.

Weinreb, P. H., W. G. Zhen, A. W. Poon, K. A. Conway and P. T. Lansbury (1996). "NACP, a protein implicated in Alzheimer's disease and learning, is natively unfolded." Biochemistry **35**(43): 13709-13715.

Welle, S., K. Burgess, C. A. Thornton and R. Tawil (2009). "Relation between extent of myostatin depletion and muscle growth in mature mice." American Journal of Physiology-Endocrinology and Metabolism **297**(4): E935-E940.

Wickenden, A. D., R. Kaprielian, Z. Kassiri, J. N. Tsoporis, R. Tsushima, G. I. Fishman and P. H. Backx (1998). "The role of action potential prolongation and altered intracellular calcium handling in the pathogenesis of heart failure." Cardiovasc Res **37**(2): 312-23.

Wilfinger, W. W., K. Mackey and P. Chomczynski (1997). "Effect of pH and ionic strength on the spectro-photometric assessment of nucleic acid purity." Biotechniques **22**(3): 474-&.

Winn, N., A. Paul, A. Musaro and N. Rosenthal (2002). "Insulin-like growth factor isoforms in skeletal muscle aging, regeneration, and disease." Cold Spring Harb Symp Quant Biol **67**: 507-18.

Wisneski, J. A., C. N. Pfeil, D. G. Wyse, R. Mitchell, S. H. Rahimtoola and E. W. Gertz (1981). "LEFT-VENTRICULAR EJECTION FRACTION CALCULATED FROM VOLUMES AND AREAS - UNDERESTIMATION BY AREA METHOD." Circulation **63**(1): 149-151.

Witke, W. (2004). "The role of profilin complexes in cell motility and other cellular processes." Trends Cell Biol **14**(8): 461-9.

Wollert, K. C., G. P. Meyer, J. Lotz, S. Ringes-Lichtenberg, P. Lippolt, C. Breidenbach, S. Fichtner, T. Korte, B. Hornig, D. Messinger, L. Arseniev, B. Hertenstein, A. Ganser and H. Drexler (2004). "Intracoronary autologous bone-marrow cell transfer after myocardial infarction: the BOOST randomised controlled clinical trial." Lancet **364**(9429): 141-148.

Woo, Y. J., C. M. Panlilio, R. K. Cheng, G. P. Liao, P. Atluri, V. M. Hsu, J. E. Cohen and H. W. Chaudhry (2006). "Therapeutic delivery of cyclin A2 induces myocardial regeneration and enhances cardiac function in ischemic heart failure." Circulation **114**: I206-I213.

World Health Organisation (2003). "World Health Report 2003."

Xiong, D., T. Yajima, B.-K. Lim, A. Stenbit, A. Dublin, N. D. Dalton, D. Summers-Torres, J. D. Molkentin, H. Duplain, R. Wessely, J. Chen and K. U. Knowlton (2007). "Inducible cardiac-restricted expression of enteroviral protease 2A is sufficient to induce dilated cardiomyopathy." Circulation **115**(1): 94-102.

Xu, G. J., E. Hannappel, J. Morgan, J. Hempstead and B. L. Horecker (1982). "SYNTHESIS OF THYMOSIN-BETA-4 BY PERITONEAL-MACROPHAGES AND ADHERENT SPLEEN-CELLS." Proceedings of the National Academy of Sciences of the United States of America-Biological Sciences **79**(13): 4006-4009.

Xue, B., A. H. Aguda and R. C. Robinson (2007). Models of the actin-bound forms of the beta-thymosins. Thymosins in Health and Disease: First International Symposium. **1112:** 56-66.

Yacoub, M. H. (2001). "A novel strategy to maximize the efficacy of left ventricular assist devices as a bridge to recovery." Eur Heart J **22**(7): 534-40.

Yang, F., X. P. Yang, Y. H. Liu, J. Xu, O. Cingolani, N. E. Rhaleb and O. A. Carretero (2004). "Ac-SDKP reverses inflammation and fibrosis in rats with heart failure after myocardial infarction." Hypertension **43**(2): 229-36.

Yang, H., M. L. Adamo, A. P. Koval, M. C. McGuinness, H. Ben-Hur, Y. Yang, D. LeRoith and C. T. Roberts, Jr. (1995). "Alternative leader sequences in insulin-like growth factor I mRNAs modulate translational efficiency and encode multiple signal peptides." Mol Endocrinol **9**(10): 1380-95.

Yang, Y. P., Z. Q. Liang, Z. L. Gu and Z. H. Qin (2005). "Molecular mechanism and regulation of autophagy." Acta Pharmacologica Sinica **26**(12): 1421-1434.

Yang, Z., J. Huang, J. Geng, U. Nair and D. J. Klionsky (2006). "Atg22 recycles amino acids to link the degradative and recycling functions of autophagy." Molecular Biology of the Cell **17**(12): 5094-5104.

Ye, L., K. O. Lee, L. P. Su, W. C. Toh, H. K. Haider, P. K. Law, W. Zhang, S. P. Chan and E. K. W. Sim (2009). "Skeletal myoblast transplantation for attenuation of hyperglycaemia, hyperinsulinaemia and glucose intolerance in a mouse model of type 2 diabetes mellitus." Diabetologia **52**(9): 1925-1934.

Yesilay, A. B., O. Karakurt, R. Akdemir, G. Erden, H. Kilic, S. Acikel, B. Karasu, M. Sari, M. Balci and M. Aksoy (2011). "Thymosin beta4 levels after successful primary percutaneous coronary intervention for acute myocardial infarction." Turk Kardiyoloji Dernegi arsivi : Turk Kardiyoloji Derneginin yayin organidir **39**(8): 654-60.

Yndestad, A., J. K. Damas, E. Oie, T. Ueland, L. Gullestad and P. Aukrust (2006). "Systemic inflammation in heart failure - The whys and wherefores." Heart Failure Reviews **11**(1): 83-92.

Yoshizumi, M., W. S. Lee, C. M. Hsieh, J. C. Tsai, J. Li, M. A. Perrella, C. Patterson, W. O. Endege, R. Schlegel and M. E. Lee (1995). "DISAPPEARANCE OF CYCLIN-A CORRELATES WITH PERMANENT WITHDRAWAL OF CARDIOMYOCYTES FROM THE CELL-CYCLE IN HUMAN AND RAT HEARTS." Journal of Clinical Investigation **95**(5): 2275-2280.

Zahedi, R. P., U. Lewandrowski, J. Wiesner, S. Wortelkamp, J. Moebius, C. Schuetz, U. Walter, S. Gambaryan and A. Sickmann (2008). "Phosphoproteome of resting human platelets." Journal of Proteome Research **7**(2): 526-534.

Zarbock, J., H. Oschkinat, E. Hannappel, H. Kalbacher, W. Voelter and T. A. Holak (1990). "SOLUTION CONFORMATION OF THYMOSIN-BETA-4 - A NUCLEAR-MAGNETIC-RESONANCE AND SIMULATED ANNEALING STUDY." Biochemistry **29**(34): 7814-7821.

Zeltsman, D. and M. A. Acker (2002). "Surgical management of heart failure: An overview." Annual Review of Medicine **53**: 383-391.

Zhang, J., Z. G. Zhang, D. Morris, Y. Li, C. Roberts, S. B. Elias and M. Chopp (2009). "Neurological functional recovery after thymosin beta4 treatment in mice with experimental auto encephalomyelitis." Neuroscience.

Zhang, Y., C. Riesterer, A. M. Ayrall, F. Sablitzky, T. D. Littlewood and M. Reth (1996). "Inducible site-directed recombination in mouse embryonic stem cells." Nucleic Acids Research **24**(4): 543-548.

Zhang, Y., M. Yuan, K. M. Bradley, F. Dong, P. Anversa and J. Ren (2012). "Insulin-Like Growth Factor 1 Alleviates High-Fat Diet-Induced Myocardial Contractile Dysfunction Role of Insulin Signaling and Mitochondrial Function." Hypertension **59**(3): 680-U349.

Zhou, J., Y. P. Jang, S. R. Kim and J. R. Sparrow (2006). "Complement activation by photooxidation products of A2E, a lipofuscin constituent of the retinal pigment epithelium." Proceedings of the National Academy of Sciences of the United States of America **103**(44): 16182-16187.

Zhou, J., J. Qu, X. P. Yi, K. Graber, L. Huber, X. Wang, A. M. Gerdes and F. Li (2007). "Upregulation of gamma-catenin compensates for the loss of gamma-catenin in adult cardiomyocytes." American Journal of Physiology-Heart and Circulatory Physiology **292**(1): H270-H276.

Zhu, J., L.-P. Su, L. Ye, K.-O. Lee and J.-H. Ma (2012). "Thymosin beta 4 ameliorates hyperglycemia and improves insulin resistance of KK Cg-Ay/J mouse." Diabetes Research and Clinical Practice **96**(1): 53-59.

Zhu, X. D. and P. D. Sadowski (1995). "CLEAVAGE-DEPENDENT LIGATION BY THE FLP RECOMBINASE - CHARACTERIZATION OF A MUTANT FLP PROTEIN WITH AN ALTERATION IN A CATALYTIC AMINO-ACID." Journal of Biological Chemistry **270**(39): 23044-23054.